Lung cancer cachexia

LUNG CANCER CACHEXIA

Decoding molecular mechanisms and imaging the dynamics of muscle wasting

Wouter R. P. H. van de Worp

Lung cancer cachexia

Decoding molecular mechanisms and imaging the dynamics of muscle wasting

Wouter Robertus Paulus Hendrik van de Worp

ISBN: 978-94-6458-711-1

Provided by thesis specialist Ridderprint, ridderprint.nl
Printing: Ridderprint
Layout and cover design: Birgit Vredenburg, persoonlijkproefschrift.nl

The research described in this thesis was performed at the Department of Respiratory Medicine, NUTRIM School of Nutrition and Translational Research in Metabolism at Maastricht University Medical Centre+, Maastricht, the Netherlands.

The Research Conducted in this doctoral thesis was supported by a grant of Danone Nutricia Research.

Lung cancer cachexia

Decoding molecular mechanisms and imaging the dynamics of muscle wasting

Dissertation

To obtain the degree of doctor at Maastricht University,
on the authority of the Rector Magnificus, prof. dr. Pamela Habibović
in accordance with the decision of the Board of Deans,
to be defended in public on Wednesday 14th December 2022 at 16:00 hours

by

Wouter Robertus Paulus Hendrik van de Worp

Supervisor
Prof. dr. A.M.W.J. Schols

Co-supervisors
Dr. R.C.J. Langen
Dr. A. van Helvoort
Dr. J. Theys

Assessment Committee
Prof. dr. M.K.C. Hesselink (chair)
Prof. dr. D.K.M. De Ruysscher
Prof. dr. D. Guttridge, Medical University of South Carolina, USA
Dr. L. Hendriks
Dr. L. Sylow, University of Copenhagen, Denmark

CONTENT

1

General introduction and outline of this thesis

GENERAL INTRODUCTION

1. CANCER CACHEXIA

Cancer cachexia is a complex multifactorial catabolic syndrome that leads to significant unintentional body weight loss, characterized by an ongoing loss of skeletal muscle mass with or without a reduction in fat mass. This loss of body weight cannot be fully reversed by conventional nutritional support [1]. Cancer cachexia is estimated to affect up to 30% of all patients with cancer, with the highest prevalence in lung, pancreatic and liver cancer patients [2]. Cancer cachexia is associated with poor clinical outcome, decreased overall survival [3] and negatively influences tumor therapy, as is illustrated by increased post-operative mortality and decreased response to anticancer therapy [4-6].

There are many definitions of cancer cachexia. The most generally accepted criteria to define cachexia are weight loss of greater than 5% of total body weight over the last 6 months, or ongoing weight loss of greater than 2% when body mass index (BMI) is lower than 20 kg/m^2 and sex-specific skeletal muscle index (SMI) consistent with sarcopenia [1]. Although weight loss and BMI generally distinguish patients with and without cachexia and is associated with overall survival [7], the use of more sophisticated analysis methods such as computed tomography (CT) to obtain body composition has been suggested as a better tool [8, 9]. Indeed, a recent study in patients with pancreatic ductal adenocarcinoma challenged the consensus definition with CT analysis. While the traditional definition classified 56.6% of patients as being cachectic, the CT analysis detected tissue loss of more than 5% in 81% of the patients [10]. This indicates that the opportunistic use of oncologic CT images for more precise assessment of body composition should be applied to detect cancer cachexia as early as possible.

2. LUNG CANCER

Lung cancer is the third most common cancer in both men and women. More than 13.000 people per year are diagnosed with lung cancer in the Netherlands [11]. The incidence of lung cancer increases with age, and in combination with the improved screening methods, the number of patients diagnosed with lung cancer has increased by 22% over the past ten years [11]. Lung cancer is currently by far the leading cause of cancer-related deaths worldwide [12]. Importantly, the number of deaths from lung cancer continues to decrease, partly because of decreased smoking rates and advances in early detection and treatment [11]. Lung cancer is

subdivided in two major subtypes including both small cell lung cancer (SCLC) and non-small cell lung cancer (NSCLC). Approximately 85% of the new lung cancer cases is diagnosed with NSCLC [13, 14]. At diagnosis, NSCLC is staged according to the TNM classification system in which the cancer is characterized based on the size and extend of the main tumor (T), the degree of spread to regional lymph nodes (N) and metastasis to distant sides (M) [15]. Based on the TNM staging system there are four stages of NSCLC. Stage I-II represents early-stage "localized" disease, stage III "loco regionally advanced" disease and stage IV "metastatic" disease. Patients with NSCLC typically present late with advanced, unresectable disease and have a poor prognosis. The average 5-year survival rate is 17% [11]. For patients diagnosed with stage I this is 61%, while for patients with advanced metastatic NSCLC (stage IV) the 5-year survival rate is only 3% [11].

The development of NSCLC is linked to somatic mutations in many different genes [16]. Only in rare cases, the genetic mutation is inherited. Activation mutation in KRAS and EGFR and a loss of function mutation in TP53 represent the most common somatic mutations in NSCLC [13, 16]. KRAS and EGFR encode for a GTPase and receptor tyrosine kinase, respectively, and play an important role in cell proliferation. TP53 produces the p53 protein, which regulates cell proliferation and division by monitoring DNA damage. KRAS- and EGFR-mutant NSCLC display different biological characteristics and are clinically distinct. The KRAS mutation accounts for approximately 10-30% of the cases of NSCLC and is related to smoking, whereas the EGFR mutation account for 10-40% and is unrelated to smoking [13].

The guidelines for the treatment of NSCLC differ per stage and mutation. The recommended treatment of stage I and II NSCLC is surgical removal of the tumor, followed by postoperative platinum-based adjuvant chemotherapy (ChT) in stage II disease [17, 18]. For patients with comorbidities or any patients refusing surgery, stereotactic radiotherapy (RT) is the refereed treatment [17, 18]. In stage III NSCLC a distinction is made between resectable and unresectable tumors. In resectable stage III NSCLC the tumor is removed by surgery followed by postoperative platinum-based ChT [17, 18]. In patients with unresectable stage III NSCLC, the treatment of choice is concurrent chemoradiotherapy (cCRT) followed by 1 year of durvalumab immunotherapy with curative intent [17, 18]. If cCRT is not possible, for any reason, sequential cCRT represents an effective alternative [17, 18]. In stage IV NSCLC, treatment is not aimed at curing the disease, but at extending life expectancy and quality of life. Approximately half of the stage IV patients is eligible for systemic therapy. The type of systemic therapy is dependent on PD-L1

expression and the presence of an oncogenic driver mutation in tumor cells. ChT with platinum doublets in combination with immunotherapy should be considered in all stage IV NSCLC patients without mutation [19]. In patients where at least 50% of the tumor cells express PD-L1, Pembrolizumab (immunotherapy inhibiting the binding between PD-1 and PD-L1) is considered as the first-line option [19]. Stage IV NSCLC patients with an active oncogenic driver mutation are treated with therapies targeting the activity of the oncogenic driver [19]. Besides the stage of the disease, the manifestation of cancer cachexia is an important contributing factor for the overall prognosis and the success rate of the anti-cancer treatment.

3. THE PREVALENCE AND IMPACT OF CACHEXIA IN LUNG CANCER

Weight loss is frequently observed in patients with lung cancer. Based on multiple observational studies, approximately 60% of the NSCLC patients experience body weight loss prior to diagnosis and 37% of the newly diagnosed NSCLC patients develop cachexia according to the consensus definition [2, 4, 20]. These studies showed that NSCLC patients with cachexia at diagnosis have a significant shorter survival time compared to patients without cachexia [4, 20-22]. A retrospective study showed that patients with metastatic lung cancer (stage IV) have a higher risk to develop cachexia compared to patients without metastatic disease [23]. In addition, they showed that the number of metastatic sites correlates with the likelihood to develop cachexia. Interestingly, they also showed for the first time that having a mutation in KRAS correlates with the risk to develop cachexia [23].

Several studies have examined the incidence of treatment-induced toxicities in NSCLC patients. It has been reported that patients with NSCLC with weight loss at diagnosis have a significantly increased incidence of hematologic toxicities and worse progression-free survival compared to those without unintentional weight loss [20, 24]. In addition, patients with weight loss are more likely to quit chemotherapy early than those without weight loss [20]. The influence of cachexia on disease management and treatment outcomes for patients receiving radiotherapy are poorly described. Recently, a retrospective study showed that the presence of cachexia at diagnosis does not preclude the use of radiotherapy as a curative modality [25]. However, cachexia at diagnosis of NSCLC is prognostic factor for worse outcomes despite curative intent therapy [25]. Up till now, there is marginal clinical evidence of a relationship between cachexia and failure of immune inhibitors. Shiroyama et al. suggested that NSCLC patients with low muscle mass receiving immune checkpoint inhibitors have a greater chance of tumor progression compared to those without low muscle mass [26]. More recently, it was shown that weight loss,

characterized by loss of subcutaneous and visceral adipose tissues, at week 6 of treatment with nivolumab, is a significant poor prognostic factor for survival in patients with Stage IV NSCLC [27, 28]. Turner et al. demonstrated that there was an association of Pembrolizumab clearance with overall survival suggesting that NSCLC patients with cachexia have an increased catabolism of immune checkpoint inhibitors [5].

4. MUSCLE LOSS: A HALLMARK IN CANCER CACHEXIA

Skeletal muscle loss is a characteristic of cancer cachexia and is an important contributing factor to muscle weakness, which adversely affects performance status, quality of life and hospitalization risk [29]. The pathogenesis of (lung) cancer cachexia is multifactorial and incompletely understood, but a distinction can be made between intra-cellular signaling pathways in the skeletal muscle (Figure 1), and the extra-cellular (extra-muscular) triggers generated by or in response to the tumor (Figure 2), which initiate loss of muscle mass.

4.1. Intra-cellular mechanism of muscle wasting in cancer cachexia

Skeletal muscle is the largest tissue in the body and is essential for voluntary movement, including mobility, maintenance of body posture and stability, swallowing and breathing. However, skeletal muscle is not just a locomotor organ, but also contributes to numerous metabolic processes including substrate disposal and thermogenesis [30]. The skeletal muscle is a highly dynamic and plastic tissue and can rapidly respond to changes in functional or metabolic demand [31]. Following resistance exercise, muscles undergo hypertrophy and increase in muscle mass and strength [31, 32]. Conversely, in response to an insult such as cancer cachexia the same parameters decline resulting in muscle atrophy [31]. The mechanisms that contribute to the plasticity of skeletal muscle mass include both protein turnover and myonuclear turnover [31, 33, 34]. Under normal conditions, the absolute rates of protein synthesis and proteolysis, and the recruitment of new nuclei (regeneration) and apoptosis are balanced to maintain homeostasis. However, during muscle wasting the balance within these processes shifts in favor of skeletal muscle catabolism. This subsequently results in net loss of muscle proteins and consequently the loss of muscle mass and strength.

4.1.1. Muscle protein turnover

Skeletal muscle growth requires protein synthesis and is mainly controlled by the insulin-like growth factor 1 (IGF-1) signaling pathway. IGF-1 induces muscle growth by activating the phosphoinositide-3-kinase (PI3K)/Akt pathway. Subsequently,

active Akt stimulates protein synthesis by activating mammalian target of rapamycin (mTOR) and its downstream effectors, 4E-binding protein 1 (4E-BP1) and S6 kinase 1 (S6k1). It should be noted that mTOR responds also to multiple signals other than Akt, including amino acids and physical activity [31, 33].

Skeletal muscle wasting involves a reduction in myofiber cross sectional area due to the net loss of myofibrillar proteins, organelles and cytoplasm. The two main degradation pathways involved in muscle atrophy include the ubiquitin proteasome system (UPS) and the autophagy lysosome pathway (ALP). The activation of the degradation pathways is transcriptionally regulated by a common subset of genes, also called atrophy-related genes or "atrogenes". The upregulation of these atrogenes is under normal conditions blocked by Akt through negative regulation of Forkhead box O (FoxO) transcription factors[31].

The UPS is responsible for the degradation of sarcomeric proteins (e.g. myosin and actin) as well as some specific regulatory proteins after marking with ubiquitin. This is an enzymatic process relying on E1 ubiquitin-activating enzymes, E2 ubiquitin conjugates and E3 ubiquitin ligases [35]. The polyubiquitinated proteins are transferred to the 26S proteasome, where they are degraded. The proteolytic activity of the UPS is in part determined by the expression of rate-limiting muscle specific E3 ligase, including atrogin-1 and muscle RING finger 1 (MuRF1).

The ALP is the other degradation pathway and is used for the degradation and recycling of cytoplasm, long-lived proteins and organelles [36]. Autophagy begins with the formation of a phagophore that engulfs the intra-cellular cargo, thereby sequestering the cargo in an autophagosome. The autophagosome fuses with the lysosome, promoting the degradation of the autophagosomal content. The proteolytic activity of the ALP is in part determined by the activation of Ulk-1/2 by mTOR. In addition, the synthesis and processing of microtubule-associated protein light chain 3 (LC3B) and GABARAP are increased during autophagy, making it other key read outs of autophagy [37].

From experimental models of cancer cachexia, there is abundant evidence for decreased protein synthesis and increased protein degradation, mainly through UPS and ALP, in the skeletal muscle [38, 39]. However, data from clinical studies is rare and considerable more controversial [40]. Op den Kamp et al. observed increased Akt phosphorylation to the total protein ratio in cachectic NSCLC patients compared with healthy control. In contrast, none of the downstream signaling proteins, such as FoxO and mTOR, showed significant changes in phosphorylation.

In addition, they found increased expression of autophagy markers (BNIP3 and LC3B) in muscle biopsies of patients with cachexia compared with healthy control, but no changes in muscle specific E3 ligases [41]. In other cancer types, several studies have reported increased expression of autophagy markers in patients with cachexia [42-45]. However, multiple other studies did not observe any impairment in signaling pathways involved in protein synthesis and degradation pathways in skeletal muscle of cancer patients with cachexia [46-49].

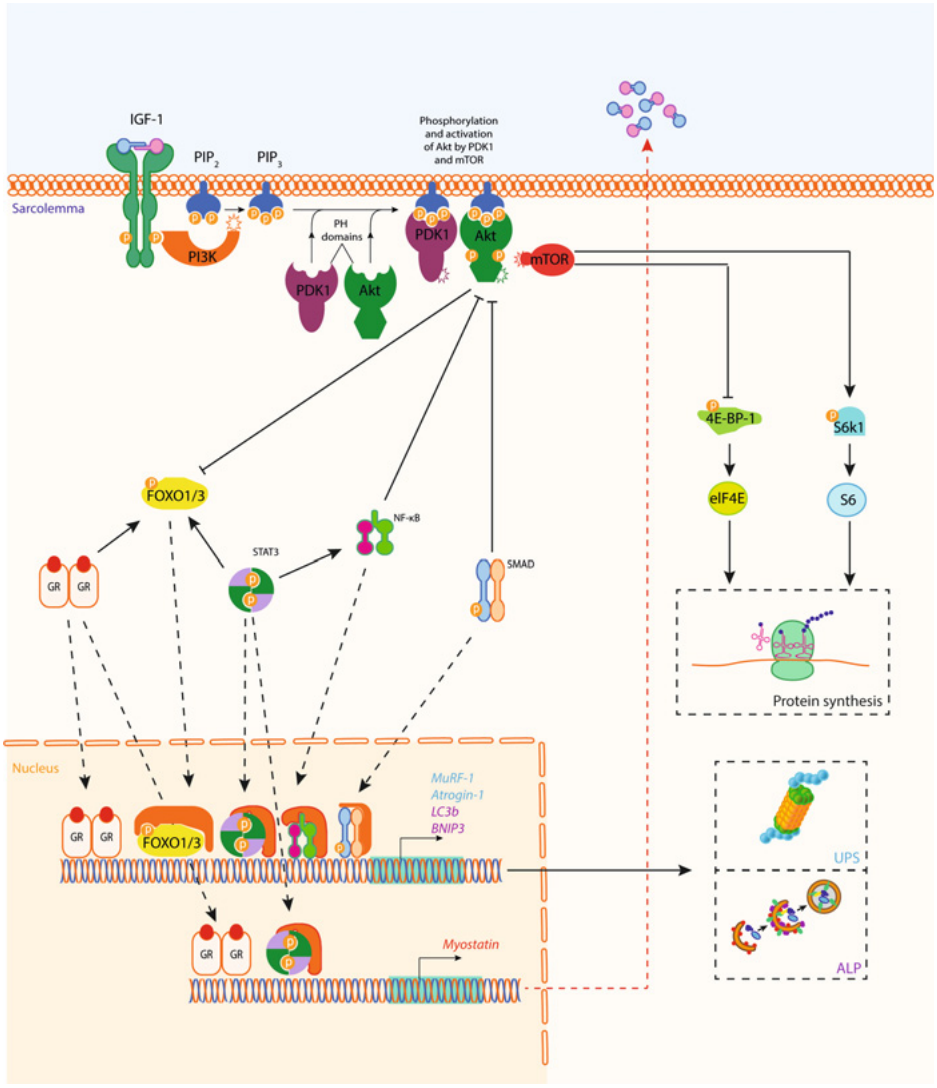

Figure 1: *Schematic signaling diagram illustrating the intra-cellular mechanisms of muscle protein turnover, which can be deregulated during muscle wasting in cancer cachexia.*

4.1.2. Myonuclear turnover

Myonuclear turnover, the balance between myonuclear accretion and apoptosis, is an additional important mechanism that contributes to the plasticity of muscle mass. Myonuclear accretion is the last step of postnatal myogenesis and relies on the donation of satellite cell-derived myonuclei to muscle fibers [50]. In adults, satellite cells reside in a quiescent state and show limited gene transcription and translation [51]. Upon external triggers (e.g. physical activity or injury), satellite cells are activated and proliferate into myoblasts [51-53]. The myoblasts either return into quiescence to prevent depletion of the satellite pool, or differentiate and fuse with muscle fibers to contribute to muscle fiber regeneration, repair and growth [51, 53].

From both clinical and experimental studies there is evidence that cancer cachexia is associated with impaired myonuclear turnover [54-57]. However, missing from these studies is an understanding of whether the impairment of muscle regeneration is simply a consequence of muscle atrophy, or instead a contributing factor leading to the loss of muscle mass and function. Additional well-designed studies using both human subjects and animal models are required to fully elucidate the causes of dysfunctional muscle regeneration during cancer cachexia.

4.1.3. Regulation of muscle mass by microRNAs

MicroRNAs (miRNAs), approximately 22 nucleotides long single-stranded RNAs, have the ability to regulate the synthesis of individual proteins allowing them to fine-tune the proteome of the cell. MiRNAs regulate muscle biology at multiple levels, influencing many important cellular processes including protein and myonuclear turnover [58, 59]. More in-depth information on the biology of miRNAs and studies of differential expression of miRNAs and the pathways they control in muscle atrophy are provided in chapter 2 of this thesis [60].

4.2. Extra-cellular mechanisms of muscle wasting in cancer cachexia

The intra-cellar processes, as describes above, can change upon triggers from outside the skeletal muscle (Figure 2). The extra-cellular stimuli of atrophy in cancer cachexia can be subdivided into direct and indirect effects of the tumor. On the one hand, tumor cells continuously secrete cytokines and growth factors, such as interleukin-6 (IL-6), interleukin-8 (IL-8) and transforming growth factor-β (TGF-β), which can directly stimulate muscle atrophy via several pathways. On the other hand, the tumor secreted factors can result in chronic activation of the immune system and a negative energy balance which are both well-known contributors to muscle wasting. Chronic-systemic inflammation may potentiate muscle wasting

through several mechanism regulated by cytokines and hormones that either directly or indirectly act on skeletal muscle.

There is evidence from both clinical and experimental animal studies that inflammation plays a crucial role in cancer cachexia. Multiple clinical studies have described increased levels of inflammatory markers in cancer patients with cachexia. In NSCLC patients with cachexia, significant higher levels of IL-6, IL-8 and soluble tumor necrosis factor-α receptor 1 (TNFα-R1) and lower levels of albumin and IGF-1 have been observed [41, 61]. More recently, a systematic review showed that there is a consistent association between CT-derived SMI/skeletal muscle density and systematic inflammation, as evidenced by C reactive protein (CRP), albumin and neutrophil lymphocyte ratio [62]. Similarly, in animal models of cancer cachexia, the association between systemic inflammation and muscle wasting has been extensively reported [63-65]. In addition, several researcher have found evidence that the enhanced catabolism is mediated primarily by increases in pro-inflammatory cytokines such as tumor necrosis factor alpha (TNF-α), interleukin 1 (IL-1) and IL-6 [66-69]. Combined these studies strongly support the hypothesis that there is a causal relationship between inflammation and cancer cachexia

4.3. Extra-cellular triggers that directly induce muscle wasting

Many of the extra-cellular stimuli coordinate via receptors the intra-cellular processes through signal transduction pathways. Signaling via these pathways leads to activation of inducible transcription factors, including NF-κB, STAT and Smad, which in turn affect protein turnover and/or myonuclear turnover. These pathways are briefly discussed below.

4.3.1. NF-κB signaling

Pro-inflammatory cytokines, including TNF-α and IL-1, directly affect the skeletal muscle by activating nuclear factor κ light chain enhancer of activated B cells (NF-κB). Under normal conditions, NF-κB is maintained in the inactive state by binding inhibitory protein IκB. Increased levels of pro-inflammatory cytokines cause the activation of an IκB kinase complex that phosphorylates IκB, which results in the ubiquitination and degradation. This leads to the nuclear translocation of NF-κB and activation of NF-κB-mediated gene transcription [70]. NF-κB activation has been implicated as an important step in inflammation-induced muscle wasting. In tumor-bearing animal models, both pharmacological and muscle-specific genetic inhibition of NF-κB prevented muscle wasting [71, 72].

The exact role of NF-κB in muscle metabolism is still poorly understood. However, NF-κB activation has been implicated in increasing UPS proteolytic activity indicated by increased expression of Atrogin-1 and MuRF1 [31]. Furthermore, NF-κB has been shown to inhibit Akt leading to increased expression of FoxO [73].

4.3.2. JAK-STAT signaling

The Janus kinases (JAK)-signal transducer and activator of transcription (STAT) signaling pathway is activated by IL-6 and leukemia inhibitory factor (LIF) [74, 75]. IL-6 and LIF binding to the receptor complex, respectively IL-6r-Gp130 and LIFr-Gp130, results in the phosphorylation of JAK. After activation, the JAK proteins dimerize and phosphorylate downstream STAT3 proteins [76]. The activated STAT3 transcription factors dimerize and translocate to the nucleus where they regulate the transcription of CCAAT/enhancer binding protein (C/EBPδ). Subsequently, STAT3-C/EBPδ activation increases myostatin, Atrogin-1 and MuRF1 expression in skeletal muscle, stimulating protein degradation [77].

4.3.3. Smad signaling

The Smad signaling pathway is activated by ligands of the TGF-β family, including myostatin and activin A. Myostatin is produced by the skeletal muscle and act as a negative regulator of muscle growth, as shown by the findings that myostatin mutations in various mammalian species cause muscle hypertrophy [78]. Myostatin has also been found to be associated with cancer cachexia and its expression is stimulated by the JAK-STAT pathway. In the skeletal muscle, binding of myostatin to its receptor, ActRIIB, results in the phosphorylation and nuclear translocation of Smad2 or Smad3 transcription factors. Activated of Smad signaling leads to inhibition of Akt activity resulting in increased proteolysis [31].

4.4. Extra cellular triggers that indirectly induce muscle wasting

Circulating pro-inflammatory cytokines either produced by the tumor or by the host in response to the tumor also cause dysregulation of tissue that indirectly contribute to the development of cancer cachexia. As such, increased glucocorticoid synthesis, anorexia and hypermetabolism are important well-known contributors to the progression of cancer cachexia.

4.4.1. Increased glucocorticoid synthesis

Glucocorticoids, such as cortisol, are a class of steroid hormones that play an important role in glucose metabolism and have potent anti-inflammatory functions [79]. Because of the latter characteristic synthetic glucocorticoids are used to treat diseases caused by an overactive immune system, such as asthma, sepsis and autoimmune diseases. However, long-term use of these synthetic glucocorticoids have been found to cause muscle wasting. Since this observation, the role of glucocorticoids in cancer cachexia has been extensively studied.

Under normal physiological conditions, glucocorticoids are synthesized in the zona fasciculate of the adrenal cortex [80]. During inflammation, pro-inflammatory cytokines increase the synthesis and release of glucocorticoids from the adrenal cortex [81]. In turn, the glucocorticoids activate a negative feedback loop to shut down its own release. During cancer cachexia, the continues release of pro-inflammatory cytokines cause dysregulation of the negative feedback loop leading to high levels of circulating glucocorticoids [82]. Glucocorticoids have been shown to induce muscle wasting by increasing FoxO signaling, stimulating UPS and ALP mediated muscle protein degradation [83-85], and increasing myostatin production [86].

4.4.2. Anorexia

Anorexia, loss of appetite, is commonly present in patients with lung cancer [87, 88]. Anorexia in cancer has many causes, but is primary caused by the activity of pro-inflammatory cytokines that modulate central nervous system neurotransmitter cascades. Administration of IL-1, TNF-α and IFN-γ [89-91], but not IL-6 [92], has been demonstrated to reduce food intake. These pro-inflammatory cytokines produce anorexia either peripherally or centrally. They can cross the blood-brain barrier [93, 94] or by activating ascending fibers of the vagus nerve [95]. The anorexia is thought to occur as a result of increased stimulation of serotonin and corticotrophin releasing factor in the hypothalamus [96, 97]. The reduced release of neuropeptide Y may also contribute to anorexia. Antibodies to IL-1, TNF-α and IFN-γ enhance food intake in tumor bearing rodents [90, 98, 99]. The TNF-α rs800629 single-nucleotide polymorphism is associated with anorexia in patients with NSCLC [100].

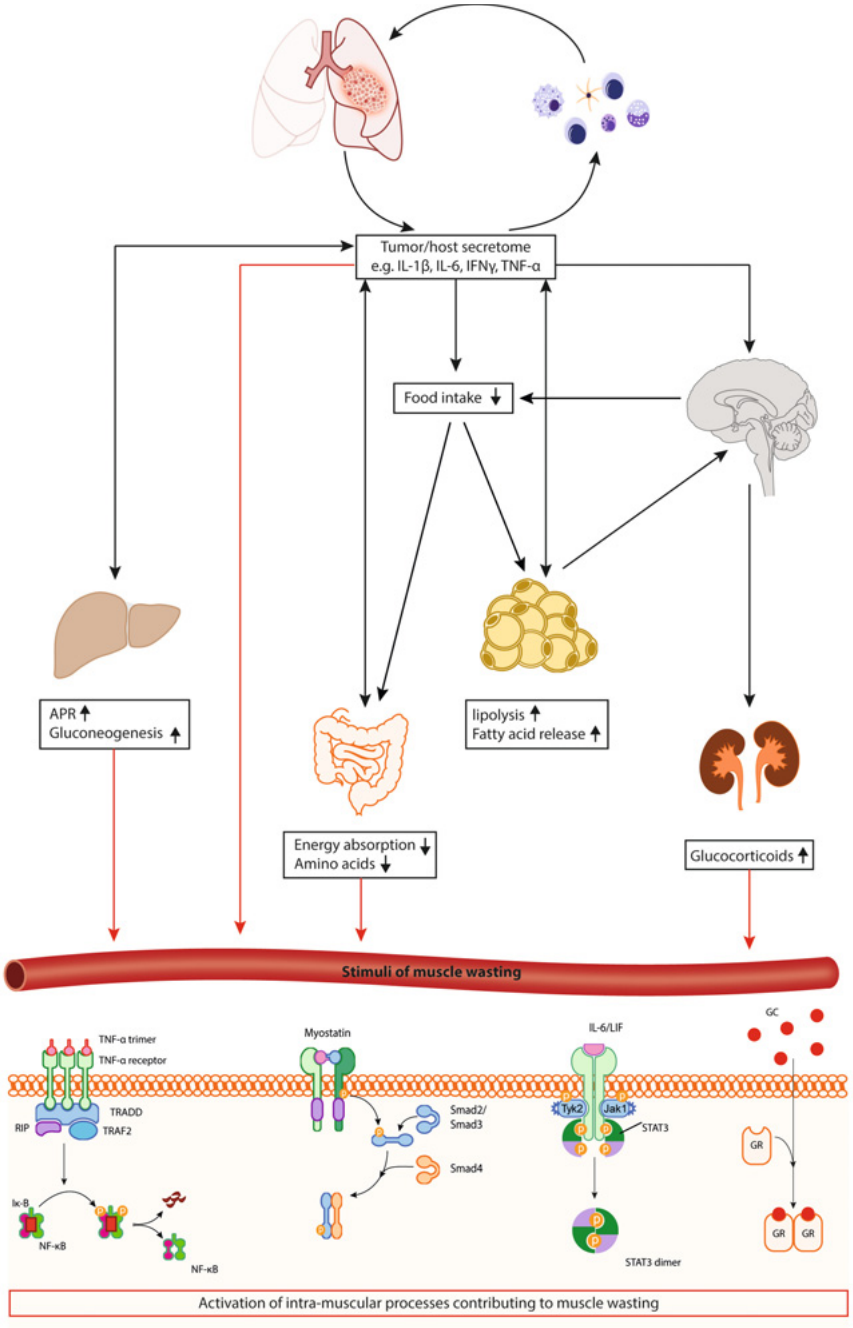

Figure 2: *schematic illustration showing extra-cellular mechanisms of muscle wasting in cancer cachexia. The indirect and direct triggers (black and red arrows, respectively) of muscle wasting are indicated. The intra-muscular processes contributing to muscle wasting are shown in Fig. 1.*

4.4.3. Hypermetabolism

Resting energy expenditure (REE) represents the main component of the total daily energy expenditure. Increased REE, hypermetabolism, is often described in patients with cancer cachexia [101, 102]. Hypermetabolism is related to the increased production pro-inflammatory cytokines and is frequent in advanced NSCLC [101, 103]. In response to the circulating cytokines, a series of changes in the liver is initiated that is referred to as the hepatic acute-phase response (APR). Most importantly, hepatocytes increase the synthesis of positive acute-phase proteins (e.g. C-reactive protein) essential to the inflammatory process. At the same time, the production of a number of other proteins is decreased; these proteins are referred to as negative acute-phase proteins (e.g. albumin) [104]. The increased energy demand by the liver during APR and the immune system influence the REE and initiates processes of muscle wasting. The muscle starts to release amino acids that serve as a fuel through hepatic gluconeogenesis [104]. Normally, the APR elicits a few hours after injury or infection and the majority of the response diminishes in a period of days. However, in cancer this process is converted into a continuous reaction, meaning that the energy demand is never met. As the turnover of muscle proteins occurs at a significant rate, the imbalance between protein synthesis and proteolysis describes the loss of muscle mass seen in lung cancer patients.

AIMS AND OUTLINE OF THIS THESIS

Detection, prevention and adequate treatment of cachexia are a challenge and unmet medical need, respectively, for patients with lung cancer. Therefore, using a translational research approach, the aim of this thesis was to improve our understanding of the dynamics of skeletal muscle wasting and corresponding systemic and muscle molecular changes, and evaluate the therapeutic effects of a multitarget multinutrient intervention.

In **chapter 2**, we provide an overview and describe the mode of action of microRNAs recently implicated in the molecular mechanisms of muscle atrophy. Furthermore, we discuss the challenges to explore their potential as putative therapeutic target in cachexia.

In **chapter 3**, we aimed to identify differentially expressed miRNAs putatively involved in lung cancer cachexia. To this end, we profiled and analyzed miRNA expression in quadriceps muscle biopsies of newly diagnosed treatment-naive NSCLC patients with cachexia and healthy controls.

In **chapter 4**, we review the evidence and perspectives of nutritional interventions to treat cancer cachexia, present an overview of preclinical studies focused on nutritional interventions in cancer cachexia, and discuss the limitations in currently applied experimental models and highlight opportunities for multinutrient interventions.

In **chapter 5 and 6**, we describe the development and validation of a 3D U-Net deep learning network to automatically segment and quantify muscle mass (Chapter 5) and lung tumor volume (Chapter 6) of whole-body CT images for longitudinal follow-up of the dynamics of lung cancer cachexia in mice.

In **chapter 7,** we characterize the systemic changes and muscle functional and molecular alterations during lung cancer cachexia in a novel orthotopic lung cancer mouse model, and address its translational relevance by comparative transcriptomic analysis of skeletal muscle obtained from NSCLC patients with cachexia.

In **chapter 8**, we test the therapeutic efficacy of a specific combination of nutrients as a targeted nutritional intervention on experimental cancer cachexia in the orthotopic lung cancer mouse model.

Finally, the findings of the work described in the current thesis are discussed in a broader framework in **Chapter 9**.

REFERENCES

1. Fearon K, Strasser F, Anker SD, Bosaeus I, Bruera E, Fainsinger RL, et al. Definition and classification of cancer cachexia: an international consensus. Lancet Oncol. 2011;12(5):489-95.
2. Anker MS, Holcomb R, Muscaritoli M, von Haehling S, Haverkamp W, Jatoi A, et al. Orphan disease status of cancer cachexia in the USA and in the European Union: a systematic review. J Cachexia Sarcopenia Muscle. 2019;10(1):22-34.
3. Prado CM, Lieffers JR, McCargar LJ, Reiman T, Sawyer MB, Martin L, et al. Prevalence and clinical implications of sarcopenic obesity in patients with solid tumours of the respiratory and gastrointestinal tracts: a population-based study. Lancet Oncol. 2008;9(7):629-35.
4. Dewys WD, Begg C, Lavin PT, Band PR, Bennett JM, Bertino JR, et al. Prognostic effect of weight loss prior to chemotherapy in cancer patients. Eastern Cooperative Oncology Group. Am J Med. 1980;69(4):491-7.
5. Turner DC, Kondic AG, Anderson KM, Robinson AG, Garon EB, Riess JW, et al. Pembrolizumab Exposure-Response Assessments Challenged by Association of Cancer Cachexia and Catabolic Clearance. Clin Cancer Res. 2018;24(23):5841-9.
6. Vaughan VC, Martin P, Lewandowski PA. Cancer cachexia: impact, mechanisms and emerging treatments. J Cachexia Sarcopenia Muscle. 2013;4(2):95-109.
7. Blum D, Stene GB, Solheim TS, Fayers P, Hjermstad MJ, Baracos VE, et al. Validation of the Consensus-Definition for Cancer Cachexia and evaluation of a classification model--a study based on data from an international multicentre project (EPCRC-CSA). Ann Oncol. 2014;25(8):1635-42.
8. Prado CM, Birdsell LA, Baracos VE. The emerging role of computerized tomography in assessing cancer cachexia. Curr Opin Support Palliat Care. 2009;3(4):269-75.
9. Prado CM, Gonzalez MC, Heymsfield SB. Body composition phenotypes and obesity paradox. Curr Opin Clin Nutr Metab Care. 2015;18(6):535-51.
10. Kays JK, Shahda S, Stanley M, Bell TM, O'Neill BH, Kohli MD, et al. Three cachexia phenotypes and the impact of fat-only loss on survival in FOLFIRINOX therapy for pancreatic cancer. Journal of Cachexia, Sarcopenia and Muscle. 2018;9(4):673-84.
11. (IKNL) IKN. NKR cijfers 2020. 2021.
12. Sung H, Ferlay J, Siegel RL, Laversanne M, Soerjomataram I, Jemal A, et al. Global Cancer Statistics 2020: GLOBOCAN Estimates of Incidence and Mortality Worldwide for 36 Cancers in 185 Countries. CA Cancer J Clin. 2021;71(3):209-49.
13. Herbst RS, Heymach JV, Lippman SM. Lung cancer. N Engl J Med. 2008;359(13):1367-80.
14. Rivera MP, Mehta AC, Wahidi MM. Establishing the diagnosis of lung cancer: Diagnosis and management of lung cancer, 3rd ed: American College of Chest Physicians evidence-based clinical practice guidelines. Chest. 2013;143(5 Suppl):e142S-e65S.
15. Lababede O, Meziane MA. The Eighth Edition of TNM Staging of Lung Cancer: Reference Chart and Diagrams. Oncologist. 2018;23(7):844-8.
16. Ding L, Getz G, Wheeler DA, Mardis ER, McLellan MD, Cibulskis K, et al. Somatic mutations affect key pathways in lung adenocarcinoma. Nature. 2008;455(7216):1069-75.

17. Postmus PE, Kerr KM, Oudkerk M, Senan S, Waller DA, Vansteenkiste J, et al. Early and locally advanced non-small-cell lung cancer (NSCLC): ESMO Clinical Practice Guidelines for diagnosis, treatment and follow-up. Ann Oncol. 2017;28(suppl_4):iv1-iv21.
18. Remon J, Soria JC, Peters S. Early and locally advanced non-small-cell lung cancer: an update of the ESMO Clinical Practice Guidelines focusing on diagnosis, staging, systemic and local therapy. Ann Oncol. 2021.
19. Planchard D, Popat S, Kerr K, Novello S, Smit EF, Faivre-Finn C, et al. Metastatic non-small cell lung cancer: ESMO Clinical Practice Guidelines for diagnosis, treatment and follow-up. Ann Oncol. 2018;29(Suppl 4):iv192-iv237.
20. Ross PJ, Ashley S, Norton A, Priest K, Waters JS, Eisen T, et al. Do patients with weight loss have a worse outcome when undergoing chemotherapy for lung cancers? Br J Cancer. 2004;90(10):1905-11.
21. van der Meij BS, Schoonbeek CP, Smit EF, Muscaritoli M, van Leeuwen PA, Langius JA. Pre-cachexia and cachexia at diagnosis of stage III non-small-cell lung carcinoma: an exploratory study comparing two consensus-based frameworks. Br J Nutr. 2013;109(12):2231-9.
22. Kimura M, Naito T, Kenmotsu H, Taira T, Wakuda K, Oyakawa T, et al. Prognostic impact of cancer cachexia in patients with advanced non-small cell lung cancer. Support Care Cancer. 2015;23(6):1699-708.
23. Shiono M, Huang K, Downey RJ, Consul N, Villanueva N, Beck K, et al. An analysis of the relationship between metastases and cachexia in lung cancer patients. Cancer Med. 2016;5(9):2641-8.
24. Cortellini A, Palumbo P, Porzio G, Verna L, Giordano AV, Masciocchi C, et al. Single-institution study of correlations between skeletal muscle mass, its density, and clinical outcomes in non-small cell lung cancer patients treated with first-line chemotherapy. Thoracic Cancer. 2018;9(12):1623-30.
25. Giap F, Lau SKM, Gannavaparu BS, Iyengar P. Impact of Baseline Cachexia in Non-Small Cell Lung Cancer on Radiation Therapy Utilization and Survival. International Journal of Radiation Oncology, Biology, Physics. 2016;96(2):E509.
26. Shiroyama T, Nagatomo I, Koyama S, Hirata H, Nishida S, Miyake K, et al. Impact of sarcopenia in patients with advanced non–small cell lung cancer treated with PD-1 inhibitors: A preliminary retrospective study. Scientific Reports. 2019;9(1):2447.
27. Degens J, Dingemans AC, Willemsen ACH, Gietema HA, Hurkmans DP, Aerts JG, et al. The prognostic value of weight and body composition changes in patients with non-small-cell lung cancer treated with nivolumab. J Cachexia Sarcopenia Muscle. 2021;12(3):657-64.
28. Degens J, Dingemans AC, Schols A, Willemsen ACH. Letter to the Editor. Lung Cancer. 2021;153:184.
29. Aapro M, Arends J, Bozzetti F, Fearon K, Grunberg SM, Herrstedt J, et al. Early recognition of malnutrition and cachexia in the cancer patient: a position paper of a European School of Oncology Task Force. Ann Oncol. 2014;25(8):1492-9.
30. Egan B, Zierath JR. Exercise metabolism and the molecular regulation of skeletal muscle adaptation. Cell Metab. 2013;17(2):162-84.
31. Schiaffino S, Dyar KA, Ciciliot S, Blaauw B, Sandri M. Mechanisms regulating skeletal muscle growth and atrophy. Febs j. 2013;280(17):4294-314.

32. Suetta C, Aagaard P, Rosted A, Jakobsen AK, Duus B, Kjaer M, et al. Training-induced changes in muscle CSA, muscle strength, EMG, and rate of force development in elderly subjects after long-term unilateral disuse. Journal of Applied Physiology. 2004;97(5):1954-61.
33. Glass DJ. Skeletal muscle hypertrophy and atrophy signaling pathways. The International Journal of Biochemistry & Cell Biology. 2005;37(10):1974-84.
34. Sandri M. Signaling in muscle atrophy and hypertrophy. Physiology (Bethesda). 2008;23:160-70.
35. Ciechanover A. Proteolysis: from the lysosome to ubiquitin and the proteasome. Nat Rev Mol Cell Biol. 2005;6(1):79-87.
36. Sandri M. Autophagy in skeletal muscle. FEBS Lett. 2010;584(7):1411-6.
37. Glick D, Barth S, Macleod KF. Autophagy: cellular and molecular mechanisms. The Journal of Pathology. 2010;221(1):3-12.
38. White JP, Baynes JW, Welle SL, Kostek MC, Matesic LE, Sato S, et al. The regulation of skeletal muscle protein turnover during the progression of cancer cachexia in the Apc(Min/+) mouse. PLoS One. 2011;6(9):e24650.
39. Goncalves MD, Hwang S-K, Pauli C, Murphy CJ, Cheng Z, Hopkins BD, et al. Fenofibrate prevents skeletal muscle loss in mice with lung cancer. Proceedings of the National Academy of Sciences. 2018;115(4):E743-E52.
40. Dolly A, Dumas J-F, Servais S. Cancer cachexia and skeletal muscle atrophy in clinical studies: what do we really know? Journal of Cachexia, Sarcopenia and Muscle. 2020;11(6):1413-28.
41. Op den Kamp CM, Langen RC, Snepvangers FJ, de Theije CC, Schellekens JM, Laugs F, et al. Nuclear transcription factor κ B activation and protein turnover adaptations in skeletal muscle of patients with progressive stages of lung cancer cachexia. Am J Clin Nutr. 2013;98(3):738-48.
42. Zhang Y, Wang J, Wang X, Gao T, Tian H, Zhou D, et al. The autophagic-lysosomal and ubiquitin proteasome systems are simultaneously activated in the skeletal muscle of gastric cancer patients with cachexia. Am J Clin Nutr. 2020;111(3):570-9.
43. Johns N, Hatakeyama S, Stephens NA, Degen M, Degen S, Frieauff W, et al. Clinical classification of cancer cachexia: phenotypic correlates in human skeletal muscle. PLoS One. 2014;9(1):e83618.
44. De Castro GS, Simoes E, Lima JD, Ortiz-Silva M, Festuccia WT, Tokeshi F, et al. Human cachexia induces changes in mitochondria, autophagy and apoptosis in the skeletal muscle. Cancers. 2019;11(9):1264.
45. Aversa Z, Pin F, Lucia S, Penna F, Verzaro R, Fazi M, et al. Autophagy is induced in the skeletal muscle of cachectic cancer patients. Sci Rep. 2016;6:30340.
46. MacDonald AJ, Johns N, Stephens N, Greig C, Ross JA, Small AC, et al. Habitual Myofibrillar Protein Synthesis Is Normal in Patients with Upper GI Cancer Cachexia. Clin Cancer Res. 2015;21(7):1734-40.
47. Stephens NA, Skipworth RJ, Gallagher IJ, Greig CA, Guttridge DC, Ross JA, et al. Evaluating potential biomarkers of cachexia and survival in skeletal muscle of upper gastrointestinal cancer patients. J Cachexia Sarcopenia Muscle. 2015;6(1):53-61.
48. D'Orlando C, Marzetti E, François S, Lorenzi M, Conti V, di Stasio E, et al. Gastric cancer does not affect the expression of atrophy-related genes in human skeletal muscle. Muscle Nerve. 2014;49(4):528-33.
49. Taskin S, Stumpf VI, Bachmann J, Weber C, Martignoni ME, Friedrich O. Motor protein function in skeletal abdominal muscle of cachectic cancer patients. J Cell Mol Med. 2014;18(1):69-79.

50. Relaix F, Zammit PS. Satellite cells are essential for skeletal muscle regeneration: the cell on the edge returns centre stage. Development. 2012;139(16):2845-56.
51. Dhawan J, Rando TA. Stem cells in postnatal myogenesis: molecular mechanisms of satellite cell quiescence, activation and replenishment. Trends Cell Biol. 2005;15(12):666-73.
52. Snijders T, Nederveen JP, McKay BR, Joanisse S, Verdijk LB, van Loon LJ, et al. Satellite cells in human skeletal muscle plasticity. Front Physiol. 2015;6:283.
53. Yin H, Price F, Rudnicki MA. Satellite cells and the muscle stem cell niche. Physiol Rev. 2013;93(1):23-67.
54. He WA, Berardi E, Cardillo VM, Acharyya S, Aulino P, Thomas-Ahner J, et al. NF-κB-mediated Pax7 dysregulation in the muscle microenvironment promotes cancer cachexia. J Clin Invest. 2013;123(11):4821-35.
55. Penna F, Costamagna D, Fanzani A, Bonelli G, Baccino FM, Costelli P. Muscle wasting and impaired myogenesis in tumor bearing mice are prevented by ERK inhibition. PLoS One. 2010;5(10):e13604.
56. Mehl KA, Davis JM, Berger FG, Carson JA. Myofiber degeneration/regeneration is induced in the cachectic ApcMin/+ mouse. J Appl Physiol (1985). 2005;99(6):2379-87.
57. Ramamoorthy S, Donohue M, Buck M. Decreased Jun-D and myogenin expression in muscle wasting of human cachexia. Am J Physiol Endocrinol Metab. 2009;297(2):E392-401.
58. Horak M, Novak J, Bienertova-Vasku J. Muscle-specific microRNAs in skeletal muscle development. Dev Biol. 2016;410(1):1-13.
59. Kemp PR, Griffiths M, Polkey MI. Muscle wasting in the presence of disease, why is it so variable? Biological Reviews. 2019;94(3):1038-55.
60. van de Worp W, Theys J, van Helvoort A, Langen RCJ. Regulation of muscle atrophy by microRNAs: 'AtromiRs' as potential target in cachexia. Curr Opin Clin Nutr Metab Care. 2018;21(6):423-9.
61. SIMONS JPFHA, SCHOLS AMWJ, BUURMAN WA, WOUTERS EFM. Weight loss and low body cell mass in males with lung cancer: relationship with systemic inflammation, acute-phase response, resting energy expenditure, and catabolic and anabolic hormones. Clinical Science. 1999;97(2):215-23.
62. Abbass T, Dolan RD, Laird BJ, McMillan DC. The Relationship between Imaging-Based Body Composition Analysis and the Systemic Inflammatory Response in Patients with Cancer: A Systematic Review. Cancers (Basel). 2019;11(9).
63. Cella PS, Marinello PC, Borges FH, Ribeiro DF, Chimin P, Testa MTJ, et al. Creatine supplementation in Walker-256 tumor-bearing rats prevents skeletal muscle atrophy by attenuating systemic inflammation and protein degradation signaling. Eur J Nutr. 2020;59(2):661-9.
64. Zhuang P, Zhang J, Wang Y, Zhang M, Song L, Lu Z, et al. Reversal of muscle atrophy by Zhimu and Huangbai herb pair via activation of IGF-1/Akt and autophagy signal in cancer cachexia. Support Care Cancer. 2016;24(3):1189-98.
65. Chiappalupi S, Sorci G, Vukasinovic A, Salvadori L, Sagheddu R, Coletti D, et al. Targeting RAGE prevents muscle wasting and prolongs survival in cancer cachexia. J Cachexia Sarcopenia Muscle. 2020;11(4):929-46.
66. Llovera M, López-Soriano FJ, Argilés JM. Effects of tumor necrosis factor-alpha on muscle-protein turnover in female Wistar rats. J Natl Cancer Inst. 1993;85(16):1334-9.

67. Baltgalvis KA, Berger FG, Pena MM, Davis JM, Muga SJ, Carson JA. Interleukin-6 and cachexia in ApcMin/+ mice. Am J Physiol Regul Integr Comp Physiol. 2008;294(2):R393-401.
68. Gelin J, Moldawer LL, Lönnroth C, Sherry B, Chizzonite R, Lundholm K. Role of endogenous tumor necrosis factor alpha and interleukin 1 for experimental tumor growth and the development of cancer cachexia. Cancer Res. 1991;51(1):415-21.
69. Sherry BA, Gelin J, Fong Y, Marano M, Wei H, Cerami A, et al. Anticachectin/tumor necrosis factor-alpha antibodies attenuate development of cachexia in tumor models. Faseb j. 1989;3(8):1956-62.
70. Peterson JM, Bakkar N, Guttridge DC. NF-κB signaling in skeletal muscle health and disease. Curr Top Dev Biol. 2011;96:85-119.
71. Miao C, Lv Y, Zhang W, Chai X, Feng L, Fang Y, et al. Pyrrolidine Dithiocarbamate (PDTC) Attenuates Cancer Cachexia by Affecting Muscle Atrophy and Fat Lipolysis. Front Pharmacol. 2017;8:915.
72. Cai D, Frantz JD, Tawa NE, Jr., Melendez PA, Oh BC, Lidov HG, et al. IKKbeta/NF-kappaB activation causes severe muscle wasting in mice. Cell. 2004;119(2):285-98.
73. Hanna RA, Quinsay MN, Orogo AM, Giang K, Rikka S, Gustafsson Å B. Microtubule-associated protein 1 light chain 3 (LC3) interacts with Bnip3 protein to selectively remove endoplasmic reticulum and mitochondria via autophagy. J Biol Chem. 2012;287(23):19094-104.
74. Schindler C, Levy DE, Decker T. JAK-STAT signaling: from interferons to cytokines. J Biol Chem. 2007;282(28):20059-63.
75. Seto DN, Kandarian SC, Jackman RW. A Key Role for Leukemia Inhibitory Factor in C26 Cancer Cachexia. J Biol Chem. 2015;290(32):19976-86.
76. Moresi V, Adamo S, Berghella L. The JAK/STAT Pathway in Skeletal Muscle Pathophysiology. Front Physiol. 2019;10:500.
77. Zhang L, Pan J, Dong Y, Tweardy DJ, Dong Y, Garibotto G, et al. Stat3 activation links a C/EBPδ to myostatin pathway to stimulate loss of muscle mass. Cell Metab. 2013;18(3):368-79.
78. Lee SJ. Regulation of muscle mass by myostatin. Annu Rev Cell Dev Biol. 2004;20:61-86.
79. Barnes PJ. Anti-inflammatory actions of glucocorticoids: molecular mechanisms. Clin Sci (Lond). 1998;94(6):557-72.
80. Silverman MN, Sternberg EM. Glucocorticoid regulation of inflammation and its functional correlates: from HPA axis to glucocorticoid receptor dysfunction. Ann N Y Acad Sci. 2012;1261:55-63.
81. Mastorakos G, Webster EL, Friedman TC, Chrousos GP. Immunoreactive corticotropin-releasing hormone and its binding sites in the rat ovary. J Clin Invest. 1993;92(2):961-8.
82. Braun TP, Zhu X, Szumowski M, Scott GD, Grossberg AJ, Levasseur PR, et al. Central nervous system inflammation induces muscle atrophy via activation of the hypothalamic-pituitary-adrenal axis. J Exp Med. 2011;208(12):2449-63.
83. Gayan-Ramirez G, Vanderhoydonc F, Verhoeven G, Decramer M. Acute treatment with corticosteroids decreases IGF-1 and IGF-2 expression in the rat diaphragm and gastrocnemius. Am J Respir Crit Care Med. 1999;159(1):283-9.
84. Imae M, Fu Z, Yoshida A, Noguchi T, Kato H. Nutritional and hormonal factors control the gene expression of FoxOs, the mammalian homologues of DAF-16. J Mol Endocrinol. 2003;30(2):253-62.

85. Fenton CG, Webster JM, Martin CS, Fareed S, Wehmeyer C, Mackie H, et al. Therapeutic glucocorticoids prevent bone loss but drive muscle wasting when administered in chronic polyarthritis. Arthritis Res Ther. 2019;21(1):182.
86. Pansters NA, Langen RC, Wouters EF, Schols AM. Synergistic stimulation of myogenesis by glucocorticoid and IGF-I signaling. J Appl Physiol (1985). 2013;114(9):1329-39.
87. Muliawati Y, Haroen H, Rotty LW. Cancer anorexia - cachexia syndrome. Acta Med Indones. 2012;44(2):154-62.
88. Ezeoke CC, Morley JE. Pathophysiology of anorexia in the cancer cachexia syndrome. Journal of Cachexia, Sarcopenia and Muscle. 2015;6(4):287-302.
89. Laviano A, Meguid MM, Yang ZJ, Gleason JR, Cangiano C, Rossi Fanelli F. Cracking the riddle of cancer anorexia. Nutrition. 1996;12(10):706-10.
90. Torelli GF, Meguid MM, Moldawer LL, Edwards III CK, Kim H-J, Carter JL, et al. Use of recombinant human soluble TNF receptor in anorectic tumor-bearing rats. American Journal of Physiology-Regulatory, Integrative and Comparative Physiology. 1999;277(3):R850-R5.
91. Plata-Salamán CR. Interferons and central regulation of feeding. Am J Physiol. 1992;263(6 Pt 2):R1222-7.
92. Strassmann G, Jacob CO, Evans R, Beall D, Fong M. Mechanisms of experimental cancer cachexia. Interaction between mononuclear phagocytes and colon-26 carcinoma and its relevance to IL-6-mediated cancer cachexia. J Immunol. 1992;148(11):3674-8.
93. Banks WA, Farr SA, Morley JE. Entry of blood-borne cytokines into the central nervous system: effects on cognitive processes. Neuroimmunomodulation. 2002;10(6):319-27.
94. Gutierrez EG, Banks WA, Kastin AJ. Murine tumor necrosis factor alpha is transported from blood to brain in the mouse. J Neuroimmunol. 1993;47(2):169-76.
95. Goehler LE, Busch CR, Tartaglia N, Relton J, Sisk D, Maier SF, et al. Blockade of cytokine induced conditioned taste aversion by subdiaphragmatic vagotomy: further evidence for vagal mediation of immune-brain communication. Neurosci Lett. 1995;185(3):163-6.
96. Lloyd RB, Nemeroff CB. The role of corticotropin-releasing hormone in the pathophysiology of depression: therapeutic implications. Curr Top Med Chem. 2011;11(6):609-17.
97. Uehara A, Sekiya C, Takasugi Y, Namiki M, Arimura A. Anorexia induced by interleukin 1: involvement of corticotropin-releasing factor. Am J Physiol. 1989;257(3 Pt 2):R613-7.
98. Martignoni ME, Kunze P, Friess H. Cancer cachexia. Mol Cancer. 2003;2:36.
99. Matthys P, Heremans H, Opdenakker G, Billiau A. Anti-interferon-gamma antibody treatment, growth of Lewis lung tumours in mice and tumour-associated cachexia. Eur J Cancer. 1991;27(2):182-7.
100. Jatoi A, Qi Y, Kendall G, Jiang R, McNallan S, Cunningham J, et al. The cancer anorexia/weight loss syndrome: exploring associations with single nucleotide polymorphisms (SNPs) of inflammatory cytokines in patients with non-small cell lung cancer. Support Care Cancer. 2010;18(10):1299-304.
101. Cao D-x, Wu G-h, Zhang B, Quan Y-j, Wei J, Jin H, et al. Resting energy expenditure and body composition in patients with newly detected cancer. Clinical nutrition. 2010;29(1):72-7.

102. Vazeille C, Jouinot A, Durand J-P, Neveux N, Boudou-Rouquette P, Huillard O, et al. Relation between hypermetabolism, cachexia, and survival in cancer patients: a prospective study in 390 cancer patients before initiation of anticancer therapy. The American journal of clinical nutrition. 2017;105(5):1139-47.
103. Staal-van den Brekel AJ, Dentener MA, Schols A, Buurman WA, Wouters E. Increased resting energy expenditure and weight loss are related to a systemic inflammatory response in lung cancer patients. Journal of clinical oncology. 1995;13(10):2600-5.
104. Stephens NA, Skipworth RJ, Fearon KC. Cachexia, survival and the acute phase response. Current Opinion in Supportive and Palliative Care. 2008;2(4):267-74.

2

Regulation of muscle atrophy by microRNAs: 'AtromiRs' as potential target in cachexia

Wouter R.P.H. van de Worp
Jan Theys
Ardy van Helvoort
Ramon C.J. Langen

Current Opinion in Clinical Nutrition and Metabolic Care
2018, 21:423-429

Purpose of the review

To provide an overview and describe the mode of action of miRNAs recently implicated in muscle atrophy, and discuss the challenges to explore their potential as putative therapeutic targets in cachexia.

Recent findings

Recent work showed differentially expressed miRNAs in skeletal muscle of patients with cachexia-associated diseases. Studies using experimental models revealed miRNA regulation of the anabolic IGF-1 and catabolic TGF-β/myostatin pathways, and downstream protein synthesis and proteolysis signaling in control of muscle mass.

Summary

Cachexia is a complex metabolic condition associated with progressive body weight loss, wasting of skeletal muscle mass and decrease in muscle strength. MiRNAs play a central role in post-transcriptional gene regulation by targeting mRNAs, thereby coordinating and fine-tuning many cellular processes. MiRNA expression profiling studies of muscle biopsies have revealed differentially expressed miRNAs in patients with low muscle mass or cachexia. Evaluation in experimental models has revealed muscle atrophy, inhibition of protein synthesis and activation of proteolysis in response to modulation of specific miRNAs, termed 'atromiRs' in this review. These exciting findings call for further studies aimed at exploring the conservation of differentially expressed miRNAs across diseases accompanied by cachexia, identification of miRNA clusters and targets involved in muscle atrophy, and probing whether these miRNAs might be potential therapeutic targets for cachexia.

Introduction

Cachexia is a complex metabolic condition associated with progressive body weight loss, wasting of skeletal muscle mass and decrease in muscle strength. A plethora of factors and biological mechanisms are involved in the pathophysiology of cachexia. Here, we discuss recent work on the involvement of microRNAs (miRNAs) in the regulation of skeletal muscle mass and speculate on their potential as therapeutic targets to modulate cachexia.

Cachexia

Cachexia is highly prevalent in patients with certain types of cancer and advanced stages of diseases such as chronic obstructive pulmonary disease (COPD), chronic kidney disease (CKD) and heart failure (HF). The most distinct characteristics of cachexia are progressive body weight loss and wasting of skeletal muscle. Muscle wasting is an important determinant of physical disability, diminished quality of life, and is associated with increased mortality. In addition, cachexia limits therapeutic options and efficacy as cachectic patients display reduced tolerance and responsiveness to interventions, as exemplified by dose-limiting toxicity of radiation- and chemotherapy in cachectic cancer patients (1).

At the tissue level, loss of myofibrillar protein in muscle fibers, i.e. decrease in size and not reduction in the number of myofibers, is one of the hallmarks of cachexia. The reduction in protein content is the consequence of both decreased protein synthesis and increased degradation (proteolysis). The proximal pathways that control protein synthesis and proteolysis are well described during acute changes in muscle mass. In addition, accretion of muscle progenitor (satellite) cell-derived nuclei into adult myofibers has been implicated in muscle mass homeostasis (2). However, the exact cellular mechanisms underlying altered regulation of protein and myonuclear turnover and the triggers initiating atrophy signaling in skeletal muscle in cachexia remain to be identified.

MicroRNAs, biogenesis and mode of action

MiRNAs are small, ±22 nucleotides (nt) long single-stranded RNAs that play a central role in post-transcriptional gene regulation by targeting mRNAs, thereby coordinating and fine-tuning many cellular processes. The human genome encodes more than 1000 miRNAs, regulating the expression of at least 50% of all human genes. These pivotal post-transcriptional regulators of gene expression themselves are regulated in a transient and tissue-specific manner during development, homeostasis, and disease (3).

MiRNAs are derived from protein-coding intragenic or non-coding intergenic regions of the DNA and are often found in clusters. A cluster of miRNAs is defined as several miRNA genes with high sequence homology located on the same chromosomal locus, resulting in their coordinated regulation. The observed high sequence homology between the miRNAs in a cluster confers activity towards mRNA targets of genes that operate in the same cellular pathway, allowing a miRNA cluster to regulate various components of the same biological process (4). MiRNA genes are first transcribed as long primary transcripts referred to as primary miRNA (pri-miRNA). Two serial processing reactions take place to obtain mature miRNA. The first reaction occurs in the nucleus and is executed by the Microprocessor complex. The stem-loop structure is cleaved by the nuclear RNase III Drosha to produce an approximately 70nt hairpin structure, termed precursor miRNA (pre-miRNA). The pre-miRNA is subsequently transported to the cytoplasm, where it is cleaved by a second RNase III enzyme (Dicer) to yield an approximately 22nt miRNA duplex, called mature miRNA. To exert their regulatory function, one strand of this duplex, the so-called miRNA guide strand (5p), associates with Argonaute 2 proteins to form the miRISC complex (miRNA-induced silencing complex). This miRISC complex is directly responsible for gene silencing either via mRNA degradation or translational repression. The other strand, indicated as passenger strand (3p), is thought to be degraded (3).

Individual miRNAs may engage with multiple mRNA targets, often encoding various components within the same intracellular network. Typically, the miRNA recognizes partially complementary binding sites, generally located in the 3' untranslated region (3' UTR) of target mRNA. Perfect complementarity to a stretch of 7-8 nt at the 5' end of the miRNA, referred to as seed sequence, is a major determinant in target recognition and is sufficient to trigger gene silencing. The majority of the gene regulatory impact of miRNAs occurs through mRNA degradation, while translational repression confers a distinct inhibitory mode of action by miRNAs (3).

MyomiRs: miRNAs in skeletal muscle.

Most miRNAs are ubiquitously expressed among tissues. However, a small group of miRNAs is exclusively expressed or enriched in striated muscle, i.e. skeletal and cardiac muscle tissue. These muscle-specific miRNAs are referred to as 'myomiRs' and include miR-1, miR-133a, miR-133b, miR-206, miR-208a, miR-208b, miR-486 and miR-499. The tissue specificity of myomiRs results from transcriptional regulation by muscle-specific transcription factors, and is for some myomiRs conferred by their genomic location within the myosin heavy chain (MyHC) genes. MyomiRs have been identified as essential determinants in regulatory networks of

myogenesis, muscle fiber type composition, muscle growth, and homeostasis, as extensively reviewed by Horak et al. (5).

Considering the important role of the myomiRs in myogenesis and muscle growth, alterations in their regulation and potential involvement in muscle atrophy during cachexia can be logically anticipated. Changes in expression of myomiRs have been shown in physiological and disease-induced muscle atrophy, but it is unclear whether these are causally involved or represent adaptive or compensatory responses to muscle atrophy (5). This complexity illustrates the challenge to determine the cause and effect of altered myomiR expression in muscle atrophy. Although a few articles suggested a role for myomiRs in de modulation of catabolic pathways (6), no direct involvement of altered myomiR expression in cachexia has been reported. In contrast, changes in intra-muscular levels of miRNAs not belonging to the myomiRs have been implicated in muscle atrophy and wasting conditions including cachexia.

'AtromiRs': miRNAs involved in muscle atrophy and cachexia.

Research strategies based on experimental models as well as patient-derived muscle biopsies have been deployed to identify putative miRNAs involved in muscle atrophy and specifically cachexia. We propose to term these miRNAs 'atromirs'. Using an elegant approach comparing miRNA expression profiles in skeletal muscle of unrelated experimental models of muscle atrophy, Jin Li et al. identified miR-29b as a potential atromiR, as its expression was sufficient and required for the loss of muscle mass (7). Specifically, a miRNA array was performed on the gastrocnemius muscles from rats subjected to unilateral sciatic denervation-induced muscle atrophy. Of fifteen differentially expressed miRNAs, four were conserved across species, as their increased expression was confirmed in mouse denervated gastrocnemius muscles. MiR-29b was the only miRNA which displayed increased expression levels in four additional *in vivo* models of wasting, including muscle atrophy induced by dexamethasone, fasting, cancer cachexia and aging (sarcopenia). Furthermore, in fully differentiated myotubes, miR-29b over-expression reduced myotube diameter, and decreased MyHC, indicative of *in vitro* atrophy (7). Additional studies postulate a role for miR-29b in muscle atrophy based on its increased expression in models of cardiac cachexia and aging, and causal involvement has been shown in cell culture experiments, yet its potential involvement in human cachexia awaits confirmation in patient derived muscle biopsies (7-9).

Comprehensive profiling of miRNAs for cachexia in human muscle biopsies has been scarce, due to challenges posed by heterogeneity of the clinical population, limited group sizes because of the costly profiling techniques and the invasive nature of muscle biopsies collection. In 2017, the first paper was published identifying differentially expressed miRNAs between cachectic and non-cachectic cancer patents (10). In this study a total of 8 out of 777 miRNAs from rectus abdominis biopsies from cachectic and non-cachectic pancreas and colorectal cancer patients were found to be differentially expressed. All 8 miRNAs were up-regulated, but the direct involvement of the miRNAs reported in this study remains to be addressed in experimental models of cachexia. At the end of 2017, 32 miRNAs were identified to be differentially expressed in the quadriceps of COPD patients with a low fat-free mass index (FFMI) compared with healthy controls (11). Most of the differentially expressed miRNAs were down-regulated in the skeletal muscle of patients with COPD. Only six miRNAs were up-regulated with five of them belonging to the same miRNA cluster. This corresponding differential expression suggests their common upstream regulation and putatively coordinated downstream involvement in muscle atrophy. MiR-542-3p and miR-542-5p were the most significantly increased miRNAs in the COPD cohort (11). The expression of miR-424-5p, another member of the miRNA cluster, was also highly up-regulated, and inversely proportional to physical performance (12). Remarkably, both the expression of miR-542-5p and miR-424-5p were also found to be significantly increased in patients with intensive care unit acquired weakness or amyotrophic lateral sclerosis (11-14). In both populations a direct correlation of miR-424-5p expression and disease progression was observed (12, 13). These studies are the first to identify differentially expressed miRNAs in patients with cachexia with partial conservation between different diseases (10, 11). Importantly, overlapping miRNAs associated with cachexia in cancer as well as COPD, CKD, HF and others, may potentially represent a group of miRNAs specific to muscle atrophy in cachexia per se, independent of the underlying disease (Figure 1). Therefore, comparative miRNA profiling of biopsies collected from cachectic and non-cachectic patients with these diseases is required for the identification of candidate atromiRs. Subsequently, elucidation of the regulation of atromiR expression and their targets in skeletal muscle will aid to a better understanding of the regulation of muscle breakdown in different wasting conditions.

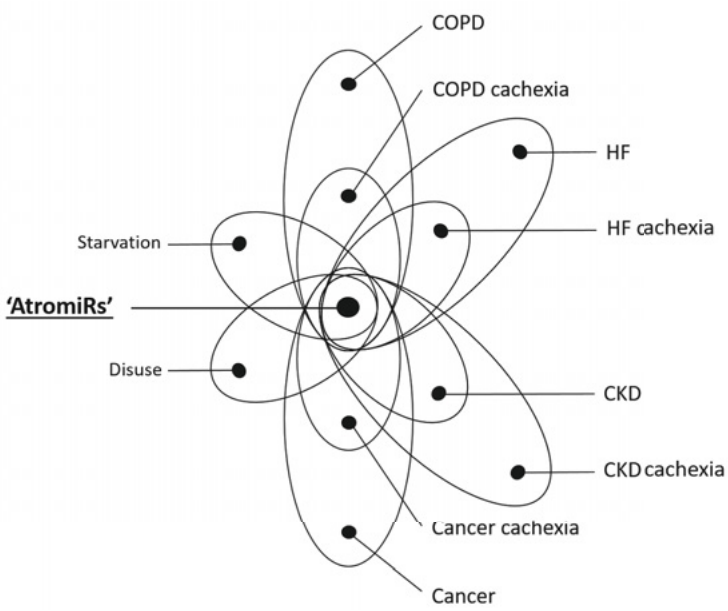

Figure 1: *Conceptual Venn diagram of differentially expressed miRNAs specifically associated with disease, disease-related muscle atrophy, or muscle atrophy independent of the underlying disease, illustrating the strategy to identify miRNAs in skeletal muscle specifically related to muscle atrophy, 'atromiRs'.*

MiRNA regulation of processes and pathways that govern muscle mass.

Muscle atrophy is the consequence of an imbalance between protein synthesis and degradation. While the insulin-like growth factor 1 (IGF-1) pathway promotes muscle growth by stimulating protein synthesis and inhibiting proteolysis, signaling induced by ligands of the transforming growth factor beta (TGF-β) family (e.g. myostatin) results in the converse. Specifically, IGF-1 binds the insulin receptor and activates the PI3K-Akt pathway; in turn Akt induces mTOR, which increases mRNA translation efficiency and capacity, although the latter is also determined by the number of ribosomes regulated independently of PI3K/Akt signaling. In contrast, TGF-β receptor activation inhibits Akt through induction of Smad signaling, resulting in repression of protein synthesis. Conversely, the rate of proteolysis depends on the activity of the ubiquitin proteasome pathway (UPP) and the autophagy-lysosome pathway (ALP). Proteolytic activity is in part determined by the expression of rate limiting enzymes, including the E3 ligase Muscle RING finger 1 (MuRF1) and Atrogin-1 in UPP, as well as by components of the ALP. Their expression is in large extent determined by the transcription factors FoxO1/3, which are subject to inhibitory phosphorylation by Akt. Consequently, inverse regulation of Akt

activity by the IGF-I and TGF-β/myostatin pathways defines their opposing effects on proteolysis. In addition, Smad signaling has also been implicated in direct transcriptional regulation of proteolysis (2).

Recently, several miRNAs associated with muscle mass were implicated in the regulation of these processes and pathways (Figure 2). MiR-424-5p, associated with skeletal muscle loss in different diseases as described above (11-14), is postulated to modulate protein synthesis. *In vitro*, it was shown that miR-424-5p targets proteins involved in ribosomal RNA (rRNA) synthesis. Over-expression of miR-424-5p in myoblasts reduces both 18S and 47S rRNA. Consistently, miR-424-5p inhibits protein synthesis measured by puromycin incorporation. These findings were confirmed *in vivo* by over-expressing miR-322-5p, the rodent orthologue of miR-424-5p, in the tibialis anterior in mice (12). Conversely, expression levels of miR-322-5p are decreased in the hypertrophying right ventricle of rats with pulmonary hypertension (15). This study also showed that miR-322-5p suppresses IGF-1 expression in C2C12 myoblasts.

Similarly, IGF-1 was also found to be the direct target gene of miR-18a, a miRNA of which expression correlates inversely with muscle growth (16). *In vitro*, myotube atrophy induced by over-expression of miR-18a was accompanied by increased expression of atrogin-1 and MuRF-1. Furthermore, miR-18a decreased the phosphorylation of both Akt and FoxO3, while inhibition of Akt/FoxO signaling blocked these effects of miR-18a (16).

Over-expression of miR-29b, identified as a potential atromiR using experimental models described above (7), causes myotube atrophy along with elevated expression of MuRF-1 and Atrogin-1, and autophagy-related genes. MiR-29b also directly targets IGF-1 and PI3K (p85α), and decreases the phosphorylation levels of downstream proteins such as Akt, FoxO3A, mTOR and P70S6K. In addition, inhibition of miR-29b expression prevents dexamethasone-, TNF-α- and H_2O_2-induced expression of proteolysis-related genes and myotube atrophy (7).

In contrast to the actions of these miRNAs, the miR-23a/27a cluster has been shown to attenuate muscle atrophy in a mouse model of CKD-induced muscle wasting. Over-expression of the miR-23a/-27a cluster in the tibialis anterior of CKD mice attenuated muscle loss, improved grip strength and decreased the expression of Atrogin-1 and MuRF-1. The latter corresponded with attenuated activity of the PI3k/Akt signaling pathway and reduced Smad2/3 phosphorylation (17). *In silico* binding site prediction implicated PTEN and Smad3, and myostatin, Smad2 and

FoxO1 as the respective targets of miR-23a and miR-27a potentially responsible for their atrophy-attenuating actions (17, 18).

MiR-542-5p has been reported to target inhibitors of the Smad signaling pathway, thereby sensitizing to TGF-β/myostatin ligands (11). Smurf1 and Smad7 function as TGF-β type 1 receptor antagonists whereas PPP2CA dephosphorylates the Smad2/3 complex, all suppressing Smad signaling. Over-expression of miR-542-5p in myoblasts reduces the mRNA expression levels of Smurf-1, Smad7, and PPP2CA, suggesting that it increases Smad signaling & reduced protein synthesis. These findings were confirmed in mice by overexpressing miR-542-3p in the tibialis anterior (11). Conversely, miR-422a was identified as a miRNA positively associated with muscle strength and mass in catabolic diseases. *In vitro*, miR-422a suppressed different members of the Smad family, including Smad2, -3 and -4, and inhibited TGF-β activity (19).

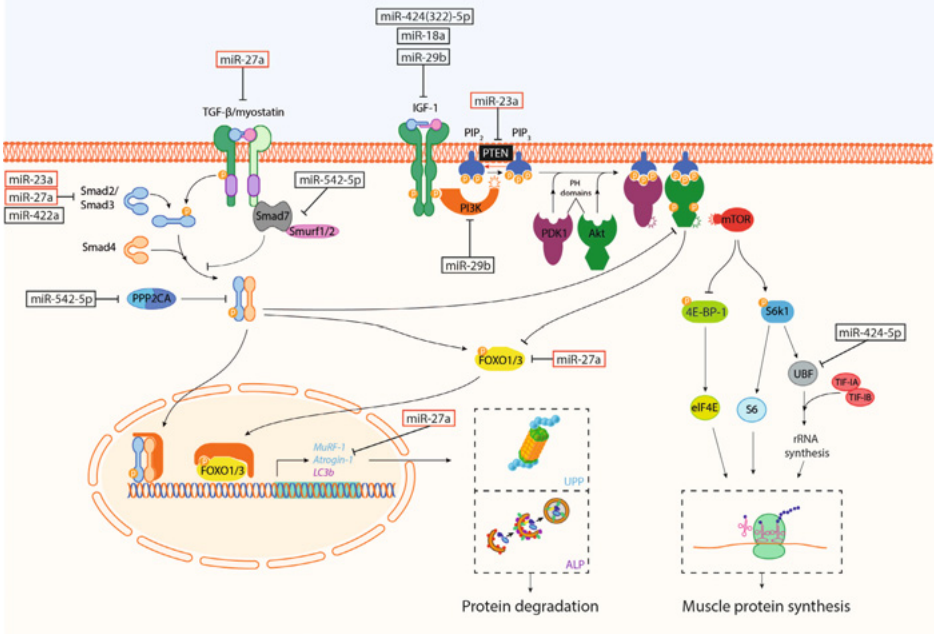

Figure 2: *Schematic signaling diagram illustrating the potential targets of muscle derived miRNAs in pathways and processes regulating muscle atrophy. MiRNAs in red boxes correspond to targets only based on in silico target prediction. Abbreviations not used in the main text: PIP_2: Phosphatidylinositol 4,5-bisphosphate ; PIP_3: Phosphatidylinositol (3,4,5)-trisphosphate; PDK1: phosphoinositide-dependent kinase-1; 4E-BP-1: Eukaryotic translation initiation factor 4E-binding protein 1; eIF4E: Eukaryotic translation initiation factor 4E; TIF: Transcription initiating factor.*

Collectively, multiple studies provide evidence that miRNAs may directly or indirectly regulate protein synthesis and degradation, and upstream signaling pathways indicating their role in muscle atrophy. Further identification of the miRNA targets in these molecular switchboards controlling muscle mass is an essential step when evaluating the potential of miRNA as therapeutic targets for cachexia.

Conclusion: MiRNA therapeutics for cachexia?

Since the discovery of miRNAs, the potential of intervening in miRNA regulated pathological processes has been investigated and miRNA-based therapeutics have been developed. To date, at least seven miRNA-targeted therapeutics are in clinical trial. The first miRNA-targeted drug to enter phase II clinical trials was Miravirsen, a locked nucleic acid (LNA)-modified antisense inhibitor of miR-122, for the treatment of hepatitis C virus infection (20, 21). Although there are no miRNA therapeutics for muscle atrophy in clinical trial yet, the potential shown in pre-clinical studies to manipulate miRNA expression and activity through systemic or local delivery raises possibilities for this new class of drugs for cachexia.

A major question in developing miRNA-based therapeutics is whether a single miRNA or miRNA cluster should be targeted. The key obstacle is posed by the numerous mRNA targets engaged by one individual miRNA or cluster. Thus, the manipulation of miRNA expression or function can have a profound impact on cellular homeostasis, making it essential to carefully and comprehensively investigate miRNA expression, and the mRNA targets of a particular miRNA. This should occur not only in skeletal muscle, but also in other tissues to ensure off-target effects, e.g. on other pathways or in other tissues are limited. In addition, further development of delivery systems with selective or high affinity for skeletal muscle will be required for miRNA-based therapeutics to effectively target skeletal muscle. Finally, the question of whether individual patients express a different set of driver atromirs remains to be addressed.

The current surge in studies related to miRNAs involvement in cachexia will aid in the identification of key atromiRs for target discovery and drug development. This rapidly increasing body of knowledge, together with comprehensive preclinical research, will clarify the feasibility of miRNA targeting and may eventually bring miRNA therapeutics to the clinic for the treatment of muscle atrophy in cachexia.

REFERENCES

1. von Haehling S, Anker SD. Prevalence, incidence and clinical impact of cachexia: facts and numbers-update 2014. J Cachexia Sarcopenia Muscle. 2014;5(4):261-3.
2. Argiles JM, Busquets S, Stemmler B, Lopez-Soriano FJ. Cancer cachexia: understanding the molecular basis. Nat Rev Cancer. 2014;14(11):754-62.
3. Krol J, Loedige I, Filipowicz W. The widespread regulation of microRNA biogenesis, function and decay. Nat Rev Genet. 2010;11(9):597-610.
4. Wang Y, Luo J, Zhang H, Lu J. microRNAs in the Same Clusters Evolve to Coordinately Regulate Functionally Related Genes. Mol Biol Evol. 2016;33(9):2232-47.
5. Horak M, Novak J, Bienertova-Vasku J. Muscle-specific microRNAs in skeletal muscle development. Dev Biol. 2016;410(1):1-13.
6. Marinho R, Alcantara PSM, Ottoch JP, Seelaender M. Role of Exosomal MicroRNAs and myomiRs in the Development of Cancer Cachexia-Associated Muscle Wasting. Front Nutr. 2017;4:69.
7. Li J, Chan MC, Yu Y, Bei Y, Chen P, Zhou Q, et al. miR-29b contributes to multiple types of muscle atrophy. Nat Commun. 2017;8:15201.
8. Moraes LN, Fernandez GJ, Vechetti-Junior IJ, Freire PP, Souza RWA, Villacis RAR, et al. Integration of miRNA and mRNA expression profiles reveals microRNA-regulated networks during muscle wasting in cardiac cachexia. Sci Rep. 2017;7(1):6998.
9. Jung HJ, Lee KP, Milholland B, Shin YJ, Kang JS, Kwon KS, et al. Comprehensive miRNA Profiling of Skeletal Muscle and Serum in Induced and Normal Mouse Muscle Atrophy During Aging. J Gerontol A Biol Sci Med Sci. 2017;72(11):1483-91.
10. Narasimhan A, Ghosh S, Stretch C, Greiner R, Bathe OF, Baracos V, et al. Small RNAome profiling from human skeletal muscle: novel miRNAs and their targets associated with cancer cachexia. J Cachexia Sarcopenia Muscle. 2017;8(3):405-16.
11. Garros RF, Paul R, Connolly M, Lewis A, Garfield BE, Natanek SA, et al. MicroRNA-542 Promotes Mitochondrial Dysfunction and SMAD Activity and Is Elevated in Intensive Care Unit-acquired Weakness. Am J Respir Crit Care Med. 2017;196(11):1422-33.
12. Connolly M, Paul R, Farre-Garros R, Natanek SA, Bloch S, Lee J, et al. miR-424-5p reduces ribosomal RNA and protein synthesis in muscle wasting. J Cachexia Sarcopenia Muscle. 2018;9(2):400-16.
13. de Andrade HM, de Albuquerque M, Avansini SH, de SRC, Dogini DB, Nucci A, et al. MicroRNAs-424 and 206 are potential prognostic markers in spinal onset amyotrophic lateral sclerosis. J Neurol Sci. 2016;368:19-24.
14. Kovanda A, Leonardis L, Zidar J, Koritnik B, Dolenc-Groselj L, Ristic Kovacic S, et al. Differential expression of microRNAs and other small RNAs in muscle tissue of patients with ALS and healthy age-matched controls. Sci Rep. 2018;8(1):5609.
15. Connolly M, Garfield BE, Crosby A, Morrell NW, Wort SJ, Kemp PR. miR-322-5p targets IGF-1 and is suppressed in the heart of rats with pulmonary hypertension. FEBS Open Bio. 2018;8(3):339-48.
16. Liu C, Wang M, Chen M, Zhang K, Gu L, Li Q, et al. miR-18a induces myotubes atrophy by down-regulating IgfI. Int J Biochem Cell Biol. 2017;90:145-54.
17. Wang B, Zhang C, Zhang A, Cai H, Price SR, Wang XH. MicroRNA-23a and MicroRNA-27a Mimic Exercise by Ameliorating CKD-Induced Muscle Atrophy. J Am Soc Nephrol. 2017;28(9):2631-40.

18. Zhang A, Li M, Wang B, Klein JD, Price SR, Wang XH. miRNA-23a/27a attenuates muscle atrophy and renal fibrosis through muscle-kidney crosstalk. J Cachexia Sarcopenia Muscle. 2018.
19. Paul R, Lee J, Donaldson AV, Connolly M, Sharif M, Natanek SA, et al. miR-422a suppresses SMAD4 protein expression and promotes resistance to muscle loss. J Cachexia Sarcopenia Muscle. 2018;9(1):119-28.
20. Rupaimoole R, Slack FJ. MicroRNA therapeutics: towards a new era for the management of cancer and other diseases. Nat Rev Drug Discov. 2017;16(3):203-22.
21. Chakraborty C, Sharma AR, Sharma G, Doss CGP, Lee SS. Therapeutic miRNA and siRNA: Moving from Bench to Clinic as Next Generation Medicine. Mol Ther Nucleic Acids. 2017;8:132-43.

3

Identification of miRNAs in skeletal muscle associated with lung cancer cachexia

Wouter RPH van de Worp
Annemie MWJ Schols
Anne-Marie C Dingemans
Céline MH Op den Kamp
Juliette HRJ Degens
Marco CJM Kelders
Susan Coort
Henry C Woodruff
Gueorqui Kratassiouk
Annick Harel-Bellan
Jan Theys
Ardy van Helvoort
and Ramon CJ Langen

Journal of Cachexia Sarcopenia and Muscle
2020, 11:452-463

ABSTRACT

INTRODUCTION: Cachexia, highly prevalent in patients with non-small cell lung cancer (NSCLC), impairs quality of life and is associated with reduced tolerance and responsiveness to cancer therapy and decreased survival. MiRNAs are small non-coding RNAs that play a central role in post-transcriptional gene regulation. Changes in intra-muscular levels of miRNAs have been implicated in muscle wasting conditions. Here, we aimed to identify miRNAs that are differentially expressed in skeletal muscle of cachectic lung cancer patients to increase our understanding of cachexia and to allow us to probe their potential as therapeutic targets.

METHODS: A total of 754 unique miRNAs were profiled and analyzed in vastus lateralis muscle biopsies of newly diagnosed treatment-naïve NSCLC patients with cachexia (n=8) and age-matched and sex-matched healthy controls (n=8). MiRNA expression analysis was performed using a TaqMan MicroRNA Array. *In silico* network analysis was performed on all significant differentially expressed miRNAs. Differential expression of the top-ranked miRNAs was confirmed using reverse transcription–quantitative real-time PCR in an extended group (n=48) consisting of NSCLC patients with (n=15) and without cachexia (n=11), and healthy controls (n=22). Finally, these miRNAs were subjected to univariate and multivariate Cox proportional hazard analysis using overall survival and treatment-induced toxicity data obtained during the follow-up of this group of patients.

RESULTS: We identified 28 significant differentially expressed miRNAs, of which five miRNAs were up-regulated and 23 down-regulated. *In silico* miRNA-target prediction analysis showed 158 functional gene targets, and pathway analysis identified 22 pathways related to the degenerative or regenerative processes of muscle tissue. Subsequently, the expression of six top-ranked miRNAs was measured in muscle biopsies of the entire patient group. Five miRNAs were detectable with reverse transcription–quantitative real-time PCR analysis, and their altered expression (expressed as fold change, FC) was confirmed in muscle of cachectic NSCLC patients compared with healthy control subjects: miR-424-5p (FC=4.5), miR-424-3p (FC=12), miR-450a-5p (FC=8.6), miR-144-5p (FC=0.59), and miR-451a (FC=0.57). In non-cachectic NSCLC patients, only miR-424-3p was significantly increased (FC=5.6) compared with control. Although the statistical support was not sufficient to imply these miRNAs as individual predictors of overall survival or treatment-induced toxicity, when combined in multivariate analysis miR-

450-5p and miR-451a resulted in a significant stratification between short-term and long-term survival.

CONCLUSION: We identified differentially expressed miRNAs putatively involved in lung cancer cachexia. These findings call for further studies to investigate the causality of these miRNAs in muscle atrophy and the mechanisms underlying their differential expression in lung cancer cachexia.

1. INTRODUCTION

Lung cancer is the leading cause of cancer deaths worldwide [1]. The majority of patients (85%) suffer from non-small cell lung carcinoma (NSCLC) and are predominantly diagnosed at an advanced stage [2], and up to 60% suffer from cancer cachexia [3]. Cachexia is characterized by ongoing loss of body weight, systemic inflammation, anorexia and pronounced loss of skeletal muscle mass and is identified as an important contributor to poor quality of life and mortality [3-5]. Cachexia also adversely affects cancer therapy as cachectic cancer patients have a decreased response to radiotherapy, chemotherapy and immunotherapy [6-8]. The proximal pathways associated with muscle wasting in response to inactivity and starvation are well described and similar to those that occur in wasting associated with disease [9]. However, the triggers and the exact underlying cellular mechanisms of muscle atrophy in lung cancer patients with cachexia remain to be further revealed.

MicroRNAs (miRNAs) are small single-stranded RNAs of approximately 22 nucleotides long that play a central role in post-transcriptional gene regulation by either promoting messenger RNA decay or inhibiting translation [10]. In addition, a number of papers have reported miRNA functioning outside this paradigm (reviewed by Dragomir *et al* [11]) underlining their importance as regulators of gene expression. MyomiRs, a class of miRNAs exclusively expressed or enriched in striated muscle, have been identified as essential determinants in regulatory networks of myogenesis, muscle fiber type composition, muscle growth, and homeostasis [12]. Several miRNAs have also been shown to play a role in different experimental models of skeletal muscle atrophy, including miR-18a, miR-23a, miR-27a, miR-29b, miR-351, miR-422a, miR-424(322)-5p, miR-542-5p and miR-675 [13-24]. AtromiRs have been dubbed as a collective term referring to miRNAs putatively involved in muscle atrophy, regulating processes and signaling pathways that contribute to muscle wasting [25, 26]. However, knowledge of the biological relevance of these miRNAs and their regulation in lung cancer cachexia is lacking.

Until now, extensive profiling of miRNAs related to muscle wasting in human muscle biopsies has been scarce. Changes in intra-muscular levels of diverse miRNAs have been implicated in muscle wasting in critical care [23], chronic obstructive pulmonary disease (COPD) [24], amyotrophic lateral sclerosis (ALS) [27, 28] and a mixed population of pancreas and colon cancer patients [29]. However, as the triggers and intracellular mechanisms of muscle atrophy in lung cancer cachexia may partly differ from these other conditions, distinct miRNAs may be involved in

lung cancer cachexia. Therefore, we designed the current study to investigate the expression profile of miRNAs in the vastus lateralis muscle of a well-characterized group of NSCLC patients with cachexia. We aimed to (i) identify differentially expressed miRNAs in lung cancer cachexia and study whether this altered expression profile is already present in lung cancer patients without cachexia; (ii) predict gene targets for the differentially expressed miRNAs and relate these to pathways involved in muscle mass modulation; and (iii) explore the predictive value of these miRNAs for overall survival (OS) and treatment induced toxicities.

2. METHODS

2.1. Study population

The human samples were used from a previously published cross-sectional study approved by the Medical Ethics Committee of the Maastricht University Medical Centre+ (MEC 06-2-015) and conducted according to local ethical guidelines and all participants provided written informed consent [30].

Briefly, newly diagnosed patients with advanced stage NSCLC admitted to the Department of Respiratory Medicine of the Maastricht University Medical Centre+ between July 2007 and July 2010 were eligible for participation in the study. Participants were divided into a non-cachectic and cachectic group according to the definition in the international cachexia consensus [4]. NSCLC was confirmed by pathological analysis, and tumor stage was determined by using the 6th Tumor-Node-Metastasis International Staging System for Lung Cancer [31].

To study a representative sample of lung cancer patients, but minimize the interference of advanced comorbidities or drugs that could have potential effects on the studied variables, patients with the following characteristics were excluded: Global Initiative for Chronic Obstructive Lung Disease stage IV COPD, Congestive Heart Failure New York Heart Association stage III-IV, and active infectious disease, as well as patients who were taking hormones or continual oral corticosteroids. Additional exclusion criteria were the presence of other malignant disease and the initiation of antitumor therapy.

Healthy control subjects were recruited through advertisements. It was confirmed that healthy control subjects had no recent body weight loss or any of the diseases or used any of the medications described in the exclusion criteria. Samples from eight NSCLC patients with cachexia and eight healthy controls were used for miRNA

array analysis. The extended group included samples from 22 healthy controls, 15 NSCLC patients with cachexia and 11 NSCLC patients without cachexia.

2.2. Body composition

Body height, and waist and hip circumferences were measured to the nearest centimeter. Body weight was measured to the nearest 0.1 kg using a standard lance beam scale. Body mass index was calculated as weight/height squared.

Dual energy X-ray absorptiometry (DEXA: DPX-L, Lunar Radiation Corp., Madison, WI) was used to determine whole-body composition, including fat mass index (FMI), fat free mass index (FFMI) and appendicular skeletal muscle index. Appendicular skeletal muscle index was calculated as the lean mass of the extremities divided by body height squared. DEXA measurements were performed in the fasted state.

2.3. Muscle strength

Isokinetic strength of quadriceps muscle was measured by using a Biodex dynamometer (Biodex system version 3.3). Isokinetic muscle-strength testing was performed at an angle of 60 degrees (three repetitions). Muscle strength was defined as the highest muscular force output (peak torque) in newton meters (N·m).

2.4. Muscle biopsies

Percutaneous needle biopsies of quadriceps muscle (vastus lateralis muscle) were obtained under local anesthesia using the Bergström technique [32]. Muscle specimens for biochemical analysis were immediately frozen in liquid nitrogen, and stored at -80°C until further use. Before analysis, muscle biopsies were crushed with a mortar and pestle in liquid nitrogen.

2.5. RNA extraction and miRNA expression analysis

For miRNA expression analysis, TRI Reagent (Sigma-Aldrich) was used according to the manufacturers' protocol. Muscle specimens (10-30 mg) were homogenized in TRI Reagent by using a Mini bead beater (Cole Parmer) sample homogenizer, and total RNA was extracted. A NanoDrop ND-1000 spectrophotometer (Isogen Lifescience) and Agilent 2100 Bioanalyzer (Agilent Technologies) was used to measure the quantity, purity and integrity of the RNA (Supporting Information, Table S1).

2.6. TaqMan® Array Human MicroRNA

Single-stranded cDNA was synthesized from total RNA samples using the TaqMan® MicroRNA Reverse Transcription (RT) Kit (Applied Biosystems) and the

Megaplex™ RT primers (human pool set v3.0; Applied Biosystems). A total of 754 miRNAs were profiled from vastus lateralis muscle biopsies (out of a total of 1917 precursors and 2654 mature sequences annotated in miRBase v22)[33]. Briefly, 400 ng of RNA was added to the Megaplex™ RT primer solution containing 0.8 µL Megaplex™ RT primers (10x), 0.2 µL deoxynucleotide triphosphate [dNTP; 100 mM], 0.9 µL $MgCl_2$ [25 mM], 0.1 µL RNase inhibitor [20 U/µL], 1.5 µL MultiScribe™ reverse transcriptase [50 U/µL], 10x RT buffer, and 0.2 µL nuclease-free water. RT reactions were carried out according to the manufacturers' protocol.

For TaqMan® Array Human MicroRNA, 6 µL of the Megaplex™ RT product was mixed with 2x TaqMan® Universal PCR Master Mix (Applied Biosystems) and 444 µL nuclease-free water. For each sample, 100 µL of the PCR reaction mix was loaded into each port of the TaqMan® Array cards (Human MicroRNA A+B Set v3.0; Applied Biosystems). The TaqMan® Array was carried out on the 7900HT Fast Real Time PCR System (Applied Biosystems) according to the manufacturers' protocol. The real-time expression data were analyzed using the 7900 SDS RQ Manager software. The resultant C_q values were exported. GeNorm was used to select the most stable reference gene, *Mamm*U6 (gene stability measure M: 0.019 & 0.012, respectively). All C_q values were normalized to *Mamm*U6, using the $\Delta\Delta C_t$ method. Cut-off number of cycles was set as 35. The thresholds used to determine significance of differentially expressed miRNAs was set as $P<0.05$ and a $\Delta\Delta C_t \geq 1$ cycle.

2.7. Reverse transcription quantitative real-time PCR (RT-qPCR)

A fixed volume of 5 ng/µL of total RNA was used for the RT reaction. First-strand cDNA synthesis was performed using the miRCURY® LNA® RT kit according to the manufacturers' protocol (Exiqon). cDNA was diluted (1:80) in nuclease-free H_2O and stored at 4 °C, cDNA stocks were stored at – 20 °C. For real-time PCR amplification, each reaction contained 5µl ExiLENT SYBR® Green master mix (Exiqon), 1 µL miRCURY® LNA® PCR primer mix (Exiqon) and 4 µL diluted cDNA template. PCR settings were 95 °C for 10 min, followed by 45 cycles of 95 °C for 10 s and 60 °C for 1 min, carried out on a Roche LightCycler480 system. Melt curves were made using a gradual increase in temperature of 0.11 °C/s with 5 acquisitions/s and a temperature range of 60 °C to 90 °C. The melt curves were examined using the LightCycler480 software (Roche). PCR efficiency was determined using LinRegPCR software (Suppl. Table 1). The resultant C_q values were exported and normalized to loading control (UniSp6; Exiqon), using the $\Delta\Delta C_t$ method. Cut-off number of cycles was set as 40. The thresholds used to determine

significance of differentially expressed miRNAs was set as $P<0.05$ and a $\Delta\Delta C_t \geq 1$ cycle. The primers used are listed in Supporting Information, Table S2.

2.8. Network analysis

Cytoscape 3.6.1, a widely adopted network visualization and analysis tool, was used to build a miRNA-gene-pathway network [34]. The differentially expressed miRNAs were imported into Cytoscape. Using the CyTargetLinker app in Cytoscape [35], experimentally validated miRNA-gene interactions from miRTarBase 7.0 [36] were added creating a miRNA-target interaction (MTI) network. The targeted genes were reviewed for expression in the skeletal muscle using The Human Protein Atlas [37]. In addition, an overrepresentation analysis was performed in PathVisio 3.3.0 [38] with the miRNA target genes using the human curated analysis collection of WikiPathways [39] and the human gene identifier mapping database (Ensembl 89) [40]. The pathways were then ranked based on a standardized difference score (Z score). A pathway was considered involved when the Z score > 1.96 and permutation p value < 0.05. Finally, the MTI network was extended with the selected pathways using the human WikiPathways [39] linkset in the CyTargetLinker app resulting in a miRNA-gene-pathway network. In this network the miRNA expression levels were visualized. The biological network platform NDEx [41] was used to share and publish the network.

2.9. Exploration of miRNAs as prognostic factor

Univariate Cox proportional hazards models were constructed using the expression levels of the five differentially expressed miRNAs confirmed in the entire group to assess their potential as prognostic factors for OS and/or treatment induced toxicities. OS was defined as the time period between the date of diagnose and the date of death, and the β-coefficient and associated hazard ratio (HR) were computed, as well as the significance and the Wald statistics [42]. Further survival analysis was performed using the median of the survival predictions of multivariate Cox proportional hazards model to stratify the group of patients into distinct survival groups. The logarithms of the expression rates of the miRNAs were considered as continuous variables. Common terminology criteria for adverse events (CTCAE) v5.0 was used to classify treatment-induced toxicities. CTCAE score of 3 was used as cut-off point, and random forest classifier models were used to explore cross-correlation effects between varying combinations of miRNA expression levels on toxicity and the presence of NSCLC, using out-of-bag error estimation, and the results are reported as the area under the curve (AUC) of the receiver operator characteristic curve.

2.10. Statistics

Clinical and demographic data of patients and controls are presented as mean ± standard deviation for normally distributed variables and as median (interquartile range) for variables that were not normally distributed. Independent samples t-test and One-factor ANOVA were used to calculated differences between continuous variables. Chi-square test and Fisher's exact test were used to calculate differences between categorical variables. Differences in miRNA expression data were calculated using Student's t-test and One-factor ANOVA for normally distributed data or by Mann-Whitney U test and Kruskal-Wallis test for non-parametric data. The log-rank test for censored survival data was used to calculate the significance of the Cox proportional hazards models. Data were analyzed with Statistical Package for the Social Sciences software (SPSS version 23 for Windows) and R version 3.4.3 [43]. Significance was set at $P<0.05$.

3. RESULTS

3.1. Clinical characterization of non-small cell lung cancer patients with and without cachexia and control subjects

Basic characteristics of the study population are detailed in Table 1. There was no significant difference between study groups in gender and age. Body weight loss was found to be significantly different between the groups ($P<0.001$). Non-cachectic and cachectic patients with NSCLC showed no significant differences in tumor stage or histological subtype. The majority of these patients (non-cachexia: 64%; cachexia: 73%) suffered from metastatic NSCLC (Table 1 and Supporting Information Table S3). At NSCLC diagnosis, non-cachectic patients showed a mean body weight loss of 1.7% in 6 months before diagnosis, whereas patients with cachexia had a mean body weight loss of 12.7% ($P<0.001$). Moreover, FFMI was significantly lower in patients with cachexia compared with both healthy controls and non-cachectic patients ($P<0.05$) while fat mass index was not different between groups. Muscle strength in patients with cachexia was 47% less than in healthy controls ($P<0.05$). Non-cachectic patients showed less pronounced but significantly reduced muscle strength compared with healthy controls (23%, $P<0.05$).

Table 1: Clinical characteristics of the entire study population

		Non-small cell lung carcinoma (NSCLC)	
	Healthy control (n=22)	**Non-cachexia (n=11)**	**Cachexia (n=15)**
Gender (male/female)	13/9	9/2	8/7
Age (years)	61.4 ± 7.0	63.3 ± 10.3	58.9 ± 7.8
Height (m)	1.73 ± 0.10	1.76 ± 0.06	1.72 ± 0.10
Body weight loss (kg)	0 ± 0	1.3 ± 1.1[A]	9.7 ± 3.9[B,C]
Body weight loss (%)	0 ± 0	1.7 ± 1.3[A]	12.7 ± 4.9[B,C]
Body mass index (BMI) (kg/m²)	24.1 ± 3.3	25.3 ± 3.4	23.1 ± 4.9
Fat mass index (FMI) (kg/m²)	6.5 ± 2.5	7.6 ± 2.8	6.8 ± 3.1
Fat free mass index (FFMI) (kg/m²)	18.4 ± 2.2	18.2 ± 1.8	16.6 ± 2.8[B]
Appendicular skeletal muscle index (ASMI) (kg/m²)	7.7 ± 1.0	7.1 ± 0.84	6.2 ± 0.97 [B,C]
IL-6 (pg/mL)	42.6 (34, 79)	55.7 (44, 82)	130.6 (81, 199)[B,C]
CRP (mg/L)	1.0 (0.5. 1.5)	9.5 (5, 40)[A]	49.5 (25, 86)[B,C]
Disease stage (IIIB/IV)	-	4/7	4/11
Histology (adeno/squamous cell)	-	8/3	8/7
Peak torque flexion 60° (N·m)	73,9 ± 20,8	57,3 ± 19,7[A]	37,4 ± 16,7[B,C]
Peak torque extension 60° (N·m)	120.0 ± 31.2	92.1 ± 27.8[A]	63.6 ± 28.3[B,C]

CRP, C-reactive protein; IL, interleukin.
Cachexia was defined as body weight loss of >5% in the past 6 months, or body weight loss of >2% in combination with either a BMI <20kg/m², or an appendicular skeletal muscle index consistent with sarcopenia determined by DEXA (male<7.26 kg/m²; female<5.45 kg/m²). Data are presented as mean ± standard deviation for normally distributed variables and as median (inter-quartile range) for variables that were not normally distributed. Significance was calculated by one-factor analysis of variance and least significant difference post hoc testing for normally distributed variables and by Mann Whitney U test for variables that were not normally distributed.
[A]P < 0.05 (non-cachexia compared with control subjects).
[B]P < 0.05 (cachexia compared with control subjects).
[C]P < 0.05 (non-cachexia compared with cachexia).

3.2. Identification of differentially expressed microRNAs in non-small cell lung cancer cachexia using TaqMan Array Human MicroRNA

Muscle biopsies from eight NSCLC patients with cachexia and eight gender-matched and age-matched healthy controls were subjected to TaqMan Array to identify miRNAs associated with lung cancer cachexia. Clinical and demographic data of the patients and controls are detailed in Supporting Information, Table S4. A total of 754 miRNAs were profiled from vastus lateralis muscle biopsies. Twenty-eight miRNAs were found to be differentially expressed in cachectic NSCLC patients compared with healthy controls (Figure 1 and Supporting Information Table S5). A total of 5 miRNAs were up-regulated (fold-change (FC)≥2 and a P<0.05). Remarkably, four of them (miR-450a-5p, miR-450b-5p, miR-424-5p and miR-424-3p) belong to the same miRNA cluster. The majority of the differentially expressed miRNAs (82%) were down-regulated (FC≤0.5 and a P<0.05). Hierarchical cluster analysis of all subjects using Ward's method was conducted (Figure 1), resulting in a separation into two equal clusters consisting of cachectic NSCLC patients and healthy controls respectively. These findings suggest a disease-related difference in miRNA expression profile between NSCLC patients with cachexia and healthy controls.

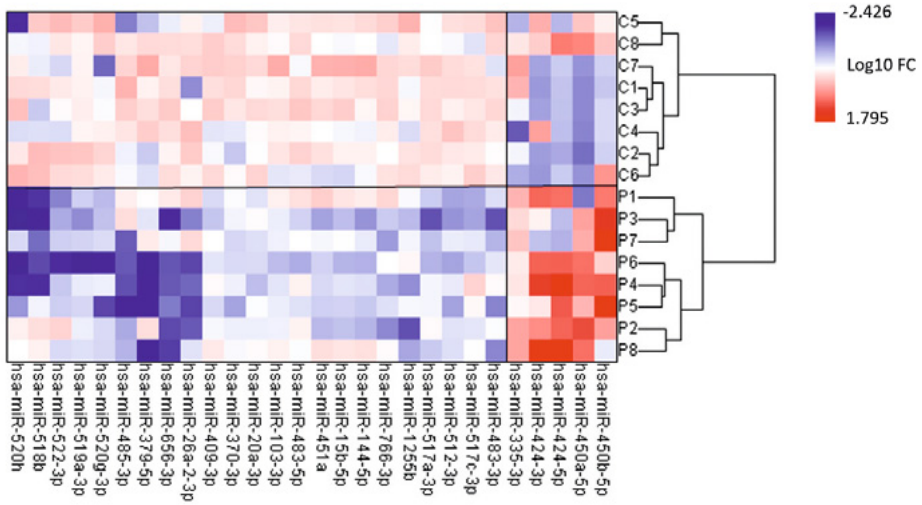

Figure 1: *Heatmap showing the 28 microRNAs (miRNAs) found to be differentially expressed in skeletal muscle of non-smal cell lung cancer (NSCLC) patients with cachexia (P, n=8) in comparison with age-matched healthy controls (C, n=8). The expression of miRNAs was measured by TaqMan® Array Human MicroRNA in vastus lateralis muscle biopsies as described in methods. Red: up-regulated miRNAs; blue: down-regulated miRNAs. Only those miRNA with a P<0.05 and fold change (FC) ≥2 are shown (two-tailed t-test). The numbers on the legend are log10-transformed values. Hierarchical cluster analysis of all subjects using Ward's method was conducted, resulting in a separation into cachectic NSCLC patients and healthy controls, respectively.*

3.3. Predicted microRNA–gene–pathway network

Differentially expressed miRNAs may contribute to regulation of muscle wasting in lung cancer cachexia, which implies that relevant biochemical pathways in the muscle are targeted. To identify potentially involved pathways linked to these miRNAs, miRTarBase was utilized for miRNA target prediction based on experimentally validated targets. This *in silico* analysis revealed that 3215 miRNA target genes and 5164 miRNA - target interactions were found. Only miRNA target genes with a confirmed functional interaction were selected. For 24 out of 28 differentially expressed miRNAs, functional gene targets were present in miRTarBase. Analysis showed 158 genes to be targeted, some of which by more than one of the miRNAs. Of these target genes, 114 are functionally expressed in the skeletal muscle and several of them have already been studied in the context of cancer cachexia or other muscle wasting disorders (Supporting Information, Table S6).

Using the 158 genes, an overrepresentation analysis was performed in PathVisio using the human-curated analysis collection of WikiPathways. Out of 463 pathways, 181 met the criteria (Z score > 1.96 and permutation P-value < 0.05). A selection of pathways considered relevant based on existing literature implying their involvement in muscle tissue regenerative and degenerative processes was added into the network (Figure 2 and Supporting Information, Tables S7a and S7b) and included interleukin-6, transforming growth factor-β, insulin, PI3K-Akt, and tumor necrosis factor-α signaling pathways. A table of all significantly targeted pathways is available in Supporting Information, Table S8.

3.4. Confirmation and comparison of the top-ranked differentially expressed microRNAs in the entire study population

To assess whether this miRNA expression pattern is specific to lung cancer, or lung cancer cachexia, a selection of six top-ranked miRNAs was measured in the muscle biopsies of the entire group, consisting of treatment-naïve NSCLC patients with cachexia (n=15) and without cachexia (n=11), and healthy controls (n=22). The selection of miRNAs was based on their magnitude of differences in expression and postulated relevance of these miRNAs in muscle mass modulation. The six highest-ranked miRNAs (four up-regulated and two down-regulated) were measured by reverse transcription–quantitative real-time PCR. MiR-450b-5p expression levels could not reliably be detected (C_q> 40), and were omitted from further analyses. Five miRNAs showed a significant difference between cachectic NSCLC patients and healthy controls (Figure 3). MiR-424-5p, miR-424-3p and miR-450a were 4.5-fold, 12-fold and 7.7-fold increased, respectively (Figure 3A-3C).

MiR-451a and miR-144-5p were 1.75-fold and 1.69-fold decreased, respectively (Figure 3D-3E). Only miR-424-3p was significantly increased in non-cachectic patients compared with healthy controls (Figure 3B). No gender related differences were observed in miRNA expression within the groups (data not shown). Overall, these data confirm the differential expression of five miRNAs in skeletal muscle of NSCLC patients with cachexia compared with controls and reveal intermittent changes in non-cachectic patients for induced miRNAs only.

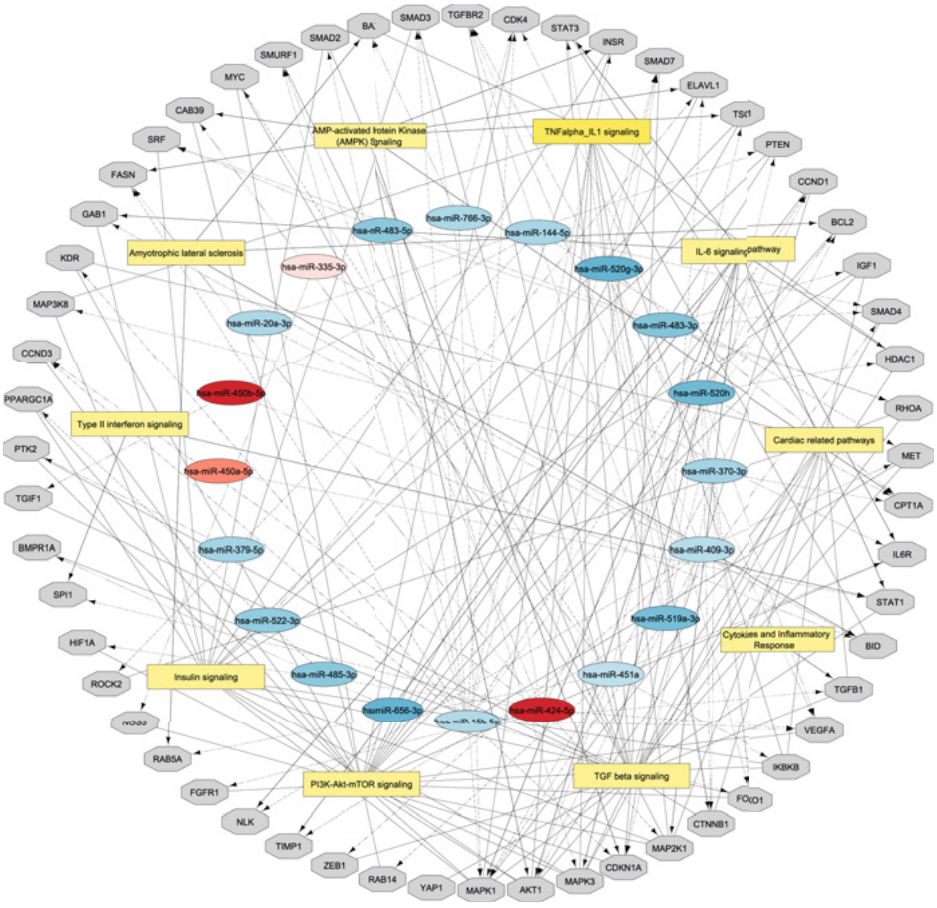

Figure 2: *microRNA (miRNA)-gene-pathway network based on miRTarBase and WikiPathways as described in the Methods section. Red: up-regulated miRNAs; blue: down-regulated miRNAs; grey: potential gene targets in the skeletal muscle; and yellow: most significantly targeted pathways. Cytoscape was used to visualize the network. The network is available via NDEx. The miRNAs and associated target genes within each pathway are included in Supporting Information, Tables S7a and S7b.*

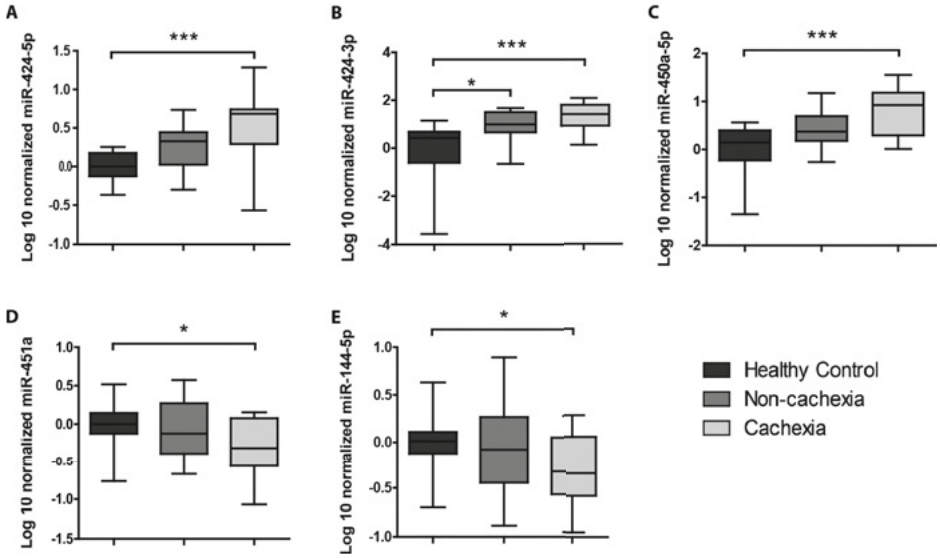

Figure 3: *Box-and-whisker plots showing that the expression of* ***(A)*** *miR-424-5p,* ***(B)*** *miR-424-3p and* ***(C)*** *miR-450a-5p are increased; and the expression of* ***(D)*** *miR-451a and* ***(E)*** *miR-144-5p is decreased in non-small cell lung cancer (NSCLC) patients with cachexia compared with control. The expression of the microRNAs was determined by quantitative PCR in vastus lateralis muscle biopsies from the extended cohort of cachectic (n=15) and non-cachectic (n=11) NSCLC patients and healthy controls (n=22) as described in the Methods section. The box-and-whisker plot shows median and min to max. *P<0.05 and ***P<0.001 Kruskal-Wallis test and Dunn post hoc testing.*

Subsequently, a machine learning approach was used to explore cross-correlation effects between varying combinations of miRNA expression levels and the presence of cachexia. A random forest classifier to differentiate between NSCLC patients and healthy individuals using miRNA expression as predictors for cachexia yielded results significantly different from random chance (AUC = 0.5) for the combination of miR-424-3p and miR-450a-5p yielding an AUC = 0.79 (95% confidence interval 0.6-0.9), and addition of miR-144-5p increasing the AUC to 0.85 (95% confidence interval 0.7-0.9). Further addition of differentially expressed miRNAs did not significantly increase the AUC. These data further confirm the correlation of these miRNAs with cachexia, and implicate miR-424-3p, miR-450a-5p and miR-144-5p as putative AtromiRs.

3.5. microRNAs as potential independent prognostic and predictive factors?

Survival data were available of this well-characterized NSCLC study population, and showed that patients with cachexia have a decreased 3-year OS rates (Figure 4A). Moreover, of the patients with a high treatment-induced toxicity score (CTCAE≥3), cachectic patients had a significantly lower OS compared with non-cachectic patients (Figure 4B). To test whether the expression levels of miRNAs are potential prognostic factors for OS and/or treatment-induced toxicities, the five differentially expressed miRNAs confirmed in the entire group were subjected to univariate Cox proportional hazards analysis. Univariate Cox proportional hazard results for OS showed no significant correlation between OS and miRNA expression. Moreover, miR-450a-5p achieved a high hazard ratio of 2.3 which, although not significantly different (P=0.09; Table 2), may indicate a potential association between the miR-450a-5p expression and OS. Multivariate analysis using the miRNAs with the lowest P-value and highest hazard ratios (miR-450a-5p and miR-451a) in linear combination yield a significant stratification into two distinct survival groups (P=0.038; Figure 4C). In linear regression analysis to find correlations with the CTCAE scale revealed, none of the miRNAs showed up as a potential classifier for treatment-induced toxicities.

Table 2: Univariate cox proportional hazards results for overall survival

miRNAs	β	HR (95% CI for HR)	Wald test	P-value
hsa-miR-424-5p	-0.09	0.9 (0.3-3.0)	0.0	0.89
hsa-miR-451a	-0.67	0.5 (0.2-1.7)	1.2	0.27
hsa-miR-144-5p	-0.46	0.6 (0.2-1.8)	0.7	0.40
hsa-miR-424-3p	-0.01	1.0 (0.5-1.9)	0.0	0.98
hsa-miR-450a-5p	0.82	2.3 (0.9-5.8)	2.9	0.09

HR, Hazards ratio; CI, confidence interval.
Five top-ranked miRNAs were subjected to univariate proportional hazards model. No significant correlation between overall survival and miRNA expression was found.

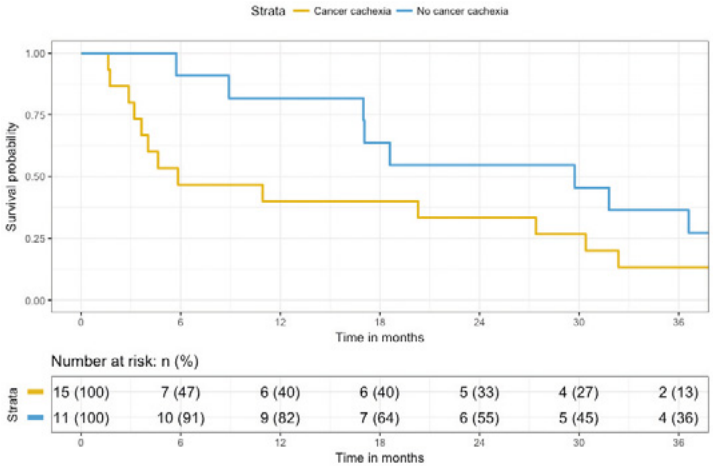
Strata
Cancer cachexia
No cancer cachexia
Survival probability
1.00
0.75
0.50
0.25
0.00
0
6
12
18
24
30
36
Time in months
Number at risk: n (%)
Strata
15 (100) 7 (47) 6 (40) 6 (40) 5 (33) 4 (27) 2 (13)
11 (100) 10 (91) 9 (82) 7 (64) 6 (55) 5 (45) 4 (36)
Time in months

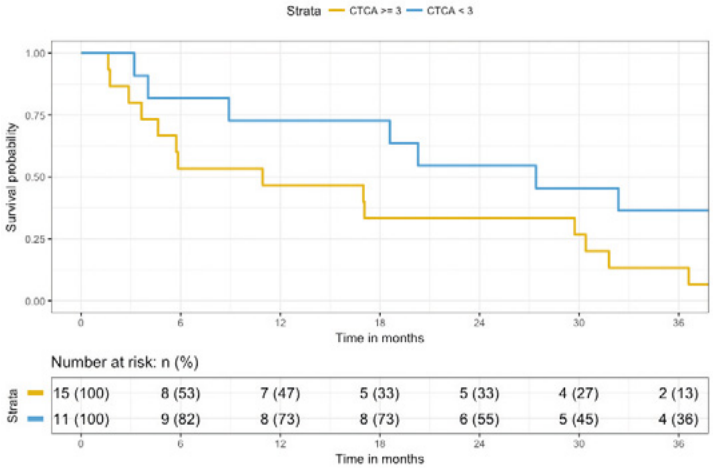
Strata
CTCA >= 3
CTCA < 3
Survival probability
1.00
0.75
0.50
0.25
0.00
0
6
12
18
24
30
36
Time in months
Number at risk: n (%)
Strata
15 (100) 8 (53) 7 (47) 5 (33) 5 (33) 4 (27) 2 (13)
11 (100) 9 (82) 8 (73) 8 (73) 6 (55) 5 (45) 4 (36)
Time in months

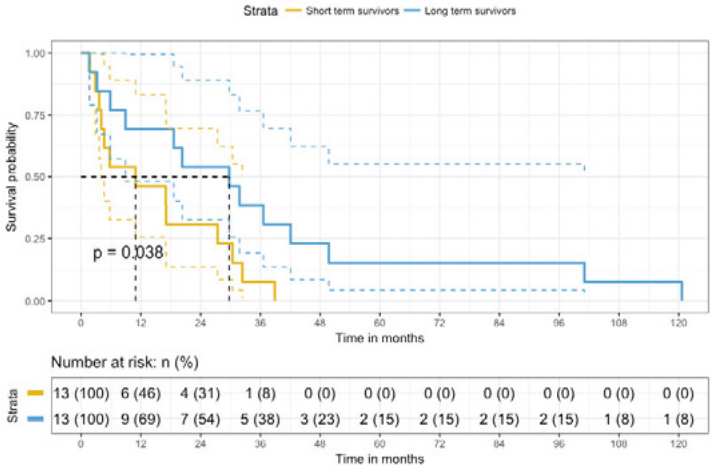
Strata
Short term survivors
Long term survivors
Survival probability
1.00
0.75
0.50
0.25
0.00
p = 0.038
0
12
24
36
48
60
72
84
96
108
120
Time in months
Number at risk: n (%)
Strata
13 (100) 6 (46) 4 (31) 1 (8) 0 (0) 0 (0) 0 (0) 0 (0) 0 (0) 0 (0) 0 (0)
13 (100) 9 (69) 7 (54) 5 (38) 3 (23) 2 (15) 2 (15) 2 (15) 2 (15) 1 (8) 1 (8)
Time in months

Figure 4: *Kaplan-Meier plots for cachexia, treatment-induced toxicity and microRNA (miRNA) expression.* ***(A)*** *Kaplan-Meier plot was constructed to assess the survival function of non-small cell lung cancer (NSCLC) patients with cachexia (n=15) vs. without cachexia (n=11). Cachectic NSCLC patients had a shorter overall survival (OS) when compared with non-cachectic NSCLC patients. The log rank P-value was not significant.* ***(B)*** *Kaplan-Meier plot was constructed to assess the survival function of NSCLC patients with a CTCAE≥3 vs. NSCLC patients with a CTCAE<3. Patients received either chemotherapy or a combination of chemotherapy and radiotherapy. NSCLC patients with a CTCAE ≥3 had a shorter OS compared with NSCLC patients with a CTCAE<3. The log rank P-value was not significant.* ***(C)*** *Kaplan-Meier plot was constructed to assess the survival function of miRNA expression in NSCLC. Multivariate analysis using the miRNAs with the lowest P-value and highest hazard ratios (miR-450a-5p and miR-451a) in linear combination yield a significant stratification into two distinct survival groups (short-term and long-term survival).*

4. DISCUSSION

Cancer cachexia treatment is an unmet medical need, and a better understanding of the underlying mechanisms is essential to develop effective interventions. In this study, we identified 28 differentially expressed miRNAs in the skeletal muscle of cachectic lung cancer patients. Subsequent validation of six top-ranked miRNAs, revealed that differential expression of four miRNAs is unique to patients with cachexia. In addition, using a random forest model trained on three differentially expressed miRNAs allowed for the classification between healthy individuals and NSCLC patients with cachexia. Extensive target prediction and pathway analyses linked the differentially expressed miRNAs to processes involved in muscle mass modulation. Finally, using Cox proportional hazard models including the top two performing miRNAs, significant stratification between short-term and long-term survival was achieved.

Of 28 differentially expressed miRNAs, five miRNAs are overexpressed in the vastus lateralis of NSCLC patients with cachexia compared with healthy controls. Remarkably, four of these miRNAs belong to the same cluster, the H19X-encoded miR-424/-503 cluster. This miRNA cluster includes six miRNAs (miR-424, miR-503, miR-542, miR-450a-1, miR-450a-2 and miR-450b) and has postulated roles in cell differentiation, proliferation, plasticity and metabolism, extensively reviewed by Wang et al. [44]. In accordance to our data, members of this miRNA cluster were previously found to be increased in the skeletal muscle of patients with other muscle wasting diseases: in patients with amyotrophic lateral sclerosis the expression levels of miR-425, miR-450b, miR-503 and miR-542 were increased [27, 28]. In addition, the expression levels of miR-424-5p/3p, miR-450a and miR-542-

5p/3p were found to be increased in COPD patients with low FFMI, and patients with intensive care unit acquired weakness [22-24].

The expression of the miR-451a cluster, including miR-451a and miR-144, is significantly decreased in the skeletal muscle of cachectic NSCLC patients. The miR-451a cluster is located on chromosome 17 [45], and is widely dysregulated in numerous human cancers in which it may play an important role in proliferation, migration and invasion of cells [46, 47]. However, knowledge of the mechanism of action of the miR-451a cluster in skeletal muscle is currently limited. Coherent with our data, miR-144 was significantly down-regulated in the skeletal muscle of chronic kidney disease patients and COPD patients with a low FFMI [23, 48]. Expression of the other member of the miR-451a cluster, miR-451a, was significantly increased in the skeletal muscle of powerlifters [49]. D'Souza et al. postulated a supportive role of miR-451a in myogenesis, and its decreased expression observed in our study may relate to impairments in the myogenesis process, which have been implicated in cancer cachexia [30, 50, 51].

Another miRNA cluster that is abundantly represented by the differentially expressed miRNAs is the C19 miRNA cluster (C19MC). The expression of nine miRNAs from the C19MC is suppressed in the vastus lateralis of NSCLC patients with cachexia. C19MC is one of the largest miRNA clusters in human genome [52, 53]. The miRNAs of the C19MC are expressed from the paternal chromosome and promote pluripotent stem cell phenotype [52], and their activity towards promoting stem cell survival has been implicated in muscle mass maintenance [24]. In general, paternally imprinted genes promote growth, which is consistent with our data revealing decreased expression of these miRNAs in cachexia. Similar to our findings, the expression of multiple members from the C19MC is suppressed in the skeletal muscle of COPD patients with low FFMI [24]. In that study, an association of C19MC expression with FFMI was observed, which was restricted to male patients with severe COPD and absent in female patients. Although a potential interaction between sex and miRNA expression on the cachexia could not be investigated in our relatively small group, sexual dimorphism of skeletal muscle regulation has been reported [54], and should be subject of future study.

Altogether, these findings show changes in expression of overlapping miRNA in different wasting disorders. Although, the number of human miRNA profiling studies related to muscle wasting is limited, these miRNA clusters seem promising targets in the search of miRNAs involved in muscle atrophy.

The current study was not designed to dissect molecular mechanisms of miRNA involvement in cachexia. However, *in silico* network analysis provided relevant information about the potential contribution of these miRNAs in lung cancer cachexia. Using miRTarBase, we identified 158 experimentally validated genes that are potentially targeted by the miRNAs. Among these genes, 114 are functionally expressed in the skeletal muscle and are involved in pathways contributing to muscle degenerative and regenerative processes. The overrepresented pathways that have been implicated in muscle mass regulation include interleukin-6 signaling pathway, transforming growth factor-β signaling pathway, tumor necrosis factor-α signaling pathway, insulin and PI3K-Akt signaling pathway, reviewed in [55-57]. The involvement of these pathways in muscle atrophy has been established in various experimental models, and their detection as targets of the differentially expressed miRNAs identified in this study, for the first time implies their potential involvement in lung cancer cachexia. Furthermore, the identification of pathways relevant to muscle mass regulation using this approach, confirms our strategy to combine miRNA expression and network analyses, and emphasizes the urgency to explore the causal involvement of differential expression of these miRNAs in cancer cachexia.

The data obtained from the miRNA screening and *in silico* network analysis, suggest a potential role for the differentially expressed miRNAs in the pathology of lung cancer cachexia. However, the experimental set-up applied in the screening approach did not allow us to discriminate between lung cancer and lung cancer cachexia specific miRNAs. For that reason, a selection of top-ranked miRNAs was measured in the entire study population consisting of healthy controls and NSCLC patients with and without cachexia. Consistent with the results of the TaqMan Array, miR-424-5p, miR424-3p and miR-450a-5p were significantly increased, and miR-451a and miR-144-5p were significantly decreased in NSCLC patients with cachexia compared with healthy controls. Except for miR-424-3p, the three up-regulated miRNAs showed a non-significant, but intermediate expression in NSCLC patients without cachexia. These intermediate expression levels might reflect a pre-cachectic stage in some of NSCLC patients classified as non-cachectic. Although the anthropomorphic data were not available beyond the cross-sectional comparison at diagnosis, up to 60% of NSCLC patients may eventually develop cachexia [3], supporting the possibility that a portion of the patients were pre-cachectic. Consequently, miR-424-5p, miR-424-3p and miR-450a-5p may play a role in the development of cachexia in lung cancer. In contrast, down-regulated miRNAs did not display intermediate expression levels in non-cachectic lung cancer patients. As decreased expression of miR-451a and miR-144-5p seems

to be lung cancer cachexia specific, this may reflect adaptive changes of these miRNAs to the cachectic state. For the prediction of cachexia, when differentiating between NSCLC patients and healthy controls we found results significantly different from random chance. These data are promising; however, given the low number of patients and relatively high number of variables (five per patient) these results are exploratory and need to be validated externally in a larger cohort.

Body weight loss has a detrimental impact on survival in NSCLC. In different study populations, it has been shown that increased body weight loss results in shorter OS [6, 58-60]. Furthermore, it has been shown that low muscle mass is associated with increased treatment induced toxicities [61]. Consistent with these findings, our data show that NSCLC patients with cachexia have a shorter 3-year survival time compared with NSCLC patients without cachexia. Moreover, we show that OS is more affected by treatment-induced toxicity in cachectic compared with non-cachectic patients. In this study, we tested the potential of miRNAs as independent prognostic factor for OS and/or treatment-induced toxicities using a univariate analysis. In addition, using a multivariate Cox proportional hazard model including the top two performing miRNAs from univariate analysis, significant stratification of the patient population into short-term and long-term survival was achieved. Extending this approach in a larger cohort of lung cancer patients is required and may yield predictive or prognostic miRNA signatures, as was shown for OS in abdominal cancer [29].

5. CONCLUSIONS

We identified 28 differentially expressed miRNAs in the skeletal muscle of lung cancer patients with cachexia, including 5 top-ranked miRNAs with high potential relevance to muscle atrophy, as demonstrated using gene target/pathway analyses, and comparison to non-cachectic lung cancer patients. Further investigation of these miRNAs to elucidate their regulation and mode of action in muscle atrophy will contribute to our understanding of cachexia, and allow us to probe their potential as therapeutic targets.

REFERENCES

1. Bray F, Ferlay J, Soerjomataram I, Siegel RL, Torre LA, Jemal A. Global cancer statistics 2018: GLOBOCAN estimates of incidence and mortality worldwide for 36 cancers in 185 countries. CA Cancer J Clin. 2018;68(6):394-424.
2. Herbst RS, Heymach JV, Lippman SM. Lung cancer. N Engl J Med. 2008;359(13):1367-80.
3. Del Ferraro C, Grant M, Koczywas M, Dorr-Uyemura LA. Management of Anorexia-Cachexia in Late Stage Lung Cancer Patients. J Hosp Palliat Nurs. 2012;14(6).
4. Fearon K, Strasser F, Anker SD, Bosaeus I, Bruera E, Fainsinger RL, et al. Definition and classification of cancer cachexia: an international consensus. Lancet Oncol. 2011;12(5):489-95.
5. Argiles JM. Cancer-associated malnutrition. Eur J Oncol Nurs. 2005;9 Suppl 2:S39-50.
6. Dewys WD, Begg C, Lavin PT, Band PR, Bennett JM, Bertino JR, et al. Prognostic effect of weight loss prior to chemotherapy in cancer patients. Eastern Cooperative Oncology Group. Am J Med. 1980;69(4):491-7.
7. Vaughan VC, Martin P, Lewandowski PA. Cancer cachexia: impact, mechanisms and emerging treatments. J Cachexia Sarcopenia Muscle. 2013;4(2):95-109.
8. Turner DC, Kondic AG, Anderson KM, Robinson AG, Garon EB, Riess JW, et al. Pembrolizumab Exposure-Response Assessments Challenged by Association of Cancer Cachexia and Catabolic Clearance. Clin Cancer Res. 2018;24(23):5841-9.
9. Schiaffino S, Dyar KA, Ciciliot S, Blaauw B, Sandri M. Mechanisms regulating skeletal muscle growth and atrophy. FEBS J. 2013;280(17):4294-314.
10. Bartel DP. Metazoan MicroRNAs. Cell. 2018;173(1):20-51.
11. Dragomir MP, Knutsen E, Calin GA. SnapShot: Unconventional miRNA Functions. Cell. 2018;174(4):1038- e1.
12. Horak M, Novak J, Bienertova-Vasku J. Muscle-specific microRNAs in skeletal muscle development. Dev Biol. 2016;410(1):1-13.
13. Soares RJ, Cagnin S, Chemello F, Silvestrin M, Musaro A, De Pitta C, et al. Involvement of microRNAs in the regulation of muscle wasting during catabolic conditions. J Biol Chem. 2014;289(32):21909-25.
14. Lee DE, Brown JL, Rosa-Caldwell ME, Blackwell TA, Perry RA, Jr., Brown LA, et al. Cancer cachexia-induced muscle atrophy: evidence for alterations in microRNAs important for muscle size. Physiological genomics. 2017;49(5):253-60.
15. Liu C, Wang M, Chen M, Zhang K, Gu L, Li Q, et al. miR-18a induces myotubes atrophy by down-regulating Igf1. Int J Biochem Cell Biol. 2017;90:145-54.
16. Wang B, Zhang C, Zhang A, Cai H, Price SR, Wang XH. MicroRNA-23a and MicroRNA-27a Mimic Exercise by Ameliorating CKD-Induced Muscle Atrophy. J Am Soc Nephrol. 2017;28(9):2631-40.
17. Zhang A, Li M, Wang B, Klein JD, Price SR, Wang XH. miRNA-23a/27a attenuates muscle atrophy and renal fibrosis through muscle-kidney crosstalk. J Cachexia Sarcopenia Muscle. 2018.
18. Li J, Chan MC, Yu Y, Bei Y, Chen P, Zhou Q, et al. miR-29b contributes to multiple types of muscle atrophy. Nat Commun. 2017;8:15201.
19. He Q, Qiu J, Dai M, Fang Q, Sun X, Gong Y, et al. MicroRNA-351 inhibits denervation-induced muscle atrophy by targeting TRAF6. Exp Ther Med. 2016;12(6):4029-34.

20. Paul R, Lee J, Donaldson AV, Connolly M, Sharif M, Natanek SA, et al. miR-422a suppresses SMAD4 protein expression and promotes resistance to muscle loss. J Cachexia Sarcopenia Muscle. 2018;9(1):119-28.
21. Connolly M, Garfield BE, Crosby A, Morrell NW, Wort SJ, Kemp PR. miR-322-5p targets IGF-1 and is suppressed in the heart of rats with pulmonary hypertension. FEBS Open Bio. 2018;8(3):339-48.
22. Connolly M, Paul R, Farre-Garros R, Natanek SA, Bloch S, Lee J, et al. miR-424-5p reduces ribosomal RNA and protein synthesis in muscle wasting. J Cachexia Sarcopenia Muscle. 2018;9(2):400-16.
23. Garros RF, Paul R, Connolly M, Lewis A, Garfield BE, Natanek SA, et al. MicroRNA-542 Promotes Mitochondrial Dysfunction and SMAD Activity and Is Elevated in Intensive Care Unit-acquired Weakness. Am J Respir Crit Care Med. 2017;196(11):1422-33.
24. Lewis A, Lee JY, Donaldson AV, Natanek SA, Vaidyanathan S, Man WD, et al. Increased expression of H19/miR-675 is associated with a low fat-free mass index in patients with COPD. J Cachexia Sarcopenia Muscle. 2016;7(3):330-44.
25. van de Worp W, Theys J, van Helvoort A, Langen RCJ. Regulation of muscle atrophy by microRNAs: 'AtromiRs' as potential target in cachexia. Curr Opin Clin Nutr Metab Care. 2018;21(6):423-9.
26. Kemp PR, Griffiths M, Polkey MI. Muscle wasting in the presence of disease, why is it so variable? Biol Rev Camb Philos Soc. 2018.
27. de Andrade HM, de Albuquerque M, Avansini SH, de SRC, Dogini DB, Nucci A, et al. MicroRNAs-424 and 206 are potential prognostic markers in spinal onset amyotrophic lateral sclerosis. J Neurol Sci. 2016;368:19-24.
28. Kovanda A, Leonardis L, Zidar J, Koritnik B, Dolenc-Groselj L, Ristic Kovacic S, et al. Differential expression of microRNAs and other small RNAs in muscle tissue of patients with ALS and healthy age-matched controls. Sci Rep. 2018;8(1):5609.
29. Narasimhan A, Ghosh S, Stretch C, Greiner R, Bathe OF, Baracos V, et al. Small RNAome profiling from human skeletal muscle: novel miRNAs and their targets associated with cancer cachexia. J Cachexia Sarcopenia Muscle. 2017;8(3):405-16.
30. Op den Kamp CM, Langen RC, Snepvangers FJ, de Theije CC, Schellekens JM, Laugs F, et al. Nuclear transcription factor kappa B activation and protein turnover adaptations in skeletal muscle of patients with progressive stages of lung cancer cachexia. Am J Clin Nutr. 2013;98(3):738-48.
31. Greene FL. AJCC Cancer Staging Manual, 6th ed. Springer-Verslag. 2002.
32. Bergstrom J. Percutaneous needle biopsy of skeletal muscle in physiological and clinical research. Scand J Clin Lab Invest. 1975;35(7):609-16.
33. Kozomara A, Birgaoanu M, Griffiths-Jones S. miRBase: from microRNA sequences to function. Nucleic Acids Res. 2019;47(D1):D155-D62.
34. Shannon P, Markiel A, Ozier O, Baliga NS, Wang JT, Ramage D, et al. Cytoscape: a software environment for integrated models of biomolecular interaction networks. Genome Res. 2003;13(11):2498-504.
35. Kutmon M, Kelder T, Mandaviya P, Evelo CT, Coort SL. CyTargetLinker: a cytoscape app to integrate regulatory interactions in network analysis. PLoS One. 2013;8(12):e82160.
36. Chou CH, Shrestha S, Yang CD, Chang NW, Lin YL, Liao KW, et al. miRTarBase update 2018: a resource for experimentally validated microRNA-target interactions. Nucleic Acids Res. 2018;46(D1):D296-D302.

37. Uhlen M, Fagerberg L, Hallstrom BM, Lindskog C, Oksvold P, Mardinoglu A, et al. Proteomics. Tissue-based map of the human proteome. Science. 2015;347(6220):1260419.
38. Kutmon M, van Iersel MP, Bohler A, Kelder T, Nunes N, Pico AR, et al. PathVisio 3: an extendable pathway analysis toolbox. PLoS Comput Biol. 2015;11(2):e1004085.
39. Slenter DN, Kutmon M, Hanspers K, Riutta A, Windsor J, Nunes N, et al. WikiPathways: a multifaceted pathway database bridging metabolomics to other omics research. Nucleic Acids Res. 2018;46(D1):D661-D7.
40. van Iersel MP, Pico AR, Kelder T, Gao J, Ho I, Hanspers K, et al. The BridgeDb framework: standardized access to gene, protein and metabolite identifier mapping services. BMC Bioinformatics. 2010;11:5.
41. Pillich RT, Chen J, Rynkov V, Welker D, Pratt D. NDEx: A Community Resource for Sharing and Publishing of Biological Networks. Methods Mol Biol. 2017;1558:271-301.
42. Wald A. Sequential Analysis. New York: Dover; 1947.
43. Team RC. R: A language and environment for statistical computing. Vienna, Austria: R Foundation for Statistical Computing; 2017.
44. Wang F, Liang R, Tandon N, Matthews ER, Shrestha S, Yang J, et al. H19X-encoded miR-424(322)/-503 cluster: emerging roles in cell differentiation, proliferation, plasticity and metabolism. Cell Mol Life Sci. 2018.
45. Kozomara A, Griffiths-Jones S. miRBase: annotating high confidence microRNAs using deep sequencing data. Nucleic Acids Res. 2014;42(Database issue):D68-73.
46. Su Z, Ni L, Yu W, Yu Z, Chen D, Zhang E, et al. MicroRNA-451a is associated with cell proliferation, migration and apoptosis in renal cell carcinoma. Mol Med Rep. 2015;11(3):2248-54.
47. Gao Z, Zhang P, Xie M, Gao H, Yin L, Liu R. miR-144/451 cluster plays an oncogenic role in esophageal cancer by inhibiting cell invasion. Cancer Cell Int. 2018;18:184.
48. Watson E, Sylvius NB, Viana JJL, Greening N, Barratt J, Smith A. MP401 -Differential miRNA expression in skeletal muscle of human CKD patients and healthy controls. Nephrology Dialysis Transplantation. 2016;31(suppl_1):i473-i4.
49. D'Souza RF, Bjornsen T, Zeng N, Aasen KMM, Raastad T, Cameron-Smith D, et al. MicroRNAs in Muscle: Characterizing the Powerlifter Phenotype. Front Physiol. 2017;8:383.
50. He WA, Berardi E, Cardillo VM, Acharyya S, Aulino P, Thomas-Ahner J, et al. NF-kappaB-mediated Pax7 dysregulation in the muscle microenvironment promotes cancer cachexia. J Clin Invest. 2013;123(11):4821-35.
51. Brzeszczynska J, Johns N, Schilb A, Degen S, Degen M, Langen R, et al. Loss of oxidative defense and potential blockade of satellite cell maturation in the skeletal muscle of patients with cancer but not in the healthy elderly. Aging (Albany NY). 2016;8(8):1690-702.
52. Mouillet JF, Ouyang Y, Coyne CB, Sadovsky Y. MicroRNAs in placental health and disease. Am J Obstet Gynecol. 2015;213(4 Suppl):S163-72.
53. Lin S, Cheung WK, Chen S, Lu G, Wang Z, Xie D, et al. Computational identification and characterization of primate-specific microRNAs in human genome. Comput Biol Chem. 2010;34(4):232-41.
54. Montalvo RN, Counts BR, Carson JA. Understanding sex differences in the regulation of cancer-induced muscle wasting. Curr Opin Support Palliat Care. 2018;12(4):394-403.

55. Belizario JE, Fontes-Oliveira CC, Borges JP, Kashiabara JA, Vannier E. Skeletal muscle wasting and renewal: a pivotal role of myokine IL-6. Springerplus. 2016;5:619.
56. Glass DJ. Skeletal muscle hypertrophy and atrophy signaling pathways. Int J Biochem Cell Biol. 2005;37(10):1974-84.
57. Sandri M. Signaling in muscle atrophy and hypertrophy. Physiology (Bethesda). 2008;23:160-70.
58. Yang R, Cheung MC, Pedroso FE, Byrne MM, Koniaris LG, Zimmers TA. Obesity and weight loss at presentation of lung cancer are associated with opposite effects on survival. J Surg Res. 2011;170(1):e75-83.
59. Takayama K, Atagi S, Imamura F, Tanaka H, Minato K, Harada T, et al. Quality of life and survival survey of cancer cachexia in advanced non-small cell lung cancer patients-Japan nutrition and QOL survey in patients with advanced non-small cell lung cancer study. Support Care Cancer. 2016;24(8):3473-80.
60. Mytelka DS, Li L, Benoit K. Post-diagnosis weight loss as a prognostic factor in non-small cell lung cancer. J Cachexia Sarcopenia Muscle. 2018;9(1):86-92.
61. Prado CM, Baracos VE, McCargar LJ, Reiman T, Mourtzakis M, Tonkin K, et al. Sarcopenia as a determinant of chemotherapy toxicity and time to tumor progression in metastatic breast cancer patients receiving capecitabine treatment. Clin Cancer Res. 2009;15(8):2920-6.
62. von Haehling S, Morley JE, Coats AJS, Anker SD. Ethical guidelines for publishing in the journal of cachexia, sarcopenia and muscle: update 2017. J Cachexia Sarcopenia Muscle. 2017;8(6):1081-3.

SUPPORTING INFORMATION

Table S2: miRCURY LNA miRNA PCR assay primers

Product name	Target sequence 5'-3'	Cat. no.	Company
hsa-miR-424-5p	CAGCAGCAAUUCAUGUUUUGAA	YP00204736	Exiqon (Qiagen)
hsa-miR-424-3p	CAAAACGUGAGGCGCUGCUAU	YP00205918	Exiqon (Qiagen)
hsa-miR-450a-5p	UUUUGCGAUGUGUUCCUAAUAU	YP00206085	Exiqon (Qiagen)
hsa-miR-450b-5p	UUUUGCAAUAUGUUCCUGAAUA	YP00205607	Exiqon (Qiagen)
hsa-miR-451a-5p	AAACCGUUACCAUUACUGAGUU	YP02119305	Exiqon (Qiagen)
hsa-miR-144-5p	GGAUAUCAUCAUAUACUGUAAG	YP00204670	Exiqon (Qiagen)

Table S3: Tumor stage and site of metastasis.

	Non-cachexia (n=11)	Cachexia (n= 15)
Tumor stage (n)		
IIIB	4	4
IV	7	11
Site of metastasis (n)		
Multiple intrapulmonary tumors (both lungs)	2	2
Bone	1	4
Liver	0	1
Lymph nodes	2	1
Peritoneal carcinomatosis	1	0
Pleurisy carcinomatosis	1	3

Table S4: Clinical and demographic data of NSCC patients with cachexia and controls subjected to TaqMan® miRNA array

	Healthy Control (n=8)	Cachexia (n=8)
Gender (male/female)	6/2	6/2
Age (years)	61.9 ± 6.7	58.3 ± 8.6
Height (m)	1.77 ± 0.1	1.74 ± 0.1
Body weight loss (kg)	-	11.2 ± 3.9***
Body weight loss (%)	-	14.2 ± 5.5***
Body Mass Index (BMI) (kg/m²)	24.3 ± 2.8	26.8 ± 6.1
Fat Mass Index (FMI) (kg/m²)	7.0 ± 3.3	7.0 ± 3.1
Fat Free Mass Index (FFMI) (kg/m²)	18.1 ± 1.1	16.3 ± 3.5
Appendicular Skeletal Muscle Index (ASMI) (kg/m²)	7.6 ± 0.69	5.9 ± 0.84***
IL-6 (pg/ml)	41.7 (35. 85)	119.3 (62. 354)*
CRP (mg/l)	1.2 (0.5. 1.6)	67.8 (26. 188)***
Disease stage of NSCLC (IIIB/IV)	-	1/7
Histology of NSCLC (adeno/squamous cell)	-	4/4
Peak torque flexion 60° (Nm)	77.8 ± 18.5	28.7 ± 18.7***
Peak torque extension 60° (Nm)	119.3 ± 29.6	49.8 ± 29.4***

*Cachexia was defined as body weight loss of >5% in the past 6 months. or body weight (BW) loss of >2% in combination with either a BMI <20kg/m². or an appendicular skeletal muscle index consistent with sarcopenia determined by DEXA (males<7.26 kg/m²; females<5.45 kg/m²). Data is presented as mean ± SD for normally distributed variables and as median (interquartile range) for variables that were not normally distributed. Significance was calculated by Independent samples t-test for equality of means (two-tailed) was used testing for normally distributed variables and by Mann Whitney U test for variables that were not normally distributed. * P<0.05 and ***P<0.001.*

Table S5: significantly differentially expressed miRNAs in cachectic NSCLC patients compared with healthy controls.

miRNA	Normalized miRNA amount relative to healthy control ($2^{-\Delta\Delta Ct}$)	P-value
hsa-miR-450a-5p	20.3	0.006
hsa-miR-424-5p	20.1	0.007
hsa-miR-450b-5p	16.1	0.003
hsa-miR-424-3p	12.9	0.014
hsa-miR-335-3p	3.9	0.049
hsa-miR-103-3p	0.49	0.020
hsa-miR-483-5p	0.49	0.041
hsa-miR-409-3p	0.46	0.020
hsa-miR-15b-5p	0.41	0.036
hsa-miR-370-3p	0.41	0.021
hsa-miR-20a-3p	0.40	0.001
hsa-miR-451a	0.39	0.039
hsa-miR-517c-3p	0.35	0.011
hsa-miR-144-5p	0.31	0.011
hsa-miR-766-3p	0.27	0.008
hsa-miR-1255b	0.23	0.009
hsa-miR-517a-3p	0.21	0.001
hsa-miR-512-3p	0.19	0.000
hsa-miR-522-3p	0.18	0.009
hsa-miR-520g-3p	0.18	0.024
hsa-miR-483-3p	0.17	0.002
hsa-miR-519a-3p	0.16	0.003
hsa-miR-26a-2-3p	0.13	0.018
hsa-miR-485-3p	0.12	0.013
hsa-miR-379-5p	0.09	0.029
hsa-miR-518b	0.09	0.009
hsa-miR-520h	0.09	0.025
hsa-miR-656-3p	0.05	0.000

4

Nutritional interventions in cancer cachexia: evidence and perspectives from experimental models

Wouter RPH van de Worp
Annemie MWJ Schols
Jan Theys
Ardy van Helvoort
and Ramon CJ Langen

Frontiers in Nutrition
2020, 7:601329

ABSTRACT

Cancer cachexia is a complex metabolic syndrome characterized by involuntary skeletal muscle loss and is associated with poor clinical outcome, decreased survival and negatively influences cancer therapy. No curative treatments are available for cancer cachexia, but nutritional intervention is recommended as a cornerstone of multimodal therapy. Optimal nutritional care is pivotal in the treatment of cancer cachexia, and the effects of nutrients may extend beyond provision of adequate energy uptake, targeting different mechanisms or metabolic pathways that are affected or deregulated by cachexia. The evidence to support this notion derived from nutritional intervention studies in experimental models of cancer cachexia is systematically discussed in this review. Moreover, experimental variables and readout parameters to determine skeletal muscle wasting and cachexia are methodologically evaluated to allow critical comparison of similar studies. Single- and multinutrient intervention studies including qualitative modulation of dietary protein, dietary fat, and supplementation with specific nutrients, such as carnitine and creatine, were reviewed for their efficacy to counteract muscle mass loss and its underlying mechanisms in experimental cancer cachexia. Numerous studies showed favorable effects on impaired protein turnover and related metabolic abnormalities of nutritional supplementation in parallel with a beneficial impact on cancer-induced muscle wasting. The combination of high quality nutrients in a multitargeted, multinutrient approach appears specifically promising, preferentially as a multimodal intervention, although more studies investigating the optimal quantity and combination of nutrients are needed. During the review process, a wide variation in timing, duration, dosing and route of supplementation, as well as a wide variation in animal models were observed. Better standardization in dietary design, and the development of experimental models that better recapitulate the etiology of human cachexia, will further facilitate successful translation of experimentally-based multinutrient, multimodal interventions into clinical practice.

1. INTRODUCTION

Cancer cachexia is a debilitating syndrome characterized by involuntary weight loss that not only affects adipose tissue but also leads to wasting and weakness of skeletal muscle. Cachexia is associated with an abnormal energy and substrate metabolism that cannot be reversed by conventional nutritional support (1). This differentiates the syndrome from (semi)starvation during which energy expenditure and protein turnover is reduced. Cachexia is highly prevalent in advanced cancers. One third of all patients with cancer loses more than 5% of their original body weight, which is a common screening criterion for cancer cachexia (1, 2). In particular, about 70% of gastric cancer patients, 80% of lung cancer patients, and 90% of liver and pancreatic cancer patients are at risk of developing cachexia (2). Cachexia is associated with poor clinical outcome, decreased survival (3) and negatively influences tumor therapy, as is illustrated by increased postoperative mortality and decreased response to radiation-, chemo- and immunotherapy (4-6). Muscle wasting is an important contributing factor to muscle weakness in cachexia, which adversely affects performance status, quality of life and hospitalization risk of cancer patients (7).

Many factors contribute to cancer-induced weight loss including anorexia, altered protein and energy metabolism, and chronic inflammation. The anorexia associated with cancer cachexia is likely caused by the activity of pro-inflammatory cytokines, such as tumor necrosis factor-α (TNF-α), interleukin-1 (IL-1), interleukin-6 (IL-6) and growth differentiation factor 15, that are produced either by the tumor or by the host in response to the tumor, which interfere with appetite signals within the anterior hypothalamus (8, 9). Some of these cytokines may also increase the metabolic rate in cancer cachexia (10). In addition to hypermetabolism, one of the major metabolic changes contributing to cancer cachexia is the alteration in protein metabolism. These changes are characterized by a net protein breakdown and an increased oxidation of branched-chain amino acids (BCAAs), especially in the skeletal muscle, to support energy production (gluconeogenesis) and to supply amino acids for elevated hepatic synthesis of acute-phase proteins (11). The breakdown of the host protein is partly stimulated by tumor-secreted factors, including proteolysis-inducing factor and lipid-mobilizing factor, and host-derived inflammatory cytokines such as TNF- α and IL-6 (12).

Undernutrition is a common problem in patients with cancer cachexia and can be a consequence of both reduced dietary intake, poor dietary quality and hypermetabolism (13). The reduced food intake is thought to be explained by

tumor-induced symptoms, such as mechanical interference with nutritional intake or absorption, treatment-related side effects, including mucositis, nausea and vomiting, and altered taste. Undernutrition not only affects the macronutrients that supply energy but also the micronutrients that are essential cofactors in metabolism and vital to preserve body mass Therefore, undernutrition is one of the main reasons that patients with cancer cachexia have an inadequate micronutrient status (14). Accordingly, inadequate micronutrient intake negatively influences the course of the disease and increases the risk of complications.

For a long time, undernutrition and cachexia remained neglected medical conditions for which a clear therapeutic strategy was lacking. A multidisciplinary approach is currently considered the best option to tackle cancer cachexia, in which nutritional intervention is recommended as an integral part of the multimodal therapy (15). Adequate nutritional care is pivotal to provide the essential building blocks to maintain and rebuild tissue in cachectic patients. Furthermore, nutrition is also crucial to supply energy and micronutrients that are vital to fuel and catalyze metabolic processes. In addition to the nourishing of the cachectic patients, various nutrients have been implied in the regulation and normalization of metabolic processes underlying the wasting in cachectic patients. Most of the metabolically active nutrients have different functions in the various intertwined processes that may be deregulated in cachexia. For nutrients and their metabolites that are rate limiting in key metabolic pathways, preventing any deficiencies will help preserve or restore metabolic homeostasis. Furthermore, an approach where multiple nutrients are combined in a well-balanced multi-nutrient intervention is likely most appropriate, as it is well recognized that nutritional modulation includes alteration of intermediates, precursors, catalyzers and regulators of many metabolic pathways. Therefore nutritional interventions have the potential to simultaneously affect multiple targets that may be involved in the cancer cachexia process including energy intake, anorexia, inflammation and anabolic signaling (Figure 1). However, identification of an optimal nutritional intervention requires systematic experimental evaluation of the specific as well as combined effects of individual components.

Nutritional support in patients with cancer cachexia aims to counteract the negative energy balance as well as the net protein breakdown, without stimulating tumor growth or negatively influencing anti-tumor therapy. To establish a net positive protein balance, specific nutrients mitigating catabolic and stimulating anabolic signals should be considered. To create an anabolic environment, adequate caloric intake and nutrient composition (e.g., quantity and quality of nutrients) is instrumental, because without sufficient nutrient availability, anabolic triggers will

not lead to muscle maintenance or an increase in muscle mass. Several nutritional agents have been proposed to tackle cancer cachexia, however, clear evidence of their efficacy is limited. A better understanding of specific nutrients' contribution to muscle anabolism in these patients can lead to the development of specialized nutritional products focusing on halting muscle mass loss in cancer cachexia.

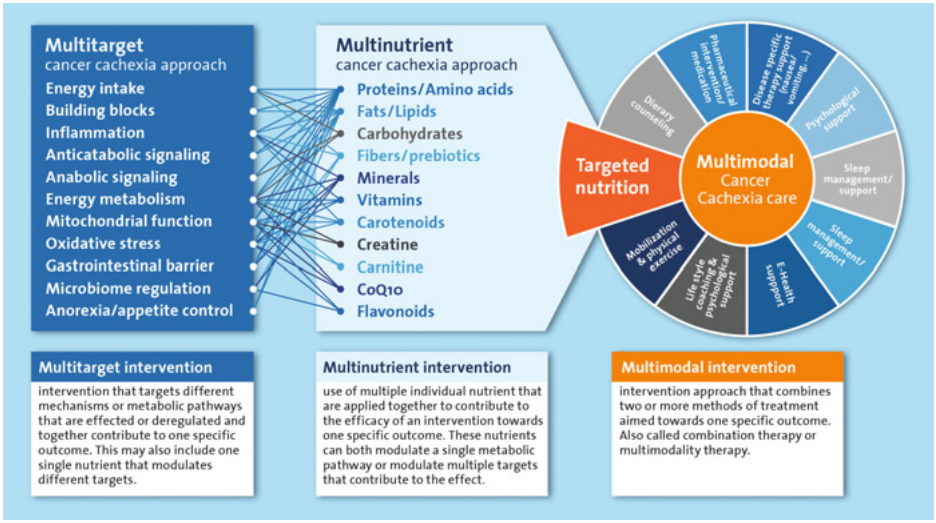

Figure 1: *Simplified representation of the multitarget and multinutrient approach and their mutual interactions as part of the multimodal cancer cachexia care. All components listed under 'multinutrient cancer cachexia approach' are systematically reviewed as single nutrients or as part of multinutrient approaches in the text.*

Experimental animal models are used extensively to study mechanisms underlying cancer cachexia and evaluate potential treatments. In this narrative review, based on a systematic evaluation of the current literature (Supporting information, Table S1), we provide an overview of preclinical studies focused on nutritional interventions in cancer cachexia, and discuss the gaps and highlight opportunities in current experimental models.

2. SINGLE NUTRIENT INTERVENTIONS

2.1 Dietary protein

Adequate supply of dietary protein is a prerequisite for maintenance or gain of skeletal muscle mass. A positive protein balance is required to increase skeletal muscle mass, and elevated plasma levels of essential amino acids from dietary protein are considered an effective anabolic stimulus (16). However, fundamental

evidence on the sufficient and optimal quantity and quality of protein intake for treating low muscle mass is lacking. The ESPEN guidelines on nutrition in cancer patients suggest a protein intake in the range of 1.0 – 1.5 g/kg/day (17). Importantly, these guidelines are recommendations and evidence-based studies to support the optimal quantity are largely missing. Evidence concerning the quality of proteins, regarding the optimal amino acid composition and their digestibility (availability) in the context of cancer cachexia, is also lacking. In contrast to their suitability for defining the optimal quantity of protein resulting from translational challenges, experimental models of cancer cachexia can readily be deployed to study optimal amino acid composition and quality of proteins to prevent or treat cancer cachexia.

2.1.1 Branched-chain amino acids

Branched-chain amino acids (BCAAs) have been hypothesized to exert a therapeutic effect in diseases accompanied by muscle wasting since they are integral components of skeletal muscle proteins and their critical role in stimulating protein synthesis (18). BCAAs may decrease proteolysis and increase protein synthesis in skeletal muscle, primarily through activation of the mTOR pathway and modulation of inflammation through glutamine production (19, 20). Of the BCAAs, leucine is most potent in stimulating muscle protein synthesis, whereas isoleucine and valine are less effective (20). In MAC16 tumor bearing mice, administration of leucine and valine significantly reversed the loss in body weight. Only leucine produced a significant recovery in muscle wet weight by increasing protein synthesis and decreasing degradation (20). In C26 tumor-bearing mice, leucine supplemented diet increased plasma amino acid concentration and counteracted muscle mass loss dose-dependently, while no effect of leucine-rich diet on body weight and/or anorexia was observed (21). In rats bearing the Walker 256 tumor, multiple studies have demonstrated that the loss of skeletal muscle mass induced by cancer cachexia was attenuated by leucine supplementation (22-26). Leucine supplementation did attenuate protein degradation, potentially through their modulatory effects on proteasome subunits; and improved protein synthesis, via activation of the mTOR pathway and downstream kinases. These actions were related to cachexia amelioration but did not increase survival time or reduce tumor growth (22, 23, 26, 27). Furthermore, a different cytokine profile was observed in tumor bearing rats fed a leucine-rich diet after 14 days. Both, the pro- inflammatory cytokines TNF-α, IL-6 and IFNγ and anti-inflammatory cytokines IL-10 and IL-4 were enhanced in the serum compared with tumor bearing control, indicating a cytokine modulatory effect (25). Altogether, these data suggest that leucine supplementation has a beneficial effect on experimental cancer cachexia.

The BCAA leucine may attenuate muscle wasting by modulating protein synthesis and proteolysis.

2.1.2 β-Hydroxy-β-Methylbutyrate

β-hydroxy-β-methylbutyrate (HMB) is synthesized in the human body through metabolism of L-leucine (28). Under normal conditions about 5% of dietary leucine is converted into HMB (29, 30). This leucine metabolite is thought to modulate protein turnover, primarily by suppressing protein degradation (28). In mice bearing the MAC16 tumor, HMB supplementation attenuated the development of weight loss accompanied by a small reduction in tumor weight (31, 32). HMB caused a significant increase in the wet weight of soleus muscle and a reduction in protein degradation. Furthermore, Smith et al. showed that HMB was not only capable of attenuating protein degradation in skeletal muscle of cachectic mice but also stimulated protein synthesis (32). In rats bearing the Walker 256 tumor, HMB supplementation significantly decreased tumor weight. These rats maintained body weight, blood metabolic parameters (glucose, lactate, triacylglycerol and cholesterol) and tissue glycogen levels comparable to non-tumor-bearing rats (33). Similar effects of HMB were obtained in rats bearing the Yoshida AH-130 tumor fed a 4% HMB-enriched diet (34). HMB supplementation led to a significant increase in body weight and a significantly attenuated gastrocnemius loss. Although, protein synthesis was not measured, HMB treatment increased phosphorylation of mTOR and p70S6k compared to both sham and tumor-bearing control, suggesting a direct modulatory effect on muscle protein anabolism (34). Given the beneficial effects of HMB on muscle protein turnover and the observed anti-tumor effect, HMB could be a useful supplement as part of the treatment of muscle wasting in cancer cachexia. However, further exploration of the efficacy of lower doses will be required, as the HMB doses used in these studies are supra-physiological and may not be feasible as intervention in a clinical setting.

2.1.3 Glutamine

Glutamine is the most abundant, non-essential, amino acid in the body that plays a role in a variety of physiological and biochemical processes (35). Glutamine is considered the main metabolic fuel for gastrointestinal enterocytes maintaining the normal integrity of the intestinal mucosa. Furthermore, glutamine plays an essential role as a precursor of peptide, protein, glucose and lipid synthesis (36, 37). Moreover, glutamine is one of the precursor amino acids of glutathione, which is a major antioxidant and a vital component of host defense (38). Although glutamine is the most abundant amino acid in the body, a marked glutamine depletion is observed in many patients with cancer (35). Consequently, glutamine might be

useful to treat cancer cachexia. Supplementation with 2% L-glutamine showed to attenuate cancer-induced cachexia, indicated as preserved body weight loss and a lower cachexia index, in rats bearing the Walker 256 tumor (39-43). Furthermore, tumor growth was inhibited in tumor-bearing rats supplemented with L-glutamine (39-42). In cachectic rats, Walker 256 tumor growth caused considerable changes in small intestine metabolism (44). L-Glutamine supplementation restored the intestinal mucosa in the duodenum and jejunum by enhancing cell proliferation as well as increasing villous height, crypt depth, and total height of the intestinal wall (40). Furthermore, L-glutamine supplementation was associated with a significant elevation of glucose and insulin levels compared to control. The resulting hyperglycemia is probably attributable to the increased activity of gluconeogenic enzymes in the small intestine due to the increased availability of glutamine as a glucose precursor. (41). All together, these studies suggest a beneficial effect of glutamine on cancer cachexia via enhancing intestinal health and energy metabolism.

2.1.4 Glycine

Glycine is a non-essential amino acid and is often considered biologically neutral. However, studies have shown that L-glycine has effective anti-inflammatory, immunomodulatory and cytoprotective properties (45). The underlying mechanisms responsible for the protective effects of glycine are not completely clear, but may include suppression of calcium signaling, inhibition of inflammatory cell activation and decreased formation of free radicals and other toxic compounds (45). In addition, dietary glycine was also reported to inhibit the growth of certain types of tumors, such as liver tumors (46) and melanoma tumors (47). Only one study investigated the effect of glycine treatment in an experimental model of cancer cachexia. In mice bearing the C26 tumor, glycine administration reduces tumor growth and attenuates cancer-induced cachexia (48). Glycine treatment partially prevented the tumor-induced loss in skeletal muscle mass and cross sectional area. This protective effect of glycine was associated with preserved muscle function. In skeletal muscle, glycine normalized IL-6 and F4/80, a marker for macrophage in filtration, mRNA expression and reduced oxidative stress. In addition, glycine treatment attenuated Atrogin-1 and MuRF1 mRNA expression. In accordance, protein expression of the initiation factor eIF3-f, a major target of Atrogin-1 and an important regulator of protein synthesis, was preserved (48). This is the first and only study to demonstrate a beneficial effect of glycine on cancer-induced cachexia. Additional research is required to confirm these promising results and to further unravel the anti-tumor and anti-cachectic effects.

2.1.5 Arginine

Arginine is a conditionally essential amino acid, i.e. the body can synthesize sufficient amounts of arginine to meet physiological demands under well-nourished, healthy conditions (49). Arginine is involved in a number of biological processes including cell growth, survival and protein synthesis. It is also a precursor in the biosynthesis of nitric oxide (50). Nitric oxide is a ubiquitous cellular messenger that stimulates the release of certain hormones, such as insulin and growth hormone, and is an important regulator of blood flow, tissue oxygenation and immune function. In addition, arginine may enhance T cell natural killer cell activity, which inhibits tumor growth (51). Therefore, supplementation with arginine could be beneficial for patients with cancer cachexia through modulation of the endogenous anti-tumor response. However, up till now, there are no data in experimental cancer cachexia models published. This could be related to the concern that arginine, or its metabolites, interfere with metabolic pathways that can induce growth of some tumors (52, 53). These findings emphasize the importance that not all nutrients that envision positive effects on muscle anabolism are applicable in the treatment of cancer cachexia.

2.2 Dietary fat

Dietary fat is an important source of energy and contributes a significant caloric value to our diet. In Western diets, dietary fat may constitute 40-45% of the total caloric intake. Dietary fat is not just a source of energy, it also functions as structural component of cell membranes, carries fat soluble vitamins, plays an important role in signal transduction and is a precursor for inflammatory mediators (54).

2.2.1 High-fat ketogenic diet

Currently, there is limited research available to substantiate an optimal energy percentage of dietary fat in cancer cachexia but the effect of ketogenic diets have been investigated in cancer. The ketogenic diet is a high-fat, low-carbohydrate diet designed to increase the blood concentration of free fatty acids and ketone bodies as alternative sources of energy to glucose (55). As tumor cells mostly rely on glucose as a substrate for anaerobic energy production, i.e., Warburg effect (56), ketogenic diets aim to reduce energy sources for the tumor, while providing free fatty acids and ketone bodies as an energy source for the muscle. Consequently, a high fat diet might be expected to prevent host catabolism during cachexia, mainly by tumor growth reduction. Only a few studies investigated the anti-cachectic effects of ketogenic diets in experimental models of cancer cachexia. In mice bearing the MAC16 tumor, Tisdale et al. showed that the cachectic phenotype can be partly reversed by a ketogenic diet [80% of calories supplied as medium

chain triglycerides (MCT)], causing reduced tumor growth and an inhibition of body weight loss (57). Body composition analysis showed retention of both fat and fat-free carcass mass in animals fed high levels of MCT. In another study, an 80% MCT-based high-fat diet reduced both tumor weight and host weight loss and restored both nitrogen balance and urea excretion to that of non-tumor-bearing mice (58). Furthermore, amino acid concentrations in plasma were also restored to control levels, suggesting that excessive nitrogen catabolism during cachexia can be prevented. More recently, the effect of an infant formula with a ketogenic composition used to treat patients with refractory epilepsy was investigated on cancer cachexia in C26 tumor-bearing mice (59). Mice receiving the ketogenic formula showed reduced body weight loss and muscle mass loss. Tumor growth and plasma IL-6 levels were significantly decreased in mice receiving the ketogenic formula compared to tumor-bearing control. It seems that the ketogenic diet inhibits tumor growth and thereby prevents host catabolism. Collectively, these studies suggest that the ketogenic diet with adequate amounts of proteins has beneficial effects on the development of cancer cachexia. However, there is some debate concerning the use of ketogenic diets and the development of dyslipidemia. Some (60, 61) but not all (62) studies indicate that a ketogenic diet produce significant increases in the plasma levels of total cholesterol and triglycerides. Elevated levels of plasma triglycerides and cholesterol are often detected in patients suffering from cancer cachexia (63), as a result of increased lipolysis (64, 65). This tumor induced dyslipidemia, in turn causes lipotoxic effects in other tissues including skeletal muscle (65, 66). Considering the potential impact of dyslipidemia to cancer cachexia, this potential effect should be further investigated to probe the feasibility of the ketogenic diets in patients with cancer cachexia.

2.2.2 Polyunsaturated fatty acids

Dietary long chain polyunsaturated fatty acids (lcPUFAs) have an effect on diverse physiological processes affecting normal health and chronic diseases (67-69). The n-3 and n-6 lcPUFA families are derived from the desaturation and elongation of the essential lcPUFAs α-linolenic and linoleic acids that are ingested as components of food. The principal members of the n-3 lcPUFA family are eicosapentaenoic acid (EPA) and docosahexaenoic acid (DHA), whereas arachidonic acid is the main derivate of the n-6 lcPUFA family. It is known that eicosanoids derived from n-6 lcPUFAs have pro-inflammatory and immune-active functions, whereas n-3 lcPUFA-derived eicosanoids have anti-inflammatory properties, attributable to their ability to inhibit the formation of n-6 lcPUFA-derived eicosanoids.

Diet supplementation with fish oil, which is rich in n-3 lcPUFAs EPA and DHA, has been investigated to preserve skeletal muscle mass in various experimental animal models of cancer cachexia. Most of these studies show that fish oil is an effective nutritional intervention to induce body weight gain, reduce tumor growth rate and reverse food intake. In 1990, Tisdale et al. showed for the first time that a diet enriched in fish oil reduced both tumor growth and weight loss produced by the MAC16 adenocarcinoma (70). Reversal of host body weight loss was associated with an increase in total body fat and muscle mass. Although the amount of fish oil required for optimal activity was high (50% of total calories), no toxicities were observed (70). Comparable results were found in Walker 256 tumor-bearing rats receiving an n-3 fish oil diet. Tumor weight gain in fish oil fed rats was reduced and these animals gained body weight and maintained blood metabolic parameters (glucose, lactate, triacylglycerol and cholesterol) similar to non-tumor-bearing rats (71). Fish oil supplementation via oral gavage reduced body weight loss and tumor weight gain to a similar extent (72). Finally, some studies investigated the effect of lifelong supplementation of the diet with fish oil on cancer cachexia (73, 74). In these studies, the diet of pregnant and lactating rats and subsequent male offspring was supplemented with fish oil. Lifelong supplementation of the diet with fish oil significantly decreased tumor growth, increased survival, reversed food intake and prevented body weight loss. Furthermore, fish oil supplementation partly preserved blood metabolic parameters in tumor-bearing rats compared to control (73, 74). However, it is difficult to predict if the effects found in these lifelong supplementation studies can be translated into a treatment regimen relevant to cancer cachexia.

While most studies reported clinically and statistically significant effects of fish oil supplementation on preventing body weight loss, Dumas et al. have found no effect (75). In rats with peritoneal carcinosis, fish oil-enriched diet delayed the occurrence of anorexia compared to the control diet. Furthermore, ascites production was lower in fish oil treated rats. However, no difference in body weight gain, fat mass and muscle mass was reported (75). The discrepancies could be due to differences in the design of the study. In the aforementioned studies, in both the treatment arm and control arm relative weight gain of animals and tissues were assessed at the same time point, whereas Dumas et al. assessed the final measurements when anorexia was evident in all animals, ensuing different time points per group. Besides fish oil, shark liver oil is a common dietary supplement rich in n-3 lcPUFAs. Prophylactic supplementation with shark liver oil promoted gain in body weight, reduction of tumor weight and maintained blood metabolic parameters in Walker

256 tumor bearing rats (76, 77). However, shark liver oil supplementation showed less potent effects compared to fish oil (77).

The anti-cachectic and anti-tumor effect of purified EPA has also been investigated in various experimental animal models. In mice bearing the cachexia-inducing MAC16 adenocarcinoma, EPA was found to stabilize weight loss, delay growth of the tumor, and increase the overall survival (78-80). Such anti-cachectic effect was not achieved by the use of DHA or linoleic acid alone (79). Supplementation with EPA inhibited tumor-induced lipolysis and reduced protein degradation without an effect on protein synthesis (78, 81, 82). In mice bearing the cachexia-inducing S180 ascites tumor, oral administration of EPA prevented body weight loss by preserving the white adipose tissue mass (83). Furthermore, EPA administration suppressed plasma levels of pro-inflammatory cytokines such as TNF-α and IL-6. Lastly, EPA treatment also preserved several key lipolytic factors and raised the mRNA levels of some adipogenic factors in the white adipose tissue (83). A higher body weight gain in response to EPA supplementation has also been reported in $Apc^{(min/+)}$ mice (84), rats implanted with MCA sarcoma (85), and rats treated with MAT-LyLu prostate tumor cells (86).

Taken together, these studies suggest that n-3 lcPUFAs, in particular EPA, are effective in preventing body weight loss and tumor growth in experimental animal models of cancer cachexia. However, little is known on the underlying mechanisms of n-3 lcPUFAs/EPA in cancer cachexia. The aforementioned data suggest that n-3 lcPUFAs/EPA is able to suppress lipolysis, probably by downregulating lipid mobilizing factors (87). Whether the anti-lipolytic activity is a direct effect of n-3 lcPUFAs/EPA or related to its anti-inflammatory properties through inhibiting pro-inflammatory cytokines, such as TNF- α and IL-6, needs to be further elucidated.

2.2.3 Conjugated linoleic acid

Conjugated linoleic acid (CLA) is a group of at least 28 isomers of linoleic acid found mostly in red meat and dairy products derived from ruminants (88). CLA is marketed as a weight-loss supplement to reduce body fat and promote lean muscle growth (e.g. Tonalin®). Experimental studies have shown that CLA has anti-carcinogenic effects (89, 90). Furthermore, CLA was protective against TNF- α and LPS induced muscle wasting (91, 92). However, data on the effect of dietary supplementation of CLA in the treatment of cancer cachexia is contradictory. In mice bearing the C26 tumor, Graves et al. showed that a diet containing 0.5% CLA preserved skeletal muscle mass and reduced TNF receptor type 1 levels in muscle homogenates (93). In mice bearing the LLC tumor, the same diet reduced skeletal

muscle wasting, but had no effect on skeletal muscle levels of TNF receptor type 1 (94). In mice bearing the B16 melanoma, 0.5% CLA did not affect skeletal muscle mass or TNF receptor type 1 levels in skeletal muscle (94). The notion that CLA has beneficial effects in cancer cachexia was also not supported by Tian et al. (95). In this study, a 1% CLA enriched diet did not affect skeletal muscle mass and adipose tissue mass. CLA supplementation did not inhibit the induction of proteolytic markers. Instead, MuRF1 expression was significantly higher in C26 tumor-bearing mice receiving a diet containing 1% CLA. In skeletal muscle, CLA enhanced tumor-induced gene expression of inflammatory markers TNF- α, IL-6 receptor and F4/80. Moreover, in epididymal adipose tissue, tumor driven lipolysis was aggravated by CLA supplementation (95). More recently, in rats bearing the Walker 256 tumor, CLA treatment aggravated cachexia symptoms, including increased inflammatory status, steatosis and hyperlipidemia (96). Collectively, these results do not provide strong support for CLA in the treatment of cancer cachexia.

2.3 Other nutrients

2.3.1 Carnitine

Carnitine is a trimethylamine, which is synthesized in the liver and kidney via the conversion of two essential amino acids, lysine and methionine. Carnitine plays a major role in the import of long chain fatty acids from the cytosol into the mitochondrial matrix for subsequent β-oxidation (97, 98). Inefficiency of this bioenergetics process results in increased oxidative stress, contributing to the development of metabolic abnormalities and the release of pro-inflammatory cytokines. Consequently, supplementation of carnitine to enhance mitochondrial β-oxidation may attenuate oxidative stress and inflammation, resulting in beneficial clinical outcomes. Carnitine supplementation has been studied in various experimental models of cancer cachexia. In rats bearing the Yoshida AH-130 tumor, L-carnitine treatment resulted in greater food intake (99, 100). Protein levels of carnitine palmitoyl transferase-1 (CPT-1) enzyme, a marker of carnitine effects, were higher in the muscles of tumor-bearing rats treated with L-carnitine compared with the non-treated cachectic animals (100). This was accompanied by an inhibition of tumor-induced muscle wasting (99, 100) and an increase in physical activity (99). Moreover, L-carnitine treatment resulted in a down-regulation of atrogin-1 and MuRF1 and a decrease in the proteasome activity in gastrocnemius muscle (99, 100). In addition, the pro-apoptotic marker caspase-3 in skeletal muscle tended to be decreased in muscle of tumor-bearing rats treated with L-carnitine (99). In mice bearing the C26 tumor, L-carnitine significantly increased food intake, muscle mass and epididymis fat weight through the upregulation of CPT (101). In addition,

the increased CPT activity was associated with reduced plasma levels of IL-6 and TNF-α (101). In cachectic rats bearing the Walker 256 tumor, CPT activity was reduced and liver and plasma triacylglycerol content was increased. L-Carnitine treatment restored these measures back to control values, showing that L-carnitine preserves hepatic lipid metabolism in experimental cancer cachexia (102). Current evidence suggests that carnitine might help to ameliorate muscle wasting in cancer, although more molecular studies investigating the exact working mechanism are needed.

2.3.2 Creatine

Creatine is a non-protein amino acid that can be endogenously synthesized in the liver, kidney and pancreas and is mainly stored and utilized in the skeletal muscle. Creatine can be phosphorylated by creatine kinase to form phosphocreatine, which plays an important bioenergetics role by providing rapid energy during muscle contraction, where phosphocreatine donates a phosphate group to adenosine diphosphate to resynthesize adenosine triphosphate (103, 104). Given that oral creatine supplementation augments its intramuscular content and has the capacity to effectively enhance muscle strength and lean body mass (105-107), makes it an interesting supplement to treat muscle-wasting diseases. Indeed, creatine supplementation has been successfully used as an adjuvant treatment in numerous myopathies (108-110). Furthermore, creatine supplementation has shown antioxidant capacities as well as effectiveness to counteract pro-inflammatory cytokines (111, 112). Despite the promising results, only a few studies have investigated the effects of creatine supplementation in experimental cancer cachexia. In rats bearing the Walker 256 tumor, creatine supplementation attenuated body weight loss and tumor growth was decreased (113-115). Cancer-induced skeletal muscle atrophy was attenuated by creatine, as evidenced by the increase in muscle fiber cross-sectional area. Creatine also prevented cancer-induced increase in Atrogin-1 and MuRF1 protein levels. Furthermore, creatine supplementation prevented the increase in plasma TNF-α and IL-6 (113, 114), while it increased plasma IL-10 (114). However, mean survival time was not different compared to tumor-bearing control (113, 115). Given the beneficial effects of creatine supplementation on skeletal muscle mass maintenance in experimental cancer cachexia and the promising results in other muscle wasting diseases, creatine could be a useful supplement to treat muscle wasting in cancer cachexia and should be the objective for future studies. It should be pointed out however that creatine supplementation may increase urinary creatinine levels, which complicates interpretation of the latter as a marker of renal dysfunction in patients with a history or risk of renal disease.

2.3.3 Flavonoids

Flavonoids are a large group of polyphenolic compounds and are ubiquitously expressed in plants. Fruits and vegetables are the main dietary sources of flavonoids for humans, along with tea and wine. As a dietary component, flavonoids are thought to have health-promoting properties due to their antioxidant, hepatoprotective, anti-inflammatory and anti-carcinogenic properties (116). Despite several known effects of flavonoids on health and disease, research into the effects of flavonoids on cachexia prevention has been limited to date. In $Apc^{(min/+)}$ mice, quercetin supplementation attenuated the progression of cancer cachexia (117). Quercetin significantly attenuated body weight loss, but did not affect the loss of epididymal fat in $Apc^{(min/+)}$ mice. After 3 weeks of supplementation, the loss of muscle mass and grip strength shown in $Apc^{(min/+)}$ mice was significantly attenuated by quercetin. Furthermore, increased plasma IL-6 levels were completely mitigated by quercetin in this model of intestinal cancer. In this study, no effect of quercetin supplementation on tumor number was observed, while a reduction of the tumor weight was found in rats bearing the Walker 256 tumor (118). Epigallocatechin-3-gallate (EGCG), the principal polyphenolic component in green tea, effectively attenuates skeletal muscle atrophy in mice bearing the Lewis lung carcinoma (LLC) tumor (119). EGCG supplementation inhibited tumor growth and the loss of body weight was significantly slowed down. Furthermore, it was shown that EGCG positively regulates the expression of muscle-specific ubiquitin ligase genes encoding MuRF-1 and Atrogin-1 (119). Another study examined the effect of isoflavones derived from soy extracts on muscle atrophy in LLC-bearing mice (120). The isoflavone diet attenuated the tumor-induced loss in wet weight and myofiber size of the gastrocnemius muscle. Moreover, the increased expression of MuRF-1 and Atrogin-1 was significantly suppressed by the supplementation of isoflavones. In parallel, the isoflavone diet significantly inhibited the phosphorylation of ERK in skeletal muscle of tumor-bearing mice. No effect of dietary isoflavones on tumor mass or pro-inflammatory cytokines IL-6 and TNF-α were observed (120). Morin, another flavonoid, was able to suppress tumor-induced skeletal muscle wasting in LLC-bearing mice (121). Dietary morin prevented the reduction of muscle wet weight and myofiber size. Moreover, the tumor mass in mice fed the morin diet was significant lower compared to mice fed the normal diet. It was suggested that morin indirectly prevents muscle atrophy by suppressing tumor growth via targeting ribosomal protein S10. The anti-proliferative effect of morin had a cell specific action that was only apparent in tumor cells, but not in muscle cells (121). Because of the variation in flavonoids and limited number of studies, there is not enough evidence to recommend flavonoids as a potential supplement to treat

muscle wasting in cancer. However, the available data merits further investigation of their potential to modulate cancer cachexia.

2.3.4 Resveratrol

Resveratrol (3,5,4'-trihydroxystilbene) is a phytoalexin, a class of compounds produced by many plants when they are infected or physically harmed (122); it has been reported to have anti-tumor effects in rats (123). Research on the potential positive effects of resveratrol in cancer cachexia is limited and contradictory. In mice bearing the MAC16 tumor with established weight loss, resveratrol partly blocked weight loss by interfering with NF-κB activity in skeletal muscle and this was accompanied by inhibition of tumor growth (124). Another study demonstrated that resveratrol inhibited skeletal muscle atrophy induced by the C26 adenocarcinoma tumor through its inhibition of NF-κB activity in skeletal muscle (125), without affecting tumor growth. In contrast to these studies, administration of resveratrol did not attenuate skeletal muscle mass loss or body weight loss in both rats bearing the Yoshida AH-130 tumor and mice bearing the LLC (126). In fact, in rats, administration of resveratrol exaggerated cancer cachexia (126). On the contrary, resveratrol was able to decrease proteolysis *in vitro* (126). After absorption, resveratrol undergoes rapid and extensive metabolism leading to low bioavailability (127, 128). With respect to the poor bioavailability it might be not surprising that resveratrol did not prevent muscle wasting, as the likelihood to reach effective levels in plasma or muscle is very low. Taking these aforementioned studies into consideration, resveratrol is not likely able to ameliorate tumor induced cachexia.

2.3.5 Prebiotic non-digestible oligosaccharides

A prebiotic is "a selectively fermented ingredient that allows specific changes, both in the composition and/or activity in the gastrointestinal microflora that confers benefits upon host well-being and health" (129). Prebiotic oligosaccharides such as galacto-oligosaccharides (GOS) and fructo-oligosaccharides (FOS) have shown to have immune modulating activities, observed in several animal experiments and clinical trials (130-132). These oligosaccharides have been associated with improved gut barrier function (133). It stimulates bifidobacteria, lactobacilli and other healthy bacteria, while it reduces harmful bacteria in the gut. Moreover, these oligosaccharides may block or activate specific receptors on immune cells leading to improved immune responses. In addition, oligosaccharides are fermented by colonic bacteria into short-chain fatty acids (133). Short-chain fatty acids have been shown to exert anti-carcinogenic as well as anti-inflammatory properties (134). Although, the exact role of the microbiome in cancer cachexia is not clear yet,

animal studies suggest that the composition of the microbiota and intestinal barrier function is affected by the presence of a tumor and the development of cancer cachexia (135). These findings support the rational to target the gut microbiota in cancer cachexia using prebiotic non-digestible oligosaccharides. The therapeutic potential of prebiotic non-digestible oligosaccharides in cancer cachexia have been barely explored. In mice bearing the C26 tumor, diet supplemented with GOS and FOS (weight ratio 9:1) significantly reduced skeletal muscle mass loss (138). Similar results were obtained when the FOS was replaced by additional GOS (138). Administration of a prebiotic candidate, pectic oligosaccharide (POS), to leukemic mice mitigated the cachectic phenotype, by delaying anorexia and preserving fat mass (139). In addition, POS increased the total number of bacteria and induced a drastic change in microbial diversity and populations. No effect on inflammation was observed (139). Due to limited research, the impact of prebiotic non-digestible oligosaccharides on cancer cachexia is currently unclear and would warrants further investigation.

3. MULTINUTRIENT INTERVENTIONS

As discussed in Single Nutrient Interventions, numerous nutrients led to positive results in experimental models of cancer cachexia, targeting different aspects of the wasting syndrome. Combining such high quality nutrients and/or nutraceuticals in a “multinutrient approach” to treat cachexia, is expected to have a superior impact compared to single nutrients. A multinutrient approach is aimed at targeting specific factors involved in cancer cachexia, e.g., anorexia, altered fat and protein metabolism, and systemic inflammation, but also the replenishment of nutrient deficiencies.

Several of these multi-nutrient approaches have been studied in experimental models of cancer cachexia. In mice bearing the MAC16 tumor, Smith et al. investigated the effect EPA combined with protein (casein), amino acid mixture (leucine, arginine and methionine) and carbohydrate on protein synthesis and degradation in gastrocnemius muscle (82). Treatment with only EPA significantly reduced protein degradation, but had no effect on protein synthesis. Combination of EPA with casein tended to increase protein synthesis. However, when combined with the amino mixture protein synthesis almost doubled. The addition of carbohydrate to stimulate insulin release had no additional effect (82). In another study, Van Norren et al. examined the effect of dietary supplementation with a specific combination of high protein (100% casein), leucine and fish oil (EPA and DHA in a ratio of 2.2:1) on body composition in mice bearing the C26 tumor (140).

The multinutrient intervention targeting catabolism, anabolism and essential amino acid supply significantly reduced loss of carcass, muscle and fat mass. Addition of the single nutrients to the diets resulted in no or marginal effects (140). In a second experiment, the effect of a more humanized diet on weight loss, muscle function and physical activity was studied, referred to as Specific Nutritional Composition, containing high protein (68% casein and 32% whey), leucine, fish oil (EPA and DHA in a ratio of 2.2:1), and the oligosaccharides GOS and FOS. The specific nutritional composition diet significantly reduced loss of body, carcass, muscle and fat mass. Furthermore, tumor weight was significantly lower compared to tumor-bearing control. Muscle performance was improved and total daily activity was normalized after intervention with the specific nutritional composition diet (140, 141). The specific nutritional composition diet also showed beneficial immune modulatory effects. The nutritional combination significantly improved the Th1 immunity and plasma levels of IL-6, TNF-α and PGE_2 were significantly reduced (141). Furthermore, this combination attenuated weight loss and inflammatory markers, and reduced pathogen levels and bacterial translocation in a chemotherapy model (142). In mice bearing the B16 melanoma, the effect of a multi-nutrient intervention with BCAAs, citric acid, L-carnitine, coenzyme Q10 and various vitamins and minerals was investigated on the development of cancer cachexia (143). The mice receiving the intervention diet showed a higher cumulative food intake compared to tumor-bearing control. In addition, tumor weight was significantly lower and lung metastasis of the B16 melanoma cells were absent in the intervention group. However, attenuation of muscle tissue loss was only observed for the suprahyoid muscles in the neck but not for gastrocnemius or soleus muscles in the lower leg (143). More recently, the effect of total nutrition formula on LLC-bearing mice was investigated (144). Total nutritional formula is an energy- and protein-dense oral nutritional supplement fortified with micronutrients such as vitamin D, vitamin A, coenzyme Q10 and selenium. Daily oral supplementation with total nutritional formula significantly suppressed tumor growth, while body weight loss and gastrocnemius muscle mass loss were significantly attenuated. Furthermore, the plasma levels of TNF-α and IL-6 were significantly decreased in LLC-bearing mice supplemented with total nutritional formula (144).

Clearly, the few studies in which the combination of nutrients was systemically compared to single nutrients alone strongly support the concept of a multinutrient approach. More experimental dietary intervention studies should focus on multi-nutrient interventions targeting multiple aspects of the disease. Furthermore, future studies should define optimal selection and balance of nutrients that work in concert to produce a health benefit that is greater than the sum of the single nutrients.

4. NUTRITIONAL INTERVENTIONS: GAPS AND OPPORTUNITIES

All of the nutritional intervention studies included in this review describe effects on phenotypic measures of cachexia, such as body weight loss and/or muscle mass loss. However, only few of the studies contribute to understanding the underlying mechanisms by which beneficial effects of nutritional interventions are mediated. Of all reviewed nutrients, only L-leucine and its metabolite HMB have been shown to attenuate tumor-induced muscle wasting by (directly) modulating muscle protein synthesis and proteolysis. For many other nutrients, the anti-cachectic effect is frequently associated with reduced tumor growth, modulation of inflammatory signaling or other extra-muscular alterations that may contribute to cachexia. In these studies, it is difficult to discriminate whether these nutrients act directly on skeletal muscle metabolism, or impact indirectly on cachexia. A better understanding of the beneficial actions of nutritional interventions will not only aid their clinical implementation, but also the systematic evaluation of additive or synergistic effects of rationally selected nutritional combinations with distinct or complementary actions.

4.1 Standardization in experimental design

Given the heterogeneity of cancer-induced cachexia, the results obtained in the reviewed studies must be considered in the context of the specific models that were used, and variations in dietary regiments that were applied. Although these variations may cause discrepancies between results across different animal models, and laboratory groups, preclinical studies per se have provided advantages and results that merit their application in cachexia research. The experimental models of cancer cachexia allow analysis of different tissues affected by cancer cachexia, and provide valuable insights in the underlying mechanisms of tested interventions. In addition, safety and efficacy parameters that are relevant and translatable to clinical practice are defined in experimental models, including identification of potentially harmful interactions with other treatment modalities. Nevertheless, various aspects in the experimental design would benefit from standardization. When evaluating the potential beneficial effects of the nutritional interventions in experimental cancer cachexia, a wide variation in timing, duration, dosing and route of supplementation was observed, as well as in animal models used (Supporting Information, Table S1).

4.1.1 Intervention as source of variation

Dietary intake, composition and dose is an often overlooked source of variation in experimental animal studies of cancer cachexia (145). The majority of the studies reviewed provide diets ad libitum, while only a few studies control daily food intake. However, it should be kept in mind that anorexia is an important contributing factor

to cancer-induced muscle wasting and that dietary intake is closely related to cachexia-related outcome measures. This stresses the importance of dietary standardization, recording of food intake or pair feeding the control group, to correlate the amount of nutrient intake with outcome measures. Details on dietary intake are often provided, however, the exact composition of the experimental diets is often not described. Many of the studies reviewed used standard laboratory chow. Standard laboratory chow diets do not have a standardized macronutrient composition and often vary from batch to batch (146). Furthermore, the ingredients of laboratory chow are rarely defined, therefore it might contain unknown nutrients that may impact study endpoints. The use of purified or semi-purified diets should be the new standard. In comparison to standard laboratory chow, the ingredients included in purified and semi-purified diets are open formulas and well-characterized (147). In addition, the formulation of the semi-purified diet can be altered by the researcher according to the research objective. Besides the choice of the background diet, the control diet and intervention diet should be matched for calories and nitrogen content. The proportions of the nutrients in relation to human intake should also be considered, improving the translatability to the clinic. Furthermore, the dose of the supplemented nutrients is a point of attention. Some of the intervention studies use supraphysiological doses that may not be feasible for a nutritional intervention. For example, a diet with 4% HMB is rather unbalanced considering that normal rodent chow contains only 12.5% protein.

The timing and duration of supplementation as well as the route of administration vary between studies and is another source of variation. The majority of the studies started supplementation before or with tumor inoculation, while only a few initiate supplementation when animals show evidence of cachexia. In both study designs, the metabolic state of the animals at the start of the intervention is different, each of which may require a different formulation of an effective nutritional intervention. Besides, nutrients might have a fundamental different action in such models, for example by affecting tumor take or growth. In addition to the timing, the duration of the intervention studies varies substantially, ranging from 24 hours to 34 days after tumor inoculation. This suggests that the cachectic state at the end of the study differs between these studies, making it difficult to compare phenotypical and biochemical data between studies.

In addition, different routes of administration were applied in the reviewed experimental intervention studies. Only a few administrated the intervention via intra-peritoneal injection, subcutaneous injection or drinking water. A significant number of studies supplemented the nutrients via oral gavage. Similar to the

injections, the advantage of administration via oral gavage is that an exact amount of the nutrient is delivered irrespective of the food intake, which minimizes variation between animals. However, by administration via oral gavage the nutrient appears as a bolus and is not part of the food matrix. Furthermore, administration via oral gavage may have impact on the food intake and the intervention diet is often not isonitrogenous and isocaloric to the control diet. In the majority of the studies the nutrients are administered via the diet, either by modification of semi-purified diets, or by incorporation into the standard laboratory chow. This allows to explore the full metabolic potential of nutritional interventions, as it takes its processing through the complete digestive tract into consideration. Moreover, from a translational perspective this may be the preferred route of administration, as its clinical application will be accordingly.

Combined, systematic attention to the aspects discussed above will contribute to further standardization in experimental design and reporting of experimental details. In turn, this will greatly stimulate the speed to explore promising leads and turn these into reproducible preclinical intervention diets, with robust translational potential in cancer cachexia.

4.1.2 Heterogeneity between animal models of cancer cachexia

Numerous well established animal models of cancer cachexia are used (Table 1). However, there is substantial variability between them in terms of cell type, site of inoculation/implantation, tumor growth (speed and size), development of metastasis, the overall dynamics of the wasting process, and putative underlying mechanisms (e.g. anorexia, inflammation) (148). This makes it difficult to compare results across animal models. Furthermore, these animal models often do not recapitulate all major clinical characteristics present in cancer cachexia, which may complicate direct translation of the findings to the clinic. For example, the kinetics by which cachexia develops in these models differs from that in patients. The effectiveness of some treatments may be of transient nature and lost in patients with chronic cachexia, while treatments that do not prove effective in acute models of cachexia might be useful for treating chronic cachexia. Furthermore, the majority of the animal models have ectopically growing tumors. Although, these animal models have been useful in investigating the underlying mechanisms of cancer cachexia, animal models of cancer cachexia with orthotopically growing tumors may more closely represent clinical cancer cachexia. Orthotopic tumor growth provides tumor cells its original stroma and microenvironment, both of these elements may determine the etiology of cachexia and affect the outcome of interventions. Indeed, recently, it has been demonstrated for a murine model of pancreatic cancer cachexia that orthotopic

implantation of tumor cells on the location of interest much better recapitulates the clinical characteristics of cancer cachexia compared to subcutaneous tumor models (149). The growth monitoring capabilities for palpable, subcutaneously grown tumors is no longer a rationale for avoiding the use of orthotopic models, as recent studies have demonstrated the routine deployment of non-invasive imaging in various models, including orthotopically grown lung and brain tumors, to follow up tumor growth (150-152). Moreover, micro-CT imaging-based automated 3D contouring algorithms have been developed to simultaneously determine muscle mass changes in a model of orthotopic lung cancer cachexia (153). Finally, orthotopic tumor models provide an opportunity to study the interaction between conventional cancer therapies (e.g. chemo-, immune- and radiation therapy) and adjuvant interventions targeting cachexia. Taken together, the development of more humanized models to study the effectiveness of interventions to treat cancer cachexia may lead to a more rapid translation into clinical trials.

4.2 Combining nutrition with cancer treatment and anti-cachexia interventions

Although not in the scope of this review, in addition to tumor activity and host responses that may drive cachexia, there is increasing clinical evidence that treatments directed at the tumor may actually contribute to the development and progression of cachexia (154, 155). Studies in healthy mice and rats have also demonstrated that some chemotherapeutic agents induce muscle wasting (156, 157). Recently, it was for the first time demonstrated that distinct metabolic derangements are present in cancer-induced and chemotherapy-induced cachexia (158). This implies that different therapeutic strategies to treat cachexia may be required. A better understanding of the tumor-, host-, and treatment-induced drivers of cachexia in combination with in-depth knowledge on the mechanism of nutritional interventions is crucial to develop effective therapeutic interventions for cancer-induced and treatment-induced cachexia.

Moreover, as in practice nutritional interventions will be used in combination with anti-cancer therapies such as chemo-, radiation- and immunotherapy, it is necessary to investigate if such combinations are safe, and whether they modulate the therapeutic effectiveness. Some nutrients, such as lcPUFAs, may improve the adherence to and efficacy of chemotherapy (159), while others, including carnitine and glutamine are suggested to reduce the toxicity of anti-cancer therapy in cachectic patients (160).

Considering cancer cachexia is a multifactorial syndrome, it is expected that a multimodal approach targeting multiple aberrant pathophysiologic pathways

simultaneously will be most efficient. In addition to optimized nutritional care, other therapeutic strategies, including exercise training and pharmacological interventions, could effectively contribute to attenuate cancer related muscle wasting. Although not all treatment modalities can be modeled in pre-clinical experimental set ups, efficacy, synergy and relevance of some combined treatment modalities have been evaluated. In particular, exercise training has some experimental evidence of benefit to mitigate skeletal muscle loss and therefore should be seen as potential tool to maximize outcomes and quality of life of patients with cancer cachexia (161-164). Exercise training stimulates the increase of muscle mass and strength and might improve cancer-associated skeletal muscle wasting by stimulating anabolic pathways as well as by down-regulating the activity of pro-inflammatory cytokines (165). In addition, exercise training has a beneficial effect on counteracting fatigue, which is one of the most severe symptoms in cancer patients (166). Combining exercise training and nutritional intervention was shown to be more effective than either one alone, highlighting the potential of multimodal interventions with a nutritional component (161, 163, 164). Besides exercise training, pharmacological agents such as appetite stimulants, anabolic steroids and non-steroidal anti-inflammatory drugs could effectively contribute to the treatment of cachexia (167). Carefully designed combination therapy may maximize the impact on treating muscle wasting while minimizing the chance for drug toxicities. Various combinations of single nutrients with exercise or pharmacological agents have been studied in experimental cancer cachexia, with some success. However, the number of studies is limited and therefore more research is needed to find the optimal combination. In future studies, attention should be paid on the interaction between the different components of the multimodal approach. It is important that the combination is safe and contributes to the total therapy effectiveness.

5. CONCLUSION

Targeted nutrition is pivotal in preserving muscle mass in cancer cachexia. A large number of studies demonstrated beneficial effects of nutritional interventions on muscle wasting. However, evidenced-based studies that indicate the optimal quantity and quality of the nutrients are often missing. Furthermore, the combination of multiple nutrients is expected to have a superior impact compared to single nutrients alone. More studies investigating the optimal quantity, quality and combination of nutrients are needed. Rationally-designed nutrition intervention studies, performed in well characterized experimental models are an essential approach in the design of multimodal therapies targeting cancer cachexia.

Table 1: Heterogeneity between well-characterized animal models of cancer cachexia

Model	Tumor origin	Host	Tumor injection site	Experimental period (days post tumor injection)	Anorexia	Inflammation	Metastasis
Mouse models							
C26	Colon	CD2F1 and BALB/c	s.c. or i.m.	11-21	No/Yes depending on experimental design	Yes (IL-6)	No
LLC	Lung	C57Bl/6	s.c. or i.m.	15-34	Yes	Yes (TNF-α, IL-6, IFN-γ)	Yes
$Apc^{(min/+)}$	Colon	C57Bl/6	genetic		No	Yes (IL-6)	No
MAC16	Colon	NMRI mice	s.c.	1-20	No	Yes (TNF-α, IL-6, IL-1)	No
B16	Melanoma	C57Bl/6	s.c.	16	Yes	Yes (TNF-α, IL-6)	No
Rat models							
Walker 256	Mammary gland	Wistar rats	s.c.	7-33	Yes	Yes (TNF-α, IL-6, PGE_2, Walker factor)	No
Yoshida AH-130	Ascites hepatoma	Wistar rats	i.p.	7-24	Yes	Yes (TNF-α, PGE_2)	No
MAT-LyLu	Prostate	Copenhagen Fisher rats	s.c.	14	No	Not reported	Yes

s.c.: subcutaneous, i.m.: intramuscular, and i.p.: intraperitoneal.

Note: Tumor volume varies significantly between models. This parameter might affect the translatability to the clinical situation. However, the data provided in the reviewed papers did not provide sufficient information to summarize relative or absolute tumor volume.

REFERENCES

1. Fearon K, Strasser F, Anker SD, Bosaeus I, Bruera E, Fainsinger RL, et al. Definition and classification of cancer cachexia: an international consensus. Lancet Oncol. 2011;12(5):489-95 DOI: 10.1016/S1470-2045(10)70218-7.
2. Anker MS, Holcomb R, Muscaritoli M, von Haehling S, Haverkamp W, Jatoi A, et al. Orphan disease status of cancer cachexia in the USA and in the European Union: a systematic review. Journal of cachexia, sarcopenia and muscle. 2019;10(1):22-34 DOI: 10.1002/jcsm.12402.
3. Prado CM, Lieffers JR, McCargar LJ, Reiman T, Sawyer MB, Martin L, et al. Prevalence and clinical implications of sarcopenic obesity in patients with solid tumours of the respiratory and gastrointestinal tracts: a population-based study. Lancet Oncol. 2008;9(7):629-35 DOI: 10.1016/S1470-2045(08)70153-0.
4. Dewys WD, Begg C, Lavin PT, Band PR, Bennett JM, Bertino JR, et al. Prognostic effect of weight loss prior to chemotherapy in cancer patients. Eastern Cooperative Oncology Group. Am J Med. 1980;69(4):491-7 DOI: 10.1016/s0149-2918(05)80001-3.
5. Vaughan VC, Martin P, Lewandowski PA. Cancer cachexia: impact, mechanisms and emerging treatments. Journal of cachexia, sarcopenia and muscle. 2013;4(2):95-109 DOI: 10.1007/s13539-012-0087-1.
6. Turner DC, Kondic AG, Anderson KM, Robinson AG, Garon EB, Riess JW, et al. Pembrolizumab Exposure-Response Assessments Challenged by Association of Cancer Cachexia and Catabolic Clearance. Clinical cancer research : an official journal of the American Association for Cancer Research. 2018;24(23):5841-9 DOI: 10.1158/1078-0432.CCR-18-0415.
7. Aapro M, Arends J, Bozzetti F, Fearon K, Grunberg SM, Herrstedt J, et al. Early recognition of malnutrition and cachexia in the cancer patient: a position paper of a European School of Oncology Task Force. Annals of oncology : official journal of the European Society for Medical Oncology. 2014;25(8):1492-9 DOI: 10.1093/annonc/mdu085.
8. Ezeoke CC, Morley JE. Pathophysiology of anorexia in the cancer cachexia syndrome. Journal of cachexia, sarcopenia and muscle. 2015;6(4):287-302 DOI: 10.1002/jcsm.12059.
9. Johnen H, Lin S, Kuffner T, Brown DA, Tsai VW, Bauskin AR, et al. Tumor-induced anorexia and weight loss are mediated by the TGF-beta superfamily cytokine MIC-1. Nat Med. 2007;13(11):1333-40 DOI: 10.1038/nm1677.
10. Vazeille C, Jouinot A, Durand JP, Neveux N, Boudou-Rouquette P, Huillard O, et al. Relation between hypermetabolism, cachexia, and survival in cancer patients: a prospective study in 390 cancer patients before initiation of anticancer therapy. The American journal of clinical nutrition. 2017;105(5):1139-47 DOI: 10.3945/ajcn.116.140434.
11. Baracos VE, Mackenzie ML. Investigations of branched-chain amino acids and their metabolites in animal models of cancer. The Journal of nutrition. 2006;136(1 Suppl):237s-42s DOI: 10.1093/jn/136.1.237S.
12. Argilés JM. Cancer-associated malnutrition. Eur J Oncol Nurs. 2005;9 Suppl 2:S39-50 DOI: 10.1016/j.ejon.2005.09.006.
13. von Meyenfeldt M. Cancer-associated malnutrition: an introduction. Eur J Oncol Nurs. 2005;9 Suppl 2:S35-8 DOI: 10.1016/j.ejon.2005.09.001.

14. Grober U, Holzhauer P, Kisters K, Holick MF, Adamietz IA. Micronutrients in Oncological Intervention. Nutrients. 2016;8(3):163 DOI: 10.3390/nu8030163.
15. Prado CM, Purcell SA, Laviano A. Nutrition interventions to treat low muscle mass in cancer. Journal of cachexia, sarcopenia and muscle. 2020;11(2):366-80 DOI: 10.1002/jcsm.12525.
16. Fujita S, Dreyer HC, Drummond MJ, Glynn EL, Cadenas JG, Yoshizawa F, et al. Nutrient signalling in the regulation of human muscle protein synthesis. J Physiol. 2007;582(Pt 2):813-23 DOI: 10.1113/jphysiol.2007.134593.
17. Arends J, Bachmann P, Baracos V, Barthelemy N, Bertz H, Bozzetti F, et al. ESPEN guidelines on nutrition in cancer patients. Clinical nutrition (Edinburgh, Scotland). 2017;36(1):11-48 DOI: 10.1016/j.clnu.2016.07.015.
18. Kobayashi H, Kato H, Hirabayashi Y, Murakami H, Suzuki H. Modulations of muscle protein metabolism by branched-chain amino acids in normal and muscle-atrophying rats. The Journal of nutrition. 2006;136(1 Suppl):234S-6S DOI: 10.1093/jn/136.1.234S.
19. Nicastro H, da Luz CR, Chaves DF, Bechara LR, Voltarelli VA, Rogero MM, et al. Does Branched-Chain Amino Acids Supplementation Modulate Skeletal Muscle Remodeling through Inflammation Modulation? Possible Mechanisms of Action. J Nutr Metab. 2012;2012:136937 DOI: 10.1155/2012/136937.
20. Eley HL, Russell ST, Tisdale MJ. Effect of branched-chain amino acids on muscle atrophy in cancer cachexia. The Biochemical journal. 2007;407(1):113-20 DOI: 10.1042/bj20070651.
21. Peters SJ, van Helvoort A, Kegler D, Argiles JM, Luiking YC, Laviano A, et al. Dose-dependent effects of leucine supplementation on preservation of muscle mass in cancer cachectic mice. Oncology reports. 2011;26(1):247-54 DOI: 10.3892/or.2011.1269.
22. Ventrucci G, Mello MA, Gomes-Marcondes MC. Leucine-rich diet alters the eukaryotic translation initiation factors expression in skeletal muscle of tumour-bearing rats. BMC cancer. 2007;7:42 DOI: 10.1186/1471-2407-7-42.
23. Cruz B, Gomes-Marcondes MC. Leucine-rich diet supplementation modulates foetal muscle protein metabolism impaired by Walker-256 tumour. Reproductive biology and endocrinology : RB&E. 2014;12:2 DOI: 10.1186/1477-7827-12-2.
24. Viana LR, Canevarolo R, Luiz AC, Soares RF, Lubaczeuski C, Zeri AC, et al. Leucine-rich diet alters the (1)H-NMR based metabolomic profile without changing the Walker-256 tumour mass in rats. BMC cancer. 2016;16(1):764 DOI: 10.1186/s12885-016-2811-2.
25. Cruz B, Oliveira A, Gomes-Marcondes MCC. L-leucine dietary supplementation modulates muscle protein degradation and increases pro-inflammatory cytokines in tumour-bearing rats. Cytokine. 2017;96:253-60 DOI: 10.1016/j.cyto.2017.04.019.
26. Ventrucci G, Ramos Silva LG, Roston Mello MA, Gomes Marcondes MC. Effects of a leucine-rich diet on body composition during nutritional recovery in rats. Nutrition (Burbank, Los Angeles County, Calif). 2004;20(2):213-7 DOI: 10.1016/j.nut.2003.10.014.
27. Gomes-Marcondes MC, Ventrucci G, Toledo MT, Cury L, Cooper JC. A leucine-supplemented diet improved protein content of skeletal muscle in young tumor-bearing rats. Brazilian journal of medical and biological research = Revista brasileira de pesquisas medicas e biologicas. 2003;36(11):1589-94 DOI: 10.1590/s0100-879x2003001100017.
28. Nissen SL, Abumrad NN. Nutritional role of the leucine metabolite β-hydroxy β-methylbutyrate (HMB). The Journal of nutritional biochemistry. 1997;8(6):300-11.

29. Van Koevering M, Nissen S. Oxidation of leucine and alpha-ketoisocaproate to beta-hydroxy-beta-methylbutyrate in vivo. The American journal of physiology. 1992;262(1 Pt 1):E27-31 DOI: 10.1152/ajpendo.1992.262.1.E27.
30. Wilson GJ, Wilson JM, Manninen AH. Effects of beta-hydroxy-beta-methylbutyrate (HMB) on exercise performance and body composition across varying levels of age, sex, and training experience: A review. Nutr Metab (Lond). 2008;5:1 DOI: 10.1186/1743-7075-5-1.
31. Mirza KA, Pereira SL, Voss AC, Tisdale MJ. Comparison of the anticatabolic effects of leucine and Ca-beta-hydroxy-beta-methylbutyrate in experimental models of cancer cachexia. Nutrition (Burbank, Los Angeles County, Calif). 2014;30(7-8):807-13 DOI: 10.1016/j.nut.2013.11.012.
32. Smith HJ, Mukerji P, Tisdale MJ. Attenuation of proteasome-induced proteolysis in skeletal muscle by {beta}-hydroxy-{beta}-methylbutyrate in cancer-induced muscle loss. Cancer research. 2005;65(1):277-83.
33. Nunes EA, Kuczera D, Brito GA, Bonatto SJ, Yamazaki RK, Tanhoffer RA, et al. Beta-hydroxy-beta-methylbutyrate supplementation reduces tumor growth and tumor cell proliferation ex vivo and prevents cachexia in Walker 256 tumor-bearing rats by modifying nuclear factor-kappaB expression. Nutrition research (New York, NY). 2008;28(7):487-93 DOI: 10.1016/j.nutres.2008.04.006.
34. Aversa Z, Bonetto A, Costelli P, Minero VG, Penna F, Baccino FM, et al. beta-hydroxy-beta-methylbutyrate (HMB) attenuates muscle and body weight loss in experimental cancer cachexia. International journal of oncology. 2011;38(3):713-20 DOI: 10.3892/ijo.2010.885.
35. Bode BP, Fischer C, Abcouwer S, Wasa M, Souba WW. Glutamine and Cancer Cachexia. Protein and Amino Acid Metabolism in Cancer Cachexia. Berlin, Heidelberg: Springer Berlin Heidelberg; 1996. p. 139-70.
36. Newsholme P, Lima MM, Procopio J, Pithon-Curi TC, Doi SQ, Bazotte RB, et al. Glutamine and glutamate as vital metabolites. Brazilian journal of medical and biological research = Revista brasileira de pesquisas medicas e biologicas. 2003;36(2):153-63 DOI: 10.1590/s0100-879x2003000200002.
37. Newsholme P, Procopio J, Lima MM, Pithon-Curi TC, Curi R. Glutamine and glutamate--their central role in cell metabolism and function. Cell Biochem Funct. 2003;21(1):1-9 DOI: 10.1002/cbf.1003.
38. Yu JC, Jiang ZM, Li DM. Glutamine: a precursor of glutathione and its effect on liver. World journal of gastroenterology. 1999;5(2):143-6 DOI: 10.3748/wjg.v5.i2.143.
39. Fracaro L, Frez F, Silva B, Vicentini G, de Souza S, Martins H, et al. Walker 256 tumor-bearing rats demonstrate altered interstitial cells of Cajal. Effects on ICC in the Walker 256 tumor model. Neurogastroenterology & Motility. 2016;28(1):101-15.
40. Martins HA, Sehaber CC, Hermes-Uliana C, Mariani FA, Guarnier FA, Vicentini GE, et al. Supplementation with l-glutamine prevents tumor growth and cancer-induced cachexia as well as restores cell proliferation of intestinal mucosa of Walker-256 tumor-bearing rats. Amino Acids. 2016;48(12):2773-84 DOI: 10.1007/s00726-016-2313-1.
41. Martins HA, Bazotte RB, Vicentini GE, Lima MM, Guarnier FA, Hermes-Uliana C, et al. l-Glutamine supplementation promotes an improved energetic balance in Walker-256 tumor-bearing rats. Tumour biology : the journal of the International Society for Oncodevelopmental Biology and Medicine. 2017;39(3):1010428317695960 DOI: 10.1177/1010428317695960.

42. Vicentini GE, Fracaro L, de Souza SR, Martins HA, Guarnier FA, Zanoni JN. Experimental Cancer Cachexia Changes Neuron Numbers and Peptide Levels in the Intestine: Partial Protective Effects after Dietary Supplementation with L-Glutamine. PloS one. 2016;11(9):e0162998 DOI: 10.1371/journal.pone.0162998.
43. Vicentini GE, Martins HA, Fracaro L, de Souza SRG, da Silva Zanoni KP, Silva TNX, et al. Does l-glutamine-supplemented diet extenuate NO-mediated damage on myenteric plexus of Walker 256 tumor-bearing rats? Food research international (Ottawa, Ont). 2017;101:24-34 DOI: 10.1016/j.foodres.2017.08.054.
44. Lima MMR, de Mello MAR, Curi R. Walker 256 tumour growth causes marked changes of glutamine metabolism in rat small intestine. Cell biochemistry and function. 2002;20(2):107-13.
45. Zhong Z, Wheeler MD, Li X, Froh M, Schemmer P, Yin M, et al. L-Glycine: a novel antiinflammatory, immunomodulatory, and cytoprotective agent. Current opinion in clinical nutrition and metabolic care. 2003;6(2):229-40 DOI: 10.1097/00075197-200303000-00013.
46. Rose ML, Cattley RC, Dunn C, Wong V, Li X, Thurman RG. Dietary glycine prevents the development of liver tumors caused by the peroxisome proliferator WY-14,643. Carcinogenesis. 1999;20(11):2075-81 DOI: 10.1093/carcin/20.11.2075.
47. Rose ML, Madren J, Bunzendahl H, Thurman RG. Dietary glycine inhibits the growth of B16 melanoma tumors in mice. Carcinogenesis. 1999;20(5):793-8 DOI: 10.1093/carcin/20.5.793.
48. Ham DJ, Murphy KT, Chee A, Lynch GS, Koopman R. Glycine administration attenuates skeletal muscle wasting in a mouse model of cancer cachexia. Clinical nutrition (Edinburgh, Scotland). 2014;33(3):448-58 DOI: 10.1016/j.clnu.2013.06.013.
49. Morris SM, Jr. Regulation of enzymes of urea and arginine synthesis. Annu Rev Nutr. 1992;12:81-101 DOI: 10.1146/annurev.nu.12.070192.000501.
50. Delage B, Fennell DA, Nicholson L, McNeish I, Lemoine NR, Crook T, et al. Arginine deprivation and argininosuccinate synthetase expression in the treatment of cancer. International journal of cancer. 2010;126(12):2762-72 DOI: 10.1002/ijc.25202.
51. Crowell JA, Steele VE, Sigman CC, Fay JR. Is inducible nitric oxide synthase a target for chemoprevention? Mol Cancer Ther. 2003;2(8):815-23.
52. Szende B, Tyihák E, Trézl L. Role of arginine and its methylated derivatives in cancer biology and treatment. Cancer cell international. 2001;1(1):3 DOI: 10.1186/1475-2867-1-3.
53. Yerushalmi HF, Besselsen DG, Ignatenko NA, Blohm-Mangone KA, Padilla-Torres JL, Stringer DE, et al. Role of polyamines in arginine-dependent colon carcinogenesis in ApcMin/+ mice. Molecular Carcinogenesis. 2006;45(10):764-73 DOI: 10.1002/mc.20246.
54. Carreiro AL, Buhman KK. Chapter 3 - Absorption of Dietary Fat and Its Metabolism in Enterocytes. In: Patel VB, editor. The Molecular Nutrition of Fats: Academic Press; 2019. p. 33-48.
55. Allen BG, Bhatia SK, Anderson CM, Eichenberger-Gilmore JM, Sibenaller ZA, Mapuskar KA, et al. Ketogenic diets as an adjuvant cancer therapy: History and potential mechanism. Redox Biology. 2014;2:963-70 DOI: https://doi.org/10.1016/j.redox.2014.08.002.
56. Liberti MV, Locasale JW. The Warburg Effect: How Does it Benefit Cancer Cells? Trends Biochem Sci. 2016;41(3):211-8 DOI: 10.1016/j.tibs.2015.12.001.

57. Tisdale MJ, Brennan RA, Fearon KC. Reduction of weight loss and tumour size in a cachexia model by a high fat diet. British journal of cancer. 1987;56(1):39-43 DOI: 10.1038/bjc.1987.149.
58. Beck SA, Tisdale MJ. Nitrogen excretion in cancer cachexia and its modification by a high fat diet in mice. Cancer research. 1989;49(14):3800-4.
59. Nakamura K, Tonouchi H, Sasayama A, Ashida K. A Ketogenic Formula Prevents Tumor Progression and Cancer Cachexia by Attenuating Systemic Inflammation in Colon 26 Tumor-Bearing Mice. Nutrients. 2018;10(2) DOI: 10.3390/nu10020206.
60. Kwiterovich J, Peter O., Vining EPG, Pyzik P, Skolasky J, Richard, Freeman JM. Effect of a High-Fat Ketogenic Diet on Plasma Levels of Lipids, Lipoproteins, and Apolipoproteins in Children. JAMA. 2003;290(7):912-20 DOI: 10.1001/jama.290.7.912.
61. Creighton BC, Hyde PN, Maresh CM, Kraemer WJ, Phinney SD, Volek JS. Paradox of hypercholesterolaemia in highly trained, keto-adapted athletes. BMJ Open Sport & Exercise Medicine. 2018;4(1):e000429 DOI: 10.1136/bmjsem-2018-000429.
62. Groesbeck DK, Bluml RM, Kossoff EH. Long-term use of the ketogenic diet in the treatment of epilepsy. Dev Med Child Neurol. 2006;48(12):978-81 DOI: 10.1017/s0012162206002143.
63. Tisdale MJ. Mechanisms of cancer cachexia. Physiol Rev. 2009;89(2):381-410 DOI: 10.1152/physrev.00016.2008.
64. Das SK, Hoefler G. The role of triglyceride lipases in cancer associated cachexia. Trends in molecular medicine. 2013;19(5):292-301 DOI: 10.1016/j.molmed.2013.02.006.
65. Das SK, Eder S, Schauer S, Diwoky C, Temmel H, Guertl B, et al. Adipose triglyceride lipase contributes to cancer-associated cachexia. Science (New York, NY). 2011;333(6039):233-8 DOI: 10.1126/science.1198973.
66. Stephens NA, Skipworth RJ, Macdonald AJ, Greig CA, Ross JA, Fearon KC. Intramyocellular lipid droplets increase with progression of cachexia in cancer patients. Journal of cachexia, sarcopenia and muscle. 2011;2(2):111-7 DOI: 10.1007/s13539-011-0030-x.
67. Fernandes G, Venkatraman JT. Role of omega-3 fatty acids in health and disease. Nutrition Research. 1993;13:S19-S45 DOI: https://doi.org/10.1016/S0271-5317(05)80282-9.
68. Sijben JW, Calder PC. Differential immunomodulation with long-chain n-3 PUFA in health and chronic disease. The Proceedings of the Nutrition Society. 2007;66(2):237-59 DOI: 10.1017/S0029665107005472.
69. Yates CM, Calder PC, Ed Rainger G. Pharmacology and therapeutics of omega-3 polyunsaturated fatty acids in chronic inflammatory disease. Pharmacology & therapeutics. 2014;141(3):272-82 DOI: https://doi.org/10.1016/j.pharmthera.2013.10.010.
70. Tisdale MJ, Dhesi JK. Inhibition of weight loss by omega-3 fatty acids in an experimental cachexia model. Cancer research. 1990;50(16):5022-6.
71. Pizato N, Bonatto S, Yamazaki RK, Aikawa J, Nogata C, Mund RC, et al. Ratio of n6 to n-3 fatty acids in the diet affects tumor growth and cachexia in Walker 256 tumor-bearing rats. Nutrition and cancer. 2005;53(2):194-201 DOI: 10.1207/s15327914nc5302_8.

72. Coelho I, Casare F, Pequito DC, Borghetti G, Yamazaki RK, Brito GA, et al. Fish oil supplementation reduces cachexia and tumor growth while improving renal function in tumor-bearing rats. Lipids. 2012;47(11):1031-41 DOI: 10.1007/s11745-012-3715-9.
73. Togni V, Ota CC, Folador A, Junior OT, Aikawa J, Yamazaki RK, et al. Cancer cachexia and tumor growth reduction in Walker 256 tumor-bearing rats supplemented with N-3 polyunsaturated fatty acids for one generation. Nutrition and cancer. 2003;46(1):52-8 DOI: 10.1207/s15327914nc4601_07.
74. Fernandez R, Piechnik J, Fabris R, Malnic G, Fernandes LC. Effect of chronic fish oil supplementation on renal function of normal and cachectic rats. Brazilian journal of medical and biological research = Revista brasileira de pesquisas medicas e biologicas. 2004;37(10):1481-9 DOI: 10.1590/s0100-879x2004001000006.
75. Dumas JF, Goupille C, Pinault M, Fandeur L, Bougnoux P, Servais S, et al. n-3 PUFA-enriched diet delays the occurrence of cancer cachexia in rat with peritoneal carcinosis. Nutrition and cancer. 2010;62(3):343-50 DOI: 10.1080/01635580903407080.
76. Iagher F, de Brito Belo SR, Naliwaiko K, Franzoi AM, de Brito GA, Yamazaki RK, et al. Chronic supplementation with shark liver oil for reducing tumor growth and cachexia in walker 256 tumor-bearing rats. Nutrition and cancer. 2011;63(8):1307-15 DOI: 10.1080/01635581.2011.607540.
77. Iagher F, de Brito Belo SR, Souza WM, Nunes JR, Naliwaiko K, Sassaki GL, et al. Antitumor and anti-cachectic effects of shark liver oil and fish oil: comparison between independent or associative chronic supplementation in Walker 256 tumor-bearing rats. Lipids in health and disease. 2013;12:146 DOI: 10.1186/1476-511x-12-146.
78. Beck SA, Smith KL, Tisdale MJ. Anticachectic and antitumor effect of eicosapentaenoic acid and its effect on protein turnover. Cancer research. 1991;51(22):6089-93.
79. Tisdale MJ, Beck SA. Inhibition of tumour-induced lipolysis in vitro and cachexia and tumour growth in vivo by eicosapentaenoic acid. Biochemical pharmacology. 1991;41(1):103-7 DOI: 10.1016/0006-2952(91)90016-x.
80. Hudson EA, Tisdale MJ. Comparison of the effectiveness of eicosapentaenoic acid administered as either the free acid or ethyl ester as an anticachectic and antitumour agent. Prostaglandins, leukotrienes, and essential fatty acids. 1994;51(2):141-5 DOI: 10.1016/0952-3278(94)90090-6.
81. Whitehouse AS, Smith HJ, Drake JL, Tisdale MJ. Mechanism of attenuation of skeletal muscle protein catabolism in cancer cachexia by eicosapentaenoic acid. Cancer research. 2001;61(9):3604-9.
82. Smith HJ, Greenberg NA, Tisdale MJ. Effect of eicosapentaenoic acid, protein and amino acids on protein synthesis and degradation in skeletal muscle of cachectic mice. British journal of cancer. 2004;91(2):408-12 DOI: 10.1038/sj.bjc.6601981.
83. Du L, Yang YH, Wang YM, Xue CH, Kurihara H, Takahashi K. EPA-enriched phospholipids ameliorate cancer-associated cachexia mainly via inhibiting lipolysis. Food & function. 2015;6(12):3652-62 DOI: 10.1039/c5fo00478k.
84. Fini L, Piazzi G, Ceccarelli C, Daoud Y, Belluzzi A, Munarini A, et al. Highly purified eicosapentaenoic acid as free fatty acids strongly suppresses polyps in Apc(Min/+) mice. Clinical cancer research : an official journal of the American Association for Cancer Research. 2010;16(23):5703-11 DOI: 10.1158/1078-0432.ccr-10-1990.

85. Jho DH, Babcock TA, Tevar R, Helton WS, Espat NJ. Eicosapentaenoic acid supplementation reduces tumor volume and attenuates cachexia in a rat model of progressive non-metastasizing malignancy. JPEN Journal of parenteral and enteral nutrition. 2002;26(5):291-7 DOI: 10.1177/0148607102026005291.
86. Dagnelie PC, Bell JD, Williams SC, Bates TE, Abel PD, Foster CS. Effect of fish oil on cancer cachexia and host liver metabolism in rats with prostate tumors. Lipids. 1994;29(3):195-203 DOI: 10.1007/bf02536729.
87. Russell ST, Tisdale MJ. Effect of eicosapentaenoic acid (EPA) on expression of a lipid mobilizing factor in adipose tissue in cancer cachexia. Prostaglandins, leukotrienes, and essential fatty acids. 2005;72(6):409-14 DOI: 10.1016/j.plefa.2005.03.002.
88. Pariza MW, Ha YL. Conjugated dienoic derivatives of linoleic acid: A new class of anticarcinogens. Medical Oncology and Tumor Pharmacotherapy. 1990;7(2):169-71 DOI: 10.1007/BF02988544.
89. Lee KW, Lee HJ, Cho HY, Kim YJ. Role of the conjugated linoleic acid in the prevention of cancer. Crit Rev Food Sci Nutr. 2005;45(2):135-44 DOI: 10.1080/10408690490911800.
90. Ip MM, Masso-Welch PA, Ip C. Prevention of mammary cancer with conjugated linoleic acid: role of the stroma and the epithelium. J Mammary Gland Biol Neoplasia. 2003;8(1):103-18 DOI: 10.1023/a:1025739506536.
91. Pariza MW, Park Y, Cook ME. Conjugated linoleic acid and the control of cancer and obesity. Toxicol Sci. 1999;52(2 Suppl):107-10 DOI: 10.1093/toxsci/52.suppl_1.107.
92. Yang M, Cook ME. Dietary conjugated linoleic acid decreased cachexia, macrophage tumor necrosis factor-alpha production, and modifies splenocyte cytokines production. Experimental biology and medicine (Maywood, NJ). 2003;228(1):51-8 DOI: 10.1177/153537020322800107.
93. Graves E, Hitt A, Pariza MW, Cook ME, McCarthy DO. Conjugated linoleic acid preserves gastrocnemius muscle mass in mice bearing the colon-26 adenocarcinoma. Research in nursing & health. 2005;28(1):48-55 DOI: 10.1002/nur.20052.
94. McCarthy DO, Graves E. Conjugated linoleic acid preserves muscle mass in mice bearing the Lewis lung carcinoma, but not the B16 melanoma. Research in nursing & health. 2006;29(2):98-104 DOI: 10.1002/nur.20115.
95. Tian M, Kliewer KL, Asp ML, Stout MB, Belury MA. c9t11-Conjugated linoleic acid-rich oil fails to attenuate wasting in colon-26 tumor-induced late-stage cancer cachexia in male CD2F1 mice. Molecular nutrition & food research. 2011;55(2):268-77 DOI: 10.1002/mnfr.201000176.
96. Gonçalves DC, Lira FS, Yamashita AS, Carnevali Junior LC, Eder R, Laviano A, et al. Liver lipid metabolism disruption in cancer cachexia is aggravated by cla supplementation -induced inflammation. Clinical Nutrition. 2019;38(5):2219-30 DOI: https://doi.org/10.1016/j.clnu.2018.09.023.
97. Bremer J. Carnitine--metabolism and functions. Physiol Rev. 1983;63(4):1420-80 DOI: 10.1152/physrev.1983.63.4.1420.
98. Longo N, Frigeni M, Pasquali M. Carnitine transport and fatty acid oxidation. Biochim Biophys Acta. 2016;1863(10):2422-35 DOI: 10.1016/j.bbamcr.2016.01.023.

99. Busquets S, Serpe R, Toledo M, Betancourt A, Marmonti E, Orpi M, et al. L-Carnitine: an adequate supplement for a multi-targeted anti-wasting therapy in cancer. Clinical nutrition (Edinburgh, Scotland). 2012;31(6):889-95 DOI: 10.1016/j.clnu.2012.03.005.
100. Busquets S, Perez-Peiro M, Salazar-Degracia A, Argiles JM, Serpe R, Rojano-Toimil A, et al. Differential structural features in soleus and gastrocnemius of carnitine-treated cancer cachectic rats. Journal of cellular physiology. 2020;235(1):526-37 DOI: 10.1002/jcp.28992.
101. Liu S, Wu H-J, Zhang Z-Q, Chen Q, Liu B, Wu J-P, et al. L-carnitine ameliorates cancer cachexia in mice by regulating the expression and activity of carnitine palmityl transferase. Cancer Biology & Therapy. 2011;12(2):125-30 DOI: 10.4161/cbt.12.2.15717.
102. Silverio R, Laviano A, Rossi Fanelli F, Seelaender M. L-Carnitine induces recovery of liver lipid metabolism in cancer cachexia. Amino Acids. 2012;42(5):1783-92 DOI: 10.1007/s00726-011-0898-y.
103. Wallimann T, Tokarska-Schlattner M, Schlattner U. The creatine kinase system and pleiotropic effects of creatine. Amino Acids. 2011;40(5):1271-96 DOI: 10.1007/s00726-011-0877-3.
104. Gualano B, Roschel H, Lancha-Jr AH, Brightbill CE, Rawson ES. In sickness and in health: the widespread application of creatine supplementation. Amino Acids. 2012;43(2):519-29 DOI: 10.1007/s00726-011-1132-7.
105. Harris RC, Söderlund K, Hultman E. Elevation of creatine in resting and exercised muscle of normal subjects by creatine supplementation. Clinical Science. 1992;83(3):367-74 DOI: 10.1042/cs0830367.
106. Terjung RL, Clarkson P, Eichner ER, Greenhaff PL, Hespel PJ, Israel RG, et al. American College of Sports Medicine roundtable. The physiological and health effects of oral creatine supplementation. Med Sci Sports Exerc. 2000;32(3):706-17 DOI: 10.1097/00005768-200003000-00024.
107. Buford TW, Kreider RB, Stout JR, Greenwood M, Campbell B, Spano M, et al. International Society of Sports Nutrition position stand: creatine supplementation and exercise. Journal of the International Society of Sports Nutrition. 2007;4(1):6 DOI: 10.1186/1550-2783-4-6.
108. Louis M, Lebacq J, Poortmans JR, Belpaire-Dethiou MC, Devogelaer JP, Van Hecke P, et al. Beneficial effects of creatine supplementation in dystrophic patients. Muscle & Nerve: Official Journal of the American Association of Electrodiagnostic Medicine. 2003;27(5):604-10.
109. Chung YI, Alexanderson H, Pipitone N, Morrison C, Dastmalchi M, Ståhl-Hallengren C, et al. Creatine supplements in patients with idiopathic inflammatory myopathies who are clinically weak after conventional pharmacologic treatment: Six-month, double-blind, randomized, placebo-controlled trial. Arthritis Care & Research. 2007;57(4):694-702.
110. Kley R, Tarnopolsky M, Vorgerd M. Creatine treatment in muscle disorders: a meta-analysis of randomised controlled trials. Journal of Neurology, Neurosurgery & Psychiatry. 2008;79(4):366-7.
111. Santos R, Bassit R, Caperuto E, Rosa LC. The effect of creatine supplementation upon inflammatory and muscle soreness markers after a 30km race. Life sciences. 2004;75(16):1917-24.
112. Bassit R, Curi R, Rosa LC. Creatine supplementation reduces plasma levels of pro-inflammatory cytokines and PGE 2 after a half-ironman competition. Amino acids. 2008;35(2):425-31.

113. Campos-Ferraz PL, Gualano B, das Neves W, Andrade IT, Hangai I, Pereira RT, et al. Exploratory studies of the potential anti-cancer effects of creatine. Amino Acids. 2016;48(8):1993-2001 DOI: 10.1007/s00726-016-2180-9.
114. Cella PS, Marinello PC, Borges FH, Ribeiro DF, Chimin P, Testa MTJ, et al. Creatine supplementation in Walker-256 tumor-bearing rats prevents skeletal muscle atrophy by attenuating systemic inflammation and protein degradation signaling. European journal of nutrition. 2020;59(2):661-9 DOI: 10.1007/s00394-019-01933-6.
115. Deminice R, Cella PS, Padilha CS, Borges FH, da Silva LE, Campos-Ferraz PL, et al. Creatine supplementation prevents hyperhomocysteinemia, oxidative stress and cancer-induced cachexia progression in Walker-256 tumor-bearing rats. Amino Acids. 2016;48(8):2015-24 DOI: 10.1007/s00726-016-2172-9.
116. Kumar S, Pandey AK. Chemistry and Biological Activities of Flavonoids: An Overview. The Scientific World Journal. 2013;2013:162750 DOI: 10.1155/2013/162750.
117. Velázquez KT, Enos RT, Narsale AA, Puppa MJ, Davis JM, Murphy EA, et al. Quercetin supplementation attenuates the progression of cancer cachexia in ApcMin/+ mice. The Journal of nutrition. 2014;144(6):868-75 DOI: 10.3945/jn.113.188367.
118. Camargo CA, da Silva ME, da Silva RA, Justo GZ, Gomes-Marcondes MC, Aoyama H. Inhibition of tumor growth by quercetin with increase of survival and prevention of cachexia in Walker 256 tumor-bearing rats. Biochemical and biophysical research communications. 2011;406(4):638-42 DOI: 10.1016/j.bbrc.2011.02.111.
119. Wang H, Lai YJ, Chan YL, Li TL, Wu CJ. Epigallocatechin-3-gallate effectively attenuates skeletal muscle atrophy caused by cancer cachexia. Cancer letters. 2011;305(1):40-9 DOI: 10.1016/j.canlet.2011.02.023.
120. Hirasaka K, Saito S, Yamaguchi S, Miyazaki R, Wang Y, Haruna M, et al. Dietary Supplementation with Isoflavones Prevents Muscle Wasting in Tumor-Bearing Mice. Journal of nutritional science and vitaminology. 2016;62(3):178-84 DOI: 10.3177/jnsv.62.178.
121. Yoshimura T, Saitoh K, Sun L, Wang Y, Taniyama S, Yamaguchi K, et al. Morin suppresses cachexia-induced muscle wasting by binding to ribosomal protein S10 in carcinoma cells. Biochemical and biophysical research communications. 2018;506(4):773-9 DOI: 10.1016/j.bbrc.2018.10.184.
122. Sales JM, Resurreccion AV. Resveratrol in peanuts. Crit Rev Food Sci Nutr. 2014;54(6):734-70 DOI: 10.1080/10408398.2011.606928.
123. Carbó N, Costelli P, Baccino FM, López-Soriano FJ, Argilés JM. Resveratrol, a natural product present in wine, decreases tumour growth in a rat tumour model. Biochemical and biophysical research communications. 1999;254(3):739-43 DOI: 10.1006/bbrc.1998.9916.
124. Wyke SM, Russell ST, Tisdale MJ. Induction of proteasome expression in skeletal muscle is attenuated by inhibitors of NF-kappaB activation. British journal of cancer. 2004;91(9):1742-50 DOI: 10.1038/sj.bjc.6602165.
125. Shadfar S, Couch ME, McKinney KA, Weinstein LJ, Yin X, Rodriguez JE, et al. Oral resveratrol therapy inhibits cancer-induced skeletal muscle and cardiac atrophy in vivo. Nutrition and cancer. 2011;63(5):749-62 DOI: 10.1080/01635581.2011.563032.

126. Busquets S, Fuster G, Ametller E, Olivan M, Figueras M, Costelli P, et al. Resveratrol does not ameliorate muscle wasting in different types of cancer cachexia models. Clinical nutrition (Edinburgh, Scotland). 2007;26(2):239-44 DOI: 10.1016/j.clnu.2006.12.001.
127. Sergides C, Chirilă M, Silvestro L, Pitta D, Pittas A. Bioavailability and safety study of resveratrol 500 mg tablets in healthy male and female volunteers. Exp Ther Med. 2016;11(1):164-70 DOI: 10.3892/etm.2015.2895.
128. Almeida L, Vaz-da-Silva M, Falcão A, Soares E, Costa R, Loureiro AI, et al. Pharmacokinetic and safety profile of trans-resveratrol in a rising multiple-dose study in healthy volunteers. Molecular nutrition & food research. 2009;53 Suppl 1:S7-15 DOI: 10.1002/mnfr.200800177.
129. Roberfroid M. Prebiotics: The Concept Revisited. The Journal of nutrition. 2007;137(3):830S-7S DOI: 10.1093/jn/137.3.830S.
130. Vos AP, Haarman M, Buco A, Govers M, Knol J, Garssen J, et al. A specific prebiotic oligosaccharide mixture stimulates delayed-type hypersensitivity in a murine influenza vaccination model. International immunopharmacology. 2006;6(8):1277-86 DOI: 10.1016/j.intimp.2006.03.010.
131. Vos AP, M'Rabet L, Stahl B, Boehm G, Garssen J. Immune-modulatory effects and potential working mechanisms of orally applied nondigestible carbohydrates. Crit Rev Immunol. 2007;27(2):97-140 DOI: 10.1615/critrevimmunol.v27.i2.10.
132. Bruzzese E, VOLPICELLI M, Salvini F, Bisceglia M, Lionetti P, Cinquetti M, et al. EARLY ADMINISTRATION OF GOS/FOS PREVENTS INTESTINAL AND RESPIRATORY INFECTIONS IN INFANTS. Journal of Pediatric Gastroenterology and Nutrition. 2006;42(5):E95.
133. Xiao L, van't Land B, van de Worp WRPH, Stahl B, Folkerts G, Garssen J. Early-Life Nutritional Factors and Mucosal Immunity in the Development of Autoimmune Diabetes. Frontiers in immunology. 2017;8(1219) DOI: 10.3389/fimmu.2017.01219.
134. den Besten G, van Eunen K, Groen AK, Venema K, Reijngoud DJ, Bakker BM. The role of short-chain fatty acids in the interplay between diet, gut microbiota, and host energy metabolism. J Lipid Res. 2013;54(9):2325-40 DOI: 10.1194/jlr.R036012.
135. Bindels LB, Neyrinck AM, Claus SP, Le Roy CI, Grangette C, Pot B, et al. Synbiotic approach restores intestinal homeostasis and prolongs survival in leukaemic mice with cachexia. Isme j. 2016;10(6):1456-70 DOI: 10.1038/ismej.2015.209.
136. Schwabe RF, Jobin C. The microbiome and cancer. Nature reviews Cancer. 2013;13(11):800-12 DOI: 10.1038/nrc3610.
137. Garrett WS. Cancer and the microbiota. Science (New York, NY). 2015;348(6230):80 DOI: 10.1126/science.aaa4972.
138. Gorselink M, van Helvoort ALB, Hageman RJJ, inventors; Nutricia NV, assignee. Use of dietary fibres against muscle wasting2006.
139. Bindels LB, Neyrinck AM, Salazar N, Taminiau B, Druart C, Muccioli GG, et al. Non Digestible Oligosaccharides Modulate the Gut Microbiota to Control the Development of Leukemia and Associated Cachexia in Mice. PloS one. 2015;10(6):e0131009 DOI: 10.1371/journal.pone.0131009.
140. van Norren K, Kegler D, Argiles JM, Luiking Y, Gorselink M, Laviano A, et al. Dietary supplementation with a specific combination of high protein, leucine, and fish oil improves muscle function and daily activity in tumour-bearing cachectic mice. British journal of cancer. 2009;100(5):713-22 DOI: 10.1038/sj.bjc.6604905.

141. Faber J, Vos P, Kegler D, van Norren K, Argiles JM, Laviano A, et al. Beneficial immune modulatory effects of a specific nutritional combination in a murine model for cancer cachexia. British journal of cancer. 2008;99(12):2029-36 DOI: 10.1038/sj.bjc.6604785.
142. Faber J, van Limpt K, Kegler D, Luiking Y, Garssen J, van Helvoort A, et al. Bacterial translocation is reduced by a specific nutritional combination in mice with chemotherapy-induced neutropenia. The Journal of nutrition. 2011;141(7):1292-8 DOI: 10.3945/jn.110.136986.
143. Awa H, Futamura A, Higashiguchi T, Ito A, Mori N, Murai M, et al. Effects of Combined Treatment with Branched-Chain Amino Acids, Citric Acid, L-Carnitine, Coenzyme Q10, Zinc, and Various Vitamins in Tumor-Bearing Mice. Biological & pharmaceutical bulletin. 2017;40(3):266-71 DOI: 10.1248/bpb.b16-00638.
144. Liu YM, Chan YL, Wu TH, Li TL, Hsia S, Chiu YH, et al. Antitumor, Inhibition of Metastasis and Radiosensitizing Effects of Total Nutrition Formula on Lewis Tumor-Bearing Mice. Nutrients. 2019;11(8) DOI: 10.3390/nu11081944.
145. Giles K, Guan C, Jagoe TR, Mazurak V. Diet composition as a source of variation in experimental animal models of cancer cachexia. Journal of cachexia, sarcopenia and muscle. 2016;7(2):110-25 DOI: 10.1002/jcsm.12058.
146. Abramson EC, Kukla LJ, Shevrin DH, Lad TE, McGuire WP, Kukreja SC. A model for malignancy-associated humoral hypercalcemia. Calcified tissue international. 1984;36(5):563-7 DOI: 10.1007/bf02405367.
147. The importance of a proper control diet [press release]. www.ResearchDiets.com2013.
148. Suzuki T, Von Haehling S, Springer J. Promising models for cancer-induced cachexia drug discovery. Expert Opinion on Drug Discovery. 2020;15(5):627-37 DOI: 10.1080/17460441.2020.1724954.
149. Michaelis KA, Zhu X, Burfeind KG, Krasnow SM, Levasseur PR, Morgan TK, et al. Establishment and characterization of a novel murine model of pancreatic cancer cachexia. Journal of cachexia, sarcopenia and muscle. 2017;8(5):824-38 DOI: 10.1002/jcsm.12225.
150. Kirsch DG, Grimm J, Guimaraes AR, Wojtkiewicz GR, Perez BA, Santiago PM, et al. Imaging primary lung cancers in mice to study radiation biology. Int J Radiat Oncol Biol Phys. 2010;76(4):973-7 DOI: 10.1016/j.ijrobp.2009.11.038.
151. Iglesias VS, Hoof SJv, Vaniqui A, Schyns LE, Lieuwes N, Yaromina A, et al. An orthotopic non-small cell lung cancer model for image-guided small animal radiotherapy platforms. The British Journal of Radiology. 2019;92(1095):20180476 DOI: 10.1259/bjr.20180476.
152. Park SS, Chunta JL, Robertson JM, Martinez AA, Oliver Wong CY, Amin M, et al. MicroPET/CT imaging of an orthotopic model of human glioblastoma multiforme and evaluation of pulsed low-dose irradiation. Int J Radiat Oncol Biol Phys. 2011;80(3):885-92 DOI: 10.1016/j.ijrobp.2011.01.045.
153. van der Heyden B, van de Worp WR, van Helvoort A, Theys J, Schols AM, Langen RC, et al. Automated CT-derived skeletal muscle mass determination in lower hind limbs of mice using a 3D U-Net deep learning network. Journal of Applied Physiology. 2020;128(1):42-9.
154. Op den Kamp CM, De Ruysscher DK, van den Heuvel M, Elferink M, Houben RM, Oberije CJ, et al. Early body weight loss during concurrent chemo-radiotherapy for non-small cell lung cancer. Journal of cachexia, sarcopenia and muscle. 2014;5(2):127-37 DOI: 10.1007/s13539-013-0127-5.

155. Sanders KJC, Hendriks LE, Troost EGC, Bootsma GP, Houben RMA, Schols AMWJ, et al. Early Weight Loss during Chemoradiotherapy Has a Detrimental Impact on Outcome in NSCLC. Journal of Thoracic Oncology. 2016;11(6):873-9 DOI: 10.1016/j.jtho.2016.02.013.
156. Le Bricon T, Gugins S, Cynober L, Baracos VE. Negative impact of cancer chemotherapy on protein metabolism in healthy and tumor-bearing rats. Metabolism: clinical and experimental. 1995;44(10):1340-8 DOI: 10.1016/0026-0495(95)90040-3.
157. Damrauer JS, Stadler ME, Acharyya S, Baldwin AS, Couch ME, Guttridge DC. Chemotherapy-induced muscle wasting: association with NF-κB and cancer cachexia. Eur J Transl Myol. 2018;28(2):7590 DOI: 10.4081/ejtm.2018.7590.
158. Pin F, Barreto R, Couch ME, Bonetto A, O'Connell TM. Cachexia induced by cancer and chemotherapy yield distinct perturbations to energy metabolism. Journal of cachexia, sarcopenia and muscle. 2019;10(1):140-54 DOI: https://doi.org/10.1002/jcsm.12360.
159. Murphy RA, Mourtzakis M, Chu QS, Baracos VE, Reiman T, Mazurak VC. Supplementation with fish oil increases first-line chemotherapy efficacy in patients with advanced nonsmall cell lung cancer. Cancer. 2011;117(16):3774-80 DOI: 10.1002/cncr.25933.
160. Savarese DMF, Savy G, Vahdat L, Wischmeyer PE, Corey B. Prevention of chemotherapy and radiation toxicity with glutamine. Cancer treatment reviews. 2003;29(6):501-13 DOI: https://doi.org/10.1016/S0305-7372(03)00133-6.
161. Penna F, Busquets S, Pin F, Toledo M, Baccino FM, López-Soriano FJ, et al. Combined approach to counteract experimental cancer cachexia: eicosapentaenoic acid and training exercise. Journal of cachexia, sarcopenia and muscle. 2011;2(2):95-104.
162. DEUSTER P, MORRISON S, AHRENS R. Endurance exercise modifies cachexia of tumor growth in rats. Medicine & Science in Sports & Exercise. 1985;17(3):385-92.
163. Salomao EM, Gomes-Marcondes MC. Light aerobic physical exercise in combination with leucine and/or glutamine-rich diet can improve the body composition and muscle protein metabolism in young tumor-bearing rats. Journal of physiology and biochemistry. 2012;68(4):493-501 DOI: 10.1007/s13105-012-0164-0.
164. Salomao EM, Toneto AT, Silva GO, Gomes-Marcondes MC. Physical exercise and a leucine-rich diet modulate the muscle protein metabolism in Walker tumor-bearing rats. Nutrition and cancer. 2010;62(8):1095-104 DOI: 10.1080/01635581.2010.492082.
165. Hardee JP, Counts BR, Carson JA. Understanding the Role of Exercise in Cancer Cachexia Therapy. Am J Lifestyle Med. 2019;13(1):46-60 DOI: 10.1177/1559827617725283.
166. Kessels E, Husson O, van der Feltz-Cornelis CM. The effect of exercise on cancer-related fatigue in cancer survivors: a systematic review and meta-analysis. Neuropsychiatr Dis Treat. 2018;14:479-94 DOI: 10.2147/ndt.S150464.
167. Advani SM, Advani PG, VonVille HM, Jafri SH. Pharmacological management of cachexia in adult cancer patients: a systematic review of clinical trials. BMC cancer. 2018;18(1):1174 DOI: 10.1186/s12885-018-5080-4.

SUPPORTING INFORMATION

Table S1: Overview of reviewed studies showing the variation in timing, duration, dosing and route of supplementation, as well as the differences in animal models used in the experimental models.

Reference	Animal + tumor model	Experimental groups	Timing (start intervention)	Duration
Branched-chain amino acids				
Eley et al., 2007	NMRI mice – MAC16 colon	TB TBN	When animals had lost approx. 5% of their starting body weight.	Animals were euthanized when the body weight loss reached 20% of their starting weight. (4-5 days)
Peters et al., 2011	CD2F1 (BALB/c x DBA/2) mice – Colon 26	C TB TBN	With tumor injection	21 days
Ventrucci et al., 2004	Wistar rats – Walker 256 (pregnant)	C TB P CN TBN PN	immediately after the confirmation of pregnancy	21 days
Ventrucci et al., 2007	Wistar rats – Walker 256 (pregnant)	C TB P CN TBN PN	immediately after the confirmation of pregnancy	20 days
Cruz et al., 2017	Wistar rats – Walker 256	C CN TB TBN	With tumor injection	7, 14, or 21 days
Viana et al., 2016	Wistar rats – Walker 256	C CN TB TBN	With tumor injection	21 days
Gomes-Marcondes et al., 2003	Wistar rats – Walker 256 (weanling)	C CN TB TBN	With tumor injection	12 days

Dose/route of administration	Background diet	Control diet Isocaloric/ isonitrogenous	Diet control
(1) Control group: PBS, daily by **oral gavage**; **(2) Leucine group:** 1 g of leucine per kg bodyweight, daily by **oral gavage.**	Rat and mouse breeding diet (Special Diet Services)	Details on energy and nitrogen correction not specified.	Ad libitum
(1) Low leucine (1g/kg food)- containing 9,6% Leu per g protein; **(2) High leucine** (8g/kg food) - containing 14,8% Leu per g protein.	AIN-93M (Research Diet Services)	Details on energy and nitrogen correction not specified.	Ad libitum
(1) Control AIN-93G modified diet containing 18% protein; and **(2) Leucine-rich diet** containing 15% protein with 3% leucine. **(-)** Leucine was obtained from Ajinomoto Interamericana Ind. & Com. Ltda. (Brazil)	AIN-93G	Isocaloric and isonitrogenous	Ad libitum/ pair fed group
(1) Control AIN-93G modified diet containing 18% protein; and **(2) Leucine-rich diet** containing 15% protein with 3% leucine. **(-)** Leucine was obtained from Ajinomoto Interamericana Ind. & Com. Ltda. (Brazil)	AIN-93G	Isocaloric and isonitrogenous	Ad libitum/ pair fed group
(1) Control AIN-93G modified diet containing 18% protein; and **(2) Leucine-rich diet** containing 15% protein with 3% leucine. **(-)** Leucine was obtained from Ajinomoto Interamericana Ind. & Com. Ltda. (Brazil)	AIN-93G	Isocaloric and isonitrogenous	Ad libitum
(1) Control AIN-93G modified diet containing 18% protein; and **(2) Leucine-rich diet** containing 15% protein with 3% leucine. **(-)** Leucine was obtained from Ajinomoto Interamericana Ind. & Com. Ltda. (Brazil)	AIN-93G	Isocaloric and isonitrogenous	Ad libitum
(1) Control AIN-93G modified diet containing 18% protein; and **(2) Leucine-rich diet** containing 15% protein with 3% leucine. **(-)** Leucine was obtained from Ajinomoto Interamericana Ind. & Com. Ltda. (Brazil)	AIN-93G	Isocaloric and isonitrogenous	Ad libitum

Supplemental Table 1: Overview of reviewed studies showing the variation in timing, duration, dosing and route of s

Reference	Animal + tumor model	Experimental groups	Timing (start intervention)	Duration
6-Hydroxy-6-Methylbutyrate (HMB)				
Smith et al., 2005	NMRI mice – MAC16 colon	TB TBN	9 days after tumor inoculation. Just before the onset of BW loss	Animals were euthanized when the body weight loss reached 25% of their starting weight.
Mirza et al., 2013	NMRI mice – MAC16 colon	TB TBN	12 to 15 days after transplantation when the tumors became palpable and weight loss had started to occur	Animals were euthanized when the tumor ulcerated, weight loss reached 20%, or the animals became moribund.
Nunes et al., 2008	Wistar rats – Walker 256	C CN TB TBN	6 weeks before tumor injection	Till 14 days after tumor inoculation (total of 8 weeks).
Aversa et al., 2011	Wistar rats – Yoshida AH-130	C CN TB TBN	16 days before tumor injection	24 days
Glutamine				
Fracaro et al., 2016	Wistar rats – Walker 256	C CN TB TBN	With tumor injection	14 days
Martins et al., 2016	Wistar rats – Walker 256	C CN TB TBN	With tumor injection	10 days

supplementation, as well as the differences in animal models used in the experimental models.

	Dose/route of administration	Background diet	Control diet Isocaloric/ isonitrogenous	Diet control
	(1) Control group: PBS, daily by **oral gavage**; **(2) HMB group:** 0.25 g per kg bodyweight, daily via **oral gavage.** **(-) HMB was obtained from Organic Technologies Inc. (Coshocton, OH)**	Rat and mouse breeding diet (Special Diet Services)	Details on energy and nitrogen correction not specified.	Ad libitum
	(1) Control group: PBS, daily by **oral gavage**; **(2) HMB group:** 0.25 g per kg bodyweight, daily via **oral gavage.** **(-)** HMB was provided by Abbot Nutrition.	Rat and mouse breeding diet (Special Diet Services)	Details on energy and nitrogen correction not specified.	Ad libitum
	(1) Control group: 10% sucrose solution, daily via **oral gavage**; **(2) HMB group**: 76 mg HMB per kg bodyweight in 10% sucrose solution, daily via **oral gavage** **(-)** HMB was obtained from Metabolic Technologies Inc (Ames, IA).	Standard commercial chow (Nutrilab-CR1; Nuvital Nutrients Ltda, Curitiba-PR, Brazil)	Details on energy and nitrogen correction not specified.	Ad libitum
	(1) Control standard pelleted chow and **(2) 4% HMB** enriched pelleted chow.	Standard pelleted chow (Mucedola, Settimo Milanese, Milan, Italy).	Details on energy and nitrogen correction not specified.	Ad libitum
	(1) Control Standard balanced Nuvital diet (Nuvilab, Colombo, PR, Brazil); **(2) L-glutamine-** received the standard diet with L-glutamine incorporated at a proportion of 2 g/100 g of diet. **(-)** L-glutamine was obtained from Deg (Sao Paulo, SP, Brazil)	Standard balanced Nuvital diet (Nuvilab, Colombo, PR, Brazil)	Details on energy and nitrogen correction not specified.	Ad libitum
	(1) Control Standard balanced Nuvital diet (Nuvilab, Colombo, PR, Brazil); **(2) L-glutamine-** received the standard diet with L-glutamine incorporated at a proportion of 2 g/100 g of diet. **(-)** L-glutamine was obtained from Fagron of Brazil Pharma Ltda (Sao Paulo, SP, Brazil)	Standard balanced Nuvital diet (Nuvilab, Colombo, PR, Brazil)	Details on energy and nitrogen correction not specified.	Ad libitum

Supplemental Table 1: Overview of reviewed studies showing the variation in timing, duration, dosing and route of s

Reference	Animal + tumor model	Experimental groups	Timing (start intervention)	Duration
Martins et al., 2017	Wistar rats – Walker 256	C CN TB TBN	With tumor injection	10 days
Vincentini et al., 2016	Wistar rats – Walker 256	C CN TB TBN	With tumor injection	14 days
Vincentini et al., 2017	Wistar rats – Walker 256	C CN TB TBN	With tumor injection	14 days
Glycine				
Ham et al., 2014	CD2F1 mice – Colon 26	C TB TBN	With tumor injection	21 days
Ketogenic High fat diets				
Tisdale et al., 1987	NMRI mice – MAC16 colon	C CN TB TBN	8 days after tumor transplantation	20 days
Beck et al., 1989	NMRI mice – MAC16 colon	C TB TBN	14 days after tumor transplantation, at which time the tumors were palpable but weight loss had not occurred.	9 days

supplementation, as well as the differences in animal models used in the experimental models.

	Dose/route of administration	Background diet	Control diet Isocaloric/ isonitrogenous	Diet control
	1) Control Standard balanced Nuvital diet (Nuvilab, Colombo, PR, Brazil); **(2) L-glutamine-** received the standard diet with L-glutamine incorporated at a proportion of 2 g/100 g of diet. **(-)** L-glutamine was obtained from Fagron of Brazil Pharma Ltda (Sao Paulo, SP, Brazil)	Standard balanced Nuvital diet (Nuvilab, Colombo, PR, Brazil)	Details on energy and nitrogen correction not specified.	Ad libitum
	1) Control Standard balanced Nuvital diet (Nuvilab, Colombo, PR, Brazil); **(2) L-glutamine-** received the standard diet with L-glutamine incorporated at a proportion of 2 g/100 g of diet. **(-)** L-glutamine was obtained from Deg (Sao Paulo, SP, Brazil)	Standard balanced Nuvital diet (Nuvilab, Colombo, PR, Brazil)	Details on energy and nitrogen correction not specified.	Ad libitum
	1) Control Standard balanced Nuvital diet (Nuvilab, Colombo, PR, Brazil); **(2) L-glutamine-** received the standard diet with L-glutamine incorporated at a proportion of 2 g/100 g of diet. **(-)** L-glutamine was obtained from Deg (Sao Paulo, SP, Brazil)	Standard balanced Nuvital diet (Nuvilab, Colombo, PR, Brazil)	Details on energy and nitrogen correction not specified.	Ad libitum
	(1) Control: subcutaneous injection of saline **(2) Glycine**: 1 g per kg bodyweight of **glycine** in PBS once daily via **subcutaneous injections.**	Standard laboratory chow (not further specified).	Details on energy and nitrogen correction not specified.	Ad libitum
	(1) Control diet: standard laboratory chow; 11.5% total kcal as fat; **(2) Medium-chain triglyceride (MCT) diet**: modified standard laboratory chow with 80% total kcal from MCT.	Standard laboratory chow (Pilsbury, Birmingham, United Kingdom)	Isocaloric and isonitrogenous	Ad libitum
	(1) Control diet: standard laboratory chow; 11.5% total kcal as fat; **(2) MCT diet**: modified standard laboratory chow with 80% total kcal from MCT.	Standard laboratory chow (Pilsbury, Birmingham, United Kingdom)	Isocaloric and isonitrogenous	Ad libitum

Supplemental Table 1: Overview of reviewed studies showing the variation in timing, duration, dosing and route of s

Reference	Animal + tumor model	Experimental groups	Timing (start intervention)	Duration
Nakamura et al., 2018	CD2F1 mice – Colon 26	C TB TBN	With tumor injection	Until moribund condition max. 21 days.
Polyunsaturated fatty acids (PUFAs)				
Tisdale et al., 1990	NMRI mice – MAC16 colon	C TB TBN	12-14 days after tumor transplantation, at which time the tumors were palpable but weight loss had not occurred.	Animals were euthenized when the tumor ulcerated, weight loss reached 6 to 7 g, or the animals became moribund
Pizato et al., 2005	Wistar rats – Walker 256	C TB TBN	8 weeks before tumor injection.	Till 14 days after tumor inoculation (total of 10 weeks).
Coelho et al., 2012	Wistar rats – Walker 256	C CN TB TBN	10 weeks before tumor injection.	Till 14 days after tumor inoculation (total of 12 weeks).

supplementation, as well as the differences in animal models used in the experimental models.

	Dose/route of administration	Background diet	Control diet Isocaloric/ isonitrogenous	Diet control
	(1) Control diet is AIN-93G (64% C, 20% P, and 16% L); **(2) ketogenic formula**, Ketonformula 817-B (Meij Co.; KF 5% C, 8% P, and 87% L).	AIN-93G	Isocaloric, not isonitrogenous	Ad libitum
	(1) Control diet: standard laboratory chow; 11.5% total kcal as fat; **(2) Fish oil (FO) diet**: modified standard laboratory chow with 5%, 10%, 25% or 50% fish oil. **(-)** Fish oil was a product of the Q.P. corporation (Shibuya, Japan)	Standard laboratory chow (Pilsbury, Birmingham, United Kingdom)	Isocaloric and isonitrogenous	Ad libitum
	(1) Control group: standard chow diet, 62% total kcal carbohydrates, 29% total kcal protein, 9% total kcal fat; **(2) High-fat FO diet:** modified standard laboratory chow, 49% total kcal fat, 29% total kcal carbohydrates, 22% total kcal protein; 66% of fat as substituted as FO.	Standard chow diet (Nuvital CR-1, Curitiba, Brazil)	Isonitrogenous, not isocaloric	Ad libitum
	1) Control group: 1 g of coconut oil per kg bodyweight, daily via **oral gavage.** **(2) FO group:** 1 g of fish oil per kg bodyweight, daily via **oral gavage.** This dose represents approximately 1.25 % (w/w) of the diet. **(-)** The FO used was a mixed marine triacylglycerol preparation containing 180 g eicosapentaenoic acid (EPA) and 120 g docosahexaenoic acid (DHA) per kg.	Standard chow diet (Nuvital CR-1, Curitiba, Brazil)	Details on energy and nitrogen correction not specified.	Ad libitum

Supplemental Table 1: Overview of reviewed studies showing the variation in timing, duration, dosing and route of s

Reference	Animal + tumor model	Experimental groups	Timing (start intervention)	Duration
Togni et al., 2003	Wistar rats – Walker 256	C_1 C_2 CN TB_1 TB_2 TBN	Lifelong supplementation: Female Wistar rats were supplemented with FO prior to mating and then throughout pregnancy and gestation, and then the male offspring were supplemented from weaning until 90 days of age. Then they were inoculated subcutaneously with tumor cells.	Till 14 days after tumor inoculation.
Fernandez et al., 2004	Wistar rats – Walker 256	C CN TB TBN	Lifelong supplementation (see Togni et al., 2003)	Till 14 days after tumor inoculation
Dumas et al., 2010	BDIX rats - DHD/ K12 cells	C TB P CN TBN PN	6 weeks before tumor injection.	Till food intake was reduced by 25% for 11 consecutive days.
Iagher et al., 2011	Wistar rats – Walker 256	C_1 C_2 CN TB_1 TB_2 TBN	7 weeks before tumor injection.	Till 14 days after tumor inoculation (total of 9 weeks).
Iagher et al., 2013	Wistar rats – Walker 256	C CN_1 CN_2 TB TBN_1 TBN_2	8 weeks before tumor injection.	Till 14 days after tumor inoculation (total of 10 weeks).

supplementation, as well as the differences in animal models used in the experimental models.

	Dose/route of administration	Background diet	Control diet Isocaloric/ isonitrogenous	Diet control
	(1) Control group: standard chow diet **(2) CO group:** 1 g of coconut oil per kg bodyweight, daily via **oral gavage.** **(3) FO group:** 1 g of fish oil per kg bodyweight, daily via **oral gavage.** **(-)** The FO used was a mixed marine triacylglycerol preparation containing 180 g eicosapentaenoic acid (EPA) and 120 g docosahexaenoic acid (DHA) per kg. **(-)** Fish oil was obtained from MaxEpa (Seven Seas, Hull, UK)	Standard chow diet	Details on energy and nitrogen correction not specified.	Ad libitum
	FO group: 1 g of fish oil per kg bodyweight, daily via **oral gavage.** This dose represents approximately 1.25 % (w/w) of the diet. **(-)** The FO used was a mixed marine triacylglycerol preparation containing 180 g eicosapentaenoic acid (EPA) and 120 g docosahexaenoic acid (DHA) per kg.	Standard chow diet (Nuvital CR-1, Curitiba, Brazil)	Details on energy and nitrogen correction not specified.	Ad libitum
	(1) Control group: standard laboratory diet **(2) FO diet:** modified standard diet, incorporated with 5% FO. **(-)** Fish oil was obtained from Phosphotech (St. Herblain, France)	Standard laboratory diet (National Institute of Research on Agronomics, INRA, Jouyen-Josas, France).	Isocaloric and isonitrogenous	Ad libitum/ pair-fed group
	(1) Control group: standard chow diet **(2) CO group:** 1 g of coconut oil per kg bodyweight, daily via **oral gavage.** **(3) SLO group:** 1 g of shark liver oil per kg bodyweight, daily via **oral gavage.** **(-) SLO** was obtained from Naturalis Alimentos Naturais Ltda (Sao Paulo, Brazil)	Standard chow diet (Nuvital CR-1, Curitiba, Brazil)	Details on energy and nitrogen correction not specified.	Ad libitum
	(1) Control group: standard chow diet **(2) FO group:** 1 g of fish oil per kg bodyweight, daily via **oral gavage.** **(3) SLO group:** 1 g of shark liver oil per kg bodyweight, daily via **oral gavage.**	Standard chow diet (Nuvital CR-1, Curitiba, Brazil)	Details on energy and nitrogen correction not specified.	Ad libitum

Supplemental Table 1: Overview of reviewed studies showing the variation in timing, duration, dosing and route of s

Reference	Animal + tumor model	Experimental groups	Timing (start intervention)	Duration
Beck et al., 1991	NMRI mice – MAC16 colon	C CN TB TBN	10 to 12 days after transplantation when the tumors became palpable and weight loss had started to occur.	Max 9 days. Animals were euthanized when the tumor ulcerated, weight loss reached 25 to 30%, the tumor weight reached 10% of the host body weight, or the animals became moribund.
Tisdale et al., 1991	NMRI mice – MAC16 colon	TB TBN_1 TBN_2 TBN_3	10 to 12 days after transplantation when the tumors became palpable and weight loss had started to occur.	5 days
Whitehouse et al., 2001	NMRI mice – MAC16 colon	C CN TB TBN	10 to 12 days after transplantation when the tumors became palpable and weight loss had started to occur.	0, 24 and 48 hours
Smith et al., 2004	NMRI mice – MAC16 colon	C TB TBN	After 5% BW loss was reached. (Weight loss was evident 10–12 days after transplantation)	4 days
Du et al., 2015	Kunming mice – S180 cells	C TB TBN	24 hours after tumor injection	14 days

supplementation, as well as the differences in animal models used in the experimental models.

	Dose/route of administration	Background diet	Control diet Isocaloric/ isonitrogenous	Diet control
	(1) Control group: solvent (liquid paraffin:water, 2:1), daily by **oral gavage**; **(2) EPA group:** 1.25 to 2.5 g of EPA per kg bodyweight, daily by **oral gavage.**	Standard laboratory chow (Pilsbury, Birmingham, United Kingdom)	Details on energy and nitrogen correction not specified.	Ad libitum
	(1) Control group: 100 uL 0.9% saline, daily by oral gavage; **(2) EPA group:** 100 mg EPA, daily by oral gavage; **(3) DHA group:** 100 mg DHA, daily by oral gavage; **(4) Linoleic acid group:** 100 mg linoleic acid, daily by oral gavage. **(-)** Linoleic acid and DHA (both 99% pure) were obtained from the Sigma Chemical Co. (Poole, U.K.), and EPA (95% pure) was obtained from Peninsula Laboratories Europe Ltd (Merseyside, U.K.).	Standard laboratory chow (Pilsbury, Birmingham, United Kingdom)	Details on energy and nitrogen correction not specified.	Ad libitum
	(1) Control group: olive oil, daily by **oral gavage**; **(2) EPA group:** 0.5 and 2.5 g of EPA per kg bodyweight, daily by **oral gavage.**	Standard laboratory chow (Special Diet Services, Witham, UK).	Details on energy and nitrogen correction not specified.	Ad libitum
	(1) Control group: olive oil, twice daily by **oral gavage**; **(2) EPA group:** 1 g of EPA per kg bodyweight, twice daily by **oral gavage.**	Economy rodent breeder diet (Special Diet Services, Essex, UK).	Details on energy and nitrogen correction not specified.	Ad libitum
	(1) Control group: 0.85% normal saline, daily by **oral gavage**; **(2) EPA-PL group:** 100 mg of EPA per kg bodyweight, daily by **oral gavage.**	Standard chow diet (Harlan Teklad LM-485).	Details on energy and nitrogen correction not specified.	Ad libitum

Supplemental Table 1: Overview of reviewed studies showing the variation in timing, duration, dosing and route of s

Reference	Animal + tumor model	Experimental groups	Timing (start intervention)	Duration
Fini et al., 2010	Apc(Min/+)	C CN_1 CN_2 TB TBN_1 TBN_2	Start 6 weeks old	12 weeks
Jho et al., 2002	Fisher 344 rats - MCA tumor	TB_1 TB_2 TBN	13 days after tumor injection.	16 days
Dagnelie et al., 1994	Fisher F1 hybrid rats - MATLy-Lu prostate tumor cells	C CN TB TBN	7 days after tumor injection.	14 days
Conjugated linoleic acid (CLA)				
Graves et al., 2005	CD2F1 mice - Colon 26	C CN TB TBN	With tumor injection and 2 weeks before tumor injection.	5 weeks (Till 21 days after tumor injection)
McCarthy et al., 2006	C57Bl/6 mice – LLC and B16 tumor cells	C CN TB TBN	With tumor injection.	17 days
Tian et al., 2011	CD2F1 mice - Colon 26	C TB TBN P	With tumor injection.	20% difference in body weight between PBS and Tumor groups (day 17 post-inoculation)

supplementation, as well as the differences in animal models used in the experimental models.

	Dose/route of administration	Background diet	Control diet Isocaloric/ isonitrogenous	Diet control
	(1) Control diet: modified AIN-93G diet, corn oil substituted for soybean oil; **(2) EPA diet:** modified AIN-93G diet, soybean oil substituted for EPA free fatty acids at 2.5% weight/weight (w/w); **(3) EPA diet:** modified AIN-93G diet, soybean oil substituted for EPA free fatty acids at 5% w/w. **(-)** EPA was obtained from ALFA, SLA Pharma AG.	AIN-93G (Research Diets)	Isocaloric and isonitrogenous	Controlled
	(1) Control: oral gavage isovolemic 5.0 g/kg of corn oil (isocaloric) combined with 10 IU vitamin E/g fat, **(2) Control:** isovolumic but non-isocaloric normal saline combined with 10 IU vitamin E/g; **(2) EPA: oral gavage** twice daily, providing 5.0 g/kg per day of EPA with 10 IU vitamin E/g fat.	Undefined	Isocaloric and isonitrogenous	Controlled
	(1) Control diet: standard laboratory chow containing 50% total kcal carbohydrates, 20% total kcal protein, 11,5 % total kcal fat. (**2) FO diet**: semi purified diet, containing 50% total kcal coming from fish oil, which substituted for carbohydrates.	Standard laboratory chow (Pilsbury, Birmingham, United Kingdom)	Isocaloric and isonitrogenous	Ad libitum
	(1) Control diet: pulverized rodent chow; (**2) CLA diet:** pulverized rodent chow supplemented with 0.5% CLA.	Standard laboratory chow	Details on energy and nitrogen correction not specified.	Ad libitum
	(1) Control diet: pulverized rodent chow; **(2) CLA diet:** pulverized rodent chow supplemented with 0.5% CLA. **(-)** CLA was obtained from Loders CrokLaan (Channahon, IL)	Standard laboratory chow	Details on energy and nitrogen correction not specified.	Ad libitum
	(1) Control diet: 7% soybean oil (PBS, Tumor and Pair-fed groups); **(2) CLA diet:** 6% soybean oil and 1% c9t11-CLA free fatty acids (C9t11-CLA FFA) **(-)** CLA was obtained from Lipid Nutrition (Wormerveer, the Netherlands)	AIN-93G (Research Diets, Brunswick, NJ, USA)	Isocaloric and isonitrogenous	Controlled (pair-fed)

Supplemental Table 1: Overview of reviewed studies showing the variation in timing, duration, dosing and route of s

Reference	Animal + tumor model	Experimental groups	Timing (start intervention)	Duration
Goncalves et al., 2019	Wistar rats – Walker 256	C_1 C_2 CN TB_1 TB_2 TBN	With tumor injection.	14 days
Carnitine				
Busquets et al., 2012	Wistar rats – Yoshida AH-130	TB TBN	With tumor injection.	7 days
Busquets et al., 2020	Wistar rats – Yoshida AH-130	TB TBN	With tumor injection.	7 days
Liu et al., 2011	BALB/c mice - Colon 26	C TB TBN	12 days after tumor injection.	7 days
Silverio et al., 2012	Wistar rats – Walker 256	C CN TB TBN	14 days before tumor injection.	28 days (Until 14 after tumor injection).
Creatine				
Campos-Ferraz et al., 2016	Wistar rats – Walker 256	C TB TBN	7 days after tumor injection.	15 and 33 days

supplementation, as well as the differences in animal models used in the experimental models.

	Dose/route of administration	Background diet	Control diet Isocaloric/ isonitrogenous	Diet control
	(1) Control group: 0.5 ml of 0.9% saline, daily by **oral gavage**; **(2) Control group:** 0.5 ml of sunflower oil, daily by **oral gavage**; **(3) CLA group:** 0.5 ml (2% w:w of total food intake) of CLA (Tonalin®), daily by **oral gavage.**	Standard balanced Nuvital diet (Nuvilab, Colombo, PR, Brazil)	Details on energy and nitrogen correction not specified.	Ad libitum
	(1) Control: corresponding volume of cornoil, daily by **oral gavage**; **(2) L-Carnitine:** 1 g of L-carnitine per kg bodyweight, daily by **oral gavage.** **(-)** L-Carnitine was obtained from Sigma (Tau, Spain)	Standard laboratoty chow (Harlan Teklad Global Diet 2014)	N.A.	Ad libitum
	(1) Control: corresponding volume of cornoil, daily by **oral gavage**; **(2) L-Carnitine:** 1 g of L-carnitine per kg bodyweight, daily by **oral gavage.** **(-)** L-Carnitine was obtained from Sigma (Tau, Spain)	Undefined	N.A.	Ad libitum
	(1) Control: 2 ml of 0.9% saline, daily by **oral gavage**; **(2) L-Carnitine:** 4.5 mg of L-carnitine per kg of bodyweight, daily by **oral gavage**; **(3) L-Carnitine:** 18 mg of L-carnitine per kg of bodyweight, daily by **oral gavage**; **(-)** L-Carnitine was obtained from Sigma-Aldrich (St. Louis, MO, USA)	Undefined	N.A.	Ad libitum
	(1) Control: 1 ml of 0.9% saline, daily by **oral gavage**; **(2) L-Carnitine:** 1 g of L-carnitine per kg of bodyweight, daily by **oral gavage**. **(-)** L-Carnitine was obtained from ICN-USA	Standard laboratory chow (NUVILAB 1, Nuvital, Brazil)	N.A.	Ad libitum
	(1) Control: 4 ml of PBS, daily by **oral gavage**; **(2) Creatine:** 4 ml of PBS containing 300 mg of creatine per kg of bodyweight, daily by **oral gavage**.	Standard laboratory chow	N.A.	Ad libitum

Supplemental Table 1: Overview of reviewed studies showing the variation in timing, duration, dosing and route of s

Reference	Animal + tumor model	Experimental groups	Timing (start intervention)	Duration
Cella et al., 2020	Wistar rats – Walker 256	C TB TBN	With tumor injection.	21 days
Deminice et al., 2015	Wistar rats – Walker 256	C TB TBN	11 days before tumor injection.	21 days (10 days after tumor injection)
Flavonoids				
Velazquez et al., 2014	C57Bl/6J and Apc(Min/+)	C CN TB TBN	Start at 15 weeks old.	21 days
Camargo et al., 2011	Wistar rats – Walker 256	TB TBN	3h before tumor injection.	15 days
Wang et al., 2011	C57Bl/6 mice – LLC cells	TB TBN_1 TBN_2	Preventative: 12 days before tumor injection. Curative: with tumor injection	32-34 days
Hirasaka et al., 2016	C57Bl/6 mice – LLC cells	C CN TB TBN	With tumor injection.	21 days
Yoshimura et al., 2018	C57Bl/6 mice – LLC cells	C CN TB TBN	With tumor injection.	21 days

supplementation, as well as the differences in animal models used in the experimental models.

	Dose/route of administration	Background diet	Control diet Isocaloric/ isonitrogenous	Diet control
	Creatine: 8 g/l creatine monohydrate in their drinking water (1.0±0.1 g/kg/day)	Standard chow diet (Nuvital CR-1, Curitiba, Brazil)	N.A.	Ad libitum
	Creatine: 8 g/l creatine monohydrate in their drinking water.	Standard chow diet (Nuvital CR-1, Curitiba, Brazil)	N.A.	Ad libitum
	(1) Quercetin: 25 mg/kg (Nutravail) mixed with orange-flavored Tang (Kraft Foods), daily via oral gavage; **(2) Control:** an equal volume of vehicle solution mix of Tang juice and water alone, daily via oral gavage.	Standard rodent unpurified diet (HarlanTeklad Rodent Diet, no. 8604)	Details on energy and nitrogen correction not specified.	Ad libitum
	Quercetin was dissolved in 0.3 mL mineral oil (Nujol) and **intraperitoneal** administered daily. **(-)** Quercetin was obtained from Sigma Chemical Co. (St. Louis, MO, USA)	Undefined	Details on energy and nitrogen correction not specified.	Ad libitum
	(1) Control: water, daily by **oral gavage**; **(2) EGCG low:** 0.2 mg of EGCG, daily by **oral gavage**; **(3) EGCG high:** 0.6 mg EGCG, daily by **oral gavage**; **(-)** EGCG was obtained from Sigma Chemical Co. (St. Louis, MO, USA)	Standard laboratory chow (laboratory rodent diet, labdiet 5001, USA)	Details on energy and nitrogen correction not specified.	Ad libitum
	(1) Control diet: standard chow, AIN-93M; **(2) Isoflavone diet:** the alpha-starch content of the isoflavone diet was reduced to adjust for the composition of other nutrients, and comprised a normal diet (based on AIN-93M) mixed with soya flavone HG (0,4% w/w; Fuji Oil Co.)	AIN-93M (Oriental Yeast Co., Ltd., Tokyo, Japan).	Isocaloric and isonitrogenous	Ad libitum
	(1) control diet: AIN-93M; **(2) morin diet:** The a-starch content of the morin diet was reduced to adjust for the composition of other nutrients, and comprised a normal diet (based on AIN-93M) mixed with morin (0.1% w/w) **(-)** Morin was obtained from Sigma Aldrich (St. Louis, MO, USA)	AIN-93M (Oriental Yeast Co., Ltd., Tokyo, Japan).	Isocaloric and isonitrogenous	Ad libitum

Supplemental Table 1: Overview of reviewed studies showing the variation in timing, duration, dosing and route of s

Reference	Animal + tumor model	Experimental groups	Timing (start intervention)	Duration
Resveratrol				
Wyke et al., 2004	NMRI mice – MAC16 colon	TB TBN	After 5% BW loss was reached. (Weight loss was evident 10–12 days after transplantation).	5 days
Shadfar et al., 2011	CD2F1 mice - Colon 26	C CN TB TBN	6 days after tumor injection.	11 days
Busquets et al., 2007	C57Bl/6 - LLC and Wistar rats - Yoshida AH-130	C CN TB TBN	With tumor injection.	C57Bl/6 mice: 15 days; Wistar rats: 7 days.
Prebiotic non-digestible oligosaccharides				
Gorselink et al., 2006	CD2F1 mice - Colon 26	C TB TBN	With tumor injection.	20 days

supplementation, as well as the differences in animal models used in the experimental models.

	Dose/route of administration	Background diet	Control diet Isocaloric/ isonitrogenous	Diet control
	(1) Resveratrol-treated: Daily i.p. dose of resveratrol (1 mg/kgBW); **(2) Control:** solvent (DMSO : PBS (1 : 20)) i.p. dose. **(-)** Resveratrol was obtained from Biomol Research Laboratories Inc. (PA, USA)	Rat and mouse breeding diet (Special Diet Services, Witham, UK)	N.A.	Ad libitum
	(1) Control 250 µl of vehicle, daily by oral gavage; **(2) Resveratrol** 100 mg/kg, 200 mg/kg, or 500 mg/kg of resveratrol, daily by oral gavage. **(-)** Resveratrol was obtained from Cayman Chemical (Ann Arbor, MI, USA)	Undefined	N.A.	Ad libitum
	C57Bl/6 mice diets: **(1) Resveratrol-treated:** i.p. dose of resveratrol (5 or 25 mg/kg BW); **(2) Control:** i.p. dose of saline (5 or 25 mg/kg BW). Wistar rats diets: **(1) Resveratrol-treated:** Daily i.p. dose of resveratrol (1 mg/kgBW); **(2) Control:** saline i.p. dose (1 mg/kgBW).	Undefined	N.A.	Ad libitum
	Experiment 1: **(1) Control:** AIN-93M; **(2) GOS/FOS diet:** The modified AIN-93 M diet consisted of 51% galacto-oligosaccharides (GOS) and fructo-polysaccharides (9:1), 19% maltodextrin, 16% lactose and 14% glucose in experiment 1. Experiment 2: **(1) Control:** AIN-93M; **(2) GOS/GOS diet:** The FOS was replaced by additional GOS.	AIN-93M diet (Research Diets)	Details on energy and nitrogen correction not specified.	Ad libitum

Supplemental Table 1: Overview of reviewed studies showing the variation in timing, duration, dosing and route of s

Reference	Animal + tumor model	Experimental groups	Timing (start intervention)	Duration
Bindels et al., 2015	BALB/c - BaF3(Bcr-Abl)	C TB TBN_1 TBN_2	1 day after tumor injection.	15 days

C: Control group, CN: control group + nutrition intervention, TB: tumor-bearing group, TBN: tumor-bearing group + nutrition intervention, P: pair-fed group, PN: pair-fed + nutrition intervention, and N.A.: Not Applicable.

A literature search was performed in PubMed. Papers published in the last 35 years were included (1985-2020). The search string was composed of three search components (SCs): SC1 nutritional intervention, SC2 cancer [and] cachexia, and SC3 laboratory animals. For each of the critical SCs, a separate search string was developed. Each component-specific search string included an extensive collection of appropriate search terms, including Medical Subject Heading and free-text terms. For SC3, a PubMed search filter for primary animal studies was used (1). In a final search, all separately developed search strings for each SC were combined to retrieve the potentially relevant studies. Papers were excluded if (i) studies did not include a dietary intervention, (ii) studies did include a pharmacological intervention, (iii) studies did not include tumor-induced cachexia models, (iv) studies did not describe the conventional phenotype of cachexia, (v) human intervention studies, and (vi) review papers.

1. Hooijmans CR, Tillema A, Leenaars M, Ritskes-Hoitinga M. Enhancing search efficiency by means of a search filter for finding all studies on animal experimentation in PubMed. Laboratory Animals. 2010;44(3):170-5 DOI: 10.1258/la.2010.009117.

supplementation, as well as the differences in animal models used in the experimental models.

	Dose/route of administration	Background diet	Control diet Isocaloric/ isonitrogenous	Diet control
	(1) Control: AIN93M; **(2) Inulin:** AIN93M supplemented with inulin (5% INU w/w); and **(3) POS:** AIN93M diet supplemented with POS (5% POS w/w).	AIN-93M (Research diets, New Brunswick, NJ, USA)	Details on energy and nitrogen correction not specified.	Ad libitum

5

Automated CT-derived skeletal muscle mass determination in lower hind limbs of mice using a 3D U-Net deep learning network

Brent van der Heyden*
Wouter RPH van de Worp*
Ardy van Helvoort
Jan Theys
Annemie MWJ Schols
Ramon CJ Langen
and Frank Verhaegen
*Authors contributed equally

Journal of Applied Physiology
2019, 128:42-49

ABSTRACT

The loss of skeletal muscle mass is recognized as a complication of several chronic diseases and is associated with increased mortality and a decreased quality of life. Relevant and reliable animal models in which muscle wasting can be monitored noninvasively over time are instrumental to investigate and develop new therapies. In this work, we developed a fully automatic deep learning algorithm for segmentation of micro cone beam computed tomography images of the lower limb muscle complex in mice, and subsequent muscle mass calculation. A deep learning algorithm was trained on manually segmented data from 32 mice. Muscle wet mass measurements were obtained from 47 mice and served as a data set for model validation and reverse model validation. The automatic algorithm performance was approximately 150 times faster than manual segmentation. Reverse validation of the algorithm showed high quantitative metrics (i.e., a Dice similarity coefficient of 0.93, a Hausdorff distance of 0.4 mm, and a center of mass displacement of 0.1 mm), substantiating the robustness and accuracy of the model. A high correlation (R^2=0.92) was obtained between the computed tomography-derived muscle mass measurements and the muscle wet masses. Longitudinal follow-up revealed time-dependent changes in muscle mass that separated control from lung tumor bearing mice, which was confirmed as cachexia.

In conclusion, this deep learning model for automated assessment of the lower limb muscle complex provides highly accurate noninvasive longitudinal evaluation of skeletal muscle mass. Furthermore, it facilitates the workflow and increases the amount of data derived from mouse studies, while reducing the animal numbers.

1. INTRODUCTION

Skeletal muscle is the largest tissue in the body and comprises approximately 40% of the total body mass in normal weight humans (13). It allows voluntary movement, including mobility and breathing, but also contributes to numerous metabolic processes, including substrate disposal and thermogenesis (9, 25). Skeletal muscle is one of the most dynamic and plastic tissues of the body, responding to changes in functional or metabolic demand, most obviously in response to increased or reduced physical activity, resulting in either hypertrophy or atrophy (27). However, these characteristics also enable skeletal muscle to be used as energy and protein reserve that can be deployed during periods of starvation or during acute and chronic catabolism, as seen during trauma or infections and cancer cachexia, leading to accelerated muscle loss (30).

Loss of skeletal muscle mass, especially in the locomotor muscles, is a recognized complication of several chronic diseases including chronic obstructive pulmonary disease, chronic heart failure, and chronic kidney disease and of most malignant cancers (35). Muscle wasting is well known to be associated with increased patient mortality and decreased quality of life (1, 21, 28). As muscle wasting is an unmet medical need, the development of effective therapeutic strategies involves preclinical research, which requires reliable assessment of muscle mass in animal models.

In the clinical setting, several imaging modalities such as computed tomography (CT), cone beam CT (CBCT), dual-energy X-ray absorptiometry (DEXA), or magnetic resonance imaging (MRI) have been applied for years as practical and precise methods to assess body composition, and skeletal muscle volumes (3, 4, 12, 14, 15, 17, 20, 26, 29). In contrast, skeletal muscle mass evaluation in preclinical studies is mostly based on assessment of muscle wet masses or muscle fiber cross sectional area by postmortem histological examination. Both methods require muscle dissection and consequently are terminal experiments. This precludes longitudinal follow-up of muscle mass changes, and assessment of time-dependent changes in muscle mass therefore requires inclusion of multiple animal groups in the experimental design. Recently, novel approaches to noninvasively determine muscle volume, including changes over time of individual experimental animals using MRI and micro CT were described (5, 6, 19, 23, 24).

Micro-CT is a dedicated X-ray-based imaging technology for small animals that allows for tissue density quantifications, which makes micro-CT a good image

technique for longitudinal muscle mass assessment. To investigate muscle mass changes quantitatively, manual segmentation of the muscle volume on the CT reconstruction of the experimental animal is required, which in itself is a delicate and very time-consuming task for the researcher.

Many efforts have been made to develop automated CT segmentation techniques for patients, but surprisingly, there have only been sparse reports on fully automatic soft tissue CT segmentation techniques in experimental animals. Baiker *et al* investigated an automatic reference atlas based whole body segmentation method in micro-CT images using a digital mouse phantom (2). More recently, our group investigated organ-at-risk segmentation in mice prior to irradiation with a multi-atlas image deformation-based approach (31). Clearly, availability of automated muscle segmentation applications for mice would tremendously facilitate CT-based assessment of skeletal muscle mass in preclinical research. Moreover, it will strongly contribute to a reduction in the number of animals used for longitudinal studies that evaluate muscle mass changes, which is in line with the 3R principle embedded in national and international legislation and regulations on the protection of animals used for scientific purposes. To our knowledge, no literature exists on the fully automatic segmentation of skeletal muscle in mice. In this work we developed and validated a new method to automatically segment skeletal muscle in mice using artificial intelligence techniques that could be widely applied in animal models used to study muscle atrophy or hypertrophy.

2. MATERIALS AND METHODS

A summarizing flowchart of the study setup is shown in Figure 1. Further details are described in the subsequent paper sections.

2.1 Mouse experimental and imaging procedures

2.1.1. Animal preparation.

This work was conducted in accordance with institutional guidelines for the care and use of laboratory animals established by the Ethics Committee for Animal Experimentation of Maastricht University, in full compliance with national legislation on animal research following the European Directive 2010/63/EU for the use of animals for scientific purposes, and is part of a set of experiments to establish an orthotopic model of lung cancer cachexia (AV01070020174168). Male and female mice at 9-10 wk old (129S2/SvPasCrl, Charles River Laboratories) were socially housed in a climate-controlled room (12:12 dark-light cycle with a constant room

temperature of 21±1°C). Mice were given *ad libitum* access to food (AIN-93M) and water. After 1 wk of acclimatization, mice were randomly allocated to either sham control (n=15) or tumor bearing (TB) group (n=68). All animals underwent surgery at the age of 12 wk, at a standardized time window during their inactive period of the day. While anesthetized using a mixture of air and isoflurane (4% induction, 2% maintenance) and appropriate analgesia, sham control mice received an intrapulmonary injection with 15µL of matrix (Matrigel, Corning) and the TB mice (orthotopic lung tumor model) received an intrapulmonary injection with 15µL of Matrigel containing lung epithelium-derived adenocarcinoma cells (10). Mice were monitored daily. Based on an animal welfare scoring list, or upon a loss of body mass >20%, humane end points were applied. Furthermore, tumors were scored for characteristics, size and progression. When a total tumor volume of 500 mm^3 was reached or in the case of signs of dyspnea because of tumor growth, pulmonary constriction or metastasis, humane end points were applied.

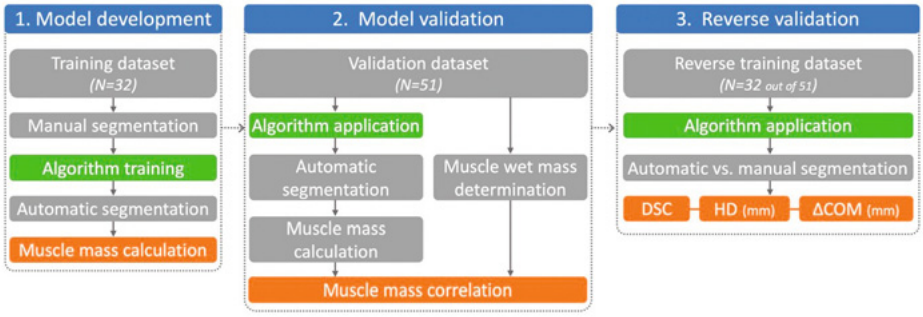

Figure 1. *Study setup flowchart. 1: Model development, the model was trained on a manually segmented data set of 32 mice. After training, the model segmented the lower limb muscle complex on micro cone beam computed tomography (µCBCT) scans and subsequently calculated the muscle mass using a pre-determined conversion curve. 2: Model validation was finally performed on a validation data set of 47 mice (4 out of 51 mice were excluded). As validation, the muscle mass determined by the model was correlated to muscle wet mass measurements. 3: a reverse validation approach was adopted to calculate three quantitative metrics between the automatic and the manual muscle segmentations. ΔCOM, center of mass displacement; DSC, Dice similarity coefficient; HD, 95th percentile Hausdorff distance.*

2.1.2. Animal imaging.

At baseline and weekly after surgery, µCBCT imaging was performed for all mice to assess lung tumor development (data not shown) and detect muscle volume changes over time. For this, mice were anesthetized as outlined above, placed in prone position with toes facing the flanks (foot and tibia angle ± 90º), and scanned using a µCBCT scanner (X-RAD 225Cx, Precision X-Ray Inc., North Branford,

USA) at an X-ray tube potential of 50 kVp, X-ray tube current of 5.6 mA, and imaging time of 2 min (34). The imaging dose of 30 cGy was verified using a PTW TN300012 Farmer-type ionization chamber (PTW, Freiburg, Germany) according to the American Association of Physicists in Medicine TG-61 protocol (18). The μCBCT projection data was reconstructed using the pilot Feldkamp back projection algorithm with a voxel dimension of 100 x 100 x 100 μm^3 (33).

At the end of the experiment, mice were scanned and subsequently euthenized using pentobarbital overdose to evaluate skeletal muscle mass. The soleus, plantaris, gastrocnemius, tibialis anterior and extensor digitorum longus muscles including tendons were collected from both hind limbs, using standardized dissection methods with a precision coefficient of 0.93 ± 0.05. Subsequently, muscles were immediately weighed in pairs on an analytical balance with precision of ± 0.1 mg and a linearity of 0.2 mg (CP64, Sartorius, Goettingen, Germany). Baseline μCBCT scans (n=32) of TB mice were used to train the newly developed algorithm and 47 mice (n=14 sham, n=33 TB) were used to validate the performance of the automatic muscle segmentation algorithm. The 47 mice were included from a group of 51 mice, of which 4 mice met the exclusion criteria (based on deviation of the expected mass-ratio of individual muscles, indicative of imperfections in the dissection procedure). Because of logistic reasons, the time interval between imaging and the muscle collection (day of euthenasia) of the validation group was either 2 days (n=24) or 0 days (n=23).

2.2. Automatic image segmentation

2.2.1. Deep learning algorithm.

As a training data set for our algorithm, the lower limb muscle complex (including the musculus gastrocnemius, soleus, plantaris, tibialis anterior and extensor digitorum longus) was manually segmented on the reconstructed cross sectional μCBCT images that were acquired at the study baseline of 32 mice. The segmentation was performed by an experienced scientist with appropriate anatomical knowledge using the SmART-ATP software (Precision X-Ray Inc., North Branford, CT) (32). During the manual segmentation of the training data set, the segmentation time was recorded to calculate the average manual segmentation time for one mouse. Images of five mice were randomly selected from the training data set and were segmented twice with a time interval of 9 mo between the segmentations to investigate the interobserver variability or reproducibility of the manual segmentations.

The deep learning algorithm [two-step three-dimensional (3D) U-Net model] was trained to segment the lower limb muscle complex volume on µCBCT images [Hounsfield units (HU)] of mice (8, 36). This 3D convolutional neural network architecture consisted of three encoding layers and three decoding layers, used weighted cross entry as loss function and used a dropout ratio of 0.5. The neural network was applied in two successive steps and made use of Tensorflow (Python 2.7) in combination with the NVIDIA CUDA Deep Neural Network library (cuDNN) computational kernels. The algorithm was executed on a NVIDIA Quadro P6000 (24 GB) graphics processing unit (GPU).

An automatic preprocessing step was performed on the µCBCT mice data set before the images were used by the deep learning algorithm. The µCBCT volume was first cropped in the transversal plane to a [256, 256, *z*] full resolution, where *z* is the number of reconstructed µCBCT slices. Next, the full resolution µCBCT volume was resized with a cubic interpolation method to an *x, y*, and *z* dimensions of [128, 128, *z* /2]. A similar method, with nearest-neighbor interpolation, was applied on the manually segmented muscle volumes. In the final preprocessing step, both the down sampled and full resolution µCBCT volumes were normalized between -400 HU and 1,000 HU.

In the first step, a 3D U-Net model was trained (350 epochs) to segment the muscle volume on the down sampled and preprocessed µCBCT images. The relative position of the automatically segmented muscle volume with respect to the down sampled µCBCT image was then used to extract a volume-of-interest (VOI) with preset dimensions (64 x 64 x 192 pixels) in the full resolution µCBCT data set. In the second step (350 epochs), the extracted full resolution VOI was used to train the second 3D U-Net.

2.2.2. Reverse validation

To evaluate the robustness and the consistency of the automatic segmentation algorithm, a reverse validation approach was applied. First, the “forward” automatic segmentation algorithm that was trained on the manually segmented data set (32 mice) was applied on a validation data set (51 mice). Here, the exclusion criterion was not adopted because the segmentations are not subject to experimental errors such as in the muscle wet mass experiments. In the reverse validation approach, a new model was trained based on the already automatically segmented muscle volumes. Here, the automatically segmented muscle volumes of 32 mice were randomly selected from the complete validation data set (51 mice) to have a similar sized trained data set compared with the original forward segmentation algorithm.

After training the “reverse” model, this model was applied to segment the training data set consisting of manual ground truth segmentations.

Finally, the automatic segmentation from the reverse algorithm was compared with the manual segmentation using three quantitative parameters, including the Dice similarity coefficient (DSC), 95th percentile Hausdorff distance (HD; in mm) and the center of mass displacement (ΔCOM; in mm). The DSC indicates the volumetric overlap between the manual and the automatic muscle segmentation, the HD calculates the maximum distance of a point in the manual segmentation to the nearest point in the automatic segmentation considering the voxel dimensions, and the ΔCOM calculates the 3D displacement of the mass centers of the manual and automatic segmentation in a Cartesian coordinate system.

2.2.3. μCBCT to mass density conversion

A μCBCT to mass density (CT2MD) conversion curve was required to calculate mass densities in every reconstructed μCBCT voxel. This CT2MD curve was obtained by scanning a cylindrical mini-phantom (diameter = 3 cm, length = 1 cm) (SmART Scientific Solutions BV, Maastricht, the Netherlands) which is composed of a solid water bulk, two air inserts, and 10 tissue mimicking inserts of 3.5 mm diameter with known mass densities (e.g., adipose 0.95 g/cm^3, soft tissue 1.06 g/cm^3, and bone inserts 1.33-1.83 g/cm^3). The mean CT numbers in HUs were calculated in circular regions-of-interest in the middle of the inserts and were then related to the certified mass densities of the cylindrical inserts in the form of a CT2MD conversion curve.

To determine muscle mass using μCBCT imaging, the CT2MD conversion curve is applied on the reconstructed μCBCT mice data set (HUs) to obtain a three-dimensional density matrix (g/cm^3). After applying the CT2MD curve on the reconstructed μCBCT mice data sets, the binary masks resulting from our automatic muscle segmentation algorithm was applied on the converted mass density volume and the knowledge of the reconstructed voxel dimensions was used to calculate the muscle mass noninvasively. An image intensity-based thresholding technique was applied on the μCBCT image data set to remove bone from the analysis.

3. RESULTS

3.1. Reverse validation and segmentation reproducibility

Three quantitative metrics (DSC, HD and ΔCOM) ± 1 standard deviation (SD) were calculated to evaluate the accuracy of the reverse automatic segmentation algorithm. On average (± 1 SD), 158±8 axial μCBCT slices were automatically segmented by the segmentation algorithm.

The DSC (± 1 SD) was equal to 0.93±0.03, the HD (± 1 SD) was equal to 0.4±0.2 mm and the ΔCOM (± 1 SD) was equal to 0.1±0.1 mm indicating a good agreement compared with the manual ground truth muscle segmentations. To investigate the manual segmentation reproducibility of the human observer, these metrics were also calculated between two manual segmentations of five mice. Here, the DSC was equal to 0.95±0.01, the HD was equal to 0.4±0.1 mm, and the ΔCOM was equal to 0.18±0.03 mm.

3.2. CT-derived muscle mass highly correlates with muscle wet masses

The combined muscle wet masses of the lower limb were determined in a validation set consisting of 47 mice and compared with the muscle masses calculated by the automatic segmentation algorithm (Figure 2). A trendline (blue) was fitted through all data points by linear regression (R^2=0.92). When separated for the time span between μCBCT scan and muscle wet mass assessment, the correlation further increased for the 23 mice for which muscle tissue was collected directly after imaging (R^2=0.96), compared with 24 mice of which muscle tissue was excised 2 days after imaging (R^2=0.80).

The ratio between the muscle wet mass and the algorithm-based muscle mass was a constant factor of 0.72±0.03 and can be attributed to the excision of a select set muscles from the hind limb musculature that can excised with high accuracy. After factor correction of the algorithm-defined muscle mass, a Bland-Altman plot was constructed to analyze the agreement between the two methods (Figure 2, right panel). No proportional bias was found, meaning that the two methods agree equally through the range of measurements.

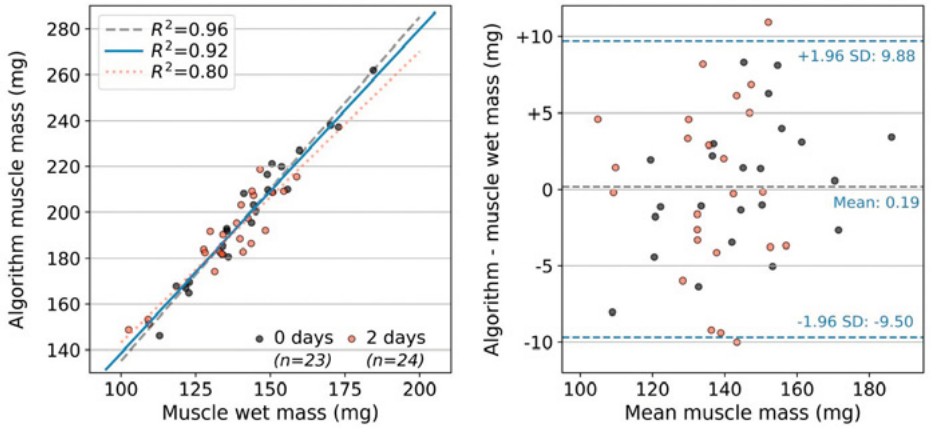

Figure 2. *Left panel: linear relationships between the muscle wet mass measurements (in one leg) and the muscle masses determined by the automatic segmentation algorithm (R^2=0.96, Y=1.50X – 14.85; Subset weighted after 0 days: R^2=0.92, Y=1.42X - 2.76; Subset weighted after 2 days: R^2=0.80, Y=1.27X + 16.04). Right panel: Bland-Altman plot between the algorithm muscle mass and the experimental muscle wet mass.*

3.3. Longitudinal assessment of muscle mass

To study muscle mass changes over time and detect the onset of muscle wasting, longitudinal evaluation of muscle mass is essential. To evaluate the automatic follow-up capabilities of our algorithm for individual mice, muscle masses were assessed for repetitive analyses of 6 randomly selected mice (3 sham control mice and 3 TB mice) in the validation data set. The muscle masses shown in Figure 3 were calculated relatively to the automatic measurement at baseline (day 0). These results show that the algorithm is capable of distinguishing muscle mass responses between sham control mice and TB mice developing muscle wasting.

One TB mouse and one sham control mouse were randomly chosen to evaluate the automatic contouring with manual contouring. In Supporting Information, animations in GIF-format are provided to visualize the automatic muscle segmentation and the manual muscle segmentation of these two mice in the axial, coronal and sagittal µCBCT viewing planes.

Figure 4 shows the automatic muscle segmentation (orange contour) and the manual muscle segmentation (yellow contour) on the µCBCT scan of these mice at the baseline measurement and at the last timepoint of the study. Because the mice were scanned at different days under different positioning conditions, a rigid deformation was applied with the Elastix software for visualization purposes (16).

For these two mice, the DSCs, HDs and ΔCOMs were calculated between the automatic and the manual segmentation at the first and last scan, respectively. For the control mouse the DSCs were equal to 0.94 and 0.95, the HDs were equal to 0.4 mm and 0.3 mm, and the ΔCOMs were equal to 0.3 mm and 0.2 mm, respectively. For the TB mouse, the DSCs were equal to 0.95 and 0.94, the HDs were equal to 0.3 mm and 0.4 mm, and the ΔCOMs were equal to 0.2 mm and 0.4 mm, respectively.

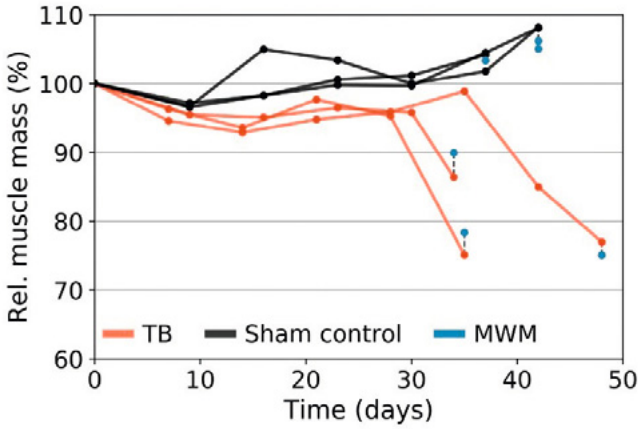

Figure 3. *Follow-up curves determined by our automatic muscle segmentation algorithm for three tumor-bearing (TB) mice (orange) and three sham control mice (black). The orange and black markers indicate the time of scanning, and the lines that connect the markers are linearly interpolated. The blue markers present the experimental muscle wet mass (MWM) at the last timepoint after applying the fitted linear relationship between the MWM and the algorithm muscle mass. The absolute (calculated) muscle mass at the baseline measurement varied slightly (time=0 days: 220.3±18.1 mg).*

3.4. Muscle segmentation algorithm

The segmentations generated by the forward two-step 3D U-Net based muscle segmentation algorithm were used to compare against muscle wet mass measurements. The first step of the 3D U-Net was trained in 5 h and 31 min, and the second step was trained in 6 h and 44 min resulting in a total duration of 12 h and 15 min. Performing the two-step 3D U-Net based automatic segmentation algorithm required an average calculation time of 6 s for one mouse, whereas the average manual segmentation time for one mouse was 17 mi. Consequently, compared with manual segmentation, the machine-based automatic method reduces the time needed to segment hind limb skeletal muscle by more than a factor of 150.

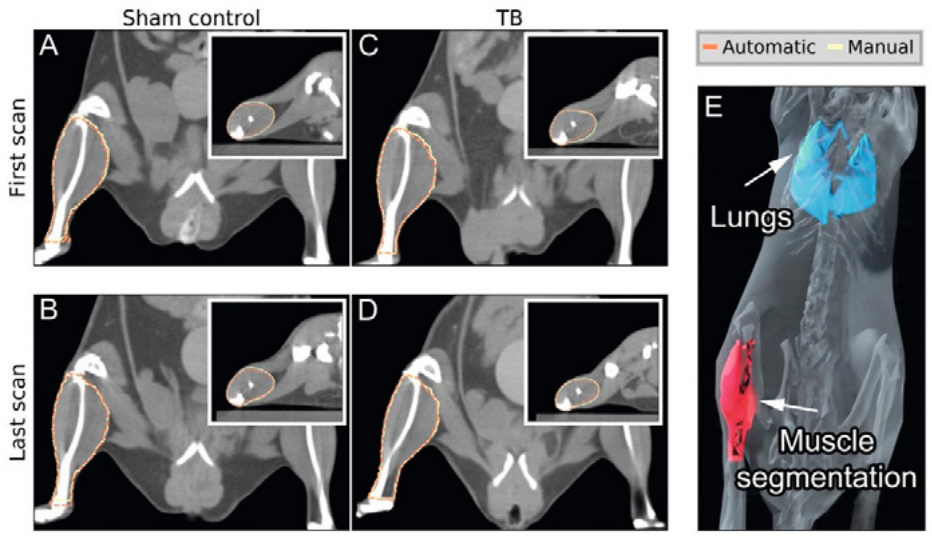

Figure 4. *Automatic (orange) and manual (yellow) hind limb muscle segmentation on a micro cone beam computed tomography (***µCBCT***) slice for a sham control mouse and a tumor bearing (TB) mouse for the scan at the baseline measurement* **(A-C)** *and the last timepoint* **(B-D)**. *Axial µCBCT slices are shown as insets in A-D. A three-dimensional model* **(E)** *of an example muscle segmentation is shown as illustration. In Supporting Information, animations of all cross sectional µCBCT slices are provided for both mice.*

4. DISCUSSION

In this paper we present a new method to noninvasively assess hind limb muscle mass in mice for cross-sectional and longitudinal purposes. It employs a deep learning algorithm trained to segment the lower muscle complex volume on µCBCT images. This algorithm or model showed a high correlation with the actual muscle wet mass measurements. Furthermore, this deep learning application enables longitudinal evaluation of skeletal muscle mass changes in experimental mouse models, significantly reducing animal numbers and analytical workload.

Biomedical image segmentation methods are commonly trained on manually segmented data sets and validated against manual segmentations on a validation data set. After automatic segmentation, statements about the algorithm's performance are then based on specific parameters (e.g. DSC, HD, or ΔCOM) compared with the manual segmentation. Although we calculated these three quantitative parameters solely for a random sham control mouse and a random TB mouse at two timepoints, we found a good agreement with the manual segmentations. The interobserver variability and reproducibility of the manual

segmentations evaluated in the image data sets of five mice showed similar results (DSC=0.95, HD=0.4 mm, ΔCOM=0.2 mm) compared with the quantitative metrics calculated between the manual and the automatic segmentation (DSC=0.95, HD=0.4 mm, and ΔCOM=0.4 mm).

In a more comprehensive quantitative analysis, we adopted a different approach to investigate whether a model can be trained on a data set that was originally segmented by the algorithm. This means that the result of the forward automatic segmentation algorithm was good enough to train a new deep learning model that in turn can segment μCBCT images with high accuracy. Using this reverse approach, we achieved mean high DSC scores of 0.93 and the HD and ΔCOM both had a submillimeter difference below 0.4 mm.

As experimental model validation, a good linear correlation (R^2=0.92) was found between the experimental wet muscle masses and the mass determined by our algorithm. The linear relationship was not equal to the unity curve which can be explained. First, not all soft tissues were extracted for the muscle wet mass measurements. Excision of the hind limb musculature was restricted to the gastrocnemius, soleus, plantaris, tibialis anterior and extensor digitorum longus muscles of both legs, as these can be collected intact and in a highly standardized manner. Consequently, remaining muscles such as the flexor digitorum longus, and the ankle plantarflexors and dorsiflexors, which contribute significantly to the lower hindlimb muscle mass (7), contributed to muscle mass calculated by the algorithm but not the muscle wet weight measurements. However, in the training data set and therefore also the automatic muscle segmentation, the whole muscle volume was segmented (in one leg) because the distinction between different muscle types requires enhanced image contrast which is not feasible with current μCBCT image quality. The muscle mass determined by our CT segmentation approach is therefore higher as it represents all muscle mass and not only the set of collected wet muscle masses. The high correlation between these two methods suggests that the relative differences between mice are maintained regardless of whether total lower hindlimb muscle mass or the cumulative wet mass of the standardized collected muscles are used.

Another source of uncertainty was the time between the last scan and the actual wet muscle mass measurements (day of euthenasia) which was ideally as short as possible (0 days), although this was not always possible for logistical reasons. The data extracted from the mice that were scanned at the day of euthenasia showed a clearly higher linear correlation (R^2=0.96) compared with the mice that

were analyzed within 2 days after imaging (R^2=0.80). The latter may be attributed to continuous changes in muscle mass, including muscle wasting in the TB mice.

Previous studies, such as Ceelen *et al.* (6), already reported a good linear correlation between the CT-derived mass and the wet muscle mass for mice (R^2=0.85), but here the CT based muscle segmentation protocol was performed manually. The correlation in that study was comparable, but slightly lower than our linear fit based on the automatically determined CT-derived muscle masses (R^2=0.92). More recently, Pasetto *et al. (24)* evaluated muscle atrophy in mouse models using micro-CT imaging. However, no CT segmentation was applied in their work; instead muscle mass was evaluated differently according to two-dimensional derived parameters including the perpendicular distance from the tibia half-length to the external hind limb muscle margin, and the distance from the upper extremity of the tibia to the medial malleolus.

The precision, accuracy, and reproducibility of DEXA in mice has already been investigated for in-vivo body parameters such as total bone mineral density, total body bone mineral, fat mass, and bone-free lean tissue mass (11, 22). In Bunckinx *et al.,* DEXA was even proposed as the reference standard for measuring muscle mass in patients. Although DEXA provides longitudinal follow-up data of bone-free lean tissue mass with low radiation exposure, this technique cannot distinguish separate muscle groups such as the lower limb muscle complex, which is possible with the µCBCT based algorithm. The use of µCBCT as imaging modality in TB mice models, in contrast to DEXA, can provide additional longitudinal follow-up information such as the tumor volume, from the same scan. MRI is an alternative high-resolution imaging technique, providing functional imaging with high soft tissue contrast. MRI does not require an imaging dose, in contrast to micro-CT, which is an important consideration when radiation dose is a critical factor in the study setup. Although MRI provides a better soft tissue contrast than micro-CT, the latter permits more rapid acquisitions at significantly lower cost. Additionally, it allows for tissue density quantifications, which makes micro-CT a suitable imaging technique for longitudinal muscle mass assessment.

In the muscle wet mass procedure, only muscles that are excisable in a highly standardized way were included, whereas the manual and automatic segmentation methods determined the entire lower hind limb muscle complex volume. The muscle complex was segmented as a whole because the µCBCT image reconstruction lacks image contrast to distinguish between individual muscle groups. In future studies, multimodality image information, such as µCBCT and MRI, could be

combined with deformable image registration to investigate the segmentation feasibility of individual muscle groups, although the μCBCT is required to convert image intensities to mass densities.

Lower limb muscle complex segmentation for multiple mice at different time points, risks amounting into a time-consuming task in a preclinical study. To illustrate this point: in our experiments, the manual segmentation by an experienced biologist of the lower limb complex on the μCBCT images required on average 20 min for one mouse. The animals were scanned at 7 different timepoints on average, resulting in 581 μCBCT scans, which would have taken more than 190 h to segment using manual contouring. In contrast, the method described here required ~11 h to segment the training data set manually, around 12 h to train the algorithm on GPU and only 6 s per automatic muscle segmentation. The latter would even enable real-time follow-up of muscle wasting during the in-vivo experiment.

Prior to implementation of the algorithm in other settings, additional validation steps may be required. In this study, the deep learning model was trained on a μCBCT image data set that was acquired with one specific imaging protocol at an X-ray tube potential of 50 kVp. However, further research is required to investigate whether the trained model is valid in imaging data sets that were acquired at different X-ray tube potential settings (e.g., with an additional scan at 90 kVp in dual-energy μCBCT), or on imaging data sets that were acquired with different spectral filtrations (33). Our training data set consisted entirely of 129S2/SvPasCrl mice. As such, further investigations are required to evaluate how the trained model will segment the lower limb muscle in mice that have age-, strain-, or pathological model-related differences in muscle size, compared with the mice that formed the training data set used in this study.

Nevertheless, we anticipate that the proposed algorithm is capable of segmenting muscle volumes in a variety of animals, as long as the study setup (i.e., X-ray acquisition protocols and reconstruction settings) and animal characteristics are consistent over time, i.e. the period in which the training data set is generated and applied to the nonsegmented data set. Therefore, we expect that for every study that uses a different imaging protocol or experimental animal species, the creation of a manually segmented training data set and the retraining of the algorithm is required to achieve the best automatic segmentation outcome.

However, this algorithm, which can be retrained depending on the study setup, will facilitate the workflow tremendously because only the training data set has to be

segmented manually. Involving experimental models using μCBCT or μCT imaging in future work will be of interest to create a larger and more diverse training data set of different animal species and settings scanned with different scan protocols and even different scanners to train a model that can be widely applied without the need for (extensive) retraining.

In conclusion, a noninvasive automatic algorithm was developed using artificial intelligence (two-step 3D U-Net) to segment skeletal muscle tissue in the lower limb complex of mice. The performance of the algorithm was in good agreement with the actual muscle wet mass measurements. This experimentally validated algorithm enables highly accurate noninvasive and automated longitudinal evaluation of skeletal muscle mass changes in mice with minimal operator involvement in the data analysis. It provides a unique possibility to collect large amounts of data from the mice, and to understand when and how muscle wasting starts and when it becomes life threatening. Furthermore, this method will allow a more accurate planning of experiments and reduce the number of mice needed for longitudinal experiments.

REFERENCES

1. Anker SD, Ponikowski P, Varney S, Chua TP, Clark AL, Webb-Peploe KM, Harrington D, Kox WJ, Poole-Wilson PA, and Coats AJ. Wasting as independent risk factor for mortality in chronic heart failure. *Lancet* 349: 1050-1053, 1997.
2. Baiker M, Milles J, Dijkstra J, Henning TD, Weber AW, Que I, Kaijzel EL, Lowik CW, Reiber JH, and Lelieveldt BP. Atlas-based whole-body segmentation of mice from low-contrast Micro-CT data. *Med Image Anal* 14: 723-737, 2010.
3. Borga M, West J, Bell JD, Harvey NC, Romu T, Heymsfield SB, and Dahlqvist Leinhard O. Advanced body composition assessment: from body mass index to body composition profiling. *J Investig Med* 66: 1-9, 2018.
4. Breiman RS, Beck JW, Korobkin M, Glenny R, Akwari OE, Heaston DK, Moore AV, and Ram PC. Volume determinations using computed tomography. *American Journal of Roentgenology* 138: 329-333, 1982.
5. Ceelen JJM, Schols A, Kneppers AEM, Rosenbrand R, Drozdz MM, van Hoof SJ, de Theije CC, Kelders M, Verhaegen F, and Langen RCJ. Altered protein turnover signaling and myogenesis during impaired recovery of inflammation-induced muscle atrophy in emphysematous mice. *Sci Rep* 8: 10761, 2018.
6. Ceelen JJM, Schols A, van Hoof SJ, de Theije CC, Verhaegen F, and Langen RCJ. Differential regulation of muscle protein turnover in response to emphysema and acute pulmonary inflammation. *Respir Res* 18: 75, 2017.
7. Charles JP, Cappellari O, Spence AJ, Hutchinson JR, and Wells DJ. Musculoskeletal Geometry, Muscle Architecture and Functional Specialisations of the Mouse Hindlimb. *PLoS One* 11: e0147669, 2016.
8. Ciçek Ö, Abdulkadir A, Lienkamp SS, Brox T, and Ronneberger O. 3D U-Net: Learning dense volumetric segmentation from sparse Annotation. *arXiv* 2016.
9. Evans DJ, Murray R, and Kissebah AH. Relationship between skeletal muscle insulin resistance, insulin-mediated glucose disposal, and insulin binding. Effects of obesity and body fat topography. *J Clin Invest* 74: 1515-1525, 1984.
10. Gibbons DL, Lin W, Creighton CJ, Rizvi ZH, Gregory PA, Goodall GJ, Thilaganathan N, Du L, Zhang Y, Pertsemlidis A, and Kurie JM. Contextual extracellular cues promote tumor cell EMT and metastasis by regulating miR-200 family expression. *Genes Dev* 23: 2140-2151, 2009.
11. Halldorsdottir S, Carmody J, Boozer CN, Leduc CA, and Leibel RL. Reproducibility and accuracy of body composition assessments in mice by dual energy x-ray absorptiometry and time domain nuclear magnetic resonance. *Int J Body Compos Res* 7: 147-154, 2009.
12. Heier CR, Guerron AD, Korotcov A, Lin S, Gordish-Dressman H, Fricke S, Sze RW, Hoffman EP, Wang P, and Nagaraju K. Non-invasive MRI and spectroscopy of mdx mice reveal temporal changes in dystrophic muscle imaging and in energy deficits. *PLoS One* 9: e112477, 2014.
13. Janssen I, Heymsfield SB, Wang ZM, and Ross R. Skeletal muscle mass and distribution in 468 men and women aged 18-88 yr. *J Appl Physiol (1985)* 89: 81-88, 1985.
14. Karlsson A, Rosander J, Romu T, Tallberg J, Gronqvist A, Borga M, and Dahlqvist Leinhard O. Automatic and quantitative assessment of regional muscle volume by multi-atlas segmentation using whole-body water-fat MRI. *J Magn Reson Imaging* 41: 1558-1569, 2015.

15. Kazemi-Bajestani SM, Mazurak VC, and Baracos V. Computed tomography-defined muscle and fat wasting are associated with cancer clinical outcomes. *Semin Cell Dev Biol* 54: 2-10, 2016.
16. Klein S, Staring M, Murphy K, Viergever MA, and Pluim JP. elastix: a toolbox for intensity-based medical image registration. *IEEE Trans Med Imaging* 29: 196-205, 2010.
17. Levine JA, Abboud L, Barry M, Reed JE, Sheedy PF, and Jensen MD. Measuring leg muscle and fat mass in humans: comparison of CT and dual-energy X-ray absorptiometry. *J Appl Physiol (1985)* 88: 452-456, 2000.
18. Ma CM, Coffey CW, DeWerd LA, Liu C, Nath R, Seltzer SM, Seuntjens JP, and American Association of Physicists in M. AAPM protocol for 40-300 kV x-ray beam dosimetry in radiotherapy and radiobiology. *Med Phys* 28: 868-893, 2001.
19. Marcuzzo S, Zucca I, Mastropietro A, de Rosbo NK, Cavalcante P, Tartari S, Bonanno S, Preite L, Mantegazza R, and Bernasconi P. Hind limb muscle atrophy precedes cerebral neuronal degeneration in G93A-SOD1 mouse model of amyotrophic lateral sclerosis: a longitudinal MRI study. *Exp Neurol* 231: 30-37, 2011.
20. Martin L, Hopkins J, Malietzis G, Jenkins JT, Sawyer MB, Brisebois R, MacLean A, Nelson G, Gramlich L, and Baracos VE. Assessment of Computed Tomography (CT)-Defined Muscle and Adipose Tissue Features in Relation to Short-Term Outcomes After Elective Surgery for Colorectal Cancer: A Multicenter Approach. *Ann Surg Oncol* 25: 2669-2680, 2018.
21. Mytelka DS, Li L, and Benoit K. Post-diagnosis weight loss as a prognostic factor in non-small cell lung cancer. *J Cachexia Sarcopenia Muscle* 9: 86-92, 2018.
22. Nagy TR, and Clair AL. Precision and accuracy of dual-energy X-ray absorptiometry for determining in vivo body composition of mice. *Obes Res* 8: 392-398, 2000.
23. Park JS, Vohra R, Klussmann T, Bengtsson NE, Chamberlain JS, and Lee D. Non-invasive tracking of disease progression in young dystrophic muscles using multi-parametric MRI at 14T. *PLoS One* 13: e0206323, 2018.
24. Pasetto L, Olivari D, Nardo G, Trolese MC, Bendotti C, Piccirillo R, and Bonetto V. Micro-computed tomography for non-invasive evaluation of muscle atrophy in mouse models of disease. *PLoS One* 13: e0198089, 2018.
25. Periasamy M, Herrera JL, and Reis FCG. Skeletal Muscle Thermogenesis and Its Role in Whole Body Energy Metabolism. *Diabetes Metab J* 41: 327-336, 2017.
26. Prado CM, Lieffers JR, McCargar LJ, Reiman T, Sawyer MB, Martin L, and Baracos VE. Prevalence and clinical implications of sarcopenic obesity in patients with solid tumours of the respiratory and gastrointestinal tracts: a population-based study. *Lancet Oncol* 9: 629-635, 2008.
27. Schiaffino S, Dyar KA, Ciciliot S, Blaauw B, and Sandri M. Mechanisms regulating skeletal muscle growth and atrophy. *FEBS J* 280: 4294-4314, 2013.
28. Schols AM, Broekhuizen R, Weling-Scheepers CA, and Wouters EF. Body composition and mortality in chronic obstructive pulmonary disease. *Am J Clin Nutr* 82: 53-59, 2005.
29. Shih R, Wang Z, Heo M, Wang W, and Heymsfield SB. Lower limb skeletal muscle mass: development of dual-energy X-ray absorptiometry prediction model. *J Appl Physiol (1985)* 89: 1380-1386, 2000.
30. Straub RH, Cutolo M, Buttgereit F, and Pongratz G. Energy regulation and neuroendocrine-immune control in chronic inflammatory diseases. *J Intern Med* 267: 543-560, 2010.

31. van der Heyden B, Podesta M, Eekers DB, Vaniqui A, Almeida IP, Schyns LE, van Hoof SJ, and Verhaegen F. Automatic multiatlas based organ at risk segmentation in mice. *Br J Radiol* 92: 20180364, 2019.
32. van Hoof SJ, Granton PV, and Verhaegen F. Development and validation of a treatment planning system for small animal radiotherapy: SmART-Plan. *Radiother Oncol* 109: 361-366, 2013.
33. Vaniqui A, Schyns L, Almeida IP, van der Heyden B, Podesta M, and Verhaegen F. The effect of different image reconstruction techniques on pre-clinical quantitative imaging and dual-energy CT. *Br J Radiol* 92: 20180447, 2019.
34. Verhaegen F, Dubois L, Gianolini S, Hill MA, Karger CP, Lauber K, Prise KM, Sarrut D, Thorwarth D, Vanhove C, Vojnovic B, Weersink R, Wilkens JJ, and Georg D. ESTRO ACROP: Technology for precision small animal radiotherapy research: Optimal use and challenges. *Radiother Oncol* 126: 471-478, 2018.
35. von Haehling S, and Anker SD. Prevalence, incidence and clinical impact of cachexia: facts and numbers-update 2014. *J Cachexia Sarcopenia Muscle* 5: 261-263, 2014.
36. Wang C, MacGillivray T, Yang G, and Newby D. A two-stage Unet framework for mutli-class segmentation on full resolution image. *arXiv* 2018.

6

Deep Learning Based Automated Orthotopic Lung Tumor Segmentation in Whole-Body Mouse CT-Scans

Wouter RPH van de Worp
Brent van der Heyden
Georgios Lappas
Ardy van Helvoort
Jan Theys
Annemie MWJ Schols
Frank Verhaegen
and Ramon CJ Langen

Cancers
2021, 13:4585

ABSTRACT

Lung cancer is the leading cause of cancer related deaths worldwide. The development of orthotopic mouse models of lung cancer, which recapitulates the disease more realistically compared to the widely used subcutaneous tumor models, is expected to critically aid the development of novel therapies to battle lung cancer or related comorbidities such as cachexia. However, follow-up of tumor take, tumor growth and detection of therapeutic effects is difficult, time consuming and requires a vast number of animals in orthotopic models. Here, we describe a solution for the fully automatic segmentation and quantification of orthotopic lung tumor volume and mass in whole-body mouse computed tomography (CT) scans. The goal is to drastically enhance the efficiency of the research process by replacing time-consuming manual procedures with fast, automated ones. A deep learning algorithm was trained on 60 unique manually delineated lung tumors and evaluated by four-fold cross validation. Quantitative performance metrics demonstrated high accuracy and robustness of the deep learning algorithm for automated tumor volume analyses (mean dice similarity coefficient of 0.80), and superior processing time (69 times faster) compared to manual segmentation. Moreover, manual delineations of the tumor volume by three independent annotators was sensitive to bias in human interpretation while the algorithm was less vulnerable to bias. In addition, we showed that besides longitudinal quantification of tumor development, the deep learning algorithm can also be used in parallel with the previously published method for muscle mass quantification and to optimize the experimental design reducing the number of animals needed in preclinical studies. In conclusion, we implemented a method for fast and highly accurate tumor quantification with minimal operator involvement in data analysis. This deep learning algorithm provides a helpful tool for the noninvasive detection and analysis of tumor take, tumor growth and therapeutic effects in mouse orthotopic lung cancer models.

1. INTRODUCTION

Lung cancer is the leading cause of cancer deaths worldwide, comprising approximately 25% of all cancer deaths [1]. Muscle wasting as a component of cancer cachexia is frequently observed in lung cancer patients and is associated with poor clinical outcome and decreased overall survival [2–5]. Preclinical research is essential for the development and evaluation of novel therapies targeting the tumor and the host. One of the greatest challenges encountered by researchers in preclinical lung cancer (cachexia) research is the translatability of animal models [6,7]. In order to study lung cancer more realistically, models in which the tumor grows in its original stroma where it can interact with the complex microenvironment are needed [8]. Such orthotopic lung cancer models have been described in mice [9–11], but are not widely used in preclinical research due to a range of challenges involved. A major challenge is the monitoring of tumor take and growth in these orthotopic lung tumor models. Unlike subcutaneous xenograft models, the tumors in orthotopic models are not visible to the eye and accessible for caliper measurements. Instead, a proxy for tumor progression in orthotopic mouse models is mostly obtained from histological assessment in terminal experiments ending at sequential time points [12,13]. However, this approach introduces variation and the number of required animals increases proportionally with each additional time point, which is not consistent with the 3R principle embedded in national and international legislation and regulations on the protection of animals used for scientific purposes [14]. A more suitable option is the use of noninvasive imaging, such as computed tomography (CT), to monitor tumor progression over time.

Micro cone beam CT (μCBCT) imaging plays an increasingly important role in preclinical cancer research. Previously, this imaging modality has been used successfully to detect tumors in lung cancer mouse models [15–20]. Analysis of the acquired imaging data by delineating the region of interest (ROI), in this case the lung tumor, allows researchers to extract quantitative information, such as tumor shape and tumor size. Traditionally, tumor segmentation is performed manually by delineating the tumor outlines in each slice of the three-dimensional (3D) CT image. However, this is labor intensive and time consuming, especially in case of repetitive CT measurements for longitudinal follow-up of tumor growth. In addition, manual delineation is a challenging task, as it requires great knowledge in anatomy and CT imaging, and it is susceptible to inter- and intra-observer variabilities. Semi-automated methods (such as thresholding and region growing) for the segmentation of lung tumors have been reported in literature already [21–23]. As such, robust and time-efficient automatic image segmentation methods to quantify

tumor development in preclinical orthotopic models will offer great benefits for the research field.

Multiple reference atlas-based approaches have been used for automatic segmentation of organs [24,25]. However, these automatic approaches often do not achieve adequate segmentation quality for heterogenic ROIs, which typically apply for tumors. The implementation of artificial intelligence (AI) in medical image processing suggests that convolutional neural networks, such as U-Nets, are an appropriate foundation for automatic ROI segmentation. Previously, we developed a deep learning algorithm trained to automatically segment the mouse calf muscle complex on μCBCT images, to derive muscle mass [26]. This algorithm showed a high correlation with the actual muscle wet mass measurements. More recently, Schoppe et al. open-sourced a deep neural network called AIMOS for automatic multi-organ segmentation of normal organs in whole-body scans of mice [27]. This model was more than two orders of magnitude faster than the atlas-based approaches, without compromising on quality. These recent developments suggest that AI will be a great platform to develop a fully automatic segmentation workflow for the quantification of lung tumors in CT images.

Here, we present the development and validation of a deep learning algorithm, based on existing AI architecture, for automated lung tumor segmentation in whole-body mouse μCBCT scans. This algorithm will be shown to be more consistent compared to human annotators and reduces the analytical workload to determine tumor size notably. In addition to longitudinal quantification of tumor development, our approach can also be deployed in parallel with the previously developed algorithm for muscle mass quantification, and to optimize the randomization and 3R animal welfare aspects of the experimental design in preclinical studies.

2. MATERIALS AND METHODS

2.1. Mouse Experimental and Imaging Procedures

2.1.1. Animals

Sixty male mice of 10 weeks (129S2/SvPasCrl, Charles River Laboratories) were socially housed (n = 3 in GM500 IVC cages (Tecniplast, Buguggiate, Italy) with corn cob bedding (JRS Lignocel, Rosenberg, Germany)) in a climate-controlled room (12:12 dark-light cycle with a constant room temperature of 21 ± 1 °C). Mice were given ad libitum access to food (AIN-93M, Bio-Services BV, Uden, NL, USA) and drinking water (autoclaved, softened and acidified (pH = 2.5)). After 1 week of

acclimatization, animals underwent surgery at a standardized time window during their inactive period of the day. Following surgery, animals were monitored daily. Data shown were derived from the combination of several experimental cohorts with identical animal characteristics and experimental procedures. The CT images of in-total 60 mice were used to create training and validation datasets.

This work was conducted in accordance with institutional guidelines for the care and use of laboratory animals established by the Ethics Committee for Animal Experimentation of the Maastricht University, in full compliance to national legislation on animal research following the European Directive 2010/63/EU for the use of animals for scientific purposes and was part of a set of experiments to establish an orthotopic model of lung cancer cachexia.

2.1.2. Tumor Model

Murine K-ras^{G12D}; p53$^{R172H\Delta G}$ lung epithelium-derived adenocarcinoma cells [28], kindly provided by Dr. J.M. Kurie, were cultured in vitro with Roswell Park Memorial Institute 1640 medium (Gibco, Rockville, MD, USA), supplemented with 9% fetal bovine serum (Gibco). Tumor cells were trypsinized in a sub-confluent state and suspended in growth factor reduced matrix (Matrigel, Corning Inc., New York, NY, USA) at a concentration 2×10^6 cells/mL. Animals were anesthetized using a mixture of air and isoflurane (4% induction, 2% maintenance) and placed in a position of right lateral decubitus. Fur was removed and a 1 cm superficial skin incision was made below the left scapula. Fat was removed, and underlying muscles (excluding intercostal muscles) were carefully lifted. While visualizing the lung motion, 10 µL of tumor cells (2×10^4 cells in 10 µL) were injected through the intercostal space into the lung. The muscles were placed back on top of the rib cage in the correct orientation and the skin was closed using a 5-0 suture. All mice receive pre-operative analgesia (Carprofen and Buprenorphine) via subcutaneous injection and post-operative analgesia (Carprofen) in the drinking water.

2.1.3. Experimental Protocol

Body weight and food intake were measured daily at a standardized time window during their inactive period of the day. At baseline and weekly after surgery, µCBCT imaging was performed for all mice to assess lung tumor development and to detect muscle volume changes over time [26]. At the end of the experiment, when mice reached cachexia related humane endpoints, mice were scanned and subsequently sacrificed using intraperitoneal pentobarbital overdose. Lungs and skeletal muscles and other organs were collected using standardized dissection methods and frozen/fixed for further analysis.

2.1.4. Animal Imaging

The anesthetized animals were placed in prone position with toes facing the flanks (foot and tibia angle ± 90°), and scanned using a μCBCT scanner (X-RAD 225Cx, Precision X-Ray Inc., North Branford, CT, USA) at an X-ray tube potential of 50 kVp, X-ray tube current of 5.6 mA, and an imaging time of 2 min [29]. The imaging dose of 30 cGy was verified using a PTW TN300012 Farmer-type ionization chamber (PTW, Freiburg, Germany) according to the AAPM TG-61 protocol [30]. The μCBCT projection data was reconstructed using the Pilot Feldkamp back projection algorithm with a voxel dimension of 100 × 100 × 100 μm^3 [31].

2.1.5. Manual Segmentation

Sixty lung tumor segmentations in the left lung were annotated manually by a scientist with appropriate anatomical knowledge using the SmART-ATP software (Precision X-ray Inc. North Branford, CT, USA and SmART Scientific Solutions BV, Maastricht, NL, USA). The annotated CT data were split randomly in four batches of 15 mice CTs each to conduct a 4-fold cross-validation. To assess inter- and intra-observer variability, one batch of mice (n = 15) was manually delineated by two additional annotators. Detailed guidelines on the annotation of the tumor (see Supporting Information) were employed to ensure reproducible annotations from all annotators.

2.2. Automatic Image Segmentation

2.2.1. Deep Learning Algorithm

The automatic tumor segmentation model contains a preprocessing step, a deep learning algorithm and a post-processing step. The preprocessing step ensures that all μCBCT scans have a fixed input size. First, air voxels were cropped by thresholding (–800 Hounsfield Units [HU]) from the original reconstructed μCBCT volume [512 × 512 × Z]. The number of cranial–caudal slices in the μCBCT reconstruction is denoted as Z. Then, the well-defined appearance of the lungs in μCBCT images was used to automatically derive the center of the cropped image volume by means of simple thresholding (–600, –200 HU) to mask low-density regions. Additionally, morphological operations (erosion and dilation using a spherical kernel of 5 × 5 × 5) were applied successively to subtract undesired low-density regions from the binary lung mask (e.g., bowel gas or trachea), and to extract the three-dimensional position of the lungs. Second, the cropped μCBCT slices around the binary lung mask (256 × 256 × Z) were resized to a 128 × 128 × Z/2 CT volume with cubic interpolation to fit the graphics processing unit (GPU) memory. Subsequently, the resized and original μCBCT volumes were normalized

between −400 and 1000 HU. Finally, to improve generalization of the network, data augmentation was performed on every μCBCT dataset and its corresponding segmentation, in every epoch. The data augmentation consisted of randomly sampled rotations (–15°, 15°) and shearing (–5, 5) operations.

An in-house developed supervised deep learning algorithm (two-step 3D U-Net) was trained to automatically segment lung tumors on μCBCT images of mice. The network architecture for both steps of the 3D U-Net was similar and consisted of three encoding layers to analyze the CT dataset, and three decoding layers to produce the tumor segmentation. Every encoding layer contained two $3 \times 3 \times 3$ convolutions followed by a rectified linear unit. Subsequently, the spatial resolution was halved in every dimension by applying $2 \times 2 \times 2$ max pooling. The decoding path was symmetrical to the encoding path, with the exception that max pooling was replaced by bilinear up sampling. The dropout ratio was set to 0.5, the number of epochs to 350, Adam was used as training optimizer [32], and the dice similarity coefficient (DSC) was adopted as optimization function to train our convolutional neural network. An illustration of the two-step 3D U-Net network architecture is shown in Figure S1.

The 3D U-Nets were applied successively in TensorFlow. The first step was applied on a rescaled low-resolution dataset ($200 \times 200 \times 200$ μm^3) to define a tumor-specific cropped 3D volume-of-interest. In the second step, this position matrix was used on a cropped full-resolution dataset to segment individual foreground voxels. The two-step network was trained, tested, and validated on a NVIDIA Quadro P6000 (24 GB) GPU and made use of the NVIDIA CUDA® Deep Neural Network library computational kernels.

The post-processing step consisted of a filling process, which was a unity check for holes in the automatic segmentation. No further post-processing steps such as filtering and morphological operations were performed.

2.2.2. μCBCT to Mass Density Conversion

For the tumor mass calculation, a μCBCT to mass density conversion (CT2MD) was utilized to convert HU values from the reconstructed μCBCT scans to 3D density matrices (g/cm^3). The CT2MD calibration curve was calculated based on scanning a cylindrical 30 mm diameter phantom dedicated for preclinical research in small animals (SmART Scientific Solutions BV, Maastricht, NL, USA). The phantom consists of a solid water structure enclosing 10 tissue-mimicking materials and 2 air holes with known and verified corresponding mass densities,

e.g., $\rho_{solid\text{-}water}$ = 1.02 g/cm^3, $\rho_{adipose}$ = 0.95 g/cm^3, $\rho_{cortical\ bone}$ = 1.33–1.82 g/cm^3. In order to calculate the tumor mass, every voxel in the reconstructed μCBCT that belongs in the corresponding ROI on the binary output predicted by the automatic deep learning model was post-processed to obtain the mass density per voxel. Finally, the voxel dimensions, e.g., pixel spacing and slice thickness, derived by the μCBCT reconstruction settings were applied to determine the tumor mass.

3. RESULTS

3.1. Quantitative Evaluation of the Segmentation Performance

In order to evaluate the performance of the automatic tumor segmentation algorithm, a four-fold cross-validation methodology was adopted. The lung tumor, ranging from 1.1 mm^3 to 81.6 mm^3, was manually delineated in 60 mice. The dataset was randomly partitioned into four equal sized batches (Batch 1–4) consisting of 15 mice each. One batch was retained as the test dataset to evaluate the model on unseen data, and the remaining three batches were used as training/test dataset. This cross-validation process was repeated four times, with each of the batches used once as the test dataset. High overlap in the tumor volumes was observed comparing the manual segmentations vs. the automatic segmentations (Batch 1: 10.19 ± 10.89 mm^3 vs. 12.3 ± 11.69 mm^3; Batch 2: 44.79 ± 26.28 mm^3 vs. 46.76 ± 30.12 mm^3; Batch 3: 27.14 ± 16.17 mm^3 vs. 26.25 ± 15.53 mm^3; and Batch 4: 26.25 ± 17.34 mm^3 vs. 25.10 ± 15.72 mm^3) (Figure 1A). Subsequently, three quantitative performance metrics (dice similarity coefficient (DSC), 95th percentile Hausdorff distance (95HD), and center of mass displacement (ΔCOM)) were calculated for each batch, which allowed quantitative evaluation of the performance of the automatic lung tumor segmentation algorithm (Figure 1B–D). The average DSC (± 1 SD) of the four batches was equal to 0.80 ± 0.10, the average HD (± 1 SD) was equal to 0.74 ± 0.48 mm and the average ΔCOM (± 1 SD) was equal to 0.30 ± 0.46 mm.

Deep learning algorithms are generally known to be fast methods for micro-CT image segmentation. Although the training of the deep learning algorithm (two-step 3D U-Net) requires an initial time investment, the processing time to segment one 3D whole-body scan of a mouse is substantially shorter compared to manual segmentation. For the automatic tumor segmentation algorithm, the first step of the two-step 3D U-Net was trained in 7 h and 18 min., and the second step was trained in 8 h and 6 min., resulting in a total duration of 15 h and 24 min. The automatic volumetric segmentation was 69 times faster: analysis of the tumor of one whole-

body μCBCT took the deep learning algorithm only 9 s, whereas the manual tumor segmentation time for one mouse was approximately 8 min.

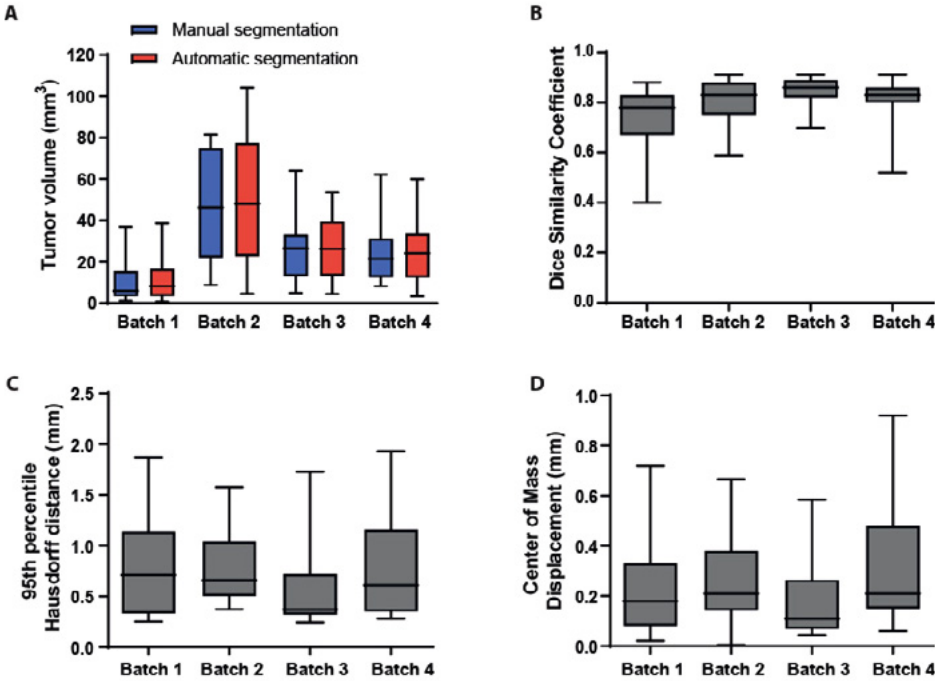

Figure 1. *Quantitative performance metrics of deep learning algorithm. (***A***) Box plots showing the distribution of the tumor volumes in mm³ per cross-validation batch (n = 15), determined by manual and automatic segmentation. (***B***–***D***) Box plots of (***B***) the dice similarity coefficient, (***C***) 95th percentile Hausdorff Distance (in mm), and (***D***) the center of mass displacement (in mm), calculated for each of the batches.*

3.2. Qualitative Evaluation of the Segmentation Performance

Visual evaluation confirmed that the automatic tumor segmentations were in the correct anatomical location and closely overlapped with the manual delineations of the training dataset (Figure 2). However, as indicated by the quantitative performance metrics, in certain cases, there was a marginal deviation from the training dataset. To understand the origin of the deviation, we further examined automatic tumor segmentations in which the DSC was more than two standard deviations lower compared to the overall mean DSC (0.80; Figure 2A). Only 6.6% of the cases had a DSC less than 0.60. In all these cases, the tumor volume was less than 9 mm³. Several automatically segmented tumor volumes had a minor overlap

with the manually delineated tumor volume, resulting in a low DSC (Figure 2B, row 2). In addition, in other cases, the automatic segmentation appeared correct, despite being different from the manually delineated training dataset (Figure 2B, row 3). This type of deviation is sometimes observed when the tumor is located in close proximity to the bronchi and/or pleura.

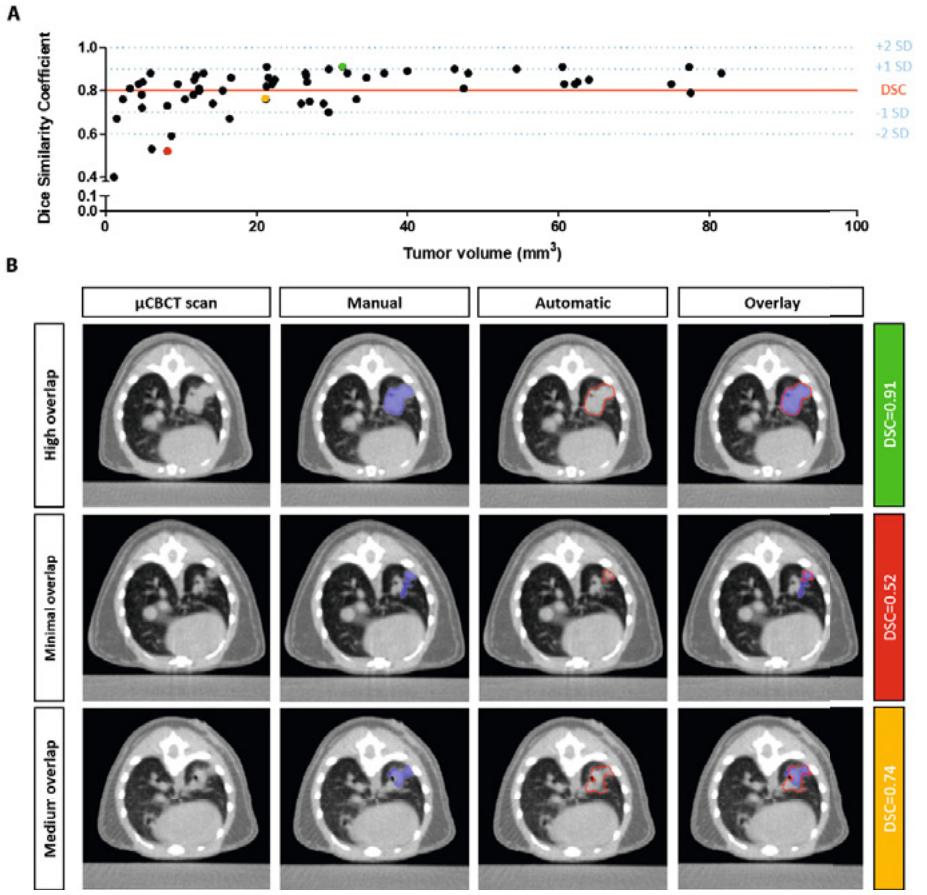

Figure 2. *Qualitative evaluation of the algorithm performance.* **(A)** *Scatterplot of the DSC versus tumor volume (n = 60). The mean DSC is indicated with a horizontal red line. The ±1SD and ±2SD are indicated with blue dotted lines.* **(B)** *Axial µCBCT images showing (from left to the right) an unsegmented scan, the manual tumor segmentation, the automatic tumor segmentation, and the overlay of the manual and automatic segmentations. The first row shows an illustrative case with a high overlap, the second row shows a case with minimal overlap, and the third row depicts a case with medium overlap. The corresponding DSCs of each row in Figure 2B are indicated in the scatterplot of Figure 2A by the green, red and yellow markers.*

3.3. Assessment of Subjectivity and Bias in Human Interpretation

In order to assess the subjectivity and bias in tumor volumes based on human interpretation, we compared the manual delineations of the training dataset (annotator 1) with the manual delineations of a second and a third independent annotator on a subset of 15 μCBCT scans. In addition, we compared the segmented tumor volumes of all three annotators with the automatic segmentations of the deep learning algorithm (trained on manual delineations of annotator 1), using the Bland and Altman method. A significant correlation was observed comparing the manually segmented tumor volumes between annotators (Table 1, Figure S2A). However, a significant difference between the tumor volumes of annotator 1 vs. annotator 2 and annotator 1 vs. annotator 3 was observed, indicative of proportional bias or disagreement (Table 1, Figure S2B). This bias was absent when comparing the tumor volumes of annotator 2 vs. annotator 3 (Table 1, Figure S2B). Subsequently, three quantitative performance metrics (DSC, 95HD and ΔCOM) were calculated for each of the comparisons (Table 1, Figure S2C). The proportion of specific agreement (DSC) was similar comparing the segmented tumor volumes of all three annotators, respectively 0.76 ± 0.13 (annotator 1 vs. annotator 2), 0.76 ± 0.13 (annotator 1 vs. annotator 3) and 0.75 ± 0.13 (annotator 2 vs. annotator 3).

Comparing the manually segmented tumor volumes of all three annotators with the automatic segmentations of the deep leaning algorithm, consistently higher correlations were observed than between annotators (Table 1, Figure S2A). However, no agreement was observed between the tumor volumes of annotator 2 vs. deep learning and annotator 3 and deep learning algorithm (Table 1, Figure S2B). Importantly, good agreement between annotator 1 vs. the deep learning algorithm was achieved (which was trained on annotator 1's contours). The DSC comparing the segmented tumor volumes of annotator 2 vs. deep learning and annotator 3 vs. deep learning were similar, respectively 0.74 ± 0.12 and 0.76 ± 0.10 (Table 1, Figure S2C). Although not significant, the DSC comparing annotator 1 vs. deep learning was higher (DSC = 0.81 ± 0.09).

Table 1. Subjectivity and bias in human interpretation.

	Segmented Tumor Volume		Quantitative Performance Metrics		
	Correlation (R^2)*	**Agreement ****	**DSC**	**95HD (mm)**	**ΔCOM (mm)**
Annotator 1 vs. Annotator 2	0.79 ($p < 0.001$)	No ($p = 0.005$)	0.76 ± 0.13	0.84 ± 0.63	0.51 ± 0.41
Annotator 1 vs. Annotator 3	0.88 ($p < 0.001$)	No ($p = 0.011$)	0.76 ± 0.13	0.82 ± 0.55	0.41 ± 0.54
Annotator 2 vs. Annotator 3	0.77 ($p < 0.001$)	Yes ($p = 0.251$)	0.75 ± 0.13	0.66 ± 0.47	0.39 ± 0.36
Annotator 1 vs. Deep learning	0.93 ($p < 0.001$)	Yes ($p = 0.365$)	0.81 ± 0.09	0.78 ± 0.53	0.30 ± 0.23
Annotator 2 vs. Deep learning	0.87 ($p < 0.001$)	No ($p = 0.001$)	0.74 ± 0.12	0.82 ± 0.41	0.51 ± 0.37
Annotator 3 vs. Deep learning	0.92 ($p < 0.001$)	No ($p = 0.007$)	0.76 ± 0.10	0.77 ± 0.39	0.45 ± 0.45

DSC: dice similarity coefficient, 95HD: 95th percentile Hausdorff distance, ΔCOM: center of mass displacement. * Linear regression. **Agreement: One sample t test on the difference between annotators. Quantitative performance metrics are presented as mean ± SD.

With these analyses, we show that manual delineations of the tumor volume are sensitive to bias in human interpretation and that the algorithm learns according to the interpretations of the annotator of a training set.

3.4. Longitudinal Assessment of Tumor Volume

To study lung tumor development and treatments effects, longitudinal evaluation of tumor volume is essential. To evaluate automated follow-up capabilities of the deep learning algorithm, lung tumor volumes were assessed for serial µCBCT images of individual animals during the study. The volumes of the automatically segmented tumors were compared qualitatively and quantitatively to the volumes of the manually delineated tumors. Data of a representative series of µCBCT images is shown in Figure 3. The automatic segmentations closely overlap with the manual segmentations, and the average DSC (± 1 SD) was equal to 0.88 ± 0.02. The total segmentation time of the deep learning algorithm was 1 min. compared to 1 h for the human annotator. These results show that the algorithm can be applied for the longitudinal follow-up of tumor development.

3.5. Simultaneous Quantification of Tumor Volume and Muscle Mass

Muscle wasting as part of cachexia is often observed in lung cancer. Previously, we developed a highly accurate ($R^2 = 0.92$, DSC = 0.93) deep learning algorithm for the quantification of hind limb muscle mass in mice [26]. Consequently, the muscle and lung tumor segmentation algorithm were executed sequentially to evaluate the feasibility of assessing both tumor and muscle mass longitudinally on serial µCBCT images (Figure 4). Experts visually verified the automatically segmented muscle and tumor volumes in the whole-body µCBCT scans. The automatic segmentation time was 13 s for both muscle and tumor. This equates to 1 min. and 31 s for an entire time series of µCBCT images of one mouse compared to 2 h and 47 min. of manual segmentation. Collectively, these data demonstrate the efficacy and feasibility of automated segmentation algorithms for the quantification of ROIs in preclinical research.

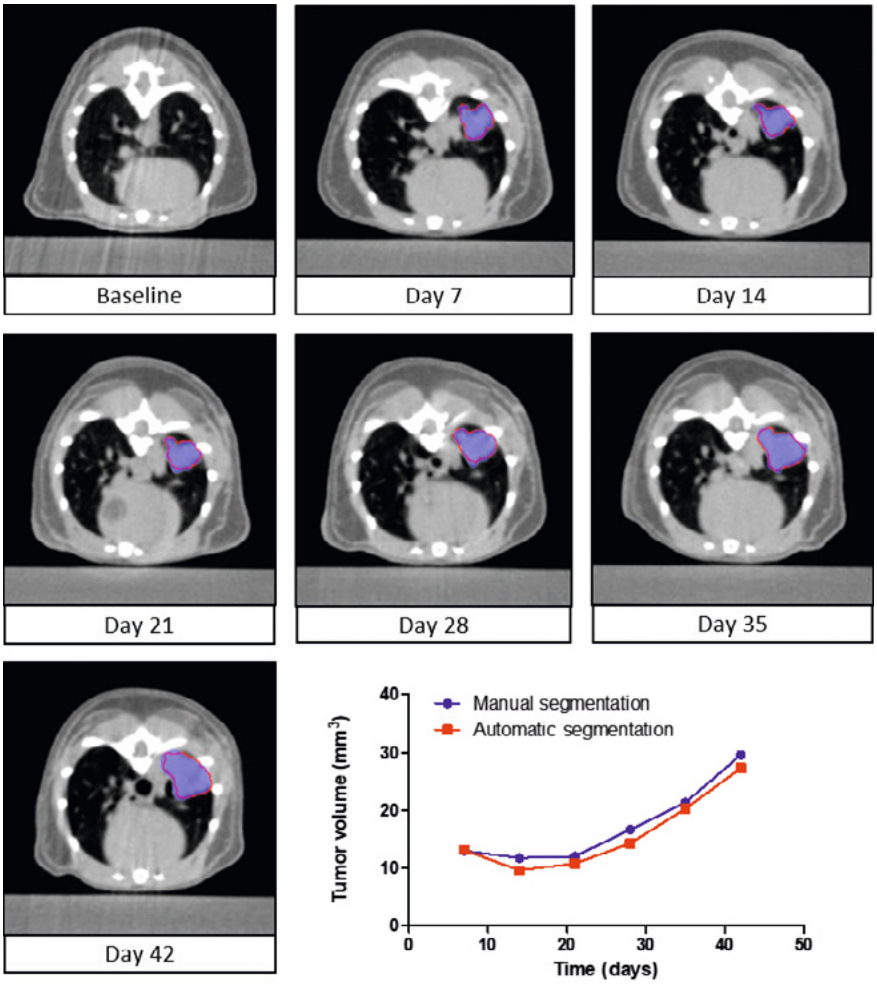

Figure 3. *Longitudinal follow-up of tumor volume. A series of axial slices of μCBCT images showing the manual segmentation (blue) and automatic segmentation (red) of the lung tumor in a single animal versus time. The μCBCT images represent one mouse at seven different time points. The quantified manual (blue) and automatically (red) segmented volumes are presented over time in the line graph.*

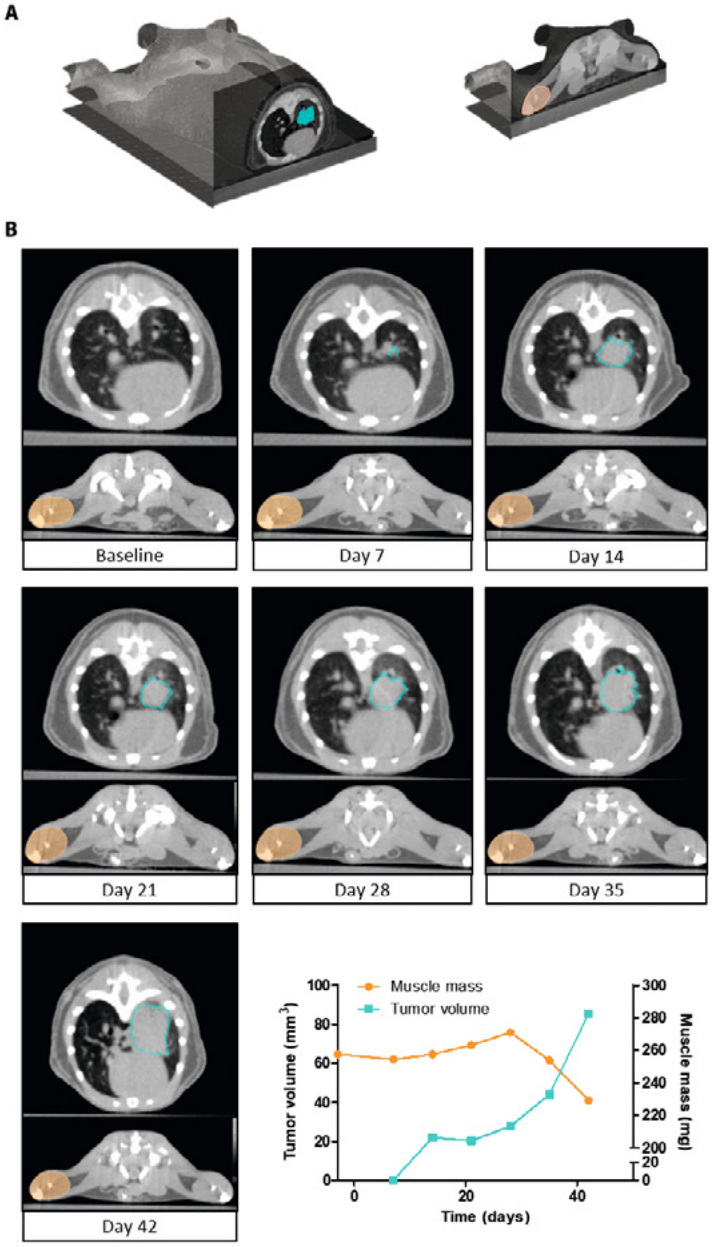

Figure 4. *Longitudinal follow-up of tumor volume and muscle mass.* **(A)** *A 3D image of a whole-body mouse μCBCT scan indicating the region of the axial slices selected for Figure 4B.* **(B)** *A series of axial slices of μCBCT images illustrating the automatic lung tumor segmentations (light blue) and lower hind limb muscle complex segmentations (orange). The μCBCT images represent one mouse at seven different time points. The quantified tumor volumes (light blue) and muscle masses (orange) are presented over time in the line graph.*

4. DISCUSSION

Manual delineation of orthotopic lung tumors visualized by CT is not only a time-consuming task, but also requires knowledge of anatomy and CT-image analysis. Additionally, this task is susceptible to human error and bias. In this paper, we introduce a deep learning algorithm for automatic tumor volume segmentation in whole-body μCBCT images. With minimal reliance on operator involvement, our deep learning method performs fast and accurate volume-mass quantifications of orthotopically growing lung tumors in mouse models.

For the development of the automatic lung tumor segmentation algorithm, we applied and optimized a two-step 3D U-Net architecture. Since its introduction in 2015 by Ronneberger et al. [33], the 2D U-Net architecture is one of the most commonly used methods in biomedical image segmentation. Shortly after the introduction of the 2D U-Net, the network architecture was modified by Milletari et al. to a 3D U-Net architecture (or V-Net) for biomedical images that have a spatial relationship in all three dimensions [34]. Medical CT, CBCT, or MRI images are a great example of imaging modalities that benefit from a 3D architecture. Previously, the 3D U-Net architecture has been shown to be a proper method for organ [35] and tumor [36,37] segmentation in medical images. However, due to the increased number of 3D convolutions performed on a large medical imaging dataset, the GPUs available on the market today are still too limited in terms of memory. Therefore, we adopted a two-step 3D U-Net architecture. The first step was applied on a downsized dataset to find the approximate tumor location, and in the second step, this position matrix was used on a cropped normal sized dataset to segment the tumor on the highest resolution.

The newly trained deep learning algorithm for automatic tumor segmentation performs 69 times faster compared to manual segmentation, saving major amounts of time in operator involvement and data analysis. Following development of the model, the algorithm's performance was assessed using specific quantitative metrics (e.g., DSC, 95HD and ΔCOM) for comparison with the manual segmentations of the training dataset. The deep learning algorithm achieves good average performance scores (DSC = 0.80, HD = 0.74 mm and ΔCOM = 0.24 mm). The performance scores of the lung tumor segmentation algorithm are slightly lower compared to the performance scores of the previously published muscle segmentation algorithm and AIMOS for normal tissue auto-segmentation [26,27]. This is not surprising, as there is wide variation in the size, shape and location of lung tumors in contrast to the muscle and other normal organs. Clearly, the low

performance scores (mean DSC−2 SD) are restricted to tumors with a volume smaller than 9 mm^3, particularly in small tumors located in close proximity to the bronchi or the pleura. In these scenarios, the acquired imaging data may contain insufficient information to distinguish between tissues, resulting in variation in the consistency of interpretation between the training dataset and the deep learning algorithm. Therefore, we recommend that for small tumors a human operator checks the results.

In accordance with previous studies [27,38,39], we found that manual annotations are sensitive to human bias in interpretation. Despite the use of detailed annotation guidelines, we showed that annotators recurrently disagree in the manual segmentations of the tumor volume. When the tumor is located in the middle of the lung free from other tissues, high agreement in the interpretation is observed. The variation in the interpretation is mainly caused by tumors located in close proximity to the bronchi. Where one annotator includes the bronchi as part of tumors the other exclude it from the delineation. Based on a relatively small dataset of only 60 manual segmentations, the agreement between the deep learning algorithm and the training dataset (annotator 1) is greater compared to human annotators. This may be due to the more consistent way in which the algorithm handles uncertainties compared to human annotators. These findings highlight the value of implementing AI in experimental preclinical and medical image segmentation. The bias in interpretation may also have an impact on the quantitative performance metrics of the algorithm if only manual segmentations of one annotator are used to create the trainings dataset. Although it is common practice in preclinical research to create training datasets generated by only one annotator [24,26,40,41], a training dataset based on two or more annotators will further increase the robustness of the model. Although it may not be necessary for the quantification of tumor volumes, this may be more important if the automatic tumor segmentations model is used for image guided high precision tumor irradiation [42,43]. Conversely, for irradiation, substantial geometrical margins are used to avoid under-irradiation.

This deep learning algorithm for lung tumor segmentation provides researchers with a helpful tool that enables fast, unbiased and interpretable quantifications of CT images. Several orthotopic mouse models have been described to study lung cancer [9–11]. What emerges unambiguously in these studies is that a tumor take of 100% is never achieved. In addition, without in vivo CT imaging, it is impossible to verify whether the tumor development is localized in the appropriate anatomical location, i.e., the lung parenchyma in our model, or if there is pleural seeding leading to the development of intra-pleural tumor growth. The automatic tumor

segmentation algorithm overcomes these limitations and offers great benefits for the quality and consistency of the research. First, it detects if a tumor grows in lung parenchyma. If the algorithm does not detect a tumor (volume = 0 mm^3), and this is confirmed by visual evaluation, mice can be excluded from an experiment reducing unnecessary distress for these animals. Then, the algorithm measures the tumor volume accurately, and subsequently, the mass of the lung tumor within one week following tumor inoculation. The tumor volumes can, for example, be used to randomize the animals into treatment groups prior to initiation of interventions, reducing variation and eventually the number of animals. In addition, we showed that the algorithm is capable of detecting changes in tumor mass over time. This is instrumental for the algorithm to be deployed as a valuable tool for preclinical lung cancer (treatment) research.

Finally, we showed that the automatic tumor segmentation algorithm can be used in combination with our previously developed algorithm for automated muscle mass determination [26]. Cancer cachexia, or muscle wasting, is a serious comorbidity and frequently occurs at advanced stage lung cancer [2]. Longitudinal assessment of both muscle mass and tumor volume will greatly aid in better understanding of the underlying mechanisms and interplay between tumor growth and muscle loss and allows studying the efficacy of therapeutic interventions on both phenomena in time.

5. LIMITATIONS

Despite the qualitatively high performance of the fully automatic AI-based lung tumor segmentation tool described here, limitations apply. Due to limited availability of µCBCT images, only 60 cases, the used dataset is small for deep learning applications. The deep learning algorithm is trained on the manual annotations of only one annotator. Furthermore, in this study, the deep learning algorithm was trained on a µCBCT image dataset collected at a single center and was acquired with one specific imaging protocol at an X-ray tube potential of 50 kVp, which can cause bias. Prior to implementation of the algorithm in other settings, further research is required to investigate whether the algorithm is valid on imaging datasets that were acquired at different X-ray tube potential settings, or on imaging datasets that were acquired with different spectral filtrations [31]. Finally, our training dataset was entirely based on 129S2/SvPasCrl mice. Nevertheless, we anticipate that the proposed algorithm is capable of segmenting tumor volumes in a variety of animals, as long as the study set-up (i.e., X-ray acquisition protocols and reconstruction settings) and animal characteristics are consistent. If the differences

in the imaging parameters are too large, transfer learning can be applied, which will reuse the knowledge from the current model to facilitate the process of retraining the model on new datasets [44].

6. CONCLUSIONS

A deep learning algorithm was developed and validated to automatically segment orthotopic lung tumors in mice. It provides fast and highly accurate tumor segmentations with minimal operator involvement in data analysis. This deep learning algorithm is a helpful tool for the non-invasive detection and analysis of tumor take, tumor growth and therapeutic effects, and can be deployed to optimize the randomization and 3R animal welfare aspects of the experimental design.

REFERENCES

1. Siegel, R.L.; Miller, K.D.; Jemal, A. Cancer statistics, 2020. *CA A Cancer J. Clin.* 2020, *70*, 7–30, doi:10.3322/caac.21590.
2. Anker, M.S.; Holcomb, R.; Muscaritoli, M.; von Haehling, S.; Haverkamp, W.; Jatoi, A.; Morley, J.E.; Strasser, F.; Landmesser, U.; Coats, A.J.S. Orphan disease status of cancer cachexia in the USA and in the European Union: A systematic review. *J. Cachexia Sarcopenia Muscle* 2019, *10*, 22–34, doi:10.1002/jcsm.12402.
3. Dewys, W.D.; Begg, C.; Lavin, P.T.; Band, P.R.; Bennett, J.M.; Bertino, J.R.; Cohen, M.H.; Douglass, H.O.; Engstrom, P.F.; Ezdinli, E.Z. Prognostic effect of weight loss prior tochemotherapy in cancer patients. *Am. J. Med.* 1980, *69*, 491–497, doi:10.1016/S0149-2918(05)80001-3.
4. Ross, P.J.; Ashley, S.; Norton, A.; Priest, K.; Waters, J.S.; Eisen, T.; Smith, I.E.; O'Brien, M.E. Do patients with weight loss have a worse outcome when undergoing chemotherapy for lung cancers? *Br. J. Cancer* 2004, *90*, 1905–1911, doi:10.1038/sj.bjc.6601781.
5. Kimura, M.; Naito, T.; Kenmotsu, H.; Taira, T.; Wakuda, K.; Oyakawa, T.; Hisamatsu, Y.; Tokito, T.; Imai, H.; Akamatsu, H. Prognostic impact of cancer cachexia in patients with advanced non-small cell lung cancer. *Support. Care Cancer* 2015, *23*, 1699–1708, doi:10.1007/s00520-014-2534-3.
6. Day, C.P.; Merlino, G.; Van Dyke, T. Preclinical mouse cancer models: A maze of opportunities and challenges. *Cell* 2015, *163*, 39–53, doi:10.1016/j.cell.2015.08.068.
7. Koontz, B.F.; Verhaegen, F.; De Ruysscher, D. Tumour and normal tissue radiobiology in mouse models: How close are mice to mini-humans? *Br. J. Radiol.* 2017, *90*, 20160441, doi:10.1259/bjr.20160441.
8. Junttila, M.R.; de Sauvage, F.J. Influence of tumour micro-environment heterogeneity on therapeutic response. *Nature* 2013, *501*, 346–354, doi:10.1038/nature12626.
9. Mordant, P.; Loriot, Y.; Lahon, B.; Castier, Y.; Lesèche, G.; Soria, J.-C.; Vozenin, M.-C.; Decraene, C.; Deutsch, E. Bioluminescent Orthotopic Mouse Models of Human Localized Non-Small Cell Lung Cancer: Feasibility and Identification of Circulating Tumour Cells. *PLoS ONE* 2011, *6*, e26073, doi:10.1371/journal.pone.0026073.
10. Justilien, V.; Fields, A.P. Utility and applications of orthotopic models of human non-small cell lung cancer (NSCLC) for the evaluation of novel and emerging cancer therapeutics. *Curr. Protoc. Pharmacol.* 2013, *62*, 14.27.11–14.27.17, doi:10.1002/0471141755.ph1427s62.
11. Iglesias, V.S.; Van Hoof, S.J.; Vaniqui, A.; Schyns, L.E.; Lieuwes, N.; Yaromina, A.; Spiegelberg, L.; Groot, A.J.; Verhaegen, F.; Theys, J. An orthotopic non-small cell lung cancer model for image-guided small animal radiotherapy platforms. *Br. J. Radiol.* 2019, *92*, 20180476, doi:10.1259/bjr.20180476.
12. Yamaura, T.; Murakami, K.; Doki, Y.; Sugiyama, S.; Misaki, T.; Yamada, Y.; Saiki, I. Solitary lung tumors and their spontaneous metastasis in athymic nude mice orthotopically implanted with human non-small cell lung cancer. *Neoplasia* 2000, *2*, 315–324, doi:10.1038/sj.neo.7900098.

13. Lee, J.; Han, Y.-A.; Yang, H.-S.; Song, J.-A.; Yang, Y.-S.; Kwon, S.; Kang, M.-S.; Lee, K.; Heo, J.-D.; Cho, K.-H. The Incidence Rate and Severity of Orthotopic Lung Cancer in an Animal Model Depends on the Number of A549 Cells and Transplantation Period. *Lab. Anim. Res.* 2010, *26*, 369–375, doi:10.5625/lar.2010.26.4.369.
14. Prescott, M.J.; Lidster, K. Improving quality of science through better animal welfare: The NC3Rs strategy. *Lab. Anim* 2017, *46*, 152–156, doi:10.1038/laban.1217.
15. De Clerck, N.M.; Meurrens, K.; Weiler, H.; Van Dyck, D.; Van Houtte, G.; Terpstra, P.; Postnov, A.A. High-resolution X-ray microtomography for the detection of lung tumors in living mice. *Neoplasia* 2004, *6*, 374–379, doi:10.1593/neo.03481.
16. Cavanaugh, D.; Johnson, E.; Price, R.E.; Kurie, J.; Travis, E.L.; Cody, D.D. In Vivo Respiratory-Gated Micro-CT Imaging in Small-Animal Oncology Models. *Mol. Imaging* 2004, *3*, 15353500200403184, doi:10.1162/15353500200403184.
17. Cody, D.D.; Nelson, C.L.; Bradley, W.M.; Wislez, M.; Juroske, D.; Price, R.E.; Zhou, X.; Bekele, B.N.; Kurie, J.M. Murine lung tumor measurement using respiratory-gated micro-computed tomography. *Investig. Radiol.* 2005, *40*, 263–269, doi:10.1097/01.rli.0000160070.67270.05.
18. Haines, B.B.; Bettano, K.A.; Chenard, M.; Sevilla, R.S.; Ware, C.; Angagaw, M.H.; Winkelmann, C.T.; Tong, C.; Reilly, J.F.; Sur, C. A quantitative volumetric micro-computed tomography method to analyze lung tumors in genetically engineered mouse models. *Neoplasia* 2009, *11*, 39–47, doi:10.1593/neo.81030.
19. Fushiki, H.; Kanoh-Azuma, T.; Katoh, M.; Kawabata, K.; Jiang, J.; Tsuchiya, N.; Satow, A.; Tamai, Y.; Hayakawa, Y. Quantification of mouse pulmonary cancer models by microcomputed tomography imaging. *Cancer Sci.* 2009, *100*, 1544–1549, doi:10.1111/j.1349-7006.2009.01199.x.
20. Kirsch, D.G.; Grimm, J.; Guimaraes, A.R.; Wojtkiewicz, G.R.; Perez, B.A.; Santiago, P.M.; Anthony, N.K.; Forbes, T.; Doppke, K.; Weissleder, R. Imaging primary lung cancers in mice to study radiation biology. *Int. J. Radiat. Oncol. Biol. Phys.* 2010, *76*, 973–977, doi:10.1016/j.ijrobp.2009.11.038.
21. Namati, E.; Thiesse, J.; Sieren, J.C.; Ross, A.; Hoffman, E.A.; McLennan, G. Longitudinal assessment of lung cancer progression in the mouse using in vivo micro-CT imaging. *Med. Phys.* 2010, *37*, 4793–4805, doi:10.1118/1.3476454.
22. Rodt, T.; von Falck, C.; Dettmer, S.; Hueper, K.; Halter, R.; Hoy, L.; Luepke, M.; Borlak, J.; Wacker, F. Lung tumour growth kinetics in SPC-c-Raf-1-BB transgenic mice assessed by longitudinal in-vivo micro-CT quantification. *J. Exp. Clin. Cancer Res.* 2012, *31*, 15, doi:10.1186/1756-9966-31-15.
23. Rudyanto, R.D.; Bastarrika, G.; de Biurrun, G.; Agorreta, J.; Montuenga, L.M.; Ortiz-de-Solorzano, C.; Muñoz-Barrutia, A. Individual nodule tracking in micro-CT images of a longitudinal lung cancer mouse model. *Med. Image Anal.* 2013, *17*, 1095–1105, doi:10.1016/j.media.2013.07.002.
24. Baiker, M.; Milles, J.; Dijkstra, J.; Henning, T.D.; Weber, A.W.; Que, I.; Kaijzel, E.L.; Löwik, C.W.; Reiber, J.H.; Lelieveldt, B.P. Atlas-based whole-body segmentation of mice from low-contrast Micro-CT data. *Med. Image Anal.* 2010, *14*, 723–737, doi:10.1016/j.media.2010.04.008.
25. Van Der Heyden, B.; Podesta, M.; Eekers, D.B.; Vaniqui, A.; Almeida, I.P.; Schyns, L.E.; Van Hoof, S.J.; Verhaegen, F. Automatic multiatlas based organ at risk segmentation in mice. *Br. J. Radiol.* 2019, *92*, 20180364, doi:10.1259/bjr.20180364.

26. van der Heyden, B.; van de Worp, W.R.; van Helvoort, A.; Theys, J.; Schols, A.M.; Langen, R.C.; Verhaegen, F. Automated CT-derived skeletal muscle mass determination in lower hind limbs of mice using a 3D U-Net deep learning network. *J. Appl. Physiol.* 2020, *128*, 42–49.
27. Schoppe, O.; Pan, C.; Coronel, J.; Mai, H.; Rong, Z.; Todorov, M.I.; Müskes, A.; Navarro, F.; Li, H.; Ertürk, A. Deep learning-enabled multi-organ segmentation in whole-body mouse scans. *Nat. Commun.* 2020, *11*, 5626, doi:10.1038/s41467-020-19449-7.
28. Gibbons, D.L.; Lin, W.; Creighton, C.J.; Rizvi, Z.H.; Gregory, P.A.; Goodall, G.J.; Thilaganathan, N.; Du, L.; Zhang, Y.; Pertsemlidis, A. Contextual extracellular cues promote tumor cell EMT and metastasis by regulating miR-200 family expression. *Genes Dev.* 2009, *23*, 2140–2151, doi:10.1101/gad.1820209.
29. Verhaegen, F.; Dubois, L.; Gianolini, S.; Hill, M.A.; Karger, C.P.; Lauber, K.; Prise, K.M.; Sarrut, D.; Thorwarth, D.; Vanhove, C. ESTRO ACROP: Technology for precision small animal radiotherapy research: Optimal use and challenges. *Radiother. Oncol.* 2018, *126*, 471–478, doi:10.1016/j.radonc.2017.11.016.
30. Ma, C.M.; Coffey, C.W.; DeWerd, L.A.; Liu, C.; Nath, R.; Seltzer, S.M.; Seuntjens, J.P. AAPM protocol for 40-300 kV x-ray beam dosimetry in radiotherapy and radiobiology. *Med. Phys.* 2001, *28*, 868–893, doi:10.1118/1.1374247.
31. Vaniqui, A.; Schyns, L.E.J.R.; Almeida, I.P.; Van Der Heyden, B.; Podesta, M.; Verhaegen, F. The effect of different image reconstruction techniques on pre-clinical quantitative imaging and dual-energy CT. *Br. J. Radiol.* 2019, *92*, 20180447, doi:10.1259/bjr.20180447.
32. Kingma, D.P.; Ba, J. Adam: A method for stochastic optimization. *arXiv* 2014, arXiv:1412.6980.
33. Ronneberger, O.; Fischer, P.; Brox, T. U-Net: Convolutional Networks for Biomedical Image Segmentation. arXiv 2015.
34. Milletari, F.; Navab, N.; Ahmadi, S.-A. V-net: Fully convolutional neural networks for volumetric medical image segmentation. In Proceedings of the 2016 Fourth International Conference on 3D Vision (3DV); IEEE; 2016.
35. Yang, J.; Veeraraghavan, H.; Armato III, S.G.; Farahani, K.; Kirby, J.S.; Kalpathy-Kramer, J.; van Elmpt, W.; Dekker, A.; Han, X.; Feng, X. Autosegmentation for thoracic radiation treatment planning: A grand challenge at AAPM 2017. *Med Phys.* 2018, *45*, 4568–4581, doi:10.1002/mp.13141.
36. Chiu, T.-W.; Tsai, Y.-L.; Su, S.-F. Automatic detect lung node with deep learning in segmentation and imbalance data labeling. *Sci. Rep.* 2021, *11*, 11174, doi:10.1038/s41598-021-90599-4.
37. Islam, M.; Vibashan, V.S.; Jose, V.J.M.; Wijethilake, N.; Utkarsh, U.; Ren, H. Brain Tumor Segmentation and Survival Prediction Using 3D Attention UNet. *arXiv* 2020.
38. Warfield, S.K.; Zou, K.H.; Wells, W.M. Validation of image segmentation by estimating rater bias and variance. *Med. Image Comput. Comput. Assist. Interv.* 2006, *9 Pt 2*, 839–847, doi:10.1007/11866763_103.
39. Joskowicz, L.; Cohen, D.; Caplan, N.; Sosna, J. Inter-observer variability of manual contour delineation of structures in CT. *Eur. Radiol.* 2019, *29*, 1391–1399, doi:10.1007/s00330-018-5695-5.
40. Akselrod-Ballin, A.; Dafni, H.; Addadi, Y.; Biton, I.; Avni, R.; Brenner, Y.; Neeman, M. Multimodal Correlative Preclinical Whole Body Imaging and Segmentation. *Sci. Rep.* 2016, *6*, 27940, doi:10.1038/srep27940.

41. Wang, H.; Han, Y.; Chen, Z.; Hu, R.; Chatziioannou, A.F.; Zhang, B. Prediction of major torso organs in low-contrast micro-CT images of mice using a two-stage deeply supervised fully convolutional network. *Phys. Med. Biol.* 2019, *64*, 245014, doi:10.1088/1361-6560/ab59a4.
42. Almeida, I.P.; Vaniqui, A.; Schyns, L.E.; Van Der Heyden, B.; Cooley, J.; Zwart, T.; Langenegger, A.; Verhaegen, F. Exploring the feasibility of a clinical proton beam with an adaptive aperture for pre-clinical research. *Br. J. Radiol.* 2019, *92*, 20180446, doi:10.1259/bjr.20180446.
43. Van Hoof, S.J.; Verde, J.B.; Verhaegen, F. Dose painting by dynamic irradiation delivery on an image-guided small animal radiotherapy platform. *Br. J. Radiol.* 2019, *92*, 20180744.
44. Yang, L.; Hanneke, S.; Carbonell, J. A theory of transfer learning with applications to active learning. *Mach. Learn.* 2013, *90*, 161–189, doi:10.1007/s10994-012-5310-y.

SUPPORTING INFORMATION

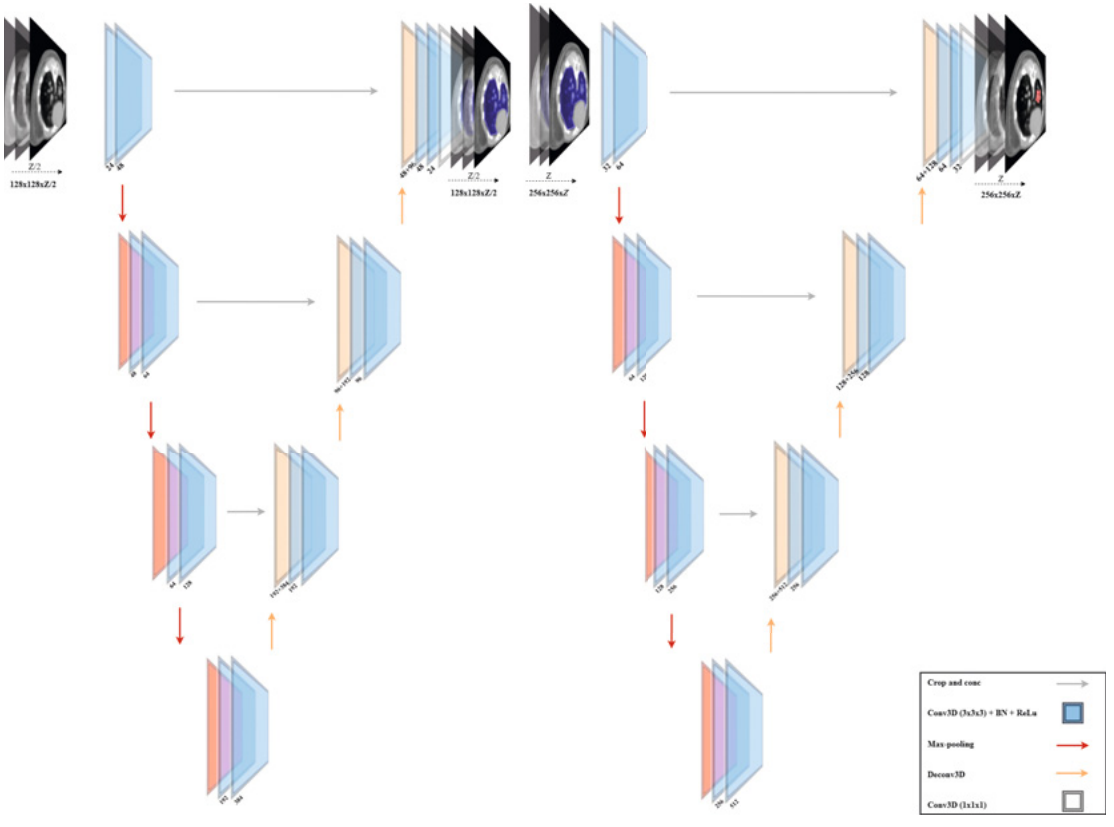

Figure S1. *The two-step 3D U-Net network architecture implemented in TensorFlow.*

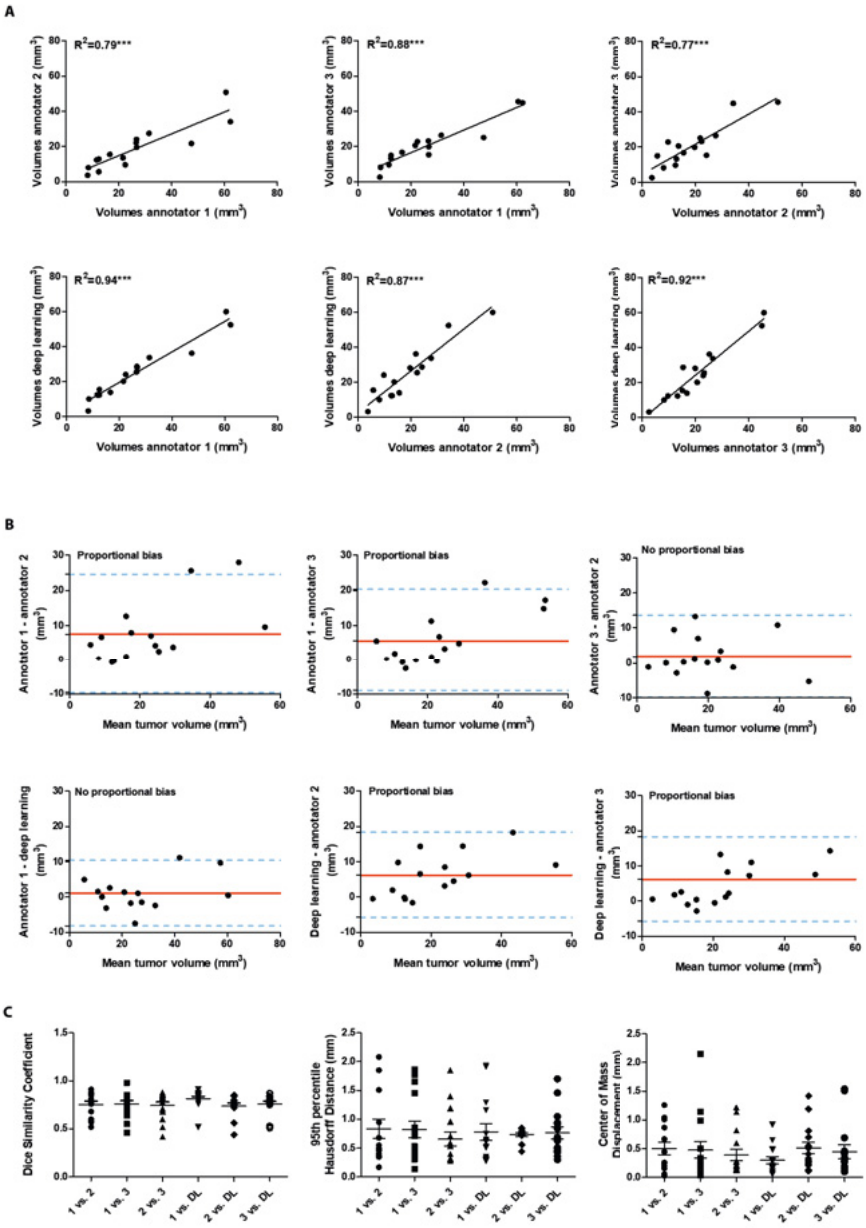

Figure S2. Subjectivity and bias in human interpretation. (A) *Linear relationship between annotators and annotators-deep learning algorithm. *** P-value < 0.001.* ***(B)*** *The Bland-Altman plot indicating agreement or disagreement between tumor volume segmentations. The dotted blue lines indicate the upper- and lower 95% confidence intervals. The red line indicates the mean.* ***(C)*** *Aligned dot plot (n=15) of the quantitative performance scores (dice similarity coefficients, 95th percentile Hausdorff Distance (in mm), and center of mass displacement (in mm)) calculated for each of the comparisons.*

7

A novel orthotopic mouse model replicates human lung cancer cachexia

Wouter RPH van de Worp
Jan Theys
Alba Sanz González
Brent van der Heyden
Frank Verhaegen
Duncan Hauser
Florian Caiment
Hubertus JM Smeets
Annemie MWJ Schols
Ardy van Helvoort
and Ramon CJ Langen.

Journal of Cachexia Sarcopenia and Muscle
Submitted 2022

ABSTRACT

INTRODUCTION: Cancer cachexia, highly prevalent in lung cancer, is a debilitating syndrome characterized by involuntary loss of skeletal muscle mass, and is associated with poor clinical outcome, decreased survival and negative impact on tumor therapy. Various lung tumor-bearing animal models have been used to explore underlying mechanisms of cancer cachexia. However, these models do not simulate anatomical and immunological features key to lung cancer and associated muscle wasting. Overcoming these shortcomings is essential to translate experimental findings into the clinic. We therefore evaluated whether a syngeneic, orthotopic lung cancer mouse model replicates systemic and muscle-specific alterations associated with human lung cancer cachexia.

METHODS: Immune competent, 11 weeks old male 129S2/Sv mice, were randomly allocated to either (1) sham control group or (2) tumor-bearing group. Syngeneic lung epithelium-derived adenocarcinoma cells (*K-ras*^{G12D}*; p53*$^{R172H\Delta G}$) were inoculated intrapulmonary into the left lung lobe of the mice. Body weight and food intake were measured daily. At baseline and weekly after surgery, grip strength was measured and tumor growth and muscle volume were assessed using micro cone beam CT imaging. After reaching humane endpoints-based surrogate survival endpoint, animals were euthanized and skeletal muscles of the lower hind limbs were collected for biochemical analysis.

RESULTS: Two-third of the tumor-bearing mice developed cachexia based on predefined criteria. Final body weight (-13.7 ± 5.7%; P<0.01), muscle mass (-13.8 ± 8.1%; P<0.01) and muscle strength (-25.5 ± 10.5%; P<0.001) were reduced in cachectic mice compared with sham controls and median survival time post-surgery was 33.5 days until humane endpoint. Markers for proteolysis, both ubiquitin proteasome system (*Atrogin-1* and *MuRF-1*) and autophagy-lysosomal pathway (*Gabarapl* and *Bnip3*), were significantly upregulated, whereas markers for protein synthesis (Akt, S6k1 and 4E-BP1) were significantly decreased in the skeletal muscle of cachectic mice compared with control. The cachectic mice exhibited increased pentraxin-2 (P<0.001) and CXCL1/KC (P<0.01) expression levels in blood plasma and increased mRNA expression of *IκBα* (P<0.05) in skeletal muscle, indicative for the presence of systemic inflammation. Strikingly, RNA sequencing, pathway enrichment and miRNA expression analyses of mouse skeletal muscle strongly mirrored alterations observed in muscle biopsies of patients with lung cancer cachexia.

CONCLUSION: We developed an orthotopic model of lung cancer cachexia in immune competent mice. Since this model simulates key aspects specific to cachexia in lung cancer patients, it is highly suitable to further investigate the underlying mechanisms of lung cancer cachexia, and to test the efficacy of novel intervention strategies.

1. INTRODUCTION

Lung cancer is the leading cause of cancer related mortality worldwide [1]. About 85% of the lung cancers are non-small cell lung cancer (NSCLC) [2, 3]. With an average 17% 5-year survival rate and increasing incidence rates [1], NSCLC remains a devastating disease. Many patients with lung cancer experience cancer cachexia, defined as unintentional weight loss and muscle wasting [4]. Cachexia may be the primary cause of mortality in end stage disease and contributes to poor survival by increasing postoperative mortality and lowering patient tolerance to chemo-, radiation- and immunotherapy [5-8]. In addition to earlier diagnosis and more effective treatment of NSCLC, prevention and treatment of cachexia is an additional target to improve patients' wellbeing and survival.

Therapies to prevent or treat cachexia are currently lacking [9]. Many therapies proven effective in experimental animal models of cancer cachexia appear unsuccessful in patients. A major factor that may contribute to the failure of these trials is that existing models of cancer cachexia fail to fully replicate the etiology of the human disease [10]. The most widely used animal models for cancer cachexia are subcutaneous tumor allograft transplants in rodents [11, 12]. Although, these animal models have been useful in investigating the underlying mechanisms of cancer cachexia, they differ from the situation seen in patients with respect to tumor burden and anatomical location. In addition, these subcutaneous mouse models have a relatively rapid onset and progression of cachexia compared to human, complicating the translatability of these models. To better characterize the systemic impact of human tumors, patient-derived xenografts have been developed [13]. However, the need to use immune-deficient recipient mice limits their use for modeling cancer cachexia. In order to simulate lung cancer cachexia more realistically, animal models needs to recreate the context in which the tumor can interact with the complex microenvironment and immune system, as happens in humans [14]. This relevant microenvironment can only be created in the organ of tumor origin, the lung. These so-called orthotopic animal models are more clinically relevant than their subcutaneous counterparts as the establishment of a tissue-specific tumor microenvironment may determine the etiology of cachexia and affect the outcome of therapies. Lung-specific genetic engineered mouse models (GEMMs) have been developed and used to study cancer cachexia [15]. However, these GEMM require intratracheal or intranasal viral delivery to accomplish Cre recombinase mediated activation of tumor growth, which might elicit interfering immune responses. Alternatively, orthotopic inoculated lung cancer mouse models have been described [16, 17], but have never been designed and characterized to

study lung cancer cachexia. The monitoring of orthotopic lung tumors is no longer an obstacle to avoid the use of these models, as we recently demonstrated the routine deployment of non-invasive micro computed tomography (μCT) imaging to follow up and quantify tumor growth longitudinally [18]. Moreover, we developed a deep learning algorithm to simultaneously automatically determine muscle mass changes on the same μCT images, allowing real time monitoring of muscle wasting during cachexia [19].

Thus, in order to develop promising targeted cachexia intervention strategies, new models that better recapitulate clinical lung cancer cachexia are needed. Such a model should exhibit: (1) orthotopic tumor growth; (2) immune competence; (3) prolonged disease progression; (4) skeletal muscle mass loss; (5) systemic inflammation; and (6) muscle specific alterations that reflect changes in patient muscle biopsies. Here, we present the development and characterization of a novel orthotopic lung cancer cachexia (OLCC) mouse model, which meets these criteria.

2. MATERIALS AND METHODS

2.1. Animals

Male 129 mice of 11 weeks (129S2/SvPasCrl, Charles River Laboratories, Germany) were socially housed (n=3) in GM500 IVC cages (Tecniplast, Buguggiate, Italy) with Corn cob bedding (JRS Lignocel, Rosenberg, Germany), shelter and nesting material in a climate-controlled room (12:12 dark-light cycle with a constant room temperature of 21±1°C). Mice were given *ad libitum* access to food (AIN-93M, Bio Services BV, Uden, the Netherlands) and drinking water (autoclaved, softened and acidified (pH=2.5)). After 1 week of acclimatization, animals were randomly allocated to either the sham control group (n=8) or the 344P tumor bearing group (n=15; Figure S1). Following surgery, animals were monitored daily. Cachexia was defined as more than 5% of body weight loss in combination with confirmed muscle mass loss measured by micro Cone Beam Computed Tomography (μCBCT). Based on an animal welfare scoring list (incl. body weight, body composition, activity, fur/skin and posture), cachexia-related humane endpoints were applied (surrogate survival endpoint). Furthermore, tumors were scored for location and size. If the primary tumor did not appear in the lung, mice were excluded. When a total tumor volume of 100 mm^3 was reached or in case of signs of dyspnea due to tumor growth or pulmonary constriction, humane endpoint was reached and the animals were sacrificed.

This work was conducted in accordance with institutional guidelines for the care and use of laboratory animals established by the Ethics Committee for Animal Experimentation of the Maastricht University and in full compliance to national legislation on animal research following the European Directive 2010/63/EU for the use of animals for scientific purposes.

2.2. Tumor model – transpleural orthotopic lung tumor cell injection

Murine 344P lung epithelium-derived adenocarcinoma cells were cultured with Roswell Park Memorial Institute 1640 medium (Gibco, Rockville, MD) supplemented with 9% fetal bovine serum (Gibco). Tumor cells were trypsinized in a sub-confluent state and suspended in Matrigel matrix (Corning) at a well-established concentration (2 x 10^6 cells/ml). Animals were anesthetized using a mixture of air and isoflurane (4% induction, 2% maintenance) and placed in a position of right lateral decubitus. Fur was removed and a 1 cm superficial skin incision was made below the left scapula. Fat tissue was moved aside and underlying muscles (excluding intercostal muscles) were carefully lifted. While visualizing the lung motion, 10 µl of Matrigel only (sham) or with tumor cells (2 x 10^4 cells in 10 µl) was injected through the intercostal space into the lung. The muscles were placed back on top of the rib cage in the correct orientation and the skin was closed using a 5-0 suture. All mice received a single dose of pre-operative analgesia (Carprofen and Buprenorphine) via subcutaneous injection and post-operative analgesia (Carprofen) in the drinking water for two days.

2.3. Experimental protocol

All procedures of the experimental protocol were performed at a standardized time window during their inactive period of the day. Body weight and food intake were measured daily. At baseline and weekly after surgery, forelimb grip strength was measured with a calibrated grip strength tester (Bioseb, Vitrolles, France) and µCBCT imaging was performed for all mice to assess lung tumor development [18] and to detect muscle volume changes over time[19] with an extensively verified 3D deep convolutional neural network . At the end of the experiment, mice were scanned under anesthesia and subsequently sacrificed using pentobarbital overdose. Skeletal muscles (e.g. m. soleus, m. plantaris, m. gastrocnemius, m. tibialis anterior (TA) and m. extensor digitorum longus (EDL)) were collected from both hind limbs, using standardized dissection methods. Subsequently, muscles were immediately weighed in pairs on an analytical balance and snap frozen in liquid nitrogen. The experimental setup is depicted in Figure S2.

2.4. Clinical validation

To assess whether the OLCC mouse model mimics the muscle intracellular changes related to human lung cancer cachexia, human samples were used from a previously published cross-sectional study [20, 21]. Vastus lateralis muscle biopsies of newly diagnosed treatment-naïve NSCLC patients with cachexia (n = 8) and age-matched and sex-matched healthy controls (n = 8) were processed for RNA sequencing.

2.5. RNA extraction

For mRNA expression analysis, TRI Reagent (Sigma-Aldrich) was used according to the manufacturers' protocol. Muscle gastrocnemius (mouse) and muscle vastus lateralis (human) were grinded into powder and homogenized in TRI Reagent by using a Mini bead beater (Cole Parmer) sample homogenizer, and total RNA was extracted. A Qubit fluorometer (Invitrogen) and the Agilent 4200 Tapestation system (Agilent Technologies) were used to measure the quantity, purity and integrity of the RNA. The RNA integrity number (RIN) values for all mouse samples were between 8.4 and 9.1, and the RIN values for all human samples were greater than 7.4.

2.6. Reverse transcription quantitative real time PCR (RT-qPCR)

A fixed amount of 400 ng of total RNA was used for the reverse transcriptase reaction. First-strand cDNA synthesis was performed using the Tetro cDNA Synthesis Kit according to the manufacturers' protocol (GC-Biotech). cDNA was diluted (1:50) in nuclease-free H_2O and stored at 4 °C, cDNA stocks were stored at – 20 °C. For real-time PCR amplification, each reaction contained 5 µl SyBr-green mix (Sensimix SYBR & Fluorescein, GC Biotech), 0.6 µl PCR primer mix (5 µM forward primer + 5 µM reverse primer) and 4.4 µl diluted cDNA template. PCR settings were 95 °C for 10 min, followed by 45 cycles of 95 °C for 10 s and 60 °C for 20 s, carried out on a Roche LightCycler480 system. Melt curves were made using a gradual increase in temperature of 0.11 °C/s with 5 acquisitions/s and a temperature range of 60 °C to 90 °C. The melt curves were examined using the LightCycler480 software (Roche). PCR efficiency was determined using LinRegPCR software. The resultant N_0 values were exported and normalized to the geometric average of five reference genes using GeNorm. Cut-off number of cycles was set as 40. The thresholds used to determine significance of differentially expressed mRNAs were set as $P<0.05$ and a $C_q \geq 1$ cycle. The primers used are listed in Table S1.

2.7. RNA sequencing

Pure, intact mRNA was isolated from 1 µg of total RNA using the NEXTFLEX Poly (A) Beads 2.0 kit (PerkinElmer). The purified mRNA was used to prepare directional, strand specific RNA libraries for sequencing using the NEXTFLEX Rapid Directional RNA-Seq kit 2.0 (PerkinElmer) according to manufacturer's instruction. The NETFLEX RNA-Seq 2.0 Unique Dual Index Barcodes (PerkinElmer) were used as adapter. A Qubit fluorometer (Invitrogen) and the Agilent 4200 Tapestation system (Agilent Technologies) were used to measure the quantity and quality of the libraries. Equal amounts (1.6 nM) of libraries were pooled and sequenced using the S2 flow cell (200 cycles) of the Illumina NovaSeq 6000.

The obtained raw data was first trimmed using fastp and the remaining reads were mapped to either the Ensembl mouse genome (release 100) or Ensembl human genome (release 100) using STAR (version 2.7.3a) and quantified using RSEM (v.1.3.1). The resultant raw read counts were processed using the R package DESeq2. Low expressed genes, defined as more than 75% of the samples of any given condition not detected (0 read), were first removed from the analysis. Genes were considered differentially expressed with an adjusted p-value (FDR) below 0.01.

2.8. In silico gene set enrichment analysis

Overrepresentation analysis was performed on the up- and down-regulated differentially expressed genes (DEGs) using g:Profiler (g:GOSt). DEGs were mapped to biological pathway databases (KEGG, Reactome and WikiPathways) and statistically significant enriched pathways were detected ($P<0.01$).

2.9. Protein isolation and Western Blot

Muscle gastrocnemius was grinded into powder and homogenized in 400 µl whole cell lysate buffer (20 mM Tris pH 7.4, 150 mM NaCl, 1% Nonidet, 1 mM DTT, cOmplete mini protease inhibitor cocktail and PhosSTOP) by using a Polytron PT 1600 E (Kinematica). The homogenates were incubated for 30 min on ice and centrifuged (14.000 x g) for 30 min at 4°C. Subsequently, supernatant fraction was separated from the pellet fraction. Protein concentration of the fractions were determined by using a BCA protein assay kit (Pierce, Thermo Fischer Scientific).

For Western Blot analysis, Laemmli buffer (0.25 M Tris-HCl pH 6.8, 8% (w/v) SDS, 40% (v/v) glycerol, 0.4 M DTT and 0.02% (w/v) Bromophenol blue) was added in a 1:4 dilution to the supernatant fraction and were incubated for 5 min at 95°C. Equal amounts of protein were loaded per lane on a Criterion XT Precast 4-12%

Bis-Tris gel (Bio-Rad). Proteins were separated by electrophoresis (100-140 V). The proteins were transferred to a 0.45 µm nitrocellulose membranes (Bio-Rad) by electroblotting (Bio-Rad Criterion Blotter) at 100 V for 1 h. Membranes were blocked during 1 h at room temperature in 5% non-fat dried milk (ELK, Campina) diluted in Tris-bufferd saline with 0.05% Tween-20 (TBS-T). Membranes were washed with TBS-T and overnight exposed at 4°C with specific primary antibodies (1:1000). Subsequently, membranes were washed with TBS-T and were incubated with secondary antibodies (1:10.000) of anti-mouse IgG peroxidase (Vector) or anti-rabbit peroxidase (Vector). Detection was performed using SuperSignal West Pico Chemiluminescent substrate (Thermo Fischer Scientific) according to the manufacturers' protocol. Membranes were imaged (Amersham Imager 600, GE Life Sciences) and quantified using the ImageQuantTL software (GE life sciences). The primary antibodies used are listed in Table S2.

2.10. Cytokine quantification

Blood was centrifuged (2.000 x *g* for 10 min at 4ºC) and plasma was stored at -20ºC. Serum Pentraxin-2 and IL-8 (Quantikine ELISA, R&D Systems) levels were quantified according to manufacturer's protocol.

3. RESULTS

3.1. Cachexia characteristics in the orthotopic lung cancer mouse model

Mice were orthotopically injected with lung tumor cells that express an activation mutation in *Kras* as well as a loss of function mutation in *p53*. One week after surgery, 80% of the mice developed a solitary tumor centrally in the left lung lobe (Figure S1). Sixty-seven percent of the tumor-bearing mice developed cachexia, defined as more than 5% of body weight loss in combination with confirmed muscle mass loss measured by non-invasive CT-imaging [19]. The other 33% of the tumor-bearing mice reached humane endpoint criteria before they developed cachexia (Figure S1). Tumor development was monitored by non-invasive CT-imaging[18], with a maximum tumor burden of 0.5% of total body weight (Figure 1A-B). The OLCC mice reached surrogate survival endpoint at a median of 33.5 days post-surgery and showed significant loss of body weight over time compared with sham control mice (Figure 2C-D). At the endpoint, on average OLCC mice lost 13.7% ($P<0.01$) of total body weight (Figure 2E). No differences in food intake were observed between OLCC and sham control mice (Figure 2F).

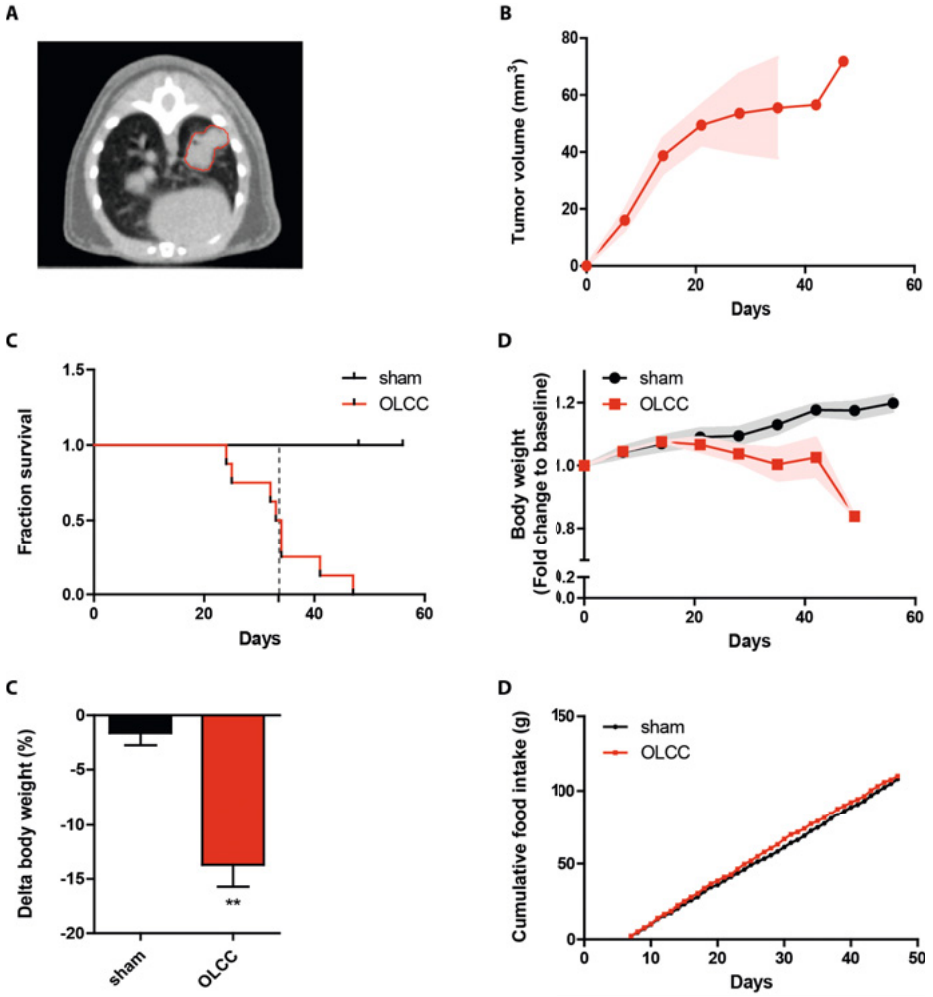

Figure 1: Tumor, body weight and survival characteristics in orthotopic lung cancer cachexia (OLCC) mice. (A) *Representative axial slice of a μCBCT image illustrating a single nodule in the left lung lobe of the OLCC mouse.* **(B)** *Tumor volume (mm³) in OLCC mice over time, measured by μCBCT.* **(C)** *Kaplan-Meier survival plot for sham and OLCC mice. The dotted vertical line indicates the median surrogate survival time for the OLCC mice (33.5 days).* **(D)** *Total mouse body weight over time, normalized to body weight at baseline (pre-surgery).* **(E)** *Relative change (%) in body weight (ΔBW) at the end of the experiment.* **(F)** *Cumulative food intake from 7 days post-surgery. Data is presented as mean ± SEM, sham control n=8 and OLCC mice n=8. Comparisons were statistically tested with the Mann-Whitney U test. Significance is shown as **P<0.01.*

The loss of body weight in OLCC mice was accompanied by significant loss of muscle mass, which became visible by non-invasive CT imaging 21 days post-surgery (Figure 2A). At endpoint, OLCC mice lost 13.8% (P<0.01) muscle mass of the hind limbs (Figure 2B). CT-based hind limb muscle wasting was reflected

by the significant loss in m. plantaris (P<0.01), m. gastrocnemius (P<0.05) and m. TA (P<0.01) wet masses (Figure 2C). In addition, OLCC mice showed decreased muscle function (p<0.001) measured by forelimb grip strength (Figure 2D-E). Importantly, CT-derived muscle mass correlated with muscle function (r=0.397, n=98; p<0.01) (Figure 2F).

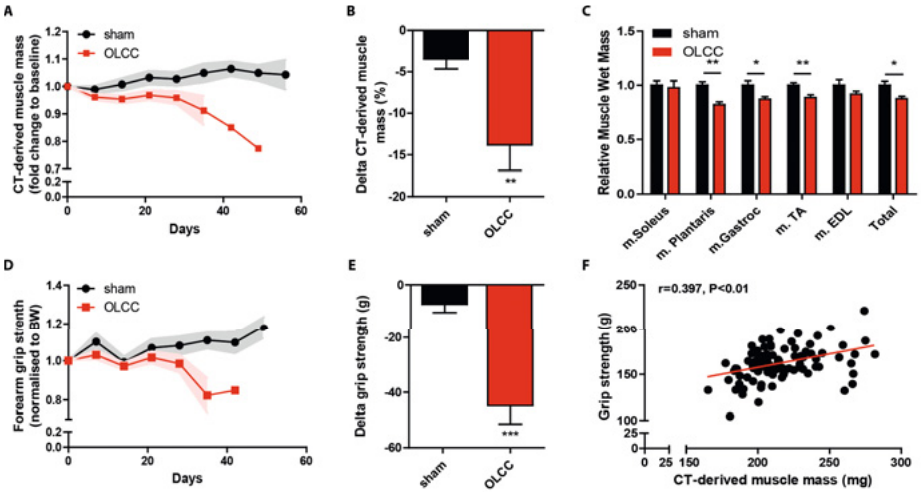

Figure 2: Loss of muscle mass and function in OLCC mice. (A) *µCBCT-derived muscle mass over time, normalized to µCBCT-derived muscle mass at baseline (pre-surgery).* **(B)** *Relative change (%) in µCBCT-derived muscle mass at the end of the experiment.* **(C)** *Relative change in muscle wet mass at the end of the experiment.* **(D)** *Forearm grip strength over time, normalized to total body weight at baseline.* **(E)** *Absolute change in grip strength (gram) at the end of the experiment.* **(F)** *Correlation between forearm grip strength and µCBCT-derived muscle mass (mg), r=0.397 (n=98). The correlation was statistically tested with Pearson's correlation coefficient (two-tailed). Data is presented as mean ± SEM, sham control n=8 and OLCC mice n=8. Comparisons were statistically tested with two-tailed unpaired t-test for normally distributed data or Mann-Whitney U test for non-parametric data. Significances are shown as *P<0.05; **P<0.01, and ***P<0.001.*

3.2. Increased proteolysis signaling in atrophied muscle of orthotopic lung cancer cachexia mice

Next, to assess activation of proteolysis signaling, we measured the expression of genes coding for components of the ubiquitin proteasome system (UPS) and autophagy lysosomal pathway (ALP), which have been implicated in cancer-induced muscle atrophy [22]. The observed muscle wasting was associated with increased mRNA expression of the ubiquitin E3 ligases *Atrogin-1* (P<0.001) and *MuRF1* (P<0.01), but not *NEDD4* (Figure 3A). The mRNA expression levels of *Gabarapl* (P<0.01) and *Bnip3* (P<0.05) were upregulated (Figure 3A) and the ratio of

phosphorylated ULK over total ULK was decreased (P<0.05; Figure 3B), suggesting increased activation of the ALP. Finally, the protein levels of phosphorylated FoxO over total FoxO was decreased (P<0.05; Figure 3C) mainly by elevated levels of total FoxO protein (P<0.05), which is consistent with increased mRNA expression of *FoxO1* (P<0.05; Figure 3A). Combined these findings indicate increased proteolysis signaling in the muscle of OLCC compared with sham control mice.

3.3. Decreased protein synthesis signaling in atrophied muscle of orthotopic lung cancer cachexia mice

To assess the anabolic activity in the skeletal muscle of OLCC mice, the activity of multiple components of the Akt/mTOR signaling pathway were measured. The protein levels of phosphorylated Akt over total Akt were decreased (P<0.05) in OLCC compared with sham control mice (Figure 4A). Protein levels of mTOR did not show significant changes in phosphorylation status (Figure 4B). Downstream of mTOR, the phosphorylation status of S6K1 (P<0.05) and 4E-BP1 (P<0.001) were decreased in the muscle of OLCC compared with sham control mice (Figure 4C-D). Finally, the mRNA expression of *REDD1*, an inhibitor of mTOR, was increased in OLCC mice (P<0.01; Figure 4E). Altogether, these observations indicate decreased protein synthesis signaling in the muscle of OLCC mice.

3.4. Increased systemic inflammation and inflammatory signaling in atrophied muscle of orthotopic lung cancer cachexia mice

As markers of systemic inflammation, circulating levels of the pro-inflammatory chemokine CXCL1/KC (murine interleukin-8 (IL-8) orthologue) and acute phase protein pentraxin-2 were assessed and found to be increased in blood plasma of OLCC mice compared with sham control (respectively P<0.01 and P<0.001; Figure 5A-B). In addition, the mRNA expression of *IκBα* was increased in muscle of OLCC compared with sham control mice (P<0.05); Figure 5C), suggesting increased inflammatory signaling in the skeletal muscle of OLCC mice.

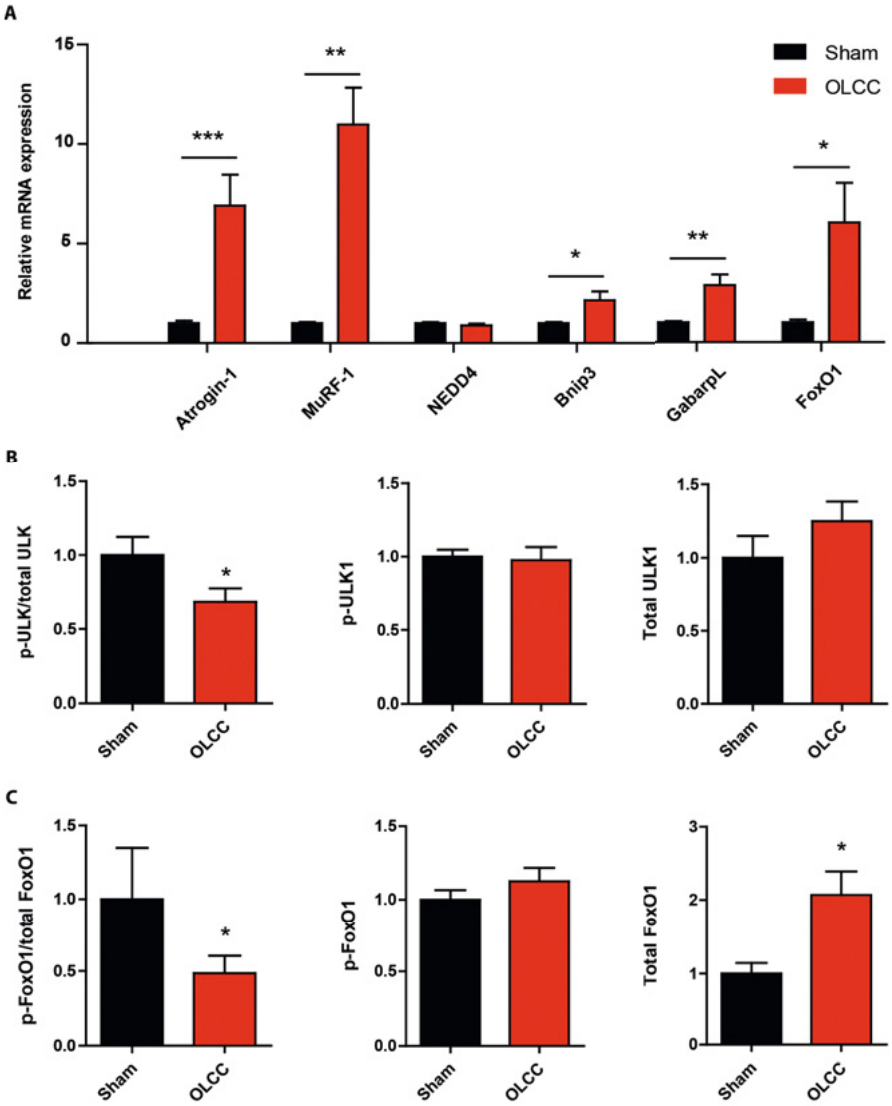

Figure 3: Increased proteolysis signaling in the muscle of OLCC mice. (A) *Relative mRNA expression levels of Atrogin-1, MuRF-1, NEDD4, Bnip3, GabarapL and FoxO1 measured in the m. gastrocnemius.* **(B)** *Ratio of phosphorylated ULK (Ser757) over total ULK, and the relative protein expression of phosphorylated ULK (Ser757) and total ULK.* **(C)** *Ratio of phosphorylated FoxO1 (Ser256) over total FoxO1, and the relative protein expression of phosphorylated FoxO1 (Ser256) and total FoxO1. Representative pictures of the Western Blot data are shown in Figure S3. Data is presented as mean ± SEM, sham control n=8 and OLCC mice n=8. Comparisons were statistically tested with two-tailed unpaired t-test for normally distributed data or Mann-Whitney U test for non-parametric data. Significances are shown as *P<0.05; **P<0.01, and ***P<0.001.*

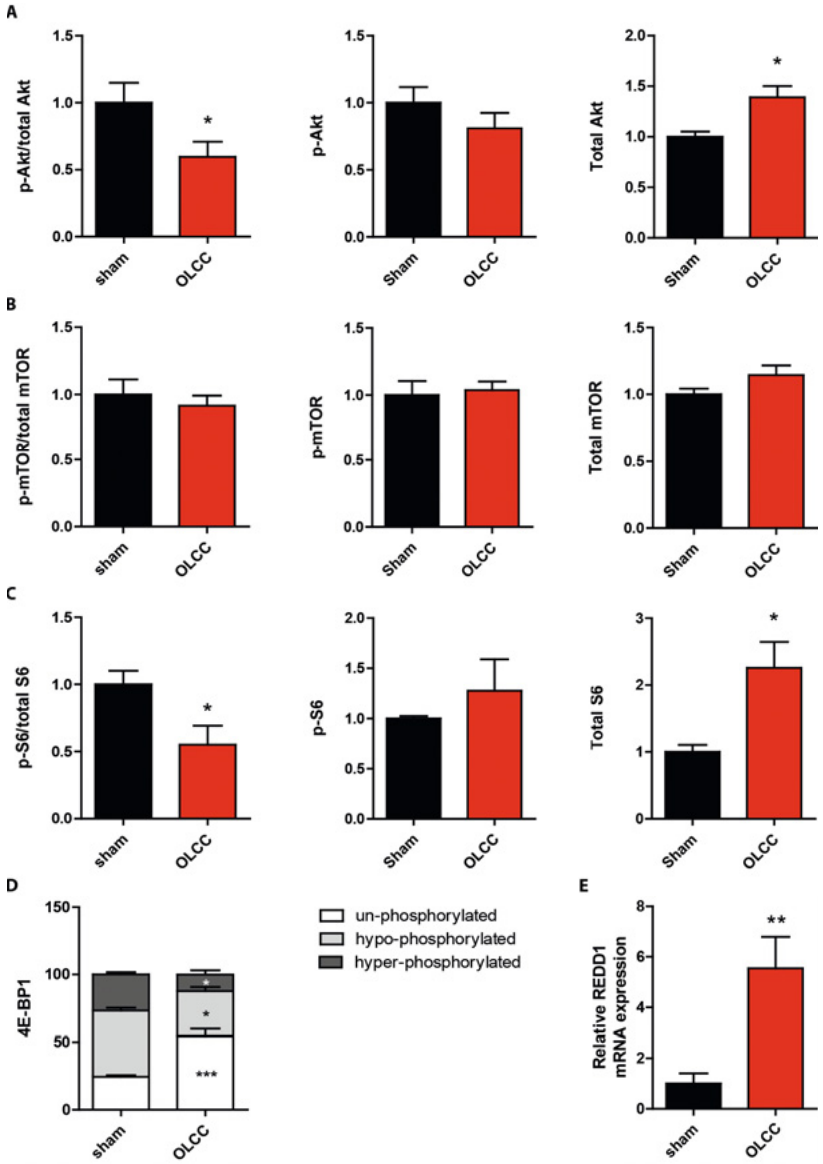

Figure 4: Decreased protein synthesis signaling in the muscle of OLCC mice. (A) *Ratio of phosphorylated Akt (Ser473) over total Akt, and the relative protein expression of phosphorylated Akt (Ser473) and total Akt.* **(B)** *Ratio of phosphorylated mTOR (Ser2448) over total mTOR, and the relative protein expression of phosphorylated mTOR (Ser2448) and total mTOR.* **(C)** *Ratio of phosphorylated S6 (Ser235/236) over total S6, and the relative protein expression of phosphorylated S6 (Ser235/236) and total S6.* **(D)** *Phosphorylation distribution of 4E-BP1. Representative pictures of the Western Blot data are shown in Figure S2.* **(E)** *Relative mRNA expression of REDD1. Data is presented as mean ± SEM, sham control n=8 and OLCC mice n=8. Comparisons were statistically tested with two-tailed unpaired t-test for normally distributed data or Mann-Whitney U test for non-parametric data. Significances are shown as *P<0.05; **P<0.01, and ***P<0.001.*

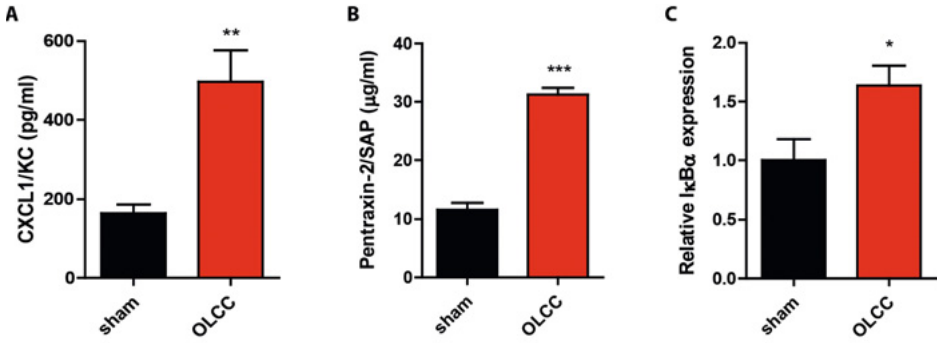

Figure 5: Increased systemic inflammation and inflammatory signaling in the muscle of OLCC mice. *Blood plasma expression levels of* **(A)** *CXCL1/KC in pg/ml and* **(B)** *Pentraxin-2 in µg/ml.* **(C)** *Relative mRNA expression of IκBα measured in the m. gastrocnemius. Data is presented as mean ± SEM, sham control n=8 and OLCC mice n=8. Comparisons were statistically tested with two-tailed unpaired t-test for normally distributed data or Mann-Whitney U test for non-parametric data. Significances are shown as *P<0.05; **P<0.01, and ***P<0.001.*

3.5. Intracellular changes specifically associated with muscle atrophy in NSCLC patients are preserved in OLCC mouse muscle.

Given the limitations of the currently available animal models of lung cancer cachexia, we assessed whether the OLCC mouse model comprehensively recapitulates the muscle intracellular changes related to human lung cancer cachexia. To this end, we applied a comparative transcriptomic analysis in muscle biopsies of cachectic NSCLC patients and OLCC mice. Gene expression profiling in NSCLC patients with cachexia resulted in 225 DEGs compared with healthy control subjects, using a FDR of < 0.01 (Figure 6A). The majority of the genes (63%) were downregulated. In the mouse model, we identified a total of 3956 DEGs between sham control and OLCC mice (Figure 6B). Here, 45% of the DEGs were downregulated. Subsequently, pathway enrichment analysis was deployed to identify similarly regulated pathways and processes in human and mouse cachectic muscle. Although we did not found any enrichment among the upregulated DEGs in cachectic patients with NSCLC, enrichment analysis on the upregulated DEGs of the OLCC mice resulted in pathways related to mRNA processing, mitophagy, autophagy, FoxO signaling (Figure S4). Remarkable overlap was observed in enrichment analysis of the downregulated DEGs of the cachectic NSCLC patients (Figure 6C) and OLCC mice (Figure 6D), identifying significant alterations in pathways related to metabolism, oxidative phosphorylation and mitochondrial functioning. These findings suggest similar alterations in the molecular processes governing muscle metabolism characterizing cachectic muscle of lung cancer patients and OLCC mice.

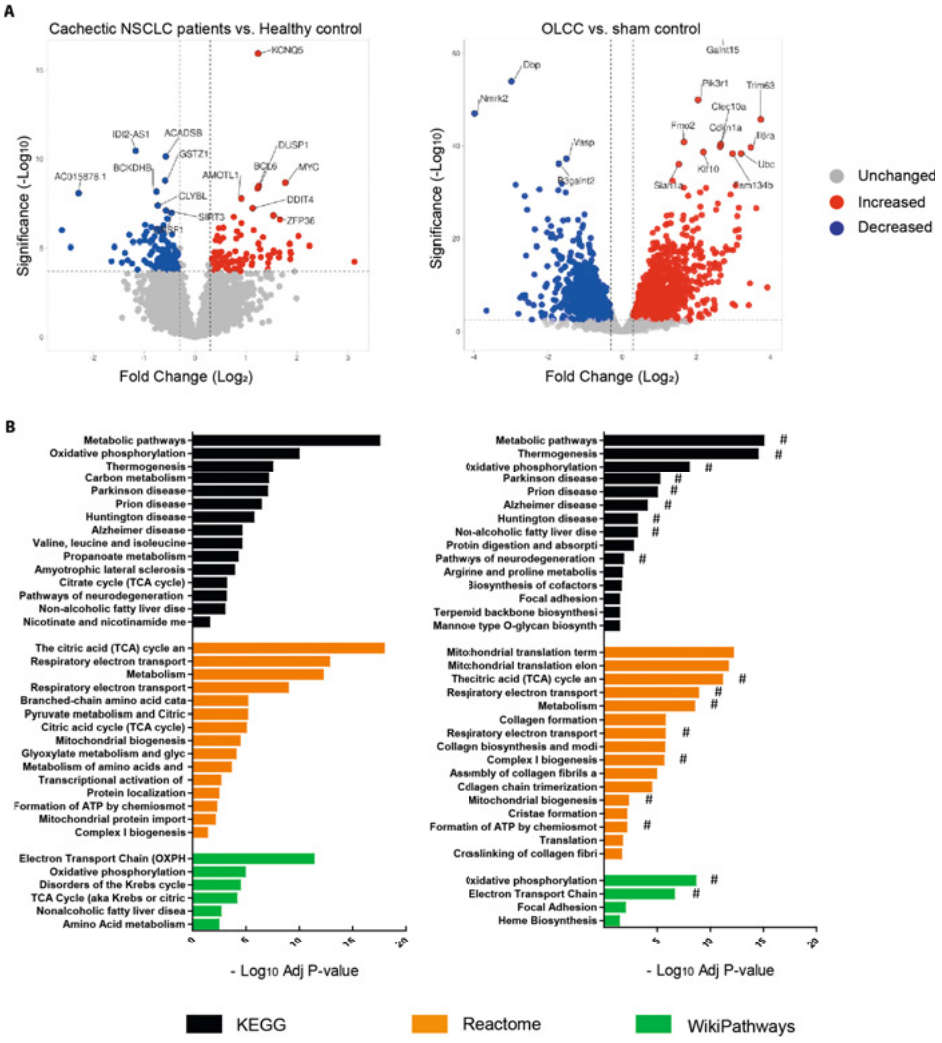

Figure 6: Comparative transcriptomic analysis in muscle biopsies of cachectic NSCLC patients and OLCC mice. (A) *Volcano plot of RNA sequencing data of newly diagnosed treatment naïve non-small cell lung cancer (NSCLC) patients with cachexia (n=8) compared with age- and gender-matched healthy controls (n=8; left panel) and OLLC mice (n=4) compared with sham control (n=4; right panel). Volcano plots are depicted with fold change (Log 2) and significance (-Log 10 Adjacent P-value). Significantly upregulated genes are shown in red, while significantly downregulated genes are shown in blue.* **(B)** *Horizontal bar chart of enriched biological pathways among significantly downregulated genes in NSCLC patients with cachexia (left panel) and OLCC mice (right panel). Enriched biological pathways are derived from three independent databases: Kyoto Encyclopedia of Genes and Genomes (KEGG; black bars), Reactome (orange bars) and WikiPathways (green bars). Overlapping pathways NSCLC patients with cachexia and OLCC mice are indicated with a hashtag (#).*

3.6. Differential miRNA expression in atrophied muscle of orthotopic lung cancer cachexia mice

In previous work we showed alterations in miRNA expression in muscle of cachectic lung cancer patients[21]. Specifically, the expression of miR-322(424)-5p and miR-450a-5p were significantly upregulated and the expression of miR-451a and miR-144-5p significantly downregulated in the skeletal muscle of lung cancer patients with cachexia. In accordance, the intramuscular expression of miR-322(424)-5p and miR-450a-5p were increased and the expression of miR-451a and miR-144-5p decreased in OLCC (Figure 7A-D). These findings indicate that similar processes are involved in the muscle of both OLCC mice and patients with lung cancer cachexia.

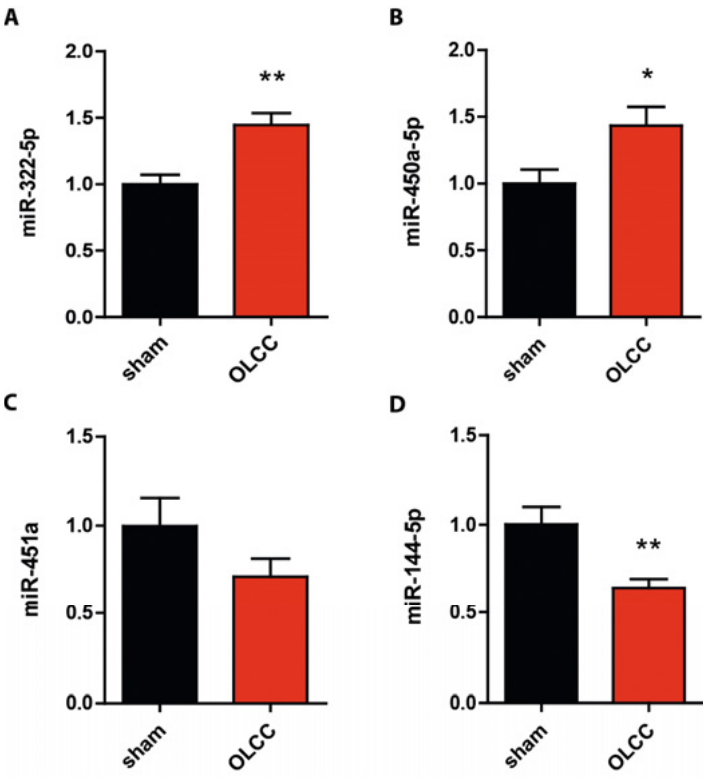

Figure 7: *Relative miRNA expression of* **(A)** *mmu-miR-322-5p* **(B)** *mmu-miR-450a-5p,* **(C)** *mmu-miR-451a, and* **(D)** *mmu-miR-144-5p measured in the m. gastrocnemius. Data is presented as mean ± SEM, sham control n=8 and orthotopic lung cancer cachexia (OLCC) n=8. Comparisons were statistically tested with two-tailed unpaired t-test for normally distributed data or Mann-Whitney U test for non-parametric data. Significances are shown as *P<0.05; **P<0.01, and ***P<0.001.*

4. DISCUSSION

In this study, we evaluated whether a syngeneic, orthotopic lung cancer mouse model replicates systemic and muscle-specific alterations associated with human lung cancer cachexia. Lung epithelium-derived adenocarcinoma cells derived from *Kras^{G12D}; p53$^{R172H\Delta G}$* mice were implanted in the lung of immune competent mice. The OLCC mice showed significant loss of skeletal muscle mass and function. The observed muscle wasting was accompanied by increased systemic inflammation and alterations in the regulation of muscle protein turnover, reflecting increased proteolysis and suppressed protein synthesis. Finally, we showed that the muscle transcriptome of the mouse model simulates key aspects specific to cachexia in lung cancer patients.

The Lewis lung carcinoma (LLC) mouse model is by far the most commonly used animal model in lung cancer cachexia research [23, 24]. In this mouse model, the LLC NSCLC cells are injected subcutaneous in immunocompetent mice [25]. This model has several advantages, including technical feasibility (easy to setup, absence of anesthesia) and tumor accessibility (direct measurement with caliper). However, the LLC model is limited by differences between tumor origin and (lung) microenvironment, including extra cellular matrix and immune infiltration, which may determine the etiology of cachexia. In addition, the LLC mouse model as used in cachexia research, develops relatively large ectopic growing tumors, which often represent more than 10% of the total body mass[24]. This may strongly impact the metabolism and energy requirements of the host and consequently determine the rapid cachexia symptom onset and a relatively short survival time typically observed in this model [24, 26, 27].

In orthotopic mouse models, the tumor grows in the appropriate anatomical site and local cellular context, which increases the relevance of experimental models, including those to study cancer cachexia [10, 28]. Previously, there only have been a few efforts to develop mouse models of lung cancer cachexia that focus on tumors arising in their original tissue, including a GEMM [15] and an intravenous metastasis model [29]. However, these models are limited by their discrepancies with respect to the clinical situation, as these models have hundreds of primary tumors that are difficult to follow up and quantify. In contrast to these models, the OLCC mouse model develops a single primary tumor of max 0.5% of total body weight in the left lung lobe of the mice, which better reflects the tumor burden in NSCLC patients and is easier to follow up. Approximately 67% of the tumor-bearing mice developed cachexia. This is similar in magnitude to the incidence observed

in the *Kras*$^{G12D/+}$*; Lkb1*$^{f/f}$ GEMM [15]. It is important to note that anorexia is absent in this model and that the symptom onset is less rapid compared with the widely used subcutaneous mouse models [11, 24], which makes the OLCC model highly suitable to study the therapeutic effects of (nutritional) intervention options.

Skeletal muscle loss is a major hallmark of cancer cachexia. In alignment with cachexia in patients with lung cancer [20] and different animal models of cancer cachexia [10, 25, 28, 30, 31], we demonstrate that the OLCC mice lose significant amount of muscle mass compared with sham control. Skeletal muscle wasting is an important contributing factor to muscle weakness. Cachectic patients have a lower hand grip strength compared with patients without cachexia [32, 33]. Muscle weakness in cachexia adversely affects performance status, quality of life and hospitalization risk of cancer patients [34]. In murine models of cancer cachexia, a decreased grip strength has been observed in cachectic mice compared with control mice [31, 35]. In line with these findings, the OLCC mice have significantly decreased grip strength compared with sham control, illustrating that progressive loss of muscle mass and function as major hallmarks of cancer cachexia are evident in the OLCC mouse model.

Systemic inflammation may be an important contributing factor to cancer-induced muscle atrophy [36, 37]. We showed that OLCC mice exhibit increased pentraxin-2 and CXCL1/KC (murine IL-8 orthologue) expression levels in the blood plasma. Pentraxin-2, also known as serum amyloid P component, is a major acute phase plasma protein in mice belonging to the same family as C-reactive protein (CRP) in human [38]. Increased circulating levels of CRP have been observed in cancer patients with cachexia compared with weight stable cancer patients and healthy controls [20, 39-41]. Raised levels of IL-8 have also been found in NSCLC patients [20] and pancreatic cancer patients with cachexia [42]. Furthermore, it has been shown that IL-8 is an independent predictor of survival in pancreatic cancer patients[42]. It has been suggested that IL-8 can directly contribute to muscle atrophy [43]. Besides increased IL-8 plasma levels, we found increased mRNA expression of *IκBα* in the skeletal muscle of cachectic mice, which is also reported in muscle biopsies of patients with lung cancer cachexia [20]. As *IκBα* is a target gene of the *NF-κB* transcription factor [44], this finding suggests increased inflammatory signaling in the muscle of the cachectic mice.

Intracellularly, the skeletal muscle wasting observed in OLCC mice is associated with increased proteolysis, involving both through UPS and ALP, and decreased protein synthesis. From experimental models of cancer cachexia, there is abundant

evidence for increased protein degradation and decreased protein synthesis [10, 15, 29, 45]. Compared to these results from animal models, evidence from human patients is rather inconclusive. Increased activation of the UPS in correlation with disease severity has been shown in skeletal muscle of patients with gastric cancer, although before the clinical onset of cachexia [46, 47]. In contrast, a study in lung cancer patients with cachexia did not find increased expression of UPS components in skeletal muscle [20]. In line with the OLCC mouse model, several studies have reported increased expression of autophagy markers in patients with cancer cachexia [48-51]. Op den Kamp et al. found increased expression of autophagy markers (*BNIP3* and *LC3B*) in muscle biopsies of NSCLC patients with cachexia compared with healthy control [20]. Available data on decreased protein synthesis, or activation status of the Akt/mTOR signaling pathway, in cancer patients is very limited. In one study on patients with pancreatic cancer and weight loss, decreased activation of Akt, mTOR and p70S6k was observed in skeletal muscle tissue compared with pancreatic cancer patients without weight loss [52]. Another study on cachectic NSCLC patients reported increased activation of Akt compared with healthy controls [20]. In contrast, none of the downstream signaling proteins, such as mTOR and 4E-BP1, showed significant changes in phosphorylation [20]. These differences between the mouse model and the patients can be explained by the different kinetics by which cachexia develops. While in the mouse model cachexia progresses within a few weeks, in the patient the progression is comprises several months. The gradual nature of the process in patients together with the constant turnover of muscle suggests that imbalances in muscle protein synthesis and breakdown may be more subtle and consequently difficult to detect in cachectic muscle.

A major drawback of many mouse models used in prior cancer cachexia research, including the LLC model, is the fact that the gene signatures in mouse skeletal muscle are completely distinct from those in cachectic patients [10]. To comprehensively assess whether the OLCC model reproduces the muscle intracellular changes related to human lung cancer cachexia, we compared the DEGs in OLCC mice with the DEGS in cachectic NSCLC patients. Using pathway-enrichment analysis, we found a remarkable overlap in the down-regulated DEGs, demonstrating similar alterations in the molecular processes governing muscle metabolism between the OLCC mice and cachectic NSCLC patients. Interestingly, many of the enriched pathways are suggestive of mitochondrial dysfunction in the skeletal muscle in lung cancer cachexia. This is in line with previous work reporting impairment of mitochondrial quality and function [53, 54], and calls for follow-up research to further unravel the role of mitochondrial dysfunction in cancer

cachexia. In addition, we measured the expression levels of four miRNAs potentially involved in the regulation of muscle atrophy in the skeletal muscle of OLCC mice. We found an identical miRNA expression pattern (up- and down-regulated) in the skeletal muscle of the OLCC mice as has been found in NSCLC patients [21]. This observation warrants further investigation into the role of these miRNAs in cancer cachexia. Combined, these expression data demonstrate that intracellular changes specifically associated with muscle atrophy in NSCLC patients are preserved in OLCC mouse muscle.

To conclude, we developed and characterized an orthotopic lung cancer mouse model in immune competent mice which simulates key aspects of human lung cancer cachexia. The model presented here provides opportunities to advance cancer cachexia research, including understanding the etiology of lung cancer cachexia and the development and evaluation of novel intervention strategies.

REFERENCES

1. Sung H, Ferlay J, Siegel RL, Laversanne M, Soerjomataram I, Jemal A, Bray F: Global Cancer Statistics 2020: GLOBOCAN Estimates of Incidence and Mortality Worldwide for 36 Cancers in 185 Countries. *CA Cancer J Clin* 2021, 71(3):209-249.
2. Herbst RS, Heymach JV, Lippman SM: Lung cancer. *N Engl J Med* 2008, 359(13):1367-1380.
3. Rivera MP, Mehta AC, Wahidi MM: Establishing the diagnosis of lung cancer: Diagnosis and management of lung cancer, 3rd ed: American College of Chest Physicians evidence-based clinical practice guidelines. *Chest* 2013, 143(5 Suppl):e142S-e165S.
4. Anker MS, Holcomb R, Muscaritoli M, von Haehling S, Haverkamp W, Jatoi A, Morley JE, Strasser F, Landmesser U, Coats AJS *et al*: Orphan disease status of cancer cachexia in the USA and in the European Union: a systematic review. *J Cachexia Sarcopenia Muscle* 2019, 10(1):22-34.
5. Dewys WD, Begg C, Lavin PT, Band PR, Bennett JM, Bertino JR, Cohen MH, Douglass HO, Jr., Engstrom PF, Ezdinli EZ *et al*: Prognostic effect of weight loss prior to chemotherapy in cancer patients. Eastern Cooperative Oncology Group. *Am J Med* 1980, 69(4):491-497.
6. Ross PJ, Ashley S, Norton A, Priest K, Waters JS, Eisen T, Smith IE, O'Brien ME: Do patients with weight loss have a worse outcome when undergoing chemotherapy for lung cancers? *Br J Cancer* 2004, 90(10):1905-1911.
7. Turner DC, Kondic AG, Anderson KM, Robinson AG, Garon EB, Riess JW, Jain L, Mayawala K, Kang J, Ebbinghaus SW *et al*: Pembrolizumab Exposure-Response Assessments Challenged by Association of Cancer Cachexia and Catabolic Clearance. *Clin Cancer Res* 2018, 24(23):5841-5849.
8. Degens J, Dingemans AC, Willemsen ACH, Gietema HA, Hurkmans DP, Aerts JG, Hendriks LEL, Schols A: The prognostic value of weight and body composition changes in patients with non-small-cell lung cancer treated with nivolumab. *J Cachexia Sarcopenia Muscle* 2021, 12(3):657-664.
9. Roeland EJ, Bohlke K, Baracos VE, Bruera E, Fabbro Ed, Dixon S, Fallon M, Herrstedt J, Lau H, Platek M *et al*: Management of Cancer Cachexia: ASCO Guideline. *Journal of Clinical Oncology* 2020, 38(21):2438-2453.
10. Talbert EE, Cuitiño MC, Ladner KJ, Rajasekerea PV, Siebert M, Shakya R, Leone GW, Ostrowski MC, Paleo B, Weisleder N *et al*: Modeling Human Cancer-induced Cachexia. *Cell Rep* 2019, 28(6):1612-1622.e1614.
11. van de Worp W, Schols A, Theys J, van Helvoort A, Langen RCJ: Nutritional Interventions in Cancer Cachexia: Evidence and Perspectives From Experimental Models. *Front Nutr* 2020, 7:601329.
12. Suzuki T, Von Haehling S, Springer J: Promising models for cancer-induced cachexia drug discovery. *Expert Opinion on Drug Discovery* 2020, 15(5):627-637.
13. Delitto D, Judge SM, Delitto AE, Nosacka RL, Rocha FG, DiVita BB, Gerber MH, George TJ, Jr., Behrns KE, Hughes SJ *et al*: Human pancreatic cancer xenografts recapitulate key aspects of cancer cachexia. *Oncotarget* 2017, 8(1):1177-1189.
14. Whiteside TL: The tumor microenvironment and its role in promoting tumor growth. *Oncogene* 2008, 27(45):5904-5912.

15. Goncalves MD, Hwang S-K, Pauli C, Murphy CJ, Cheng Z, Hopkins BD, Wu D, Loughran RM, Emerling BM, Zhang G *et al*: Fenofibrate prevents skeletal muscle loss in mice with lung cancer. *Proceedings of the National Academy of Sciences* 2018, 115(4):E743-E752.
16. Justilien V, Fields AP: Utility and applications of orthotopic models of human non-small cell lung cancer (NSCLC) for the evaluation of novel and emerging cancer therapeutics. *Curr Protoc Pharmacol* 2013, 62:14.27.11-14.27.17.
17. Sosa Iglesias V, van Hoof SJ, Vaniqui A, Schyns LE, Lieuwes N, Yaromina A, Spiegelberg L, Groot AJ, Verhaegen F, Theys J *et al*: An orthotopic non-small cell lung cancer model for image-guided small animal radiotherapy platforms. *Br J Radiol* 2019, 92(1095):20180476.
18. van de Worp WR, van der Heyden B, Lappas G, van Helvoort A, Theys J, Schols AM, Verhaegen F, Langen RC: Deep Learning Based Automated Orthotopic Lung Tumor Segmentation in Whole-Body Mouse CT-Scans. *Cancers* 2021, 13(18):4585.
19. van der Heyden B, van de Worp WR, van Helvoort A, Theys J, Schols AM, Langen RC, Verhaegen F: Automated CT-derived skeletal muscle mass determination in lower hind limbs of mice using a 3D U-Net deep learning network. *Journal of Applied Physiology* 2020, 128(1):42-49.
20. Op den Kamp CM, Langen RC, Snepvangers FJ, de Theije CC, Schellekens JM, Laugs F, Dingemans AM, Schols AM: Nuclear transcription factor κ B activation and protein turnover adaptations in skeletal muscle of patients with progressive stages of lung cancer cachexia. *Am J Clin Nutr* 2013, 98(3):738-748.
21. van de Worp WR, Schols AM, Dingemans AMC, Op den Kamp CM, Degens JH, Kelders MC, Coort S, Woodruff HC, Kratassiouk G, Harel-Bellan A: Identification of microRNAs in skeletal muscle associated with lung cancer cachexia. *Journal of cachexia, sarcopenia and muscle* 2020, 11(2):452-463.
22. Schiaffino S, Dyar KA, Ciciliot S, Blaauw B, Sandri M: Mechanisms regulating skeletal muscle growth and atrophy. *Febs j* 2013, 280(17):4294-4314.
23. Mayo JG: Biologic characterization of the subcutaneously implanted Lewis lung tumor. *Cancer Chemother Rep 2* 1972, 3(1):325-330.
24. Ballarò R, Costelli P, Penna F: Animal models for cancer cachexia. *Curr Opin Support Palliat Care* 2016, 10(4):281-287.
25. Murphy KT, Chee A, Gleeson BG, Naim T, Swiderski K, Koopman R, Lynch GS: Antibody-directed myostatin inhibition enhances muscle mass and function in tumor-bearing mice. *Am J Physiol Regul Integr Comp Physiol* 2011, 301(3):R716-726.
26. Pin F, Busquets S, Toledo M, Camperi A, Lopez-Soriano FJ, Costelli P, Argilés JM, Penna F: Combination of exercise training and erythropoietin prevents cancer-induced muscle alterations. *Oncotarget* 2015, 6(41):43202-43215.
27. Chen JA, Splenser A, Guillory B, Luo J, Mendiratta M, Belinova B, Halder T, Zhang G, Li YP, Garcia JM: Ghrelin prevents tumour- and cisplatin-induced muscle wasting: characterization of multiple mechanisms involved. *J Cachexia Sarcopenia Muscle* 2015, 6(2):132-143.
28. Michaelis KA, Zhu X, Burfeind KG, Krasnow SM, Levasseur PR, Morgan TK, Marks DL: Establishment and characterization of a novel murine model of pancreatic cancer cachexia. *J Cachexia Sarcopenia Muscle* 2017, 8(5):824-838.
29. Arneson-Wissink PC, Ducharme AM, Doles JD: A novel transplantable model of lung cancer-associated tissue loss and disrupted muscle regeneration. *Skeletal Muscle* 2020, 10(1):6.

30. Argilés JM, Figueras M, Ametller E, Fuster G, Olivan M, de Oliveira CCF, López-Soriano FJ, Isfort RJ, Busquets S: Effects of CRF2R agonist on tumor growth and cachexia in mice implanted with Lewis lung carcinoma cells. *Muscle & Nerve* 2008, 37(2):190-195.
31. Zhou X, Wang JL, Lu J, Song Y, Kwak KS, Jiao Q, Rosenfeld R, Chen Q, Boone T, Simonet WS *et al*: Reversal of Cancer Cachexia and Muscle Wasting by ActRIIB Antagonism Leads to Prolonged Survival. *Cell* 2010, 142(4):531-543.
32. Agelaki S, Rounis K, Papadaki C, Monastirioti AA, Vamvakas L, Gioulbasanis I, Mavroudis D, Makrakis DA: Cancer cachexia, sarcopenia and hand-GRIP strength (HGS) in the prediction of outcome in patients with metastatic non-small cell lung cancer (NSCLC) treated with immune checkpoint inhibitors (ICIs): A prospective, observational study. *Journal of Clinical Oncology* 2019, 37(15_suppl):9099-9099.
33. Burtin C, Bezuidenhout J, Sanders KJC, Dingemans AC, Schols A, Peeters STH, Spruit MA, De Ruysscher DKM: Handgrip weakness, low fat-free mass, and overall survival in non-small cell lung cancer treated with curative-intent radiotherapy. *J Cachexia Sarcopenia Muscle* 2020, 11(2):424-431.
34. Aapro M, Arends J, Bozzetti F, Fearon K, Grunberg SM, Herrstedt J, Hopkinson J, Jacquelin-Ravel N, Jatoi A, Kaasa S *et al*: Early recognition of malnutrition and cachexia in the cancer patient: a position paper of a European School of Oncology Task Force. *Ann Oncol* 2014, 25(8):1492-1499.
35. Puppa MJ, Murphy EA, Fayad R, Hand GA, Carson JA: Cachectic skeletal muscle response to a novel bout of low-frequency stimulation. *Journal of applied physiology (Bethesda, Md : 1985)* 2014, 116(8):1078-1087.
36. Webster JM, Kempen L, Hardy RS, Langen RCJ: Inflammation and Skeletal Muscle Wasting During Cachexia. *Front Physiol* 2020, 11:597675.
37. Argilés JM, Busquets S, López-Soriano FJ: Anti-inflammatory therapies in cancer cachexia. *European Journal of Pharmacology* 2011, 668:S81-S86.
38. Lu J, Mold C, Du Clos TW, Sun PD: Pentraxins and Fc Receptor-Mediated Immune Responses. *Front Immunol* 2018, 9:2607-2607.
39. Bilir C, Engin H, Can M, Temi YB, Demirtas D: The prognostic role of inflammation and hormones in patients with metastatic cancer with cachexia. *Medical Oncology* 2015, 32(3):56.
40. Stephens NA, Skipworth RJ, Gallagher IJ, Greig CA, Guttridge DC, Ross JA, Fearon KC: Evaluating potential biomarkers of cachexia and survival in skeletal muscle of upper gastrointestinal cancer patients. *J Cachexia Sarcopenia Muscle* 2015, 6(1):53-61.
41. Burney BO, Hayes TG, Smiechowska J, Cardwell G, Papusha V, Bhargava P, Konda B, Auchus RJ, Garcia JM: Low Testosterone Levels and Increased Inflammatory Markers in Patients with Cancer and Relationship with Cachexia. *The Journal of Clinical Endocrinology & Metabolism* 2012, 97(5):E700-E709.
42. Hou Y-C, Wang C-J, Chao Y-J, Chen H-Y, Wang H-C, Tung H-L, Lin J-T, Shan Y-S: Elevated Serum Interleukin-8 Level Correlates with Cancer-Related Cachexia and Sarcopenia: An Indicator for Pancreatic Cancer Outcomes. *J Clin Med* 2018, 7(12):502.
43. Callaway CS, Delitto AE, Patel R, Nosacka RL, D'Lugos AC, Delitto D, Deyhle MR, Trevino JG, Judge SM, Judge AR: IL-8 Released from Human Pancreatic Cancer and Tumor-Associated Stromal Cells Signals through a CXCR2-ERK1/2 Axis to Induce Muscle Atrophy. *Cancers (Basel)* 2019, 11(12).
44. Peterson JM, Bakkar N, Guttridge DC: NF-κB signaling in skeletal muscle health and disease. *Curr Top Dev Biol* 2011, 96:85-119.

45. White JP, Baynes JW, Welle SL, Kostek MC, Matesic LE, Sato S, Carson JA: The regulation of skeletal muscle protein turnover during the progression of cancer cachexia in the Apc(Min/+) mouse. *PLoS One* 2011, 6(9):e24650.
46. Bossola M, Muscaritoli M, Costelli P, Bellantone R, Pacelli F, Busquets S, Argilès J, Lopez-Soriano FJ, Civello IM, Baccino FM *et al*: Increased muscle ubiquitin mRNA levels in gastric cancer patients. *Am J Physiol Regul Integr Comp Physiol* 2001, 280(5):R1518-1523.
47. Bossola M, Muscaritoli M, Costelli P, Grieco G, Bonelli G, Pacelli F, Rossi Fanelli F, Doglietto GB, Baccino FM: Increased muscle proteasome activity correlates with disease severity in gastric cancer patients. *Ann Surg* 2003, 237(3):384-389.
48. Zhang Y, Wang J, Wang X, Gao T, Tian H, Zhou D, Zhang L, Li G, Wang X: The autophagic-lysosomal and ubiquitin proteasome systems are simultaneously activated in the skeletal muscle of gastric cancer patients with cachexia. *Am J Clin Nutr* 2020, 111(3):570-579.
49. Johns N, Hatakeyama S, Stephens NA, Degen M, Degen S, Frieauff W, Lambert C, Ross JA, Roubenoff R, Glass DJ *et al*: Clinical classification of cancer cachexia: phenotypic correlates in human skeletal muscle. *PLoS One* 2014, 9(1):e83618.
50. De Castro GS, Simoes E, Lima JD, Ortiz-Silva M, Festuccia WT, Tokeshi F, Alcântara PS, Otoch JP, Coletti D, Seelaender M: Human cachexia induces changes in mitochondria, autophagy and apoptosis in the skeletal muscle. *Cancers* 2019, 11(9):1264.
51. Aversa Z, Pin F, Lucia S, Penna F, Verzaro R, Fazi M, Colasante G, Tirone A, Rossi Fanelli F, Ramaccini C *et al*: Autophagy is induced in the skeletal muscle of cachectic cancer patients. *Sci Rep* 2016, 6:30340.
52. Schmitt TL, Martignoni ME, Bachmann J, Fechtner K, Friess H, Kinscherf R, Hildebrandt W: Activity of the Akt-dependent anabolic and catabolic pathways in muscle and liver samples in cancer-related cachexia. *J Mol Med (Berl)* 2007, 85(6):647-654.
53. Fontes-Oliveira CC, Busquets S, Toledo M, Penna F, Paz Aylwin M, Sirisi S, Silva AP, Orpí M, García A, Sette A *et al*: Mitochondrial and sarcoplasmic reticulum abnormalities in cancer cachexia: altered energetic efficiency? *Biochim Biophys Acta* 2013, 1830(3):2770-2778.
54. Antunes D, Padrão AI, Maciel E, Santinha D, Oliveira P, Vitorino R, Moreira-Gonçalves D, Colaço B, Pires MJ, Nunes C *et al*: Molecular insights into mitochondrial dysfunction in cancer-related muscle wasting. *Biochim Biophys Acta* 2014, 1841(6):896-905.
55. von Haehling S, Morley JE, Coats AJS, Anker SD: Ethical guidelines for publishing in the Journal of Cachexia, Sarcopenia and Muscle: update 2019. *J Cachexia Sarcopenia Muscle* 2019, 10(5):1143-1145.

SUPPORTING INFORMATION

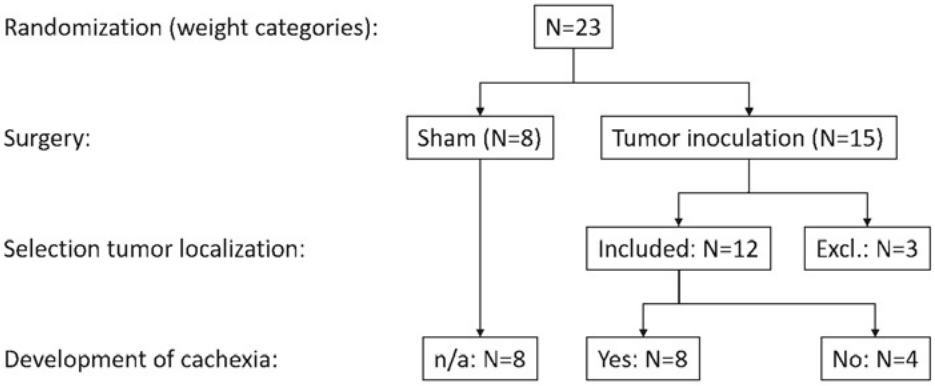

Figure S1: Flowchart of the animal experiment. *Mice, 11-weeks old, were randomly allocated to either sham control group (N=8) or tumor-bearing group (N=15). One week after surgery, animals without a primary tumor in the left lung were excluded (N=3). Only the tumor-bearing mice which developed cachexia (OLCC; N=8) were included for further analysis.*

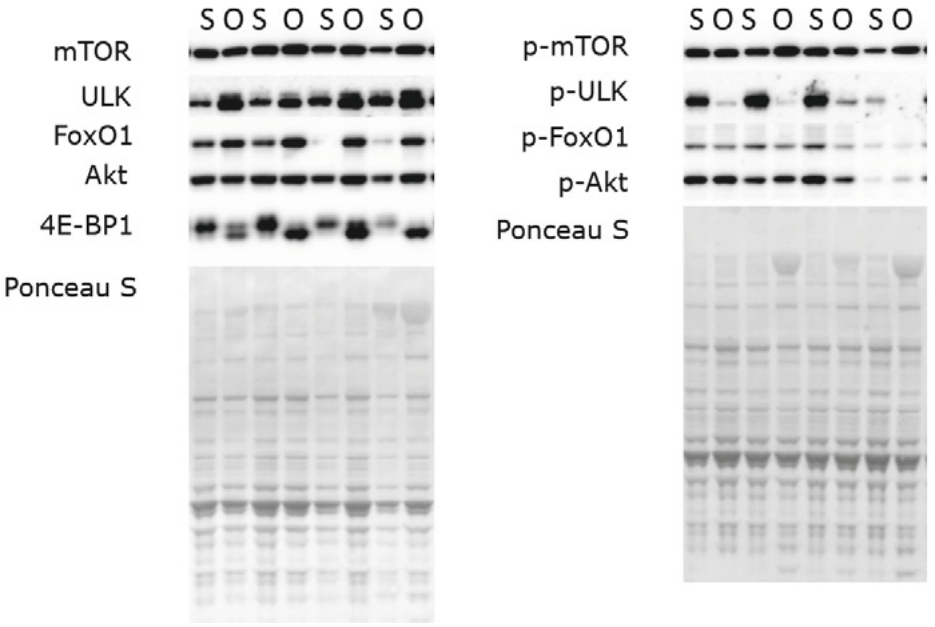

Figure. S2: Representative images of Western Blot data. *S: sham, O: OLCC. The intensity of the bands was normalized to Ponceau S.*

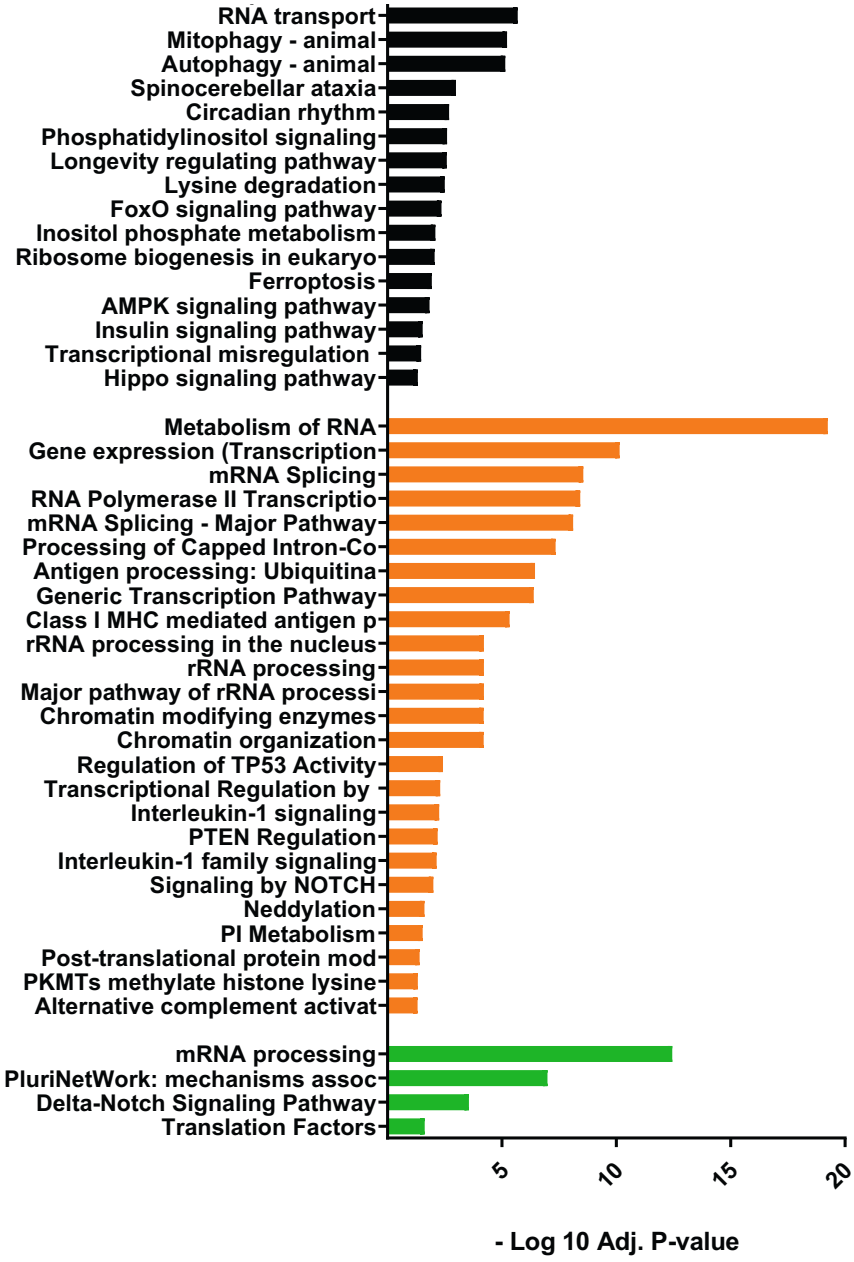

Figure S3: Horizontal bar chart of enriched biological pathways among significantly upregulated genes in OLCC mice. *Enriched biological pathways are derived from three independent databases: Kyoto Encyclopedia of Genes and Genomes (KEGG; black bars), Reactome (orange bars) and WikiPathways (green bars).*

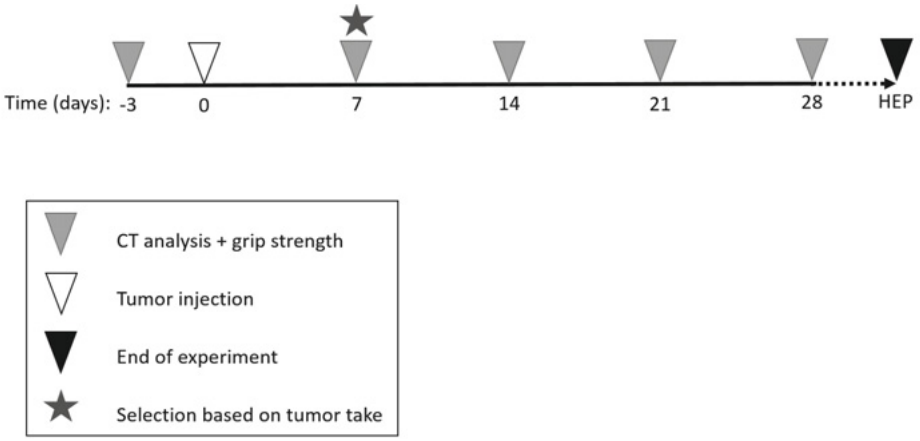

Figure S4: Experimental setup animal experiment. *Body weight and food intake were measured daily. At baseline (T-3) and weekly after tumor injection (T0), forelimb grip strength was assessed and CT-imaging was performed to assess tumor growth and muscle mass. At T0, tumor cells were injected intrapulmonary into the left lung lobe of the mice. At T7, only animals with an appropriate tumor take and location (N=12) were included in follow up analyses. After reaching cachexia-related Humane Endpoint (HEP), animals were euthanized and tissues were collected.*

Table S1: List of primers.

Gene name	Forward primer	Reverse primer
Atrogin-1	CAGCAGCTGAATAGCATCCAGAT	TCTGCATGATGTTCAGTTGTAAGC
MuRF-1	CTTCCTCTCAAGTGCCAAGCA	GTGTTCTAAGTCCAGAGTAAAGTAGTCCAT
NEDD4	GCTGCCAAGAGCACACACCTG	CAACGCCATCAAAGCCCTGT
Bnip3	AGGTTTTCCTTCCATCTCTGTTACTG	TGTGTGAACAGAAGTCAGATCCAAA
GabarapL	CCCTCCCACCAGTGCTACCAT	TCATCACTGTAGGCCACATACAGAAAA
FoxO1	ACACACAGCTGGGTGTCAGGCT	GGAAAGTGCTGCCGCTGTTG
REDD1	TCGGCGCTTCACTACTGACC	CCTAACACCCACCCCATTCC
IκBα	GCTACCCGAGAGCGAGGAT	GCCTCCAAACACACAGTCATCA
Glul	GGCCATGCGGGAGGAGA	GGTGCCTCTTGCTCAGTTTGTCA
KLF15	TCACCCTCCTCCAGACACCA	TTGGCATCCACCAGACCTGT
RPLP0	GGACCCGAGAAGACCTCCTT	GCACATCACTCAGAATTTCAATGG
RPL13A	CACTCTGGAGGAGAAACGGAAGG	GCAGGCATGAGGCAAACAGTC
B2M	CTTTCTGGTGCTTGTCTCACTGA	GTATGTTCGGCTTCCCATTCTC
Cyclophilin	TTCCTCCTTTCACAGAATTATTCCA	CCGCCAGTGCCATTATGG
HPRT	TGGATATGCCCTTGACTATAATGAGTAC	AGGACTCCTCGTATTTGCAGATTC

Table S2: List of primary antibodies.

Primary Antibodies	Supplier	Cat. No.
mTOR	Cell Signaling	2983
p-mTOR (Ser2448)	Cell Signaling	5536
ULK	Cell Signaling	8054
p-ULK (ser757)	Cell Signaling	6888
FoxO1	Cell Signaling	2880
p-FoxO1 (Ser256)	Cell Signaling	9461
Akt	Cell Signaling	9272
p-Akt (Ser473)	Cell Signaling	9271
S6	Cell Signaling	2317
p-S6 (Ser235/236)	Cell Signaling	4856
4E-BP1	Cell Signaling	9452


8
EMBARGOED

Targeted nutritional intervention attenuates experimental lung cancer cachexia

Wouter RPH van de Worp
Jan Theys
Cecile JA Wolfs
Frank Verhaegen
Annemie MWJ Schols
Ardy van Helvoort
and Ramon CJ Langen

9

General discussion

GENERAL DISCUSSION

Cancer cachexia is a complex multifactorial syndrome and is frequently observed in patients with advanced stage lung cancer [1]. The treatment of cancer cachexia is an unmet medical need and a better understanding of its dynamics and underlying mechanisms is essential to develop effective interventions and improve management of cachexia. In this final chapter, the findings and advances described in this thesis are placed in a broader perspective and opportunities for future research are discussed.

I. EARLY DETECTION AND DYNAMICS OF CANCER CACHEXIA

The international consensus guidelines postulate a continuum of three stages of cancer cachexia: pre-cachexia, cachexia and refractory cachexia [2]. The consensus report suggests that especially during the pre-cachectic phase preemptive intervention strategies could be effective in the treatment of cachexia. This demands early detection of cancer cachexia, emphasizing the need for access to practical and sensitive tools. Moreover, future therapeutic interventions may target mechanisms of a certain cachectic stage, requiring assessment modalities for follow-up of the dynamics of cachexia and differentiate between its stages. Clinical implementation of body composition analysis on routinely obtained Computed Tomography (CT)-scans, and identification of novel biomarkers for cancer cachexia could make an important contribution required for early detection of cachexia.

CT-based body composition analysis

For patients with lung cancer, CT imaging is an integral part of the diagnosis and the evaluation of the treatment response. The potential for body composition assessment for the detection of cancer cachexia was already recognized a decade ago [3]. In clinical research, typically skeletal muscle and adipose tissue are most often manually delineated on a single CT-slice (at the level of lumbar (L) disc 3 or L1), which has been shown to correlate to total muscle mass [4, 5]. However, this time-consuming manual tissue segmentation and limited availability of CT-scans during cancer treatment complicates application of CT image analyses to identify onset of and subsequent dynamics of cancer cachexia.

In addition to the CT images obtained for diagnoses and treatment evaluation, daily volumetric imaging of the tumor is part of the treatment workflow in radiotherapy (RT). Prior to every RT treatment fraction cone-beam (CB) CT images are acquired

for localization of the tumor [6]. CBCT is also commonly used for preclinical studies. In chapter 5 and 6 of this thesis, we showed that these CBCT images can be used to quantify skeletal muscle mass and tumor volume for longitudinal follow-up in mice [7, 8]. We were the first to develop a fully automatic workflow, using artificial intelligence, for the segmentation and quantification of muscle mass and tumor volume. This information was used to monitor the dynamics of cachexia, and will facilitate to study the precise timing between tumor growth (and treatment response) and cachexia, as well as evaluation of the therapeutic effects of new interventions. In addition to muscle and tumor tissue, subcutaneous adipose tissue is also clearly visible and easy to distinguish from other tissue on these CBCT-images. In future research, deep learning algorithms for the automatic segmentation and quantification of subcutaneous adipose tissue will be developed following our previously applied methodology.

For the development of these automatic workflows, a convolutional neural network (3D U-Net) was trained to automatically delineate the skeletal muscle and lung tumor on CBCT images. Such a 3D U-Net architecture is specifically designed for segmentation of biomedical images obtained from various species including human [9]. Recently, several research groups trained a convolutional neural network for the automatic segmentation of skeletal muscle mass, subcutaneous adipose tissue and visceral adipose tissue in patients on diagnostic CT images [10, 11]. However, in the clinical setting, CBCT images are currently not used for body composition assessment due to inferior quality compared to diagnostic CT. It would be of great benefit to dissect the information embedded in these images and deploy it for dynamic evaluation of skeletal muscle and fat wasting associated with cancer cachexia.

The development of an automatic workflow for clinical CBCT images may be more complicated as these images can contain many artefacts compared to diagnostic CT images, which potentially decrease the performance of automatic segmentation algorithms. To enhance the quality of the CBCT images, first, a generative adversarial network has to be trained to generate images of CT quality (synthetic CT images) from the CBCT images [12]. Subsequently, the synthetic CT images can be used to train the convolutional neural network for automatic body composition assessment. These advances in artificial intelligence (AI) for medical image analysis, make implementation of body composition analysis in clinical practice progressively more feasible. Moreover, the development of automatic workflows would allow us to delineate all slices of the (CB)CT image, which is more reliable for longitudinal assessment of body composition because of motion

of the visceral organs. This AI technology will be essential for large scale data collection and analysis, providing the basis for improved understanding of the dynamics of cancer cachexia and treatment-induced cachexia, which until now is an underexplored research area. Finally, it will be essential to early detect the onset of cancer cachexia and distinguish the different stages of cachexia.

Biomarkers of cancer cachexia

In addition to AI-driven CT based body composition analysis, the identification and validation of novel biomarkers is another approach for early detection of cancer cachexia [13, 14]. An effective biomarker should not only be predictive, but should also allow to monitor the progression/dynamics of cachexia and the effects of putative interventions [13, 14]. While a number of molecules have been proposed as biomarkers of cachexia including pro-inflammatory cytokines (Interleukin-6 [IL-6] and tumor necrosis factor alpha [TNF-α]), hormones (leptin and ghrelin), prostaglandins (prostaglandin E2 [PGE2]) and peptides, such as C-terminal agrin fragment, none have been clinically established [14].

In addition to these secreted ligands, miRNAs have also been proposed as potential biomarkers in disease, including cancer. Nowadays, in cancer research it is possible to stratify human cancers based on a miRNA signature [15-17]. In particular, miRNAs discriminate tumor from non-tumor tissues, metastatic from non-metastatic tumors, different histotypes of the same tumor type, or in treated patients, responders from non-responders [18-20]. Considering these advances in translating insights in tumor biology to detecting and monitoring cancer development and responses, the potential for miRNAs as effective biomarker for cancer cachexia has to be explored.

Several miRNA profiling studies performed in skeletal muscle, both, derived from experimental models of cancer cachexia and patients with cancer cachexia, have provided an important basis for the understanding of miRNAs in skeletal muscle and their role in cancer cachexia (reviewed in Chapter 2 [21]). A small group of muscle-specific miRNAs, called myomiRs, have been identified as essential determinants in regulatory networks of myogenesis, muscle fiber type composition, muscle growth, and homeostasis [22]. Consequently, alterations in myomiRs have been implicated as drivers and adaptive responses of muscle atrophy during muscle wasting diseases including cachexia. In addition, changes in intra-muscular levels of non-muscle specific miRNAs (not belonging to the myomiRs) have been implicated in the regulation of muscle atrophy as well. In chapter 2, we proposed to term miRNAs directly associated with muscle atrophy “atromiRs” [21]. In chapter

3, we were the first to demonstrate a differential expression profile of miRNAs in skeletal muscle of lung cancer patients with cachexia [23]. However, whether these miRNAs are specific to cancer cachexia and can be used to stratify lung cancer patients with and without cachexia requires follow-up research, including validation of our findings in an external cohort.

Importantly, analysis of miRNAs in skeletal muscle may not be feasible for application as a biomarker, as biopsy procedures are relatively invasive, require skilled operators and may not easily be integrated in routine clinical practice. In contrast to intramuscular miRNAs, assessment of circulating miRNAs as biomarker could be a promising tool [24]. An attractive feature of circulating miRNAs is their remarkable stability, due to their small size and the inclusion in protein complexes (i.e. vesicles) that preserve them from RNase activity [25, 26]. Circulating miRNA's high stability, the non-invasive way to collect, to detect and to quantify them, are all features required for ideal biomarkers.

Some studies have reported that low concentrations of myomiRs in blood correlate with poor prognosis in NSCLC, melanoma, strocytoma, orosteosacroma [27-30]. However, studies comparing miRNA expression profiles in both skeletal muscle and blood plasma are lacking. This is essential to understand the relation between miRNA expression pattern in the skeletal muscle and the miRNA profile in the blood. More research is needed to explore (circulating) miRNAs as potential biomarker for cancer cachexia. For future research, not only attention should be paid to myomiRs or other miRNAs released by the muscle, but also miRNAs released by the (cachexia-inducing) tumor hold promise as circulating biomarkers for cancer cachexia.

II. INTRA-CELLULAR MECHANISMS OF MUSCLE WASTING IN CANCER CACHEXIA

Muscle protein turnover

A characteristic feature of cachexia is the unintentional loss of muscle mass, also known as muscle wasting or muscle atrophy, which is the consequence of an imbalance between the rates of protein synthesis (anabolism) and degradation (catabolism) [2, 31]. Muscle protein synthesis is mainly regulated by the insulin-like growth factor-1 (IGF-1) signaling pathway [32, 33]. Two main pathways of protein catabolism implicated in muscle atrophy are the ubiquitin proteasome system (UPS) and the autophagy lysosomal pathway (ALP) [32, 34, 35]. In alignment with different animal models of cancer cachexia [36-38], we showed that muscle

wasting observed in the novel orthotopic lung cancer cachexia (OLCC) mouse model was accompanied by alterations in protein turnover signaling indicative of increased protein degradation, involving both through UPS and ALP, and decreased protein synthesis (Chapter 7). Molecular analyses from patient derived muscle biopsies is less decisive on muscle protein synthesis and UPS. Data on decreased muscle protein synthesis, or activation status of the IGF-1 signaling pathway, in cancer patients is limited. One study observed decreased activation of Akt, mTOR and p70S6k (downstream signaling proteins of the IGF-1 signaling pathway) in the skeletal muscle of pancreatic cancer patients with weight loss compared to pancreatic cancer patients without weight loss [39]. In contrast, another study on NSCLC patients with cachexia reported increased activation of Akt compared with healthy controls [40]. Moreover, activation of UPS signaling in skeletal muscle of patients with gastric cancer correlated with disease severity, although before the clinical onset of cachexia [41, 42], no alterations were observed in expression of UPS components in skeletal muscle of lung cancer patients with cachexia [40]. The differences in observations between clinical research studies can be explained by the use of varying definitions of cachexia, and the relatively small and heterogeneous (cachexia stage, cancer type) patient populations. Therefore, in future research, the disturbances in protein turnover signaling should be properly investigated for the three different stages of cachexia, which will contribute to our better understanding of the dynamics. Specific attention may be focused on involvement of the ALP pathway. In contrast to alterations in UPS or protein synthesis signaling, ALP activity seems very consistently affected in cancer patients with cachexia [40, 43-46]. The OLCC mouse model as well showed increased expression of markers of the ALP, therefore this model is suitable for more in depth investigation of the role of ALP alternations in cancer cachexia.

Myonuclear turnover

In addition to impaired protein turnover, there is some evidence that muscle atrophy is also associated with impaired myonuclear turnover, the balance between myonuclear accretion and apoptosis (chapter 1) [47-50]. Different animal models of cancer cachexia showed increases in the expression of Pax7 protein and/or the number of Pax7+ cells [47, 51, 52]. Whereas this is generally indicative of a regenerative response, the Pax7+ precursor cells in the muscle of tumor-bearing mice do not proceed forward in the regeneration program, and appeared arrested prior to differentiation [47]. The mechanism by which muscle regeneration becomes dysregulated is not fully understood and requires further investigation. It will be of interest to explore whether the regenerative properties of other muscle progenitor cells (e.g. mesoangioblasts, fibroadipogenic progenitors) are equally affected by

(lung) cancer cachexia [53]. Moreover, studies should be devised to distinguish between cell intrinsic alterations and effects of the cachectic environment on impaired satellite cell function, as this will provide insights that may be critical for determining appropriate treatment strategies. The newly developed OLCC mouse model (Chapter 7) in combination with the previously developed *in vitro* model for the assessment of postnatal myonuclear accretion [54] can be valuable tools the further unravel the mechanism of dysfunctional muscle regeneration in cancer cachexia.

MiRNAs in the regulation of muscle atrophy

In the section 'early detection and dynamics of cancer cachexia', miRNAs were discussed as potential biomarkers of cancer cachexia. These small single strand RNAs are known to directly affect growth and development of skeletal muscle by regulating genes that control muscle homeostasis [22]. Protein turnover and myonuclear turnover are two of the major intramuscular processes regulated by miRNAs, making them interesting therapeutic targets.

Research studies with experimental models of cancer cachexia have been conducted to identify atromiRs (reviewed in chapter 2 [21]). MiRNA profiling studies for cachexia in human muscle biopsies have been scarce and non-existing in lung cancer patients. In this thesis, by using TaqMan Human miRNA Array, 754 unique miRNAs were profiled in vastus lateralis muscle biopsies collected from 8 newly diagnosed treatment-naïve NSCLC patients with cachexia and 8 age- and sex-matched healthy controls (Chapter 3 [23]). We identified 28 differentially expressed miRNAs in the skeletal muscle of lung cancer patients with cachexia, including several H19X-encoded miRNAs with high potential relevance to muscle atrophy, as demonstrated using miRNA-gene-pathway analyses. In line with our finding, several H19X-encoded miRNAs were also found upregulated in the skeletal muscle of patients with amyotrophic lateral sclerosis [55, 56], chronic obstructive pulmonary disease patients with low fat free mass index [57] and patients with intensive care unit acquired weakness [58]. Following the publication of our manuscript, Liang et al. demonstrated that the levels of H19X-encoded miRNAs are inversely related to skeletal muscle growth [59]. In addition, they illustrated that that these miRNAs regulate skeletal muscle growth and atrophy by regulating the abundance of translation initiation factors (eIF4E, eIF4G1, eIF4B, eIF2B5 and eIF3M), thereby protein synthesis Combined these observations may suggest a causal link between H19X-encoded miRNAs and the regulating of muscle mass, which should be tested in translationally relevant preclinical models. Importantly, the expression of these H19X-encoded miRNAs was also found upregulated in

the atrophied muscle of OLCC mice (Chapter 7), emphasizing the suitability of our model to conduct clinically relevant mechanistic research and explore potential intervention strategies. Neutralizing the activities of these miRNAs may provide a new possibility to attenuate muscle atrophy. MiRNAs can be inhibited from binding their targets by complementary oligonucleotides (antimiRs). The first antimiR drug to enter phase II clinical trial was Miravirsen to treat hepatitis C virus infection [60], which shows promising effects. Whether this new class of drugs is also effective for treating conditions affecting skeletal muscle remains to be investigated.

Mitochondrial dysfunction in cancer cachexia

A major effect of lung cancer cachexia that is preserved in skeletal muscle of NSCLC patients and OLCC mice concerns mitochondrial function, as revealed by bioinformatics analysis on RNA-sequencing data described in Chapter 7. Mitochondrial dysfunction has been associated with muscle wasting in cancer cachexia, resulting from both alterations in organelle biogenesis, dynamics and clearance. In the muscle of tumor-bearing mice, the expression levels of markers for mitochondrial fusion and fission, two processes of mitochondrial dynamics, are downregulated [61-64], suggesting impaired mitochondrial adaptation. In addition to altered mitochondrial biogenesis and dynamics, the clearance of mitochondria (mitophagy) is also affected in the skeletal muscle of cachectic mice, indicated by increased expression of mitophagy markers [61, 65, 66]. The alterations in biogenesis and clearance of mitochondria are in accordance with the common finding of reduced levels of mitochondrial protein and content of mitochondrial DNA [61-63, 67]. Interestingly, in lewis lung carcinoma tumor-bearing mice it has been demonstrated that mitochondrial dysfunction occurs before the onset of cachexia [68]. Mechanistically, it has been suggested that the early development of mitochondrial dysfunction promotes mitochondrial ROS production and the oxidation of muscle contractile proteins which increases the activation of catabolic pathways and accelerates muscle protein breakdown, leading to muscle wasting. Importantly, mitochondrial alterations have recently been reported in the skeletal muscle of patients with cancer cachexia. De Castro *et al.* showed for the first time disruption of mitochondrial morphology, dysfunctional autophagy and increased apoptosis in the skeletal muscle of patients with gastrointestinal associated cancer cachexia [45]. Future research should investigate whether mitochondrial dysfunction is part of the cachectic phenotype or a trigger of cachexia, as well as how the mitochondrial dysfunction is induced (directly or indirectly by the tumor). These insights will ultimately provide a basis to consider studies aimed at restoring muscle mitochondrial function to prevent muscle atrophy during cancer.

III. EXTRA-CELLULAR MECHANISMS/TRIGGERS OF CANCER CACHEXIA

Cancer cachexia is highly associated with particular tumor types (i.e. lung, pancreatic, gastric, head and neck) suggesting that specific tumor-host interaction play a prominent role in the etiology of cachexia [1, 69]. Circulating factors secreted directly by tumor cells, or by the host in response to the tumor, are potential cachexia-inducing factors (CIFs) responsible for the impact of cancer on host physiology. CIFs can either directly target the skeletal muscle or indirectly by inducing metabolic reprogramming of peripheral organs (i.e. liver, brain, adipose tissue) to create a chronic negative energy state (reviewed in chapter 1), resulting in muscle wasting as a direct or compensatory response [70-72]. Notably, pro-inflammatory factors such as TNF-α, IL-6, IL-8 or growth differentiation factor 15, which are often found increased in the serum of patients and/or rodents with cancer cachexia have been postulated as potential CIFs [73]. Among these pro-inflammatory factors, TNF-α [74-76] and IL-6 [77] have been targeted in humans to treat cachexia. However, all these studies failed to identify any meaningful changes in cachexia-related parameters, suggesting that the most important CIFs have not yet been identified.

Comprehensive analysis of the gene expression profile of cachexia-inducing tumors can help to unravel their secretome and subsequent identification of putative tumor-derived CIFs [78, 79]. RNA sequencing in combination with algorithms for signal peptide prediction (i.e. SignalP, SecretomeP and TargetP) have become useful tools to predict tumor secretome based on gene expression data [80, 81]. Using such a workflow, Robinson et al. compared secreted protein expression changes across different cancer types and healthy tissues to identify candidate biomarkers detectable in the circulation [82]. Freire and colleagues used a similar approach to compare the expression profiles of secreted proteins in multiple tumor types with different prevalence of cachexia [83]. They revealed a tumor-specific expression profile of 25 potential CIFs that were associated with poor prognosis and correlated with the prevalence of cancer cachexia. However, these findings were not experimentally validated, and therefore, it is unknown whether these potentially tumor-derived CIFs are capable of directly contributing to muscle atrophy.

To better understand the tumor – muscle communication, we need to identify the messenger molecules (i.e. protein ligands, miRNAs) passed between the cells. After receiving the message, muscle cells trigger downstream signaling through cognate receptors, generally culminating in altered transcription factor activity

and gene expression. Measuring the downstream signaling in the muscle cells is fundamental to understand the directionality, magnitude and biological relevance of the communication pathways. The downstream signaling in the muscle cells subsequently can be used to identify the tumor-derived messenger molecules based on ligand-receptor pairing. In such an approach RNA sequencing data of cachexia-inducing tumors and the atrophied muscle is combined to explore tumor - muscle communication. Subsequent, experimental validation *in vitro* and *in vivo* is needed to assess their biological relevance and therapeutic potential in cancer cachexia. This unbiased, funnel shaped approach is currently pursued in our lab to identify tumor secreted ligands with cachexia inducing activity.

Treatment-induced cachexia

In addition to tumor activity and host responses that may drive muscle atrophy, cancer cachexia can also be induced or even accelerated by treatments directed at the tumor. As described in chapter 1, concurrent chemotherapy and radiotherapy (CCRT) followed by one year of durvalumab immunotherapy is the standard of care in fit patients with locally advanced NSCLC [84]. CCRT is a toxic treatment that can directly contribute to weight loss independent of nutritional intake and treatment-induced esophagitis in the first weeks of treatment [85]. Previous studies have demonstrated that early weight loss of more than 5% during the first week of CCRT has a negative impact on overall survival and outcome in patients with NSCLC [86]. The early weight loss during CCRT was associated with a significant drop in muscle strength. As muscle strength strongly correlates with muscle mass, this suggests loss of muscle mass early on during CCRT. More recently, it was demonstrated that early loss of fat mass, measured by BIA, is a negative prognostic factor for overall survival in NSCLC [87]. Moreover, human association studies indicated that stage IV (metastatic) NSCLC patients with cachexia benefit less from immunotherapy [88-90]. Clearly, better understanding of the dynamics and molecular mechanisms of CCRT-induced cachexia is essential to develop tailored interventions to improve the therapeutic effect of anti-cancer therapy.

Experimental animal studies investigating the underlying mechanisms of treatment-induced cachexia are scarce and limited to chemotherapy. Several studies have demonstrated that chemotherapeutic agents induce muscle wasting in rodents. However, data on the underlying mechanisms are still controversial. Some studies demonstrated that cancer and chemotherapy contribute to muscle loss by common processes, including upregulation of the UPS and mitochondrial dysfunction [91-94]. In contrast, others showed that chemotherapy-induced muscle loss was independent of the cancer associated upregulation in UPS [95, 96].

More recently, Pin et al performed a metabolomics approach to investigate the similarities and differences between cancer-induced and chemotherapy-induced cachexia [97]. The results of this study demonstrated for the first time that cancer-induced and chemotherapy-induced cachexia are characterized by a number of distinct metabolic derangements [97]. These studies highlight the complexity of chemotherapy-induced muscle wasting and suggest that more detailed studies are needed. The majority of these studies administrated chemotherapy in healthy animals and as a result the complexity of the interactions between tumor- and chemotherapy driven mediators was not taken into consideration. This is a limitation as it is plausible that chemotherapy has an impact on the tumor secretome, or may differentially influence tissues already affected by cancer. In contrast to chemotherapy-induced muscle loss, the effects of radiotherapy and consequently CCRT on body weight loss and/or muscle mass loss have not been studied in preclinical models.

Preclinical radiotherapy studies in the context of treatment-induced muscle loss are only meaningful in relevant models. Radiotherapy is a local treatment. This means specific area of the body is targeted. Thus, when studying muscle loss associated with radiotherapy alone or in combination with chemotherapy it is essential that the anatomical location and microenvironment of the tumor reflect those observed in the patient. Subcutaneous mouse models are often used to assess antitumor activity because of their high reproducibility and ease of monitoring tumor growth, however, lack translational relevance for this research question. In contrast, orthotopic mouse models are thought to reproduce the aspects of the microenvironment and are thought to be more clinically relevant. Orthotopic mouse models emulate a number of important biological features of cancer progression, vascularization, immune infiltration and sensitivity to therapy [98]. Importantly, the tumor characteristics of the OLCC mouse model are reflecting those observed in the patient (Chapter 6 and 7) and therefore will be a relevant model to study radiotherapy- or CCRT-induced cachexia. In addition, the combination of the deep learning algorithms for the longitudinal quantification of tumor volume and skeletal muscle mass will be very valuable in evaluating the effectivity of the anti-cancer therapy, and unraveling their mutual relationship as a determinant of the dynamics of the wasting process.

IV. MANAGEMENT OF CANCER CACHEXIA

Disease management is the concept to improve the health and quality of life of patients with a (chronic) condition and reduce the costs from avoidable complications by identifying and treating the condition more quickly and more

effectively, thus slowing down the progression [99]. The management of cancer cachexia is a major challenge for clinicians and an unmet medical need [100]. In this section, the current state and potential or remaining steps for implementation of the advances described in this thesis into the management of cachexia are described from the perspective of detection, monitoring and mechanisms of cachexia as outlined in sections I-III of the discussion chapter.

Detection and monitoring of cachexia

The first step in the management of cancer cachexia is identification of patients at risk for cachexia/pre-cachectic patients. Given that CT-scans are an integral part of the diagnosis and evaluation of the response to cancer therapy, assessment of body composition captured on these CT-scans should be implemented in daily clinical practice. For lung cancer patients receiving radiation therapy, body composition analysis on CBCT scans could be an additional strategy. Especially with the ongoing advances in AI for medical image analysis, development of tools to generate metrics that can be implemented as part of patient assessment becomes progressively more feasible. Routine body composition assessment will allow clinicians to screen patients for starting low muscularity, early skeletal muscle loss, and monitor the dynamics and treatment efficacy of cachexia-targeting interventions. In addition, as discussed in chapter 1, changes in body composition are associated with treatment-related dose-limiting toxicities [101, 102]. Therefore, longitudinal body composition assessment may also support early detection of patients developing treatment-related toxicities, allowing for timely adaptation of treatment regimens. However, limited data is currently available on implementation of body composition assessment in daily clinical practice, and application and feasibility research is needed in this setting.

Besides imaging, the identification and validation of biomarkers could be an opportunity for the management of cancer cachexia. In contrast to body composition analysis, testing for blood-based biomarkers is routinely applied and easy to implement in daily clinical practice. Tests for biomarkers are usually fast, minimally invasive and acceptable to patients and clinicians. Although a number of molecules have been proposed as biomarkers of cachexia, none have been clinically established. Circulating miRNAs could be promising as biomarker as discussed in section I, but more research is needed to explore their potential as biomarker. Furthermore, a potential novel biomarker first needs to be clinically validated before it can be implemented as screening tool. Evaluation of cancer cachexia using biomarkers may allow identification of critical time points for

personalized intervention with specific targeting agents, and effective markers for examination of cachexia-related characteristics.

Intervention options for cancer cachexia

Identification of the (pre)cachectic patient, will allow for initiation of targeted therapy. A wide range of intervention options, including pharmacological agents and nutrients, have been studied to treat cancer cachexia. However, currently, there are no US Food and Drug Administration (FDA)-approved therapies for cachexia and no standard of care [100]. Clinical trials have mainly focused on unimodal therapies that target either skeletal muscle anabolism, food intake or inflammation. Although some studies reported beneficial effects of unimodal therapies, they offer insufficient evidence to endorse any therapy to improve cancer cachexia outcomes [100]. This may not be unexpected considering cancer cachexia is a multifactorial condition characterized by metabolic changes, reduced nutritional intake and chronic inflammation [103]. As such, testing (combination) therapies that aim to modulate various aspects of cachexia simultaneously, i.e. multitarget interventions, are warranted [104]. Multinutrient interventions, as shown in chapter 8, in which a specific combination of nutrients are applied together to treat cachexia is a good example of such a multitarget intervention [105]. Nutritional interventions, as such, are a fundamental cornerstone of the multimodal intervention or combination therapy. Multimodal therapy is an intervention approach combines two or more methods of treatment, and is currently considered the best option to treat cancer cachexia.

In chapter 8, we tested the therapeutic efficacy of a specific combination of multiple metabolically and anti-inflammatory acting nutrients in a multitarget multinutrient approach on the development of experimental lung cancer cachexia. The intervention diet was specifically designed to target undernutrition, muscle mass (stimulate anabolism and reduce catabolism), immunological state and responsiveness, and microbiome. We showed for the first time that a targeted nutritional intervention delays the onset of cachexia, and attenuates the progression of body and muscle mass loss during cachexia. These findings are very promising and await further validation in patients with cancer cachexia. Delaying the onset of cancer cachexia would not only be associated with improved performance status and quality of life of the patients, but also with reduced treatment-related toxicities and prolonged survival. Consequently, this can lead to an increased capacity of the patient to endure anti-cancer therapy. In practice, cancer cachexia will not be treated in isolation, but in parallel or even prior to anti-cancer therapy such as

chemo-, radiation- and immunotherapy. Therefore, the next step is to test whether the combination is safe and contributes to the total therapy effectiveness.

With optimized nutritional support as basis, other therapeutic strategies, including pharmacological interventions and exercise training, could effectively contribute to attenuate cancer related muscle wasting. Carefully designed combination therapy may maximize the impact on attenuating muscle wasting while minimizing treatment-related toxicities and failures. However, the evidence to support this is limited and the number of open clinical trials is scarce. Therefore, more research is needed to design the best combination of therapeutic strategies and to test the efficacy and safety in patients with cancer cachexia.

Conclusion and directions for future research

The incomplete comprehension of the underlying mechanisms of cancer cachexia hamper the successful management of this complex syndrome. This thesis contributes to the better understanding of a pathophysiology of (lung) cancer cachexia, and describes the development of relevant models and tools to study the therapeutic efficacy of novel interventions. To increase the odds of cancer cachexia treatment, future research could focus on a number of aspects. First, research should focus on the implementation and validation of tools for the early detection of patients at risk for developing cachexia. A second opportunity for cancer cachexia research is to use more relevant models and research approaches to generate and test novel therapies to target cachexia. As anti-cancer therapy can contribute to cachexia as well, a better understanding of the underlying mechanisms of treatment-induced cachexia is necessary to improve treatment outcome. Finally, the evaluation of multitarget/multimodal therapies in patients with cancer cachexia should be emphasized in future research.

REFERENCES

1. Anker MS, Holcomb R, Muscaritoli M, von Haehling S, Haverkamp W, Jatoi A, Morley JE, Strasser F, Landmesser U, Coats AJS *et al*: Orphan disease status of cancer cachexia in the USA and in the European Union: a systematic review. *J Cachexia Sarcopenia Muscle* 2019, 10(1):22-34.
2. Fearon K, Strasser F, Anker SD, Bosaeus I, Bruera E, Fainsinger RL, Jatoi A, Loprinzi C, MacDonald N, Mantovani G *et al*: Definition and classification of cancer cachexia: an international consensus. *Lancet Oncol* 2011, 12(5):489-495.
3. Prado CM, Birdsell LA, Baracos VE: The emerging role of computerized tomography in assessing cancer cachexia. *Curr Opin Support Palliat Care* 2009, 3(4):269-275.
4. Sanders KJC, Degens J, Dingemans AC, Schols A: Cross-sectional and longitudinal assessment of muscle from regular chest computed tomography scans: L1 and pectoralis muscle compared to L3 as reference in non-small cell lung cancer. *Int J Chron Obstruct Pulmon Dis* 2019, 14:781-789.
5. Shen W, Punyanitya M, Wang Z, Gallagher D, St-Onge MP, Albu J, Heymsfield SB, Heshka S: Total body skeletal muscle and adipose tissue volumes: estimation from a single abdominal cross-sectional image. *J Appl Physiol (1985)* 2004, 97(6):2333-2338.
6. Purdie TG, Bissonnette JP, Franks K, Bezjak A, Payne D, Sie F, Sharpe MB, Jaffray DA: Cone-beam computed tomography for on-line image guidance of lung stereotactic radiotherapy: localization, verification, and intrafraction tumor position. *Int J Radiat Oncol Biol Phys* 2007, 68(1):243-252.
7. van der Heyden B, van de Worp WR, van Helvoort A, Theys J, Schols AM, Langen RC, Verhaegen F: Automated CT-derived skeletal muscle mass determination in lower hind limbs of mice using a 3D U-Net deep learning network. *Journal of Applied Physiology* 2020, 128(1):42-49.
8. van de Worp WR, van der Heyden B, Lappas G, van Helvoort A, Theys J, Schols AM, Verhaegen F, Langen RC: Deep Learning Based Automated Orthotopic Lung Tumor Segmentation in Whole-Body Mouse CT-Scans. *Cancers* 2021, 13(18):4585.
9. Milletari F, Navab N, Ahmadi S-A: V-net: Fully convolutional neural networks for volumetric medical image segmentation. In: *2016 fourth international conference on 3D vision (3DV): 2016*: IEEE; 2016: 565-571.
10. Koitka S, Kroll L, Malamutmann E, Oezcelik A, Nensa F: Fully automated body composition analysis in routine CT imaging using 3D semantic segmentation convolutional neural networks. *Eur Radiol* 2021, 31(4):1795-1804.
11. Hsu TH, Schawkat K, Berkowitz SJ, Wei JL, Makoyeva A, Legare K, DeCicco C, Paez SN, Wu JSH, Szolovits P *et al*: Artificial intelligence to assess body composition on routine abdominal CT scans and predict mortality in pancreatic cancer- A recipe for your local application. *Eur J Radiol* 2021, 142:109834.
12. Yi X, Walia E, Babyn P: Generative adversarial network in medical imaging: A review. *Medical Image Analysis* 2019, 58:101552.
13. Palus S, Springer J: Biomarkers for cancer cachexia: where do we stand? *J Cachexia Sarcopenia Muscle* 2020, 11(6):1388-1389.
14. Loumaye A, Thissen J-P: Biomarkers of cancer cachexia. *Clinical Biochemistry* 2017, 50(18):1281-1288.

15. Calin GA, Croce CM: MicroRNA signatures in human cancers. *Nat Rev Cancer* 2006, 6(11):857-866.
16. Di Leva G, Croce CM: miRNA profiling of cancer. *Curr Opin Genet Dev* 2013, 23(1):3-11.
17. Lu J, Getz G, Miska EA, Alvarez-Saavedra E, Lamb J, Peck D, Sweet-Cordero A, Ebert BL, Mak RH, Ferrando AA *et al*: MicroRNA expression profiles classify human cancers. *Nature* 2005, 435(7043):834-838.
18. Donzelli S, Mori F, Bellissimo T, Sacconi A, Casini B, Frixa T, Roscilli G, Aurisicchio L, Facciolo F, Pompili A *et al*: Epigenetic silencing of miR-145-5p contributes to brain metastasis. *Oncotarget* 2015, 6(34):35183-35201.
19. Lindholm EM, Ragle Aure M, Haugen MH, Kleivi Sahlberg K, Kristensen VN, Nebdal D, Børresen-Dale A-L, Lingjaerde OC, Engebraaten O: miRNA expression changes during the course of neoadjuvant bevacizumab and chemotherapy treatment in breast cancer. *Mol Oncol* 2019, 13(10):2278-2296.
20. Søkilde R, Persson H, Ehinger A, Pirona AC, Fernö M, Hegardt C, Larsson C, Loman N, Malmberg M, Rydén L *et al*: Refinement of breast cancer molecular classification by miRNA expression profiles. *BMC Genomics* 2019, 20(1):503.
21. van de Worp W, Theys J, van Helvoort A, Langen RCJ: Regulation of muscle atrophy by microRNAs: 'AtromiRs' as potential target in cachexia. *Curr Opin Clin Nutr Metab Care* 2018, 21(6):423-429.
22. Horak M, Novak J, Bienertova-Vasku J: Muscle-specific microRNAs in skeletal muscle development. *Dev Biol* 2016, 410(1):1-13.
23. van de Worp WR, Schols AM, Dingemans AMC, Op den Kamp CM, Degens JH, Kelders MC, Coort S, Woodruff HC, Kratassiouk G, Harel-Bellan A: Identification of microRNAs in skeletal muscle associated with lung cancer cachexia. *Journal of cachexia, sarcopenia and muscle* 2020, 11(2):452-463.
24. Belli R, Ferraro E, Molfino A, Carletti R, Tambaro F, Costelli P, Muscaritoli M: Liquid Biopsy for Cancer Cachexia: Focus on Muscle-Derived microRNAs. *International Journal of Molecular Sciences* 2021, 22(16):9007.
25. Cortez MA, Bueso-Ramos C, Ferdin J, Lopez-Berestein G, Sood AK, Calin GA: MicroRNAs in body fluids--the mix of hormones and biomarkers. *Nat Rev Clin Oncol* 2011, 8(8):467-477.
26. Izzotti A, Carozzo S, Pulliero A, Zhabayeva D, Ravetti JL, Bersimbaev R: Extracellular MicroRNA in liquid biopsy: applicability in cancer diagnosis and prevention. *Am J Cancer Res* 2016, 6(7):1461-1493.
27. Hu Z, Chen X, Zhao Y, Tian T, Jin G, Shu Y, Chen Y, Xu L, Zen K, Zhang C *et al*: Serum microRNA signatures identified in a genome-wide serum microRNA expression profiling predict survival of non-small-cell lung cancer. *J Clin Oncol* 2010, 28(10):1721-1726.
28. Li M, Zhang Q, Wu L, Jia C, Shi F, Li S, Peng A, Zhang G, Song X, Wang C: Serum miR-499 as a novel diagnostic and prognostic biomarker in non-small cell lung cancer. *Oncol Rep* 2014, 31(4):1961-1967.
29. Tian R, Liu T, Qiao L, Gao M, Li J: Decreased serum microRNA-206 level predicts unfavorable prognosis in patients with melanoma. *Int J Clin Exp Pathol* 2015, 8(3):3097-3103.
30. Zhang C, Yao C, Li H, Wang G, He X: Serum levels of microRNA-133b and microRNA-206 expression predict prognosis in patients with osteosarcoma. *Int J Clin Exp Pathol* 2014, 7(7):4194-4203.

31. Aapro M, Arends J, Bozzetti F, Fearon K, Grunberg SM, Herrstedt J, Hopkinson J, Jacquelin-Ravel N, Jatoi A, Kaasa S *et al*: Early recognition of malnutrition and cachexia in the cancer patient: a position paper of a European School of Oncology Task Force. *Ann Oncol* 2014, 25(8):1492-1499.
32. Schiaffino S, Dyar KA, Ciciliot S, Blaauw B, Sandri M: Mechanisms regulating skeletal muscle growth and atrophy. *Febs j* 2013, 280(17):4294-4314.
33. Glass DJ: Skeletal muscle hypertrophy and atrophy signaling pathways. *The International Journal of Biochemistry & Cell Biology* 2005, 37(10):1974-1984.
34. Sandri M: Autophagy in skeletal muscle. *FEBS Lett* 2010, 584(7):1411-1416.
35. Glick D, Barth S, Macleod KF: Autophagy: cellular and molecular mechanisms. *The Journal of Pathology* 2010, 221(1):3-12.
36. Talbert EE, Cuitiño MC, Ladner KJ, Rajasekerea PV, Siebert M, Shakya R, Leone GW, Ostrowski MC, Paleo B, Weisleder N *et al*: Modeling Human Cancer-induced Cachexia. *Cell Rep* 2019, 28(6):1612-1622.e1614.
37. Goncalves MD, Hwang S-K, Pauli C, Murphy CJ, Cheng Z, Hopkins BD, Wu D, Loughran RM, Emerling BM, Zhang G *et al*: Fenofibrate prevents skeletal muscle loss in mice with lung cancer. *Proceedings of the National Academy of Sciences* 2018, 115(4):E743-E752.
38. White JP, Baynes JW, Welle SL, Kostek MC, Matesic LE, Sato S, Carson JA: The regulation of skeletal muscle protein turnover during the progression of cancer cachexia in the Apc(Min/+) mouse. *PLoS One* 2011, 6(9):e24650.
39. Schmitt TL, Martignoni ME, Bachmann J, Fechtner K, Friess H, Kinscherf R, Hildebrandt W: Activity of the Akt-dependent anabolic and catabolic pathways in muscle and liver samples in cancer-related cachexia. *J Mol Med (Berl)* 2007, 85(6):647-654.
40. Op den Kamp CM, Langen RC, Snepvangers FJ, de Theije CC, Schellekens JM, Laugs F, Dingemans AM, Schols AM: Nuclear transcription factor κ B activation and protein turnover adaptations in skeletal muscle of patients with progressive stages of lung cancer cachexia. *Am J Clin Nutr* 2013, 98(3):738-748.
41. Bossola M, Muscaritoli M, Costelli P, Bellantone R, Pacelli F, Busquets S, Argilès J, Lopez-Soriano FJ, Civello IM, Baccino FM *et al*: Increased muscle ubiquitin mRNA levels in gastric cancer patients. *Am J Physiol Regul Integr Comp Physiol* 2001, 280(5):R1518-1523.
42. Bossola M, Muscaritoli M, Costelli P, Grieco G, Bonelli G, Pacelli F, Rossi Fanelli F, Doglietto GB, Baccino FM: Increased muscle proteasome activity correlates with disease severity in gastric cancer patients. *Ann Surg* 2003, 237(3):384-389.
43. Zhang Y, Wang J, Wang X, Gao T, Tian H, Zhou D, Zhang L, Li G, Wang X: The autophagic-lysosomal and ubiquitin proteasome systems are simultaneously activated in the skeletal muscle of gastric cancer patients with cachexia. *Am J Clin Nutr* 2020, 111(3):570-579.
44. Johns N, Hatakeyama S, Stephens NA, Degen M, Degen S, Frieauff W, Lambert C, Ross JA, Roubenoff R, Glass DJ *et al*: Clinical classification of cancer cachexia: phenotypic correlates in human skeletal muscle. *PLoS One* 2014, 9(1):e83618.
45. De Castro GS, Simoes E, Lima JD, Ortiz-Silva M, Festuccia WT, Tokeshi F, Alcântara PS, Otoch JP, Coletti D, Seelaender M: Human cachexia induces changes in mitochondria, autophagy and apoptosis in the skeletal muscle. *Cancers* 2019, 11(9):1264.
46. Aversa Z, Pin F, Lucia S, Penna F, Verzaro R, Fazi M, Colasante G, Tirone A, Rossi Fanelli F, Ramaccini C *et al*: Autophagy is induced in the skeletal muscle of cachectic cancer patients. *Sci Rep* 2016, 6:30340.

47. He WA, Berardi E, Cardillo VM, Acharyya S, Aulino P, Thomas-Ahner J, Wang J, Bloomston M, Muscarella P, Nau P *et al*: NF-κB-mediated Pax7 dysregulation in the muscle microenvironment promotes cancer cachexia. *J Clin Invest* 2013, 123(11):4821-4835.
48. Penna F, Costamagna D, Fanzani A, Bonelli G, Baccino FM, Costelli P: Muscle wasting and impaired myogenesis in tumor bearing mice are prevented by ERK inhibition. *PLoS One* 2010, 5(10):e13604.
49. Mehl KA, Davis JM, Berger FG, Carson JA: Myofiber degeneration/regeneration is induced in the cachectic ApcMin/+ mouse. *J Appl Physiol (1985)* 2005, 99(6):2379-2387.
50. Ramamoorthy S, Donohue M, Buck M: Decreased Jun-D and myogenin expression in muscle wasting of human cachexia. *Am J Physiol Endocrinol Metab* 2009, 297(2):E392-401.
51. Talbert EE, Guttridge DC: Impaired regeneration: A role for the muscle microenvironment in cancer cachexia. *Seminars in cell & developmental biology* 2016, 54:82-91.
52. Talbert EE, Metzger GA, He WA, Guttridge DC: Modeling human cancer cachexia in colon 26 tumor-bearing adult mice. *J Cachexia Sarcopenia Muscle* 2014, 5(4):321-328.
53. Costamagna D, Duelen R, Penna F, Neumann D, Costelli P, Sampaolesi M: Interleukin-4 administration improves muscle function, adult myogenesis, and lifespan of colon carcinoma-bearing mice. *J Cachexia Sarcopenia Muscle* 2020, 11(3):783-801.
54. Kneppers A, Verdijk L, de Theije C, Corten M, Gielen E, van Loon L, Schols A, Langen R: A novel in vitro model for the assessment of postnatal myonuclear accretion. *Skelet Muscle* 2018, 8(1):4.
55. de Andrade HM, de Albuquerque M, Avansini SH, de SRC, Dogini DB, Nucci A, Carvalho B, Lopes-Cendes I, França MC, Jr.: MicroRNAs-424 and 206 are potential prognostic markers in spinal onset amyotrophic lateral sclerosis. *J Neurol Sci* 2016, 368:19-24.
56. Kovanda A, Leonardis L, Zidar J, Koritnik B, Dolenc-Groselj L, Ristic Kovacic S, Curk T, Rogelj B: Differential expression of microRNAs and other small RNAs in muscle tissue of patients with ALS and healthy age-matched controls. *Sci Rep* 2018, 8(1):5609.
57. Connolly M, Paul R, Farre-Garros R, Natanek SA, Bloch S, Lee J, Lorenzo JP, Patel H, Cooper C, Sayer AA *et al*: miR-424-5p reduces ribosomal RNA and protein synthesis in muscle wasting. *J Cachexia Sarcopenia Muscle* 2018, 9(2):400-416.
58. Garros RF, Paul R, Connolly M, Lewis A, Garfield BE, Natanek SA, Bloch S, Mouly V, Griffiths MJ, Polkey MI *et al*: MicroRNA-542 Promotes Mitochondrial Dysfunction and SMAD Activity and Is Elevated in Intensive Care Unit-acquired Weakness. *Am J Respir Crit Care Med* 2017, 196(11):1422-1433.
59. Liang R, Shen X, Wang F, Wang X, DesJarlais A, Syed A, Saba R, Tan Z, Yu F, Ji X *et al*: H19X-encoded miR-322(424)/miR-503 regulates muscle mass by targeting translation initiation factors. *Journal of cachexia, sarcopenia and muscle* 2021, 12(6):2174-2186.
60. Janssen HL, Reesink HW, Lawitz EJ, Zeuzem S, Rodriguez-Torres M, Patel K, van der Meer AJ, Patick AK, Chen A, Zhou Y *et al*: Treatment of HCV infection by targeting microRNA. *N Engl J Med* 2013, 368(18):1685-1694.

61. Ballarò R, Beltrà M, De Lucia S, Pin F, Ranjbar K, Hulmi JJ, Costelli P, Penna F: Moderate exercise in mice improves cancer plus chemotherapy-induced muscle wasting and mitochondrial alterations. *The FASEB Journal* 2019, 33(4):5482-5494.
62. Barreto R, Mandili G, Witzmann FA, Novelli F, Zimmers TA, Bonetto A: Cancer and Chemotherapy Contribute to Muscle Loss by Activating Common Signaling Pathways. *Frontiers in Physiology* 2016, 7.
63. White JP, Baltgalvis KA, Puppa MJ, Sato S, Baynes JW, Carson JA: Muscle oxidative capacity during IL-6-dependent cancer cachexia. *American Journal of Physiology-Regulatory, Integrative and Comparative Physiology* 2011, 300(2):R201-R211.
64. van der Ende M, Grefte S, Plas R, Meijerink J, Witkamp RF, Keijer J, van Norren K: Mitochondrial dynamics in cancer-induced cachexia. *Biochimica et Biophysica Acta (BBA) - Reviews on Cancer* 2018, 1870(2):137-150.
65. Penna F, Ballarò R, Martinez-Cristobal P, Sala D, Sebastian D, Busquets S, Muscaritoli M, Argilés JM, Costelli P, Zorzano A: Autophagy Exacerbates Muscle Wasting in Cancer Cachexia and Impairs Mitochondrial Function. *Journal of Molecular Biology* 2019, 431(15):2674-2686.
66. Ballarò R, Penna F, Pin F, Gómez-Cabrera MC, Viña J, Costelli P: Moderate Exercise Improves Experimental Cancer Cachexia by Modulating the Redox Homeostasis. *Cancers* 2019, 11(3):285.
67. Molinari F, Pin F, Gorini S, Chiandotto S, Pontecorvo L, Penna F, Rizzuto E, Pisu S, Musarò A, Costelli P *et al*: The mitochondrial metabolic reprogramming agent trimetazidine as an 'exercise mimetic' in cachectic C26-bearing mice. *Journal of Cachexia, Sarcopenia and Muscle* 2017, 8(6):954-973.
68. Brown JL, Rosa-Caldwell ME, Lee DE, Blackwell TA, Brown LA, Perry RA, Haynie WS, Hardee JP, Carson JA, Wiggs MP *et al*: Mitochondrial degeneration precedes the development of muscle atrophy in progression of cancer cachexia in tumour-bearing mice. *Journal of Cachexia, Sarcopenia and Muscle* 2017, 8(6):926-938.
69. Baracos VE, Martin L, Korc M, Guttridge DC, Fearon KCH: Cancer-associated cachexia. *Nat Rev Dis Primers* 2018, 4:17105.
70. Tsoli M, Robertson G: Cancer cachexia: malignant inflammation, tumorkines, and metabolic mayhem. *Trends Endocrinol Metab* 2013, 24(4):174-183.
71. Twelkmeyer B, Tardif N, Rooyackers O: Omics and cachexia. *Curr Opin Clin Nutr Metab Care* 2017, 20(3):181-185.
72. Argilés JM, Stemmler B, López-Soriano FJ, Busquets S: Inter-tissue communication in cancer cachexia. *Nat Rev Endocrinol* 2018, 15(1):9-20.
73. Paval DR, Patton R, McDonald J, Skipworth RJE, Gallagher IJ, Laird BJ, Collaborative tCC: A systematic review examining the relationship between cytokines and cachexia in incurable cancer. *Journal of Cachexia, Sarcopenia and Muscle*, n/a(n/a).
74. Gueta I, Altman A, Shoenfeld Y: [The effect of blocking TNF-alpha in patients with cancer-related cachexia and anorexia]. *Harefuah* 2010, 149(8):512-514, 551, 550.
75. Jatoi A, Ritter HL, Dueck A, Nguyen PL, Nikcevich DA, Luyun RF, Mattar BI, Loprinzi CL: A placebo-controlled, double-blind trial of infliximab for cancer-associated weight loss in elderly and/or poor performance non-small cell lung cancer patients (N01C9). *Lung Cancer* 2010, 68(2):234-239.
76. Wiedenmann B, Malfertheiner P, Friess H, Ritch P, Arseneau J, Mantovani G, Caprioni F, Van Cutsem E, Richel D, DeWitte M *et al*: A multicenter, phase II study of infliximab plus gemcitabine in pancreatic cancer cachexia. *J Support Oncol* 2008, 6(1):18-25.

77. Ando K, Takahashi F, Motojima S, Nakashima K, Kaneko N, Hoshi K, Takahashi K: Possible role for tocilizumab, an anti-interleukin-6 receptor antibody, in treating cancer cachexia. *J Clin Oncol* 2013, 31(6):e69-72.
78. Mukherjee P, Mani S: Methodologies to decipher the cell secretome. *Biochimica et biophysica acta* 2013, 1834(11):2226-2232.
79. Armingol E, Officer A, Harismendy O, Lewis NE: Deciphering cell–cell interactions and communication from gene expression. *Nature Reviews Genetics* 2021, 22(2):71-88.
80. Emanuelsson O, Brunak S, von Heijne G, Nielsen H: Locating proteins in the cell using TargetP, SignalP and related tools. *Nat Protoc* 2007, 2(4):953-971.
81. Teufel F, Almagro Armenteros JJ, Johansen AR, Gíslason MH, Pihl SI, Tsirigos KD, Winther O, Brunak S, von Heijne G, Nielsen H: SignalP 6.0 predicts all five types of signal peptides using protein language models. *Nature Biotechnology* 2022.
82. Robinson JL, Feizi A, Uhlén M, Nielsen J: A Systematic Investigation of the Malignant Functions and Diagnostic Potential of the Cancer Secretome. *Cell reports* 2019, 26(10):2622-2635.e2625.
83. Freire PP, Fernandez GJ, de Moraes D, Cury SS, Dal Pai-Silva M, Dos Reis PP, Rogatto SR, Carvalho RF: The expression landscape of cachexia-inducing factors in human cancers. *Journal of cachexia, sarcopenia and muscle* 2020, 11(4):947-961.
84. Postmus PE, Kerr KM, Oudkerk M, Senan S, Waller DA, Vansteenkiste J, Escriu C, Peters S: Early and locally advanced non-small-cell lung cancer (NSCLC): ESMO Clinical Practice Guidelines for diagnosis, treatment and follow-up. *Ann Oncol* 2017, 28(suppl_4):iv1-iv21.
85. Op den Kamp CM, De Ruysscher DK, van den Heuvel M, Elferink M, Houben RM, Oberije CJ, Bootsma GP, Geraedts WH, Pitz CC, Langen RC *et al*: Early body weight loss during concurrent chemo-radiotherapy for non-small cell lung cancer. *J Cachexia Sarcopenia Muscle* 2014, 5(2):127-137.
86. Sanders KJC, Hendriks LE, Troost EGC, Bootsma GP, Houben RMA, Schols AMWJ, Dingemans A-MC: Early Weight Loss during Chemoradiotherapy Has a Detrimental Impact on Outcome in NSCLC. *Journal of Thoracic Oncology* 2016, 11(6):873-879.
87. Willemsen ACH, Degens JHRJ, Baijens LWJ, Dingemans AMC, Hoeben A, Hoebers FJP, De Ruysscher DKM, Schols AMWJ: Early Loss of Fat Mass During Chemoradiotherapy Predicts Overall Survival in Locally Advanced Squamous Cell Carcinoma of the Lung, but Not in Locally Advanced Squamous Cell Carcinoma of the Head and Neck. *Frontiers in nutrition* 2020, 7:600612-600612.
88. Degens J, Dingemans AC, Willemsen ACH, Gietema HA, Hurkmans DP, Aerts JG, Hendriks LEL, Schols A: The prognostic value of weight and body composition changes in patients with non-small-cell lung cancer treated with nivolumab. *J Cachexia Sarcopenia Muscle* 2021, 12(3):657-664.
89. Turner DC, Kondic AG, Anderson KM, Robinson AG, Garon EB, Riess JW, Jain L, Mayawala K, Kang J, Ebbinghaus SW *et al*: Pembrolizumab Exposure-Response Assessments Challenged by Association of Cancer Cachexia and Catabolic Clearance. *Clin Cancer Res* 2018, 24(23):5841-5849.
90. Roch B, Coffy A, Jean-Baptiste S, Palaysi E, Daures JP, Pujol JL, Bommart S: Cachexia - sarcopenia as a determinant of disease control rate and survival in non-small lung cancer patients receiving immune-checkpoint inhibitors. *Lung Cancer* 2020, 143:19-26.

91. Barreto R, Mandili G, Witzmann FA, Novelli F, Zimmers TA, Bonetto A: Cancer and Chemotherapy Contribute to Muscle Loss by Activating Common Signaling Pathways. *Frontiers in physiology* 2016, 7:472-472.
92. Chen J-A, Splenser A, Guillory B, Luo J, Mendiratta M, Belinova B, Halder T, Zhang G, Li Y-P, Garcia JM: Ghrelin prevents tumour- and cisplatin-induced muscle wasting: characterization of multiple mechanisms involved. *Journal of cachexia, sarcopenia and muscle* 2015, 6(2):132-143.
93. Garcia JM, Scherer T, Chen J-a, Guillory B, Nassif A, Papusha V, Smiechowska J, Asnicar M, Buettner C, Smith RG: Inhibition of cisplatin-induced lipid catabolism and weight loss by ghrelin in male mice. *Endocrinology* 2013, 154(9):3118-3129.
94. Gilliam LA, St. Clair DK: Chemotherapy-induced weakness and fatigue in skeletal muscle: the role of oxidative stress. *Antioxidants & redox signaling* 2011, 15(9):2543-2563.
95. Damrauer JS, Stadler ME, Acharyya S, Baldwin AS, Couch ME, Guttridge DC: Chemotherapy-induced muscle wasting: association with NF-κB and cancer cachexia. *Eur J Transl Myol* 2018, 28(2):7590-7590.
96. Barreto R, Waning DL, Gao H, Liu Y, Zimmers TA, Bonetto A: Chemotherapy-related cachexia is associated with mitochondrial depletion and the activation of ERK1/2 and p38 MAPKs. *Oncotarget* 2016, 7(28):43442-43460.
97. Pin F, Barreto R, Couch ME, Bonetto A, O'Connell TM: Cachexia induced by cancer and chemotherapy yield distinct perturbations to energy metabolism. *Journal of cachexia, sarcopenia and muscle* 2019, 10(1):140-154.
98. Bibby MC: Orthotopic models of cancer for preclinical drug evaluation: advantages and disadvantages. *European Journal of Cancer* 2004, 40(6):852-857.
99. Disease Management—A Great Concept, but Can You Implement It? *Disease Management* 2001, 4(3):111-119.
100. Roeland EJ, Bohlke K, Baracos VE, Bruera E, Fabbro Ed, Dixon S, Fallon M, Herrstedt J, Lau H, Platek M *et al*: Management of Cancer Cachexia: ASCO Guideline. *Journal of Clinical Oncology* 2020, 38(21):2438-2453.
101. Ross PJ, Ashley S, Norton A, Priest K, Waters JS, Eisen T, Smith IE, O'Brien ME: Do patients with weight loss have a worse outcome when undergoing chemotherapy for lung cancers? *Br J Cancer* 2004, 90(10):1905-1911.
102. Cortellini A, Palumbo P, Porzio G, Verna L, Giordano AV, Masciocchi C, Parisi A, Cannita K, Ficorella C, Bozzetti F: Single-institution study of correlations between skeletal muscle mass, its density, and clinical outcomes in non-small cell lung cancer patients treated with first-line chemotherapy. *Thoracic Cancer* 2018, 9(12):1623-1630.
103. Schmidt SF, Rohm M, Herzig S, Berriel Diaz M: Cancer Cachexia: More Than Skeletal Muscle Wasting. *Trends in Cancer* 2018, 4(12):849-860.
104. Fearon KCH: Cancer cachexia: Developing multimodal therapy for a multidimensional problem. *European Journal of Cancer* 2008, 44(8):1124-1132.
105. van de Worp W, Schols A, Theys J, van Helvoort A, Langen RCJ: Nutritional Interventions in Cancer Cachexia: Evidence and Perspectives From Experimental Models. *Front Nutr* 2020, 7:601329.

A

Summary

SUMMARY

Lung cancer is a leading cause of cancer related mortality worldwide. Approximately 13.000 patients per year are diagnosed with lung cancer in the Netherlands of which more than 11.000 diagnosed with Non-Small Cell Lung Carcinoma (NSCLC). The prevalence of NSCLC increases with the age, and in combination with the improved screening methods, the number of patients diagnosed with lung cancer has increased by 22% over the past ten years. The overall prognosis for NSCLC patients is very poor with an average 5-year survival rate of 17%.

Many patients with (advanced) lung cancer suffer from cancer cachexia. Cancer cachexia is a complex multifactorial catabolic syndrome that leads to significant unintentional body weight loss, characterized by an ongoing loss of skeletal muscle mass with or without a reduction in fat mass. This loss of body weight cannot be fully reversed by conventional nutritional support. Cachexia is associated with poor clinical outcome, decreased survival and negatively influences tumor therapy, as is illustrated by increased postoperative mortality and decreased response to radiation-, chemo- and immunotherapy. Muscle wasting is an important contributing factor to muscle weakness in cachexia, which adversely affects performance status, quality of life and hospitalization risk of cancer patients. However, despite increasing efforts to improve our knowledge of cancer cachexia required for development of therapies, the management of cancer cachexia remains a major challenge for clinicians and is until now an unmet medical need.

The overall objective of the research described in this thesis is to unravel the molecular mechanisms and dynamics of lung cancer cachexia. A combination of both translational and experimental research approaches are used to study this objective.

MicroRNAs (miRNAs) are small non-coding RNAs that play a central role in post-transcriptional gene regulation. Changes in intramuscular levels of miRNAs have been implicated in muscle wasting conditions, including cancer cachexia. In **chapter 2**, we provide an overview of miRNAs directly associated with muscle atrophy, which we proposed to term “atromiRs”. The regulation and mode of action of these atromiRs is described, and the challenges to explore their potential as putative therapeutic target in cachexia are discussed.

Our work in chapter 2 reveals that the involvement of miRNAs in cancer cachexia was hardly addressed and identified that systematic analyses of differential

regulation of miRNAs in patient-derived muscle biopsies are lacking. In **chapter 3**, we profiled 754 unique miRNAs in quadriceps muscle biopsies of NSCLC patients with cachexia in comparison to healthy controls. We identified 28 differentially expressed miRNAs of which five miRNAs were upregulated and 23 were downregulated. Bioinformatics-based analysis showed that these miRNAs were involved in pathways related to the degenerative or regenerative processes of muscle tissue. We are the first to identify differentially expressed miRNAs putatively involved in lung cancer cachexia. These findings call for further studies to investigate the causality of these miRNAs in muscle atrophy and their potential as biomarker or putative therapeutic target in cachexia.

Optimal nutritional care is pivotal in treatment of cancer cachexia, and the effects of nutrients may extend beyond the provision of adequate energy intake, targeting different mechanisms or metabolic pathways that are affected or deregulated by cachexia. The evidence to support this notion, derived from nutritional intervention studies in experimental models of cancer cachexia, is systematically discussed in **chapter 4**. The combination of high quality nutrients in a multitargeted, multinutrient approach appears explicitly promising, although more studies are needed to define optimal quantities and combinations of nutrients. We also concluded that standardization in dietary design should improve, and that development of more representative experimental models is essential to translate experimental findings faster into the clinic.

Various lung tumor-bearing animal models have been used to study cancer cachexia and to study the therapeutic effect of (nutritional) interventions. However, these models do not simulate anatomical and immunological features key to lung cancer and associated muscle wasting. In **chapter 7**, we therefore developed and characterized a syngeneic, orthotopic lung cancer cachexia (OLCC) mouse model and evaluated whether it replicates systemic and muscle-specific alterations associated with human lung cancer cachexia. The OLCC mice showed significant loss of body weight and skeletal muscle mass and function, indicating the development of cachexia. The observed muscle wasting was accompanied by increased systemic inflammation and alterations in the regulation of muscle protein turnover. Finally, we showed that the muscle transcriptome of the OLCC mice reproduces key aspects specific to cachexia in lung cancer patients. The newly developed OLCC mouse model provides opportunities to advance cancer cachexia research, including understanding the etiology of lung cancer cachexia and the development and evaluation of novel intervention strategies.

Two main readout parameters are a major challenge in monitoring the development of cancer cachexia in an orthotopic mouse model: muscle mass and tumor volume. Micro-CT is an X-ray-based imaging technology for small animals that allows tissue density quantification, which makes micro-CT a good technique for longitudinal muscle mass and tumor volume assessment. To investigate muscle mass and tumor volume changes quantitatively, manual segmentation of the muscle and tumor volume on the CT reconstruction is required, which is a very time-consuming task and prone to inter- and intra-observer bias. Therefore, we developed algorithms for the standardized, automated segmentation and quantification of muscle mass (**chapter 5**) and tumor volume (**chapter 6**) on whole-body mouse CT-scan using artificial intelligence techniques. The performance of these algorithms was in good agreement with the training dataset. In addition, the algorithms increase the amount of data derived from animal studies while reducing animal numbers and analytical workload.

In **chapter 8**, we provide proof of concept for the application of nutritional interventions to target cancer cachexia. We investigated the therapeutic effect of a multitargeted, multinutrient intervention diet containing high protein, leucine, fish oil, vitamin D, galacto-oligosaccharides and fructo-oligosaccharides on the development of cachexia in the OLCC mouse model. The intervention diet delayed the onset and progression of experimental lung cancer cachexia, while attenuating loss of muscle strength, mass and alterations in protein turnover signaing, resulting in prolonged maintenance of muscle function and average time to study endpoint.

Finally, in **chapter 9**, the findings and advances described in this thesis and opportunities for future research are discussed in a broader context of four fundamental pillars in cancer cachexia research: I) Early detection and dynamics of cancer cachexia; II) Intra-cellular mechanism of muscle wasting in cancer cachexia; III) Extra-cellular mechanism/triggers of cancer cachexia; and IV) Management of cancer cachexia.

Nederlandse samenvatting

NEDERLANDSE SAMENVATTING

Jaarlijks wordt bij meer dan 14.000 mensen in Nederland de diagnose longkanker gesteld waarvan circa 12.000 gediagnostiseerd met niet-kleincellig longkanker (NSCLC). NSCLC wordt vaak pas laat ontdekt. Daardoor is bij meer dan de helft van de patiënten de kanker al uitgezaaid bij diagnose, waardoor deze moeilijk te genezen is. De algehele prognose voor deze patiënten is slecht met een gemiddelde vijfjaarsoverleving van 17%.

Een groot deel van de patiënten met (uitgezaaide) longkanker ontwikkelt kankercachexie. Kankercachexie is een complex multifactorieel syndroom dat leidt tot ernstig ongewenst gewichtsverlies en wordt gekenmerkt door aanhoudend verlies van spiermassa met of zonder het verlies van vetmassa. Kankercachexie heeft grote gevolgen voor patiënten met (long)kanker. Kankercachexie heeft een negatieve invloed op de oncologische behandeling, en wordt gekarakteriseerd door verhoogde kans op toxiciteit en door een verlaagde respons op radiatie-, chemo- en immunotherapie. Daarnaast draagt het verlies van spiermassa bij aan een verlaagde spierfunctie. Dit heeft een negatieve impact op de inspanningscapaciteit, de kwaliteit van leven en verhoogt het risico op complicaties en ziekenhuisopname van kankerpatiënten. Echter, ondanks toenemende inspanningen om onze kennis van kankercachexie te verbeteren, is er momenteel geen effectieve behandeling die deze ingrijpende effecten van kankercachexie kan voorkomen of verminderen.

Het onderzoek, beschreven in dit proefschrift, richt zich op het ontrafelen van de moleculaire mechanismen en dynamiek van longkankercachexie en de ontwikkeling van behandelingen. In dit onderzoek is er gebruik gemaakt van een combinatie van zowel translationele als experimentele onderzoeksbenaderingen.

Een van deze experimentele benaderingen is het onderzoek naar MicroRNA's (miRNA's). MiRNA's zijn een vorm van niet-coderend RNA, van ongeveer 20 nucleotiden lang, die een belangrijke rol spelen in de regulatie van genexpressie door mRNA translatie te blokkeren of het mRNA te degraderen. Veranderingen in de expressie van deze miRNA's zijn beschreven in verschillende aandoeningen die gekenmerkt worden door spierafbraak (spieratrofie). Kankercachexie is een van deze aandoeningen. In **hoofdstuk 2** wordt een overzicht gegeven van miRNA's die in verband worden gebracht met spieratrofie. Deze miRNA's hebben we "atromiRs" genoemd. Verder wordt de regulatie en het werkingsmechanisme van deze atromiRs en de uitdagingen om hun potentieel aan te roeren als therapeutisch doelwit bij cachexie besproken.

In hoofdstuk 2 is vastgesteld dat de rol van miRNA's in kankercachexie nauwelijks onderzocht is en dat de systematische analyses van differentiële regulatie van miRNA's in spierbiopten van patiënten ontbreken. In de studie beschreven in **hoofdstuk 3** is de expressie van 754 miRNA's in spierbiopten afkomstig van de quadriceps van NSCLC-patiënten met cachexie gemeten en vergeleken met gezonde controles. Dit resulteerde in de identificatie van 28 miRNA's waarvan 5 miRNA's verhoogd en 23 miRNA's verlaagd tot expressie kwamen in de spier van NSCLC-patiënten met cachexie. Uit bio-informatica analyses bleek dat deze miRNA's mogelijk betrokken zijn bij degeneratieve en regeneratieve processen van spierweefsel. Met dit onderzoek zijn wij de eerste onderzoeksgroep die miRNA's hebben geïdentificeerd die vermoedelijk betrokken zijn bij longkankercachexie. Deze bevindingen zijn aanleiding voor vervolgstudies die de causaliteit van deze miRNA's bij spieratrofie, en hun potentieel als biomarker of als vermeend therapeutisch doelwit bij cachexie verder onderzoeken.

Optimale voedingszorg is van cruciaal belang bij de behandeling van kankercachexie, omdat specifieke voedingstoffen niet enkel voorzien in voldoende inname van energie en bouwstoffen, maar mogelijk ook gericht kunnen aangrijpen op een of meerdere mechanismen of metabole processen die beïnvloed of gedereguleerd worden door cachexie. In **hoofdstuk 4** worden voedingsinterventiestudies in dierexperimentele modellen van kankercachexie systematisch besproken en tevens het bewijs geleverd voor deze hypothese. De combinatie van verschillende hoogwaardige voedingsstoffen in één interventie lijkt met name veelbelovend, hoewel er meer onderzoek nodig is om de optimale hoeveelheden en combinaties van voedingsstoffen te definiëren. Daarnaast was de conclusie van dit review dat er meer aandacht besteed zou moeten worden aan de standaardisatie van de experimentele diëten en de ontwikkeling van meer representatieve experimentele modellen om de transleerbaarheid van de bevindingen te verhogen, en daarmee de verantwoording van dierexperimenteel onderzoek en kansrijkheid van klinische toepassing van (dieet)interventies te verhogen.

Om de mechanismen van kankercachexie en het therapeutisch effect van (voedings)interventies te bestuderen wordt er gebruik gemaakt van verschillende kanker muismodellen. Deze reeds bestaande muismodellen simuleren echter niet de anatomische en immunologische kenmerken die bepalend kunnen zijn voor het verloop van longkankercachexie in de patiënt. Daarom is in de studie beschreven in **hoofdstuk 7** een orthotoop longkankercachexie (OLCC) muismodel ontwikkeld en gekarakteriseerd. Daarnaast is er bestudeerd of de systemische

en spier-specifieke veranderingen ten gevolge van longkankercachexie in het muismodel overeenkomen met die in de patiënt. Zoals ook het geval is bij longkankercachexie, ontwikkelen OLCC-muizen na verloop van tijd een significant verlies van lichaamsgewicht, spiermassa en spierfunctie, welke een indicatie zijn voor de ontwikkeling van kankercachexie. Het waargenomen spiermassaverlies gaat gepaard met verhoogde systemische ontstekingseiwitten in het bloed, en een ontregeling van de balans tussen eiwitopbouw en eiwitafbraak in de skeletspier. Ten slotte is aangetoond dat het spiertranscriptoom van de OLCC-muizen belangrijke aspecten reproduceert die specifiek zijn voor cachexie bij longkankerpatiënten. Dit nieuw ontwikkelde muismodel is veelbelovend en biedt mogelijkheden om het onderzoek naar kankercachexie vooruit te helpen, waarbij men zich kan richten op zowel de etiologie van longkankercachexie als op evaluatie van nieuwe interventie strategieën.

Om de ontwikkeling van kankercachexie in het muismodel op te volgen is er gekeken naar verschillende parameters zoals lichaamsgewicht, voedselinname, spierfunctie, spiermassa en tumorvolume. Het opvolgen van de laatste twee genoemde parameters vormen echter een grote uitdaging in een orthotoop muizenmodel. Daarom is gebruik gemaakt van micro computertomografie (micro-CT), een op röntgenstraling gebaseerde beeldvormingstechnologie voor kleine dieren die het mogelijk maakt om op basis van dichtheid weefsel te kwantificeren, waarmee het mogelijk is om spiermassa en tumorvolume over tijd te volgen in een muis. Om deze veranderingen kwantitatief te onderzoeken, is het handmatige intekenen van het spier- en tumorvolume op de CT-reconstructie vereist. Dit is echter een zeer tijdrovende taak en is erg vatbaar voor subjectiviteit tussen de waarnemers. Daarom is er met behulp van kunstmatige intelligentie twee computeralgoritmen ontwikkeld voor gestandaardiseerde, geautomatiseerde intekening en kwantificatie van spiermassa (**hoofdstuk 5**) en tumorvolume (**hoofdstuk 6**) op CT-scans van muizen. De kwaliteit van de geautomatiseerde intekeningen van deze algoritmen kwamen goed overeen met de handmatig ingetekende trainingsdataset. Daarnaast dragen de algoritmen bij aan een vermindering van het aantal dieren, de analytische werklast en kosten. Ten slotte kunnen deze algoritmen gemakkelijk worden geïmplementeerd in andere onderzoekslaboratoria.

In **hoofdstuk 8** wordt er proof-of-concept geleverd voor de toepassing van voedingsinterventies voor de behandeling van kankercachexie. We onderzochten het therapeutische effect van een gericht, multi-nutriënten interventiedieet rijk aan eiwitten, leucine, visolie, vitamine D, galacto-oligosachariden en fructo-oligosachariden op de ontwikkeling van cachexie in het OLCC-muismodel.

Het interventiedieet vertraagde de aanvang en progressie van experimentele longkankercachexie hetgeen gepaard ging met een langer behoud van spierkracht. Deze studie toont het potentieel van gerichte, multi-nutriënt voedingsinterventies voor het behandelen van kankercachexie, om zo de effectiviteit van anti-tumor behandelingen en functiebehoud van de longkankerpatiënt te verhogen.

Tot slot worden in **hoofdstuk 9** de bevindingen en nieuwe inzichten beschreven in dit proefschrift, en de mogelijkheden voor toekomstig onderzoek, besproken in een bredere context, welke is onderverdeeld in vier fundamentele pijlers in kankercachexie-onderzoek: I) Vroege detectie en dynamiek van kankercachexie; II) Intracellulaire mechanismen van spierafbraak bij kankercachexie; III) Extracellulair mechanismen/triggers van kankercachexie; en IV) Management van kankercachexie.

Impact

IMPACT

Relevance for the cancer cachexia research community

Lung cancer is the second most commonly diagnosed cancer and accounts for 18% of total cancer deaths, which makes lung cancer the leading cause of cancer-related deaths worldwide [1]. The overall prognosis of lung cancer patients is extremely poor due to the difficulty of diagnosing at early-stage and the resistance to current therapies [2], and is further adversely affected by cachexia [3-5]. Approximately 80% of the lung cancer patients are at risk of developing cancer cachexia [6], which is a wasting syndrome characterized by progressive weight loss resulting from depletion of skeletal muscle mass with the loss of fat mass [7].

Cachexia is a poor prognostic factor and has major adverse clinical implications. It adversely influences performance, and quality of life and number of hospitalizations in lung cancer patients [8, 9]. In addition, decreased response to antitumor therapies has been reported in cachectic lung cancer patients. Effective treatment of cachexia has a direct impact on patient's overall health status and survival and increases the effectiveness of costly antitumor therapies [10-12]. Nevertheless, there is no FDA approved cachexia treatment and no standard of care [13]. To a large extent, this is attributable to the lack of screening tools and limited understanding of the underlying mechanisms, as a result of the complexity of the syndrome and the challenge of performing clinical trials in this fragile patient population. In cancer cachexia, studies using patients-derived muscle biopsies can provide valuable new insights in the underlying metabolism and pathways, yet are very scarce. Moreover, research in patients to study the longitudinal dynamics of the wasting process in relation to the underlying molecular mechanisms with the currently available tools, is even more demanding. Therefore, the development of relevant preclinical animal models and novel methodologies to enable such studies are required. The research described in this thesis provides new insights that contribute to unravelling the underlying mechanisms and dynamics of lung cancer cachexia, and reports on the development and validation of a novel murine model that better replicates the etiology of the human disease, and provides proof of concept for the application of nutritional interventions to target cancer cachexia.

To maximize exposure and impact for follow up in research and implementation, all the data described in this thesis is/will be published in peer reviewed journals and presented at international conferences within the field of cancer cachexia, laboratory animal sciences, nutrition and respiratory diseases.

New leads for therapeutic interventions

We aimed to identify the role of miRNAs in the regulation of muscle atrophy and specifically cachexia. We proposed to name these miRNAs 'atromiRs' (Chapter 2 [14]). Remarkably, our review revealed that the involvement of miRNAs in cachexia was hardly addressed and data from patient-derived muscle biopsies was scarce. Subsequently, we profiled 754 unique miRNAs in quadriceps muscle biopsies of NSCLC patients with cachexia in comparison to healthy controls, and used an elegant bioinformatics approach followed by confirmation in a larger cohort, which also included non-cachectic NSCLC patients. We were the first to identify differentially expressed miRNAs putatively involved in lung cancer cachexia (Chapter 3 [15]). These findings are very promising and need to be validated in an external cohort. These findings have provided leads for the development of new drugs (miRNA-based therapeutics) that affect muscle wasting directly in the skeletal muscle, and also for the development of biomarkers for early detection and intervention.

In addition to the miRNA profiling, RNA sequencing was performed on the same set of muscle biopsies (Chapter 7). The majority of the differentially expressed genes were downregulated, and pathway enrichment analysis showed that these were primarily associated with mitochondrial and metabolic processes. Dysfunctional mitochondria have been implicated in lower muscle strength and muscle wasting in experimental cancer cachexia models, however, yet poorly described in human cancer cachexia [16]. As mitochondria-targeted drugs may serve as promising therapy for mitochondrial myopathies [17], such therapies could benefit muscle wasting associated with cancer cachexia by improving mitochondrial function and positively affecting the whole body metabolome.

Overall, the observations in the muscle biopsies of this well-characterized group of NSCLC patients with cachexia not only provides new insights in lung cancer-associated muscle wasting, but may serve as a unique reference data set to evaluate the relevance of findings obtained in studies using experimental models.

A new, promising pre-clinical lung cancer cachexia model

Because of challenges posed by heterogeneity, limited group sizes and the invasive nature of sample collection, most of the information regarding the underlying mechanisms of (lung) cancer cachexia and the potential therapeutic options is derived from pre-clinical models. However, the most frequently used animal models do not simulate anatomical, physiological, and immunological features key to lung cancer and associated cachexia seen in humans. These

shortcomings hamper translating experimental findings into the clinic. Therefore, we developed and characterized a novel syngeneic orthotopic lung cancer cachexia (OLCC) mouse model in which a relatively small tumor (max 0.5% of total body weight) grows in its original stroma, the lung (Chapter 7). We showed that these lung tumor-bearing mice developed cachexia approximately 3 weeks after tumor injection. The observed muscle wasting was accompanied by increased systemic inflammation and alterations in the regulation of muscle protein turnover reflecting increased proteolysis. Strikingly, comparison of muscle transcriptomic data of lung tumor-bearing mice with cachexia and NSCLC patients with cachexia revealed a remarkable overlap in processes that were affected in muscle of man and mice. Overall, this demonstrates that our model closely overlaps the human pathophysiology and biology of lung cancer cachexia, which has two important ramifications. First, these findings answer to the need for critical assessment of the external validity of an experimental model, which is an integral part of 'Refinement' of the 3R-principles that are embedded in the EU regulation on animal research [18, 19]. Timely and robust confirmation that an experimental model captures the critical aspects of a disease or condition ensures that the use of animals and associated discomfort and costs of follow-up work based on that model are not spent in vain. Secondly, it is anticipated that mechanistic insights and interventions evaluated in this model will better translate to the human setting. This will contribute to increased clinical success rates for interventions in development, and reduce costs and patient burden.

Innovative tools for automatic tumor and muscle volume quantification

Obviously, in contrast to subcutaneous growing tumors, the tumors in orthotopic lung cancer models are not visible and accessible for caliper measurements to assess their growth. Similar to the clinical setting, cone beam computed tomography (CBCT) can be used in preclinical research to detect orthotopic growing tumors in rodent models. However, analysis of the imaging data to extract quantitative information, such as tumor size and shape, is a very labor intensive and time-consuming task. In addition, the analysis is a challenging task as it requires great expertise in anatomy and CT-imaging, and is susceptible to bias. To facilitate the quantification of orthotopic growing tumors in preclinical research, we developed and validated a deep learning algorithm for automatic lung tumor segmentation and quantification on whole-body mouse CT-scans (Chapter 6 [20]). This deep learning algorithm enables fast and highly accurate tumor quantification with minimal operator involvement in data analysis.

To detect when muscle wasting starts and study the dynamics of muscle mass changes in function of experimental life expectancy, longitudinal evaluation of muscle mass is essential. However, until now, skeletal muscle mass evaluation in preclinical animal models is mostly based on assessment of muscle wet masses, or muscle fiber cross-sectional area using histological examination of postmortem tissue. Both methods require muscle dissection and, consequently, are terminal experiments. Therefore, a similar approach as used for longitudinal tumor volume assessment was applied to develop a deep learning algorithm to automatically segment and quantify muscle mass on whole-body mouse CT-scans (Chapter 5 [21]). This deep learning application enables highly accurate non-invasive longitudinal evaluation of skeletal muscle mass changes in mice.

These deep learning algorithms provide us with the unique opportunity to study the relation between tumor development (growth speed, size and location) and muscle mass over time in mice. In addition, they increase the amount of data derived from animal studies while reducing animal numbers, analytical workload and costs. The reduction of animal numbers is an integral part of 'Reduction' of the 3R-principles that are embedded in the EU regulation on animal research [18, 19]. Importantly, these algorithms can easily be implemented in other labs interested in longitudinal evaluation of muscle atrophy and/or hypertrophy, or in research related to conditions associated with volumetric changes in other tissues.

Therapeutic efficacy of nutritional intervention

It is generally acknowledged that a multidisciplinary approach is currently considered the best option to tackle cancer cachexia, in which nutritional intervention is recommended as an integral part of the multimodal therapy [22]. Adequate nutritional care is pivotal to (1) provide building blocks for tissue maintenance, (2) provide energy and (3) regulate metabolic processes (Chapter 4). In the last chapter of this thesis, a targeted dietary intervention, directed at each of these three pillars, was tested in the newly developed mouse model of lung cancer cachexia. The intervention diet delayed the onset and progression of cachexia, and resulted in prolonged maintenance of muscle function. These data are very promising and suggest that targeted dietary interventions have the potential to support patients to maintain muscle function and mass and thereby improve tolerance to cancer and anticancer therapy, increasing quality of life and survival. Considering the high external validity of our novel model, further evaluation of the therapeutic effect of an analogous human intervention diet in a clinical trial is warranted to test its efficacy to modulate cachexia, and confirm the feasibility

of integrating dietary interventions as part the treatment regimen for patients with NSCLC.

REFERENCES

1. Sung H, Ferlay J, Siegel RL, Laversanne M, Soerjomataram I, Jemal A, Bray F: Global Cancer Statistics 2020: GLOBOCAN Estimates of Incidence and Mortality Worldwide for 36 Cancers in 185 Countries. *CA Cancer J Clin* 2021, 71(3):209-249.
2. (IKNL) IKN: NKR cijfers 2020. 2021.
3. Ross PJ, Ashley S, Norton A, Priest K, Waters JS, Eisen T, Smith IE, O'Brien ME: Do patients with weight loss have a worse outcome when undergoing chemotherapy for lung cancers? *Br J Cancer* 2004, 90(10):1905-1911.
4. van der Meij BS, Schoonbeek CP, Smit EF, Muscaritoli M, van Leeuwen PA, Langius JA: Pre-cachexia and cachexia at diagnosis of stage III non-small-cell lung carcinoma: an exploratory study comparing two consensus-based frameworks. *Br J Nutr* 2013, 109(12):2231-2239.
5. Kimura M, Naito T, Kenmotsu H, Taira T, Wakuda K, Oyakawa T, Hisamatsu Y, Tokito T, Imai H, Akamatsu H *et al*: Prognostic impact of cancer cachexia in patients with advanced non-small cell lung cancer. *Support Care Cancer* 2015, 23(6):1699-1708.
6. Anker MS, Holcomb R, Muscaritoli M, von Haehling S, Haverkamp W, Jatoi A, Morley JE, Strasser F, Landmesser U, Coats AJS *et al*: Orphan disease status of cancer cachexia in the USA and in the European Union: a systematic review. *J Cachexia Sarcopenia Muscle* 2019, 10(1):22-34.
7. Fearon K, Strasser F, Anker SD, Bosaeus I, Bruera E, Fainsinger RL, Jatoi A, Loprinzi C, MacDonald N, Mantovani G *et al*: Definition and classification of cancer cachexia: an international consensus. *Lancet Oncol* 2011, 12(5):489-495.
8. Morikawa A, Naito T, Sugiyama M, Okayama T, Aoyama T, Tanuma A, Omae K, Takahashi T: Impact of Cancer Cachexia on Hospitalization-associated Physical Inactivity in Elderly Patients with Advanced Non-small-cell Lung Cancer. *Asia Pac J Oncol Nurs* 2018, 5(4):377-382.
9. Arthur ST, Van Doren BA, Roy D, Noone JM, Zacherle E, Blanchette CM: Cachexia among US cancer patients. *Journal of Medical Economics* 2016, 19(9):874-880.
10. Dewys WD, Begg C, Lavin PT, Band PR, Bennett JM, Bertino JR, Cohen MH, Douglass HO, Jr., Engstrom PF, Ezdinli EZ *et al*: Prognostic effect of weight loss prior to chemotherapy in cancer patients. Eastern Cooperative Oncology Group. *Am J Med* 1980, 69(4):491-497.
11. Vaughan VC, Martin P, Lewandowski PA: Cancer cachexia: impact, mechanisms and emerging treatments. *J Cachexia Sarcopenia Muscle* 2013, 4(2):95-109.
12. Turner DC, Kondic AG, Anderson KM, Robinson AG, Garon EB, Riess JW, Jain L, Mayawala K, Kang J, Ebbinghaus SW *et al*: Pembrolizumab Exposure-Response Assessments Challenged by Association of Cancer Cachexia and Catabolic Clearance. *Clin Cancer Res* 2018, 24(23):5841-5849.
13. Roeland EJ, Bohlke K, Baracos VE, Bruera E, Fabbro Ed, Dixon S, Fallon M, Herrstedt J, Lau H, Platek M *et al*: Management of Cancer Cachexia: ASCO Guideline. *Journal of Clinical Oncology* 2020, 38(21):2438-2453.
14. van de Worp W, Theys J, van Helvoort A, Langen RCJ: Regulation of muscle atrophy by microRNAs: 'AtromiRs' as potential target in cachexia. *Curr Opin Clin Nutr Metab Care* 2018, 21(6):423-429.

15. van de Worp WR, Schols AM, Dingemans AMC, Op den Kamp CM, Degens JH, Kelders MC, Coort S, Woodruff HC, Kratassiouk G, Harel-Bellan A: Identification of microRNAs in skeletal muscle associated with lung cancer cachexia. *Journal of cachexia, sarcopenia and muscle* 2020, 11(2):452-463.
16. Beltrà M, Pin F, Ballarò R, Costelli P, Penna F: Mitochondrial Dysfunction in Cancer Cachexia: Impact on Muscle Health and Regeneration. *Cells* 2021, 10(11).
17. Singh A, Faccenda D, Campanella M: Pharmacological advances in mitochondrial therapy. *EBioMedicine* 2021, 65:103244.
18. Prescott MJ, Lidster K: Improving quality of science through better animal welfare: the NC3Rs strategy. *Lab Anim (NY)* 2017, 46(4):152-156.
19. Animals used for scientific purposes: Replacement, Reduction and Refinement [https://ec.europa.eu/environment/chemicals/lab_animals/3r/alternative_en.htm]
20. van de Worp WR, van der Heyden B, Lappas G, van Helvoort A, Theys J, Schols AM, Verhaegen F, Langen RC: Deep Learning Based Automated Orthotopic Lung Tumor Segmentation in Whole-Body Mouse CT-Scans. *Cancers* 2021, 13(18):4585.
21. van der Heyden B, van de Worp WR, van Helvoort A, Theys J, Schols AM, Langen RC, Verhaegen F: Automated CT-derived skeletal muscle mass determination in lower hind limbs of mice using a 3D U-Net deep learning network. *Journal of Applied Physiology* 2020, 128(1):42-49.
22. van de Worp W, Schols A, Theys J, van Helvoort A, Langen RCJ: Nutritional Interventions in Cancer Cachexia: Evidence and Perspectives From Experimental Models. *Front Nutr* 2020, 7:601329.

Acknowledgements

ACKNOWLEDGEMENTS

Every story has an end. You arrived at the last and probably most read chapter of this thesis, which means that I have finished my PhD project. The last few years have been an interesting and instructive journey. My PhD years jet packed my academic and personal development and contributed to who I am today.

The most important lesson I have learned during my PhD is that doing research and the realization of this dissertation is an absolute team effort. Many people have contributed, in one way or another, to my academic and person development leading to the successful completion of my PhD. Therefore, I would like to thank these people in my native language.

Als eerst wil ik mijn vierkoppig promotieteam bedanken voor deze leerzame en bovenal leuke periode. Vier individuen met onwijs veel kennis en kunde in verschillende facetten van het onderzoek. Samen vormen jullie een uniek team en waren jullie het fundament van mijn promotie. Het was een eer om onder jullie supervisie te promoveren en hopelijk kunnen we nog lang samenwerken.

Ramon, bedankt voor de dagelijkse begeleiding en je aanstekelijk enthousiasme voor wetenschappelijk onderzoek. Wat heb ik ongelooflijk veel van jou geleerd de afgelopen jaren. Terugkijkend op deze periode waardeer ik enorm hoeveel tijd je in mij hebt geïnvesteerd. Als dagelijks begeleider stond je deur altijd voor mij open. Ik kon ieder willekeurig moment van de dag binnenlopen voor de meest uiteenlopende vragen en jij was altijd bereidt om tijd voor mij vrij te maken. Daarnaast bewonder ik je hoge zorgvuldigheid waarmee je mijn stukken van constructieve feedback hebt voorzien. Ik had geen betere dagelijkse begeleider kunnen wensen. Tenslotte wil ik je bedanken voor het vertrouwen dat je altijd in me hebt gehad en de moeite die je hebt gedaan om mij als postdoc binnen de vakgroep te behouden.

Ardy, wat ben ik blij dat jij deel uitmaakt van mijn promotieteam. Misschien was jouw telefoontje aan Johan überhaupt de doorslaggevende factor dat ik dit project mocht starten? Door jou heb ik geleerd om op verschillende manieren naar onderzoek te kijken, niet enkel vanuit academisch perspectief. Daarnaast gaf je mij altijd het gevoel dat alles mogelijk was. Beiden hebben enorm bijgedragen aan mijn ambities en de toekomst die ik zie in het wetenschappelijk onderzoek. Ondanks je drukke agenda maakte je altijd tijd vrij voor mij en toonde je steevast oprechte interesse. Ook bel je met regelmaat om te vragen hoe het met mij is en

dat waardeer ik enorm. Tenslotte wil ik ook jou bedanken voor het vertrouwen dat je naar mij uitspreekt en de kansen die je me biedt voor de toekomst.

Jan, ook jou wil ik graag bedanken voor je betrokkenheid bij mijn promotietraject. Een van de doelstelling van mijn PhD project was het ontwikkelen van een orthotoop muizen model. Het heeft nogal wat voeten in de aarde gehad, maar het eindresultaat mag er zijn. De expertise die jij meebracht op het gebied van tumormodellen zijn hierbij van essentieel belang geweest. Daarnaast wil ik je ook graag bedanken voor je kritische blik en feedback op de geschreven stukken. Je wist de vinger altijd op de zere plek te leggen. Voor mijn vervolgonderzoek zal ik ook af en toe nog gebruik willen maken van jouw expertise. Dus ondanks dat dit hoofdstuk nu is afgelopen, is het mijn intentie om te blijven samenwerken.

Annemie, bedankt voor alle kansen (en COVID-19 ;)) die je me hebt gegeven en de ruimte die ik samen met mijn co-promotoren heb gekregen om mijn PhD traject vorm te geven. Ondanks dat onze contact momenten niet heel frequent waren, wist je me altijd te inspireren en te motiveren. Ik heb altijd met bewondering gekeken naar jouw reputatie in ons onderzoeksveld. Alleen al het noemen van jouw naam op een internationaal congres zorgt voor menig twinkeling in eenieders ogen. En stiekem heb ik hier soms gretig gebruik van gemaakt. Verder wil ik je nog bedanken voor je enthousiasme over het onderzoek, je inzichten, en kritische blik. Heel erg bedankt voor deze ervaring en op naar een succesvolle toekomst.

I would like to thank the **assessment committee** for reading and approving my thesis, and for being present at my defense. Dankjewel, thank you, tak skal du have!

Uiteraard wil ik ook mijn paranimfen Rosanne en Alex bedanken. Wat fijn dat ik te midden van jullie mijn proefschrift mag verdedigen!

Rosanne, mijn favoriete collega (Ja, dat staat er echt). Van alle PhD studenten die werkzaam waren bij PUL toen ik mijn intrede deed, ben jij nog de enige overgeblevene. Wij hebben elkaar in de tussentijd goed leren kennen, in goede en slechte perioden. Zo heb ik jou zien ontwikkelen van PhD student tot assistant professor en van basisspeler in de Eredivisie handbal tot bankspeler op de Kramsvogel (just kidding). Dit alles heeft een goede band geschept. Op het werk kan altijd bij je terecht, om te klagen, te vieren, voor een bak koffie, of voor werk gerelateerde vragen. Soms wordt weleens onderschat hoe belangrijk het is zo'n fijne collega te hebben. Ook buiten het werk om is het altijd gezellig met etentjes,

borrels en uitstapjes naar onze oud-collega's. Laten we hopen dat we nog vele jaren samen kunnen werken. En wie weet. Misschien zijn wij over een aantal jaar wel de Annemie en Ramon van de afdeling.

Alex, ik ben even in het archief gedoken en ik ontdekte dat onze eerste kennismaking op 5 mei 2017 was. Ik was net 2 weken begonnen met mijn PhD en we gingen met de collega's op stap met bevrijdingsdag. Wij bleven die avond met z'n tweeën over en eindigden bij Paul Kalkbrenner in de Complex. En hoe we binnen gekomen zijn? Daar hoef ik niet over in detail te treden. Die avond heeft de toon gezet voor de rest van onze vriendschap en sindsdien hebben we heel wat onvergetelijke avonden beleefd. Naast Duvel drinken en lol maken hebben we het ook met regelmaat over ons onderzoek. Deze gesprekken en jouw visie op onderzoek hebben significant bijgedragen aan mijn wetenschappelijk ontwikkeling de laatste jaren. Bedankt voor de afgelopen jaren en laten we proosten op een mooie toekomst.

Daarnaast zijn er nog een aantal oud-collega's die ik wil bedanken voor de gezellige jaren bij pulmonolgie.

Als eerste mijn roomie **Wessel** (aka Wessol). Op twee maanden na hebben wij het kantoor drie jaar met elkaar gedeeld. Ondanks dat wij twee totaal verschillende persoonlijkheden zijn, hebben we een bijzondere band opgebouwd. Op het werk heb ik jou altijd een fijne en relaxte collega gevonden. Je was een betrouwbare bron van informatie en praktische hulp op het lab. Daarnaast was de sfeer op ons kantoor altijd goed met een juiste verhouding tussen werk en ontspanning. Je aanwezigheid wordt dan ook nog steeds enorm gemist. Stiekem hoop ik dat we ooit weer collega's worden. Naast een fijne collega ben je ook een goede vriend geworden. Ook buiten het werk hebben we altijd lol gehad met de vele spelletjesavonden, borrels, etentjes en rondjes op de fiets. Bedankt voor alles!

Pieter, heel erg bedankt hoe jij mij verwelkomen hebt binnen de afdeling longziekten. Onder andere door de gastvrijheid van jou en uiteraard **Judith** voelde ik me onmiddellijk welkom en thuis in Maastricht. Daarnaast heb jij mij weten te overtuigen om een racefiets te kopen. Dat heb je geweten ook. Ik was al vrij snel verslaafd en sindsdien hebben we enkele duizenden kilometers samen afgelegd in het binnen- en buitenland. Als jullie dit lezen zitten jullie waarschijnlijk met het gezin in LA. Geniet ervan en ik hoor graag hoe het was als jullie terug zijn.

Anita, jij was zonder twijfel een van de sfeermakers van de afdeling. Het maakte niet uit wat we gingen doen, lunchen, koffiedrinken, borrelen, stappen, shoppen of twisteren, het was altijd gezellig. Nadat je Maastricht voor Lyon had ingeruild werd je dan ook flink gemist. Heel erg bedankt voor de gezellige periode! Ik wens jou en **Roy** heel veel succes en plezier in het zuiden van Frankrijk, en ik hoop dat we elkaar snel weer zien.

Daarnaast zijn er een aantal collega's die bij hebben gedragen aan de totstandkoming van een of meerdere wetenschappelijke artikelen in dit proefschrift.

Als eerste wil ik **Frank** en zijn physics researchteam (met name **Brent**, **Georgios** en **Cecile)** bedanken voor de succesvolle samenwerking. Zonder jullie had mijn proefschrift er heel anders uitgezien en was ik waarschijnlijk nu nog steeds CT-scans aan het intekenen. Allen heel erg bedankt voor de proactieve samenwerking. **Brent**, ik kijk nog altijd met veel plezier terug op de projecten die wij samen hebben aangepakt. Onze samenwerking was zeer doeltreffend, wat beiden onze PhD's ten goede is gekomen. Ik kan je oprecht vertellen dat dit de vruchtbaarste samenwerking was die ik ooit heb gehad! **Georgios**, after Brent left the department you took up the baton. Thank you very much for all the hard work. Very much appreciated! **Cecile**, het laatste jaar van mijn PhD heb jij mij geholpen bij het analyseren van de CT-scans. Ik kijk met veel plezier naar de toekomst waarin we hopelijk op nog vele projecten zullen samenwerken.

Natasja Lieuwes, ook jou wil ik hier nog in het bijzonder bedanken. Ik heb veel geleerd van jouw kennis en ervaring in dierexperimenteel onderzoek. Ook ben ik je enorm dankbaar voor je hulp bij het opzetten van het orthotoop muismodel en de ondersteuning bij de eerste series van operaties. Ik weet niet hoe ik dit allemaal zonder jou had moeten doen, dankjewel daarvoor!

Miriam van Dijk, jou wil ik graag bedanken voor je praktische hulp vanuit Nutricia. Of het nu ging om het bestellen van diëten, IVD gerelateerde zaken, of technische informatie met betrekking tot analyses, je was altijd bereikbaar.

Ook wil ik graag alle medewerkers van het CPV, met name **Nicole**, bedanken voor hun ondersteuning bij de experimenten en het verzorgen van de muizen.

Verder wil ik graag al mijn (oud) collega's bedanken voor de fijne samenwerkingen en de gezellige sfeer op de afdeling in de afgelopen jaren. **Harry**, bedankt voor al je input en hulp, zowel gedurende de labmeetings als daarbuiten. En natuurlijk

bedankt voor de gezelligheid en gastvrijheid als we weer met heel PUL gebruik konden maken van jullie tuin voor een borrel en/of BBQ. **Marco en Chiel**, bedankt voor jullie hulp en ondersteuning op het lab. **Karin, Juliette en Rianne**, bedankt voor jullie klinische inzichten in het cachexie onderzoek en de vele interessante discussies. **Charlotte, Debbie, Jalal, Juanita, Justine, Lieke, Lisanne, Mieke, Niki, Sandra, Sophie, Sven, Vasili en Viviënne:** bedankt voor de gezelligheid tijdens de koffie, lunch, borrels en labuitjes.

Ook wil ik graag **Merel, Rianne en Jorne**, de cachexie-collega's van de chirurgie, bedanken voor de samenwerkingen, het uitwisselen van kennis en gezelligheid de afgelopen jaren.

Vrienden en familie zijn absoluut onmisbaar tijdens een promotietraject. Zonder jullie was deze periode ongetwijfeld een stuk minder ontspannen geweest.

De asfaltvreters van het MUMC+ cycling team: **Dirk, Bart S., Rob, Youri, Michiel, Vyne, Rein, Bart B., en Dominique**. De afgelopen jaren heb ik ruim 34.000 km op de fiets afgelegd, waarvan het merendeel met een van jullie. Het samen fietsen door de Limburgse heuvels, Voerstreek en Belgische Ardennen heeft me de afgelopen jaren de nodige afleiding gegeven. Daarnaast waren de wielertripjes naar Aosta, Dolomieten, Vogezen, Annecy en Calusso een ervaring op zich. Dank voor de mooie tochten en de gezelligheid op de fiets.

Team Duvel: **George, Sybren, Noury, Tanno, Connor and Alex.** We are thinking very much along the same lines. Thank you for the all the great nights at Cafe Falstaff!

De **Zeeuwse Legenden**, de middelbare schoolvrienden. Inmiddels uitgewaaierd over heel het land. We zien elkaar soms lange tijd niet, maar als wij elkaar zien, voelt die lange tijd als de dag van gisteren. Lekker rabaten en kadouten in Malancourt was een mooie traditie. Hopelijk kunnen we deze traditie snel weer in ere herstellen. Mannen, jullie ook bedankt voor de nodige ontspanning en amusement!

Karlijn, mijn grote zus. Zonder jou was ik nu niet de persoon geweest die ik nu ben. Waar we vroeger nog weleens ruzie maakten over onzinnige dingen zijn we er nu voor elkaar als het nodig is. Na mijn Master in Utrecht verhuisde ik weer naar Maastricht. Jij woont in Amsterdam, waardoor we elkaar niet meer zo vaak zien als ik zou willen. Ik ben trots dat jij mijn zus bent en ik wil je graag bedanken voor de waardevolle tijd die we samen hebben besteed. Op een zonnige toekomst!

Mijn lieve ouders, **pa** en **ma**. Jullie hebben mij alles gegeven wat ik nodig had. Heel veel liefde, kennis en een gelukkige en onbezorgde jeugd. Jullie hebben me altijd gesteund in de keuzes die ik heb gemaakt en dat wordt ongelooflijk gewaardeerd. Ook waren jullie altijd oprecht geïnteresseerd in de vorderingen van mijn onderzoek en de status van de muizen ;). De laatste maanden werden jullie een beetje ongeduldig. Telkens als ik jullie sprak kreeg ik de vraag of het proefschrift al af was. Nu is het dan eindelijk af. Laten we het samen vieren.

Cait, de laatste woorden van mijn dankwoord zijn voor jou. Jij bent het beste wat mij is overkomen tijdens mijn PhD. Jij bent enorm belangrijk voor mij en laat me elke dag weer stralen. Ik heb altijd het maximale uit mijn PhD willen halen. Voor jou was dat zeker niet altijd even gemakkelijk. Als ik een deadline had of in het weekend naar het lab moest, was ik niet altijd even gezellig. En als klap op de vuurpijl besloot ik ook nog twee maanden naar Kopenhagen te gaan. Ondanks alles heb je me toch altijd gesteund. Tegelijkertijd laat je mij inzien dat er belangrijkere dingen in het leven zijn dan werk. Al vind ik het soms lastig hieraan toe te geven. In de tussentijd hebben we ook nog een huis gekocht en verbouwd. Nu dit bijna voorbij is wordt het tijd voor nieuwe avonturen en om te genieten. Ik heb veel mensen in dit dankwoord bedankt voor hun belangrijke bijdrage aan dit proefschrift. Ondanks dat jij niet letterlijk hebt bijgedragen was het zonder jouw steun nooit gelukt. Lieve Cait, bedankt voor je vertrouwen en steun. Ik hou van jou. Hoeveel? Heel veel!

Curriculum Vitae

CURRICULUM VITAE

Wouter van de Worp was born on March 10th, 1992 in Terneuzen. After he completed his general secondary school education in 2011 at S.s.g. De Rede in Terneuzen, Wouter studied Biomedical Science at Maastricht University. He wrote his bachelor thesis on 'the effect of dietary components in inflammatory lung diseases' at the Department of Toxicology. Wouter received his bachelor's degree in 2014. After an English Course in New York, he enrolled in the 2-years Drug Innovation Research Master at Utrecht University in February 2015. During his Master's, Wouter performed a 9-month internship at the Laboratory of Translational Immunology at UMC Utrecht. Here, he studied the underlying mechanisms of an engineered cytokine fusion protein in sensory neurons. During a second internship of 8 months, he performed research at the Utrecht Institute for Pharmaceutical Sciences in collaboration with Danone Nutricia Research. In this project, he investigated the immune modulatory effects of breast milk derived oligosaccharides.

In April 2017, Wouter started his PhD project at the Department of Respiratory Medicine at Maastricht University Medical Center+ under the supervision of prof. dr Schols, dr. Langen, dr. van Helvoort and dr. Theys focusing on lung cancer cachexia. During this PhD project, Wouter extensively studied the molecular mechanism and dynamics of muscle wasting in lung cancer cachexia, and evaluated the therapeutic effects of targeted nutritional intervention. The research performed in this project was honored with first prizes for best poster at the 11th International Conference on Cachexia, Sarcopenia and Muscle Wasting (2018) and the NUTRIM science day (2022). In addition, Wouter was selected as "next generation researcher in cancer cachexia" at the Cancer Cachexia conference (2021), and he was nominated to participate the ResearchTalent Program 2021 for high potential junior researchers. After obtaining his PhD, Wouter will continue as postdoctoral researcher in the field of cancer cachexia at the Department of Respiratory Medicine. To fund this postdoc, he was awarded with the Kootstra Talent Fellowship and the Nutricia Research Foundation grant, and he will receive funding from private partners.

List of publications

LIST OF PUBLICATIONS

Publications as part of this thesis

1. **van de Worp, W. R.,** Theys, J., van Helvoort, A., & Langen, R. C. (2018). Regulation of muscle atrophy by microRNAs: 'AtromiRs' as potential target in cachexia. Current Opinion in Clinical Nutrition & Metabolic Care, 21(6), 423-429.
2. van der Heyden, B.*, **van de Worp, W. R.*,** van Helvoort, A., Theys, J., Schols, A. M., Langen, R. C., & Verhaegen, F. (2020). Automated CT-derived skeletal muscle mass determination in lower hind limbs of mice using a 3D U-Net deep learning network. *Journal of Applied Physiology*, 128(1), 42-49. * shared first authorship
3. **van de Worp, W. R.,** Schols, A. M., Dingemans, A. M. C., Op den Kamp, C. M., Degens, J. H., Kelders, M. C., ... & Langen, R. C. (2020). Identification of microRNAs in skeletal muscle associated with lung cancer cachexia. *Journal of cachexia, sarcopenia and muscle*, *11*(2), 452-463.
4. **van de Worp, W. R.,** Schols, A. M., Theys, J., van Helvoort, A., & Langen, R. C. (2020). Nutritional interventions in cancer cachexia: evidence and perspectives from experimental models. *Frontiers in nutrition*, 7.
5. **van de Worp, W. R.,** van der Heyden, B., Lappas, G., van Helvoort, A., Theys, J., Schols, A. M., Verhaegen, F., & Langen, R. C. (2021). Deep learning based automated orthotopic lung tumor segmentation in whole-body mouse CT-scans. *Cancers. 13*(18), 4585.
6. **van de Worp, W. R.,** Theys, J., Sanz Gonzalez, A., van der Heyden, B., Verhaegen, F., Caiment, F., Hauser, D., Smeets, H. J., Schols, A. M., van Helvoort, A., & Langen, R. C. (2022). Characterization of a novel orthotopic lung cancer mouse model to study lung cancer cachexia. ***In review****: Journal of Cachexia, Sarcopenia and Muscle Wasting.*
7. **van de Worp, W. R.,** Theys, J., Wolfs C. J. A., Verhaegen, F., Schols, A. M., van Helvoort, A., & Langen, R. C. (2022). Targeted dietary intervention attenuates experimental lung cancer cachexia. ***Submitted****.*

Publications on the same topic as this thesis

8. Cortiula, F., Hendriks, L. E., **van de Worp, W. R.,** Schols, A. M., Vaes, R. D., Langen, R. C., & De Ruysscher, D. (2022). Physical exercise at the crossroad between muscle wasting and the immune system: implications for lung cancer cachexia. *Journal of Cachexia, Sarcopenia and Muscle, 13(1):55-67.*
9. Ubachs, J., **van de Worp, W. R.,** Vaes, R. D., Pasmans, K., Langen, R. C., Meex, R. C., Lambrechts, S., van Gorp, T., Kruitwagen, R. F. P. M., Olde Damink, S., Rensen, S. S. (2022). Ovarian cancer ascites induces skeletal muscle wasting in vitro and reflects sarcopenia in patients. *Journal of cachexia, sarcopenia and muscle*, *13*(1), 311-324.
10. Vaysse, P., Demers, I., van den Hout, M. F., **van de Worp, W. R.,** Baijens, L. W., Tan, B. I., Lacko, M., Vassen, L. A., van Mierlo, A., Langen, R., Speel, E. M., Heeren, R. M., Porta Siegel, T., Kremer, B. (2022). Radical oral cavity cancer resection requires sensitive metabolic profiling: Sensitivity evaluation of rapid evaporative ionization mass spectrometry. ***In press:*** *Analytical Chemistry.*

11. Aberle, M., Vaes, R., **van de Worp, W. R.,** Dubois, L. J., Lieuwes, N. G., Biemans, R., Langen, R., van Schooten, F., Dam, R., Olde Damink, S., Rensen, S. S. (2022). Novel models of human pancreatic cancer cachexia heterogeneity by transplantation of tumor organoids into mice. ***In press:*** *JCSM – Rapid communications.*
12. Webster, J. M., Waaijenberg, K., **van de Worp, W. R.,** Kelders, M., Lambrichts, S., Verhaegen, F., van der Heyden, B., Smith, C., Lavery, G., Schols, A., Hardy, R., & Langen, R. C. (2022). 11β-HSD1 determines the extent of muscle atrophy in a model of acute exacerbation of COPD. ***In review:*** *American Journal of Physiology-Lung Cellular and Molecular Physiology*

Other publications

13. de Boer, A., **van de Worp, W. R.,** Hageman, G. J., & Bast, A. (2017). The effect of dietary components on inflammatory lung diseases–a literature review. *International Journal of Food Sciences and Nutrition*, 1-17.
14. Xiao, L., van't Land, B., **van de Worp, W. R.,** Stahl, B., Folkerts, G., & Garssen, J. (2017). Early-Life Nutritional Factors and Mucosal Immunity in the Development of Autoimmune Diabetes. *Frontiers in Immunology*, *8*, 1219.
15. Xiao, L., **van De Worp, W. R.,** Stassen, R., Van Maastrigt, C., Kettelarij, N., Stahl, B., ... & van't Land, B. (2019). Human milk oligosaccharides promote immune tolerance via direct interactions with human dendritic cells. *European journal of immunology*.
16. Prado, J., Westerink, R. H., Popov-Celeketic, J., Steen-Louws, C., Pandit, A., Versteeg, S., **van de Worp, W. R.,** ... & Eijkelkamp, N. (2021). Cytokine receptor clustering in sensory neurons with an engineered cytokine fusion protein triggers unique pain resolution pathways. *Proceedings of the National Academy of Sciences*, 118(11).